Cover Page

Universiteit Leiden

The handle http://hdl.handle.net/1887/22054 holds various files of this Leiden University dissertation.

Author: Akerboom, Sebastiaan
Title: Ln(III) complexes as potential phosphors for white LEDs
Issue Date: 2013-10-29

Ln(III) complexes as potential phosphors for white LEDs

PROEFSCHRIFT

Ter verkrijging van

de graad van Doctor aan de Universiteit Leiden,

op gezag van Rector Magnificus prof. mr. C.J.J.M. Stolker,

volgens besluit van het College voor Promoties

te verdedigen op dinsdag 29 oktober 2013

klokke 10:00 uur

door

Sebastiaan Akerboom

geboren te ’s Gravenhage, Nederland in 1985

Samenstelling promotiecommissie

Promotor	Prof. Dr. E. Bouwman
Co-promotor	Dr. W.T. Fu
Overige leden	Prof. Dr. M.A.G.J. Orrit
	Prof. Dr. A. Meijerink (Universiteit Utrecht)
	Prof. Dr. C. Wickleder (Universität Siegen)
	Prof. Dr. J. Brouwer

"Unless someone discovers a means of making luminescent bodies that are vastly brighter than the best known, luminescence may be excluded altogether as a factor in artificial lighting."

(E.L. Nichols, Trans. I.E.S. **16**, 332, 1921)

aan mijn ouders

Table of Contents

1.	Introduction	7
2.	Substituted phenanthrolines as antennae in luminescent Eu(III) complexes	47
3.	Ln(III) complexes with small aromatic ligands	71
4.	Phenol-type ligands as sensitizers	87
5.	Tuning Eu(III) complexes with dibenzoylmethanates	109
6.	Triboluminescence of lanthanoid dibenzoylmethanates	129
7.	Summary, general discussion and outlook	143
8.	Appendix A, Quantum yield determination	151
	Samenvatting	158
	List of Publications	162
	Curriculum vitae	163
	Acknowledgements	164

List of abbreviations

CCT	Correlated color temperature
CIE	Commission Internationale de l'Eclairage (French)
CFL	Compact Fluorescent Lamp
Cgs	centimeter-gram-second (system of units)
CRI	Color Rendering Index
CRT	Cathode Ray Tube
CT	Charge transfer
dmf	N,N-dimethylformamide
dmso	dimethyl sulfoxide
ED	Electric dipole
ET	Energy transfer
EU-27	European Union (27 member states)
H_2fda	Furan-2,5-dicarboxylic acid
H_4tma	4-hydroxy trimesic acid
Hdbm	Dibenzoylmethane
IR	Infrared
ISC	Intersystem crossing
IUPAC	International Union of Pure and Applied Chemistry
JO theory	Judd-Ofelt theory
LED	Light-emitting diode
Lm	Lumen
LMCT	Ligand-to-metal charge transfer
MD	Magnetic dipole
MOF	Metal Organic Framework
Mtoe	Million tonnes of oil equivalent
nIR	Near infrared
nUV	Near ultraviolet
PC-WLED	Phosphor-converted white LED
PDP	Plasma Display Panel
PWh	Petawatt-hours (= 10^{15} Watt-hours)
PL	Photoluminescence
PLQY	Photoluminescence quantum yield
ppm	Parts per million
SI	Système internationale (French)
SSL	Solid State Lighting
TACN	1,4,7-Triaza-cyclononane
TL	Tube Luminescent (French)
TrL	Triboluminescence
TWh	Terawatt-hours (= 10^{12} Watt-hours)
UV	Ultraviolet
VUV	Vacuum ultraviolet
YAG	Yttrium-aluminum garnet

1 Introduction

The anticipated growth of the world population and the increasing demand for energy are in stark contrast with the earth's energy resources that are rapidly nearing depletion. Substantial amounts of energy can be saved by employing more efficient sources of artificial light. Today's light sources are reviewed together with state-of-the-art solid state light sources (SSLs) that have great energy savings potential. Emphasis is put on the phosphors required for efficient SSLs and the potential of coordination compounds of trivalent lanthanoid ions as phosphors is discussed. The chapter is concluded with a description of the contents of this thesis.

1.1 Thirst for energy

1.1.1 Global energy consumption

Year after year, the world's energy consumption has been rising [1]. With the anticipated growth of the world population in mind it is to be expected that the thirst for energy will only increase further [1-3]. In 2011, the global use of primary energy was as high as 12,275 million tons of oil equivalent (Mtoe), or approximately 143 PWh [1]. Compared to the figure of 2001 (110 PWh) this is an increase of as much as 30% in 10 years. The consumption of primary energy by the 27 member states of the enlarged European Union (EU-27) was 13.5 PWh in 2007 [4, 5]. In principle, one can think of two possible ways of dealing with the growing thirst for energy. On the one hand, the production of energy can be increased accordingly. With most of our energy production relying on fossil fuels that are rapidly approaching depletion, this seems to be an inadequate response. On the other hand, the energy can be used more effectively, i.e. by employing more efficient technology. As will be discussed in the upcoming sections (1.2 and 1.3), there is a high savings potential when it comes to artificial lighting. Recent developments in the field of semiconductor technology have opened doors towards much more efficient light sources.

1.1.2 Electric energy consumption

In 2007, the total consumption of electric energy within the EU-27 was 2.9 PWh [4, 5]. Households were responsible for using 800.7 TWh of electric energy, while the tertiary sector consumed 760.4 TWh of electric energy. Approximately 10% (84 TWh) of the residential electricity consumption was due to electric lighting, while this figure is 26% (200 TWh) for the tertiary sector [4, 5]. Similar numbers are found for the consumption of electricity in the USA: it is estimated that 22% (915 TWh) of the electric energy produced is used for electric lighting [6]. These are rather substantial amounts of energy, so there is a high energy saving potential when it comes to electric lighting. Schubert *et al.* have estimated the energy savings potential provided by *solid state lighting* (SSL) (section 1.3.3) [6]. In their calculations, the SSL-lamps are assumed to be almost three times more efficient than the current ones, which is a realistic assumption as can be seen from Table 1.1. A 20% market penetration of SSL would lead to an annual saving of 230 TWh, which is 5.5% of the total US electricity production. An SSL penetration of 60% would lead to a saving of 459 TWh per year, or 11%. The impact on annual CO_2 emissions of the US for these scenarios is estimated to be 134 Mt and 268 Mt, respectively.

1.2 Lighting technology

1.2.1 General considerations

Currently, the most commonly used lamps for indoor lighting are based on relatively old technology and have been highly optimized in the past decades. Their efficiency has reached a limit that is inherent to their operating principles, leaving little possibilities for further improvement. SSL technology on the other hand is rapidly emerging, and has made extraordinary progress in the past decade. The efficiency of SSL-based lamps is now comparable to that of fluorescent technology, and there seems to be no fundamental reason why efficiencies could not increase even further [7].

1.2.2 Incandescent lamps and halogen lamps

The development of the incandescent lamp dates back to 1879, when Thomas Edison filed his patent on the 'Electric lamp' [8-10]. The principle of operation of the incandescent lamp relies on the thermal emission of radiation by a glowing tungsten wire. The wire, or *filament*, itself is heated by resistance heating, when a sufficiently large current passes through it to make it glow. As a result of this principle, the emission spectrum of an incandescent lamp very closely resembles that of a black body radiator and can be described by the Planck radiation formula [11, 12]. The emission spectrum is continuous and broad, with its maximum depending on the emission temperature according to Wien's law: $\lambda_{max} \times T = 2.897 \times 10^{-3}$ m · K [13, 14]. A major drawback of the black body emission is that a substantial amount of radiation is emitted in the infrared region. Integration of a 2,500 K black body emission spectrum shows that only 5% of the emission energy is within the visible region, the rest is lost as heat. Following Wien's law, the emission maximum may be shifted to shorter wavelengths by increasing the filament's temperature, but this approach is limited by the evaporation rate of tungsten, with its melting point at 3,695 K [15]. In the *halogen incandescent lamp*, the net rate of tungsten evaporation is reduced by employing a tungsten-halogen cycle.

Table 1.1: Characteristics of commercially available lamps.

Lamp	η_{eff} (lm · W^{-1})	CCT (K)	CRI
Incandescent	15 - 20	2800	100
Halogen incandescent	20 - 25	2800 - 3200	100
TL / CFL	30 - 100	2700 - 6500	50 - 95
White LED (typical)	80	6500	85
Warm-white LED	67	2700	> 70

η_{eff}: luminous efficacy, lumens per watt of electrical power drawn by the lamp. TL: 'Tube Luminescent' (French), CFL: Compact Fluorescent Lamp.

During operation of the lamp, tungsten will evaporate from the filament into the gas phase. There it will react with the halogen, typically iodine, to give a volatile tungsten halide. At the high operation temperatures, this halide will stay in the gas phase and decompose close to the filament, resulting in tungsten being deposited back on it [16]. This allows higher operating temperatures of the filament and thus increases light output. However, due to the broad nature of the emission spectrum, the efficiency increase is limited, as can be seen from Table 1.1.

1.2.3 Fluorescent lamps

Fluorescent lamps were introduced in 1938 by General Electric and compact fluorescent lamps (CFL's) were made available in the 1970s [17-19]. This type of lamps relies on a gas discharge of low pressure mercury vapor. The main emission of the mercury plasma is in the deep UV at 254 nm, which is not only invisible to the human eye but also harmful [11, 20, 21]. A coating of luminescent materials, often called *phosphors*, on the inside of the tube is used to convert this UV radiation into visible light. The overall energy conversion efficiency of fluorescent lamps is limited to about 30% [11, 22]. The main energy loss occurs in the conversion of deep UV photons to visible photons, which amounts to a loss of 50%. Further energy is lost in the plasma discharge process and in the conversion process by the phosphors. It is obvious that the majority of the losses are due to the operating principles of the lamp. Since the performance of the phosphors used currently is close to their physical limit, the efficiency of fluorescent lamps cannot be improved significantly [23].

1.2.4 Light-emitting diodes

As the name suggests, a light-emitting diode (LEDs) is a diode, which generally consists of a junction of n- and p-type semiconductors. A semiconductor can be described as a substance with a valence band that holds the valence electrons and an empty conduction band. The top of the valence band is separated from the bottom of the conduction band by the bandgap, which is characteristic for the compound. A semiconductor can be doped with atoms that have excess electrons compared to the host material (n-doping). This introduces an additional dopant level with electrons within the bandgap, close to the conduction band. Doping a semiconductor with an electron-poor atom introduces an empty band near the valence band of the semiconductor. When p- and n-type semiconductors are joined together, electrons from the n-type semiconductor flow to the p-type semiconductor, occupying the holes, until equilibrium is reached. Under the influence of an external electron motive force, electrons can be pumped from the valence band of the p-type semiconductor, to the higher energy conduction band of the n-type semiconductor. At the junction, the electrons and holes can recombine under the release of energy. In the case of a direct bandgap semiconductor, this energy can be released in the form of photons, that is,

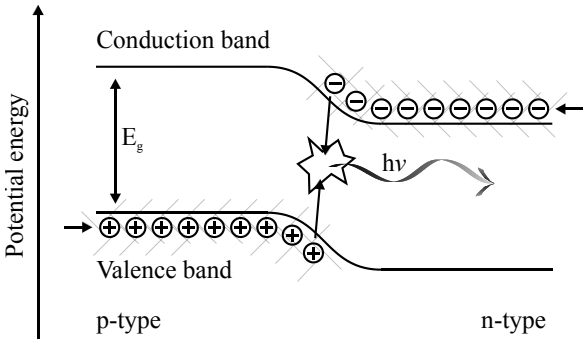

Figure 1.1: A PN-junction under forward bias, conducting a current and exhibiting luminescence as a result of radiative electron-hole recombination. E_g: bandgap, the current flows from the p-type to the n-type side of the junction.

light is emitted from the semiconductor. A schematic representation of this operating principle is given in Figure 1.1. This effect was discovered already in 1907 by H. J. Round, when testing SiC crystals as a rectifier for an early crystal-detector radio [12]. Thanks to this principle, electric energy is converted into light directly and in theory highly efficiently. Dependent on the intensity required by the application and the required color, several semiconductor systems are being used today, an overview is given in Table 1.2. Sustained development of LEDs based on GaAsP, GaP, GaAs and GaN was initiated in the 1960s. Most of the work on GaN technology was abandoned in the mid 1970s as a result of the poor efficiencies that were achieved by the early devices [12]. In 1992 however, Akasaki *et al.* demonstrated the first GaN LED emitting in the UV spectral region with a surprisingly high efficiency. From that moment on, development on GaN semiconductor technology has soared and LED technology can be used for producing all visible colors [24].

The green gap

The size of the bandgap is influenced by the dopants used in the semiconductor material and therefore dopant concentration can be used to tune the color of the light emitted by the

Table 1.2: Overview of the semiconductor systems used for commercial LEDs (source: [12]).

Semiconductor	Color	Brightness (rel.)
GaAsP:N	orange-red-IR	low
GaP:N	green	low
Al:GaAs	deep red-IR	high
$(Al_xGa_{1-x})_yIn_{1-y}P$	yellow-orange-red	high
In:GaN	nUV-blue-green	high

LED. For instance, pure GaN has a bandgap of 3.40 eV, corresponding to emission in the near-UV region at 365 nm [24]. This bandgap can be lowered by doping the material with indium, which allows the emission to shift to the blue and green spectral regions [25]. In theory, the In:GaN system could span the entire visible region, as the bandgap of pure InN is estimated to be between 0.7 and 0.8 eV, corresponding to emission in the IR region around 1600 cm^{-1} [26]. Doping the semiconductor has other effects. The $(Al_xGa_{1-x})_{0.5}In_{0.5}P$ system has a direct bandgap for $x < 0.5$ while a crossover to an indirect bandgap occurs for compositions with $x > 0.5$. The bandgap energy at the crossover point is 2.33 eV, which corresponds to 532 nm [12]. For the In:GaN system, the reasons for performance reduction at higher dopant concentrations are less well understood. It has been attributed to the immiscibility of GaN and InN and to increased strain between the In:GaN active layer and the GaN base layer [12, 27, 28]. So, while it is perfectly possible to prepare high efficiency blue and red LEDs based on GaN:In and $(Al_xGa_{1-x})_yIn_{1-y}P$, respectively, it has been proven impossible to obtain efficient green, yellow and amber LEDs. This problem is frequently referred to as the *green gap* or *yellow gap* [28, 29]. A plot of the external quantum efficiency *versus* the peak emission wavelength of commercially available LEDs is given in Figure 1.2. Also shown in this graph is the eye sensitivity curve (section 1.3.1). Since the eye is very sensitive in the region of the green gap, the inefficient LEDs still appear to exhibit bright emission.

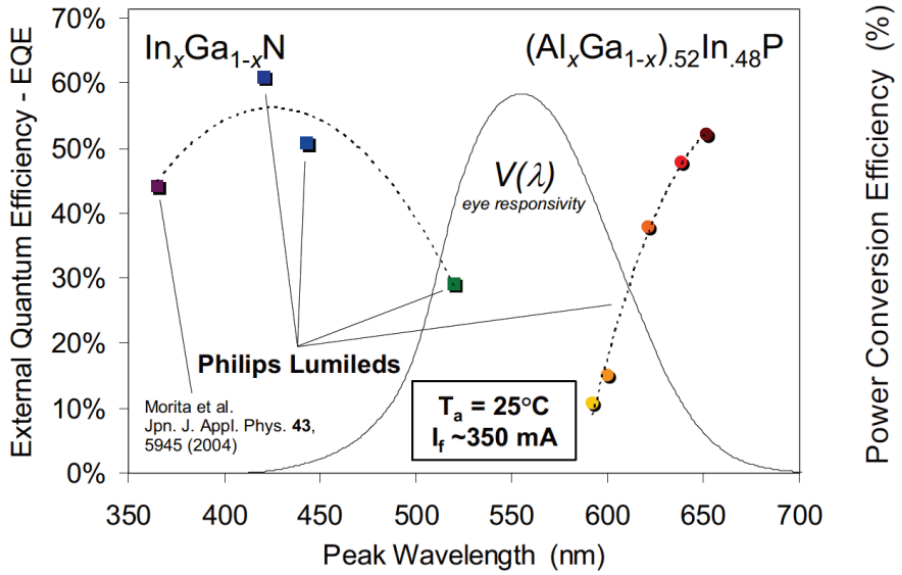

Figure 1.2: External quantum efficiency versus peak wavelength high power Philips Lumileds based on In:GaN (UV to blue region) and AlGaInP materials, superimposed on the eye sensitivity curve V(λ). The lack of high efficiency green and yellow LEDs is known as the 'green gap'. Image taken from ref. [27].

1.3 White light and light sources

1.3.1 White light

The human eye

The word *light* is used to indicate that part of the electromagnetic spectrum to which the human eye is sensitive. It is generally accepted that this part of the spectrum extends from 380 nm to 780 nm [30]. Before discussing the principles that the current light sources rely on to generate white light, it is fruitful to consider the characteristics of the human eye. In the eye, the lens focuses the light onto the retina, which contains light sensitive rod and cone cells. The rods are more sensitive to light than the cones and respond to the entire visible spectrum. They are useful in low-light conditions and do not allow color vision. The less sensitive cones require conditions of high ambient light, and there are three types of them, each of which is sensitive to a specific part of the visible spectrum, as shown in Figure 1.3. One can distinguish red-sensitive, green-sensitive and blue-sensitive cones based on their spectral response. Colors can be differentiated based on the relative stimulus of these three receptors [12, 30].

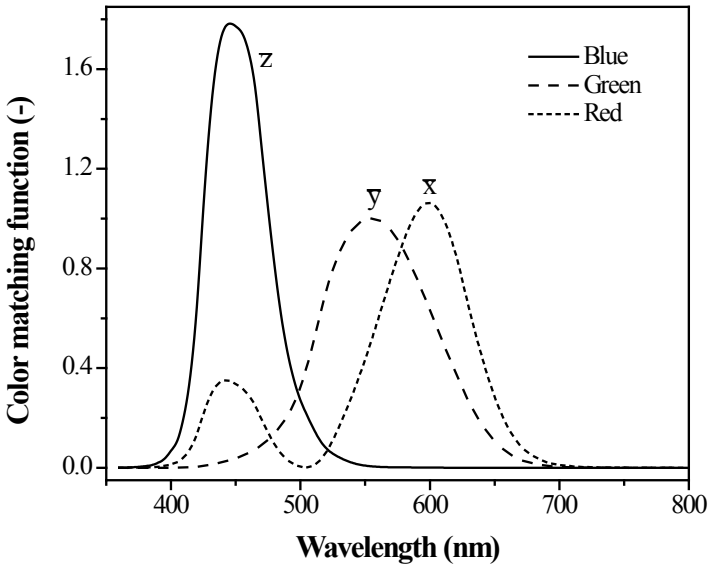

Figure 1.3: The sensitivity of the red, green and blue color receptors in the retina of the human eye. These curves are also known as the dimensionless color matching functions $\bar{x}(\lambda)$, $\bar{y}(\lambda)$ and $\bar{z}(\lambda)$. Note that $\bar{y}(\lambda)$ is equal to the eye-sensitiviy function V(λ). Redrawn using data taken from [12].

Colorimetry

The spectral response curves of the blue, red and green receptors in the eye shown in Figure 1.3 are also known as the *color matching functions* $\bar{x}(\lambda)$, $\bar{y}(\lambda)$ and $\bar{z}(\lambda)$, respectively [12, 30]. The *tristimulus values X*, *Y* and *Z* represent the degree of stimulation of each of the receptors by a light source with an emission spectrum *P(λ)* as shown in equation 1.

$$X = \int \bar{x}(\lambda) \cdot P(\lambda) d\lambda \qquad Y = \int \bar{y}(\lambda) \cdot P(\lambda) d\lambda \qquad Z = \int \bar{z}(\lambda) \cdot P(\lambda) d\lambda \qquad (1)$$

The total stimulus of the receptors in the eye is just $X + Y + Z$. This property allows for defining the ratios in equation 2, which represent the relative stimuli of the cones.

$$x = \frac{X}{X+Y+Z} \qquad y = \frac{Y}{X+Y+Z} \qquad z = \frac{Z}{X+Y+Z} \qquad (2)$$

As the value of z can be found from $z = 1 - x - y$, the z coordinate is redundant and x and y can be used to uniquely define a color in a two-dimensional color space, shown in Figure 1.4. The parameters x and y are the *chromaticity coordinates*. They can be used to locate all visible colors in the diagram; the lower left-hand corner corresponds to blue, the top to green and the right hand corner to red. As white light corresponds to equal stimulus of all three receptors, it is located in the center of the diagram.

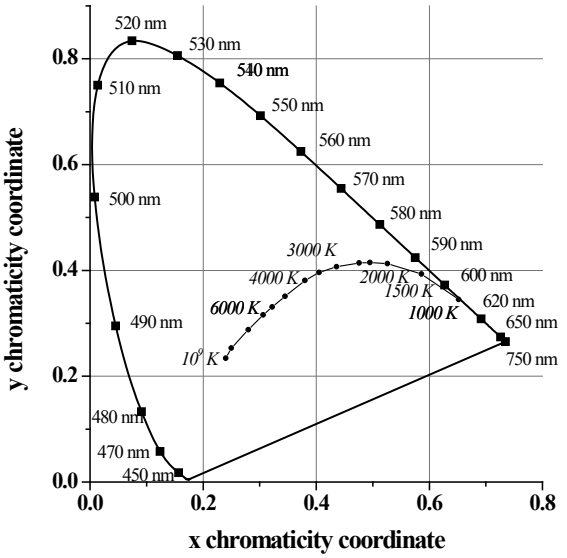

Figure 1.4: The Commission Internationale de l'Eclairage (CIE) 1931 color diagram showing the two-dimensional color space as defined by equation 2. Monochromatic colors are indicated on the perimeter of the diagram using squares. White light is located in the center at (0.33, 0.33) and the coordinates of black bodies in the temperature range from 1000 to 10^9 K are indicated by dots on the Planckian locus.

Characteristics of white light

A large number of possible optical spectra correspond to white light [12]. This is illustrated by the emission spectra shown in Figure 1.5a–e, all of which correspond to white light. Thus, a light source with a spectrum that contains only three narrow emission lines that match the maximum sensitivity of the three color receptors will be perceived as white. The same is true for a light source with an emission spectrum with a nearly constant intensity over the visible region. The difference between these two light sources can become apparent when they are used to illuminate an object. The observed color is a result of the interplay between the light source's emission spectrum and the object's light absorption spectrum. Therefore, the perceived color may differ between the two light sources. This phenomenon is described by the *color rendering index* (CRI) of the light source, which is defined as its ability to render a color with respect to a standard. The standard is usually daylight, and the CRI is specified on a scale from 0 (poor) to 100 (best). Another metric, the *correlated color temperature* (CCT), is used to indicate if a light source emits 'cold', bluish or 'warm' reddish white light. It is defined as the absolute temperature of an ideal black body emitter with its color coordinates as close as possible to that of the light source [12, 30]. For example, the CCT of a candle is somewhere between 1,500 and 2,000 K, that of an incandescent lamp 2,800 K and summer sunlight at noon between 4,900 and 5,700 K [12]. In Figure 1.4, the location of black body radiators is indicated by the *Planckian locus*. Interestingly, high color temperature light appears to be 'cold' because it is relatively rich in blue emission.

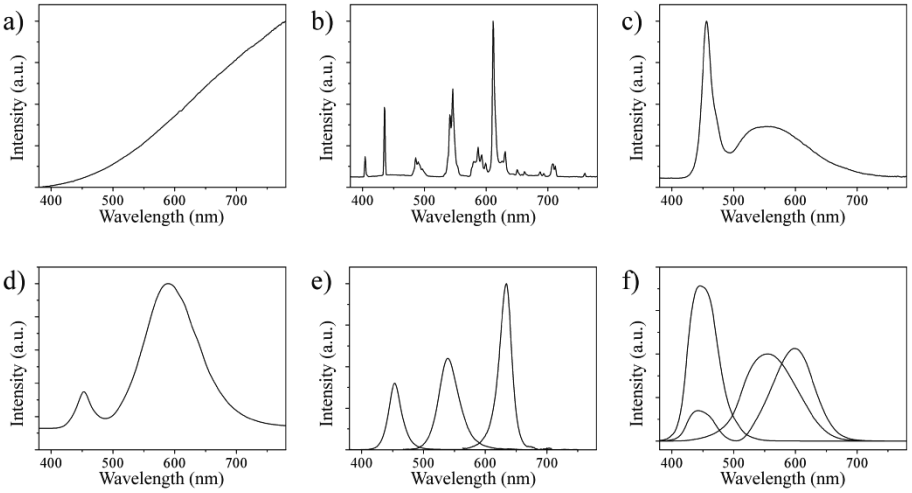

Figure 1.5: Emission spectra of a 40 W incandescent lamp (a), a typical TL lamp (b), a typical white LED (c), a warm white LED (d), a red, green and blue LED (e) and the sensitivity of the cones in the retina of the human eye (f).

Eye sensitivity

The characteristics of the eye also need to be considered when the energy performance of a lamp is measured. Although the total emitted power of radiation by a lamp is easily expressed as its *radiant flux* in units of Watts, this does not give information on the *perceived intensity*. For instance, the eye does not register the large amount of IR radiation emitted by an incandescent lamp; this is readily seen from Figure 1.5f. To take the eye sensitivity into account, *photometric units* are used. They describe the intensity of a light source as perceived by the eye. The result is expressed as *luminous efficiency* in lumens per Watt of optical power ($lm \cdot W^{-1}$). For a light source with an emission spectrum $P(\lambda)$, the luminous efficiency η_{lum} is given by equation 3 [12].

$$\eta_{lum} = 683 \frac{lm}{W} \cdot \int V(\lambda) P(\lambda) d\lambda \qquad (3)$$

In this equation, $V(\lambda)$ represents the *eye sensitivity function*, which is plotted in Figure 1.2. The maximum of the $V(\lambda)$ function is at 555 nm and the factor 683 has a historical origin [12]. The theoretical maximum luminous efficiency is thus 683 $lm \cdot W^{-1}$ for a monochromatic emitter at 555 nm. For efficient lamps and phosphor materials, a good match to the eye sensitivity function is an important prerequisite for obtaining high efficiency lighting. This is especially true for emitters in the red spectral region. The eye sensitivity falls off rapidly for wavelengths over 600 nm. For saturated red light, a red emitter with a λ_{max} of 610 nm is desired [7, 31]. This can be seen from Figure 1.4, where the lower right-hand corner corresponds to red. Use of a broad band emitter would result in substantial emission at wavelengths beyond 610 nm, reducing its luminous efficiency. Use of a line emitter that has otherwise the same λ_{max} and efficiency would reduce this spillover to longer wavelengths. As a result, the luminous efficiency of the light source has increased although the radiant flux remains unchanged. The overall efficiency of conversion of *electric power* into light by a lamp, also considering the sensitivity of the eye, is usually expressed as its *luminous efficacy*, also in $lm \cdot W^{-1}$ [12]. In this case, the Watts refer to the total electrical power drawn by the lamp.

1.3.2 Current lamps and white light

The spectrum of incandescent and halogen incandescent lamps is continuous over the entire visible region and extends deep into the infrared part. This ensures that all three receptors in the eye are stimulated, and since the spectrum is a Planck curve, the CRI of these light sources is high. In theory, a filament temperature of 6,620 K provides the best match to the human visual response and would give rise to a luminous efficiency of approximately 95 $lm \cdot W^{-1}$ [7]. The emission spectrum of fluorescent tubes strongly depends on the blend that has been applied on the inside of the tube. Typically, it consists of a mixture of phosphors with several emission lines or bands spread over the visible region, as is shown in Figure

1.5b. A comparison of characteristics of commercially available white lamps is given in Table 1.1 [9, 12, 32].

1.3.3 Solid-state lighting and white light

Although the conversion of electric energy into light can be accomplished with a high efficiency thanks to the semiconductor nature of LEDs, there is one important drawback: the emission is inherently monochromatic as it is determined by the size of the bandgap. Monochromatic light sources are useful for indicator lamps and traffic lights, but cannot be used to illuminate office-buildings and houses. Currently, several solutions to circumvent this drawback exist. The term *solid-state lighting* (SSL) is a collective expression for those LED-based white light sources.

RGB LEDs

Perhaps the most obvious solution to produce white light is to combine red, green and blue LEDs into a single device. Although this solution, also known as the *RGB LED*, has theoretically the highest efficiency, there are some downsides. The different LED chips are made using different semiconductor materials and will age at different rates, resulting in color instability of the emitted light [29]. Furthermore, the LEDs will require different driving voltages, which complicates the fabrication of an RGB LED [11, 33]. Finally, the efficiency of this solution is hampered by the comparatively low efficiency of green LED chips [29, 34]. This problem is discussed in section 1.2.4, and is inherent to the characteristics of the semiconductor materials used to produce LEDs [7, 29].

Blue LED with broadband phosphor

In an alternative approach for white light generation, a single LED chip is used to pump a layer of phosphor materials. White LEDs that rely on phosphor materials are commonly known as phosphor-converted white LEDs (PC-WLEDs). The most widely used white LEDs as of to date use an In:GaN LED emitting blue light at 470 nm combined with Ce:$Y_3Al_5O_{12}$, cerium-doped yttrium-aluminum garnet (Ce:YAG), as a phosphor material. When a current is passed through the LED, it starts emitting blue light, of which a fraction is absorbed to excite the phosphor material. The blue light of the LED, mixed with the broad band emission of the phosphor, results in white light. An emission spectrum of such device is shown in Figure 1.5c. Ever since the white LEDs of this type were commercialized in 1996, they have been applied in flashlights, bicycle lamps, car headlights and in other situations that do not require high quality white light [9, 12]. White LEDs of this type can achieve high luminous efficacies, but the lack of emission in the red spectral region generally results in high correlated color temperatures of over 6,500 K, making them unsuitable for general illumination purposes. More recently, so-called ‘warm white LEDs’ were made commercially available. The basic principle is similar: a blue LED, usually emitting at 450 nm, is used to pump a phosphor coating. The phosphor in this case

is usually a broad band emitting Eu(II)-doped $Ca_{m/2}Si_{12-m-n}Al_{m+n}O_nN_{16-n}$ (CaSiAlON) material [35, 36]. The emission from these white LEDs can achieve correlated color temperatures of 2700 K; the spectrum of such white LED is shown in Figure 1.5d. The CRI that is accomplished in this way is however limited to 70, which limits the applicability of these lamps [37-39]. In addition, degradation of the phosphor material or LED chip will cause significant color changes in time [33].

Near-UV LED with phosphor coating

An approach similar to the one taken for generating white light with fluorescent tubes is to use an LED emitting in the nUV region to pump a coating of blue, green and red phosphor materials [33, 40]. With this method it is possible to tune the color temperature and CRI just by changing the composition of the phosphor coating. At the same time, it requires driving only a single LED and provided that the phosphor materials are stable, color shifts are avoided over the entire lifespan of the LED. With this method, a high CRI as well as a high efficiency can be reached. It has been shown that a theoretical light source with three component colors can achieve a CRI of 85 at a luminous efficiency of 366 $lm \cdot W^{-1}$ [41]. Compared to the device based on a blue LED, the Stokes shift of the phosphor coating is larger when a nUV LED is used. However, this is compensated for by the higher efficiency of the nUV LED, as compared to the blue one. The effect of increasing efficiency of the In:GaN LEDs towards shorter wavelengths is illustrated by the dashed line in Figure 1.2.

1.4 Phosphor materials

1.4.1 General remarks on phosphor materials

The first phosphor material was discovered in the year 1603 by an Italian shoemaker and alchemist in Bologna, and is known as the *Bolognian stone* [42]. The material, $BaSO_4$ with traces of other elements, was found to absorb daylight and emit various colors in the dark. Other stones were found to exhibit similar behavior and these were named *phosphors*, meaning 'light bearer' in Greek. The name of the element *phosphorus* derives from the property of white phosphorus to show a faint glow when exposed to oxygen or air [42, 43]. As this glow is the result from the oxidation of phosphorus, the correct name for this process is *chemiluminescence*, not phosphorescence. Nowadays, although the meaning of *phosphor* is not clearly defined, the word generally refers to solid materials that exhibit *luminescence* [43]. Luminescence refers to the phenomenon in which a substance emits light after its electronic state has been excited by external energy. It includes both *phosphorescence* and *fluorescence*. The first refers to long afterglow phenomena linked to spin-forbidden electronic transitions, while the latter refers to extremely short afterglow associated with spin-allowed electronic transitions [13].

1.4.2 Current phosphors

Phosphor materials are widely applied in modern day technology such as luminescent tubes (*vide supra*), cathode ray tubes (CRT's) and plasma display panels (PDP's) [22, 32, 44]. These phosphors have been developed and optimized in the past several decades and have reached almost optimal photophysical properties, as strong absorption (> 90%) and high quantum efficiency (~90%). It can therefore not be expected that these properties can be significantly improved [22, 23]. Nearly all of these materials are based on inorganic compounds and are highly stable. They are, however, optimized for excitation with high energy photons. In a fluorescent lamp, a wavelength of 254 nm is used while in PDP's the phosphors are excited by vacuum UV (VUV) photons between 147 and 190 nm [11]. In CRT's, the excitation energy is even higher; a beam of high energy electrons (30 keV) is used [22]. While the current phosphors work well for those applications, they show poor absorption at 360–480 nm, limiting their usefulness for application in SSLs based on GaN LED technology.

1.4.3 Phosphors for PC-WLEDs

For the PC-WLED to become feasible, novel phosphor materials that can be excited by the LED chip are required [33, 45]. Besides Ce:YAG that is nowadays widely applied, other potential materials are investigated as phosphor for application in near-UV or blue LED based PC-WLEDs. In general, these materials comprise oxides, nitrides, oxynitrides, sulfides and silicates [33, 39, 40, 46]. Typically, most oxides show poor absorption in the nUV or blue region, while most sulfides are very sensitive to moisture and CO_2 [11, 33, 39]. Most of the oxide materials are garnet-type materials, but silicates, aluminates and borates are widely studied as well [33]. Oxynitrides and nitrides are investigated as host materials for Eu(II), as their strong crystal field results in a shift of the ion's emission into the red region. The resulting emission spectrum is of broadband nature, which is not desirable for a red phosphor. Beyond 610 nm, the sensitivity of the eye drops rapidly, as explained in section 1.3.1, so that emission at wavelengths over 610 nm contributes very little intensity. As a result, the lumen equivalent falls rapidly as the bandwidth of the red phosphor increases. The decrease in efficiency is roughly 0.15% per nanometer [7]. This can be compensated for by shifting the emission of the red phosphor to shorter wavelengths, but the lamp will not be able to render saturated red colors. To maintain a saturated red as well as a high efficiency, a narrowband phosphor emitting around 610 nm is highly desired [7]. Additional requirements, regardless of emission wavelength, arise from the very high photon flux of a typical high power LED. The excitation energy density generated by a 1 Watt In:GaN LED is estimated to be approximately 30 $W \cdot cm^{-2}$, which is nearly three orders of magnitude higher than the excitation energy density phosphors in a typical fluorescent tube are exposed to [11]. In addition, the temperature of high power LEDs can reach values of over 100 °C, because they are not perfectly efficient [47, 48].

To sum up, the perfect phosphor has [31, 49]:

1. An emission spectrum with high lumen equivalent
2. A high absorption in the n-UV to blue spectral region, matching In:GaN LEDs
3. A high quantum efficiency
4. High thermal- and photostability
5. Low thermal quenching

1.5 Trivalent lanthanoid ions

1.5.1 Lanthanoid ions and phosphor materials

The lanthanoid ions are widely used as emitting center in phosphor materials, because of their well defined and favorable photophysical properties (section 1.6). Most notable are the trivalent ions that show narrow, almost line-like emission bands that are relatively insensitive to the environment of the ion. As a result, they produce highly pure colors. The Eu(II) ion is used as emitting center in phosphors as well (*vide supra*), but it shows broad band emissions.

1.5.2 Nomenclature and discovery

When it comes to the nomenclature of the lanthanoids, there seems to be some disagreement. Although terms like *lanthanide*, *lanthanoid* and *rare earth* are loosely used, they are in fact well defined. According to the International Union of Pure and Applied Chemistry, the use of *lanthanide* should be avoided altogether as the ending '-ide' normally suggests a negative ion while the lanthanoids, being metals, only give rise to stable cations [50]. The term *lanthanoid*, meaning 'like lanthanum', is more correct and is a collective name for the elements La, Ce, Pr, Nd, Pm, Sm, Eu, Gd, Tb, Dy, Ho, Er, Tm, Yb, Lu. Although, given this definition, La should not be included in this series, it has become a member by common usage. The term 'lanthanoid' is derived from the Greek *lanthaneien*, meaning 'lying hidden' [51]. The *rare earths* encompass the lanthanoids together with Sc and Y [52]. The term 'rare earth' has an historical origin; 'earth' was commonly used to refer to oxide-type minerals in the 18th century. Earths containing the rare earth elements apparently seemed rare [53]. The history of rare earth chemistry starts in the late 18th century in Scandinavia, when Johan Gadolin discovers a new earth he names yttria. In the following years, more 'earths' were discovered, most of them consisting of a mixture of lanthanoid oxides. Successful separation into the constituent oxides was performed by Carl Gustav Mosander in the years 1839-1843. Lutetium was the last naturally-occurring rare earth to be discovered, by Urbain in 1907, while it took until 1947 to synthesize the artificial element promethium [53, 54]. It must be noted that these elements are in fact not as rare as the name suggests [53, 55, 56]. The terrestrial abundances range from 0.2 ppm for Tm to 46 ppm for Ce [56]. Thus, even the rarest rare earths are more abundant than gold (0.004 ppm), mercury (0.08 ppm) or Se (0.05 ppm) [57].

1.5.3 Mining, separation and chemical properties

Mining and separation

The lanthanoids are mainly found in nature in the minerals Bastnasite (LnFCO$_3$), Mozanite ((Ln,Th)PO$_4$) and Xenotime (Y,Ln)PO$_4$ [55, 56]. China has the world's largest lanthanoid reserve at approximately 60%, followed by the former Soviet Union at 17% and the United States at 13% [58]. The lanthanoids are extracted from the minerals by means of acid digestion, which results in the chloride salts, or by treatment with NaOH, producing lanthanoid hydroxides. Separation of the lanthanoid elements on a commercial scale is done by means of solvent extraction of lanthanoid nitrates between water and an organic solvent using tri-(*n*-butyl)phosphate as an extractant. Using repeated extractions can give the elements in a purity level of up to 99.99%, while ion-exchange methods are required to achieve purities of 99.999% [55, 56].

Basic chemical properties

Because the lanthanoids have highly similar chemical properties, it took over 100 years to completely separate them [53, 55]. They all have a stable +3 oxidation state, and the ionic radius changes smoothly from 1.06 Å for La(III) to 0.85 Å for Lu(III) [59]. The latter phenomenon is known as *lanthanoid contraction* and is tightly related to the properties of the 4f orbitals that, on going from La to Lu, are gradually filled with electrons. This 4f shell is located within the filled [Xe] core, so that the 4f orbitals are practically completely shielded from the environment by the filled 5s and 5p orbitals. In addition, the 4f electrons only partially compensate for the increase in nuclear charge, resulting in a net increase of the attractive force between the nucleus and the outer electrons and thus contraction [52]. This phenomenon is commonly known as *lanthanoid contraction*. In cases when a full ($4f^{14}$) or half full ($4f^{7}$) or empty ($4f^{0}$) shell can be achieved, additional oxidation states are possible. For this reason, Ce and Tb have a stable +4 oxidation state, while Eu and Yb can exist in a +2 oxidation state [52, 55]. The +3 oxidation state, which is common for all lanthanoids, is the result of optimal balance between ionization energy and the lattice or solvation energy [55, 60].

1.5.4 Coordination chemistry

The coordination chemistry of the lanthanoids was poorly investigated up until the mid 1960s. It was assumed that the lanthanoids would form 6-coordinate complexes, in analogy with the d-block elements [61]. However, much has been learned since. The coordination chemistry is largely governed by the +3 oxidation state, although complexes with for instance Eu(II) and Ce(IV) and Yb(II) have been reported [55, 62-64]. Owing to the properties of the shielded 4f valence electrons, the lanthanoids share many characteristics. They act as hard Lewis acids preferring hard Lewis bases such as O and F. Compared to the d-block metal ions, they all show a rather low coordination stabilization energy, and

complex formation as a result is mainly entropy-driven. Thus, polydentate ligands generally give rise to stable complexes. The stability of the bonds increases gradually on going from La(III) to Lu(III) as a result of the increased charge density on the smaller ions. Unlike d-block ions, the lanthanoid ions do not show a preferred coordination geometry and the bonding is mainly non-directional. The final geometry and coordination number are therefore mostly governed by the steric demands of the ligands. For example, spectroscopic evidence suggests that the early lanthanoids (La – Eu) form aqua complexes with a coordination number of 9, while the later ions (Dy – Lu) give rise to complexes described by $[Ln(H_2O)_8]^{3+}$ [55]. This is a direct result from lanthanoid contraction. Coordination numbers are reported to range from 2 to as high as 12 [60]. Care should be taken, though, because the coordination of the cyclopentadienyl ligand is often counted as 1 [52]. A coordination number of 8 is most commonly encountered for the lanthanoid ions. Lower coordination numbers can be achieved by increasing the steric bulk of the ligands, while higher numbers are accessible by using chelating ligands with a small coordination angle, such as the nitrate ion.

1.6 Photophysical properties of the trivalent lanthanoid ions

1.6.1 Electronic structure and energy levels

The interesting photophysical properties of the trivalent lanthanoid ions, such as the long luminescence lifetime and line-like emission spectra, are a direct result of the 4f orbitals being shielded by the 5s and 5p shells. The 4f orbitals are gradually filled on going from La(III) to Lu(III), and the electronic configuration changes from $[Xe]4f^0$ to $[Xe]4f^{14}$. Depending on the number of electrons, there are several ways to distribute them over the 4f orbitals. There are seven 4f orbitals, and each of them can hold two electrons, so there are a total of 14 positions or *spin-orbitals* available for the electrons to occupy. It can be shown that the number of possible arrangements (N) for distribution of n electrons over p orbitals is given by equation 4.

$$N = \frac{p!}{n!(p-n)!} \qquad (4)$$

The number of possible arrangements of the f electrons or *microstates*, for the trivalent lanthanoid ions is given in Table 1.3.

Table 1.3: Atomic number (Z), number of f-electrons and possible arrangements (N) and ground state energy term for the trivalent lanthanoid ions.

Ln(III)	Z	$4f^n$	N	Ground term
La	57	0	1	$^1S_0$
Ce	58	1	14	$^2F_{5/2}$
Pr	59	2	91	$^3H_4$
Nd	60	3	364	$^4I_{9/2}$
Pm	61	4	1001	$^5I_4$
Sm	62	5	2002	$^6H_{5/2}$
Eu	63	6	3003	$^7F_0$
Gd	64	7	3432	$^8S_{7/2}$
Tb	65	8	3003	$^7F_6$
Dy	66	9	2002	$^6H_{15/2}$
Ho	67	10	1001	$^5I_8$
Er	68	11	364	$^4I_{15/2}$
Tm	69	12	91	$^3H_6$
Yb	70	13	14	$^2F_{7/2}$
Lu	71	14	1	$^1S_0$

Spectroscopic terms and free-ion levels

Some electron arrangements will be more favorable than others as a result of a number of interactions that the electrons experience. By far the strongest interaction is the Coulomb repulsion between the electrons, resulting in splitting of the configuration into *spectroscopic terms*. The energy differences caused by this interaction are in the order of 10^4 cm^{-1} [65]. A spectroscopic term is characterized by the total orbital angular momentum (L) and total spin (S) corresponding to the distribution of the electrons. Following the Russel-Saunders coupling scheme, both L and S can be found from the orbital angular momentum (l) and spin (s) of the individual electrons by a vector sum, using equations 5 and 6.

$$\vec{L} = \vec{l}_1 + \vec{l}_2 + \cdots + \vec{l}_n \qquad (5)$$

$$\vec{S} = \vec{s}_1 + \vec{s}_2 + \cdots + \vec{s}_n \qquad (6)$$

A spectroscopic term has the general form $^{2S+1}\mathbf{L}$, with **L** depending on L according to Table 1.4, while the number $2S + 1$ indicates the spin multiplicity of the term.

Table 1.4: Term symbols corresponding to the first seven values of *L*.

L	0	1	2	3	4	5	6	7
L	S	P	D	F	G	H	I	K

Besides the Coulombic interaction that leads to splitting of a configuration into spectroscopic terms, there is a weaker interaction that splits the terms further into *levels*. It is the spin-orbit interaction, which results in energy differences in the order of 10^3 cm^{-1} [65]. The orbital and spin angular momenta of the electrons couple to give a total angular momentum *J*. For a given term, *J* can take values according to equation 7.

$$|\vec{L} - \vec{S}| \leq \vec{J} \leq |\vec{L} + \vec{S}| \qquad (7)$$

The number of levels within a given term is simply found from $(2L + 1) \times (2S + 1)$, and the levels are described by symbols of the general form $^{2S+1}\mathbf{L}_J$. These levels are the so-called free-ion energy levels, as up until here no influence of the environment has been taken into account. The symbol corresponding to the ground state level can be found using Hund's rules in the order given below [66].

1. The ground state level has the largest spin multiplicity
2. The ground state level has the highest orbital angular momentum
3. The *J*-value of the ground state of a $4f^n$ configuration is given by:
    - $J = |L - S|$ if $n \leq 6$
    - $J = S$ if $n = 7$
    - $J = |L + S|$ if $n \geq 8$

Crystal field splitting

When the lanthanoid ion is placed in a coordinating environment, a third and even weaker interaction must be taken into account. It is the electric field produced by the coordinating atoms, known as the crystal field, which results in splitting of the free-ion levels further into Stark levels. The energy differences caused by the crystal field are in the order of a few hundreds of cm^{-1} [65, 66]. The maximum number of Stark levels for each free ion level equals $(2J + 1)$, but the exact number depends on the geometry of the coordination sphere. As a result, the 4f – 4f transitions of the trivalent lanthanoids can be used to probe site symmetries, and the maximum number of Stark levels for a given site symmetry have been tabulated [66, 67]. The Stark levels are labeled using the symbols of the irreducible representations of the point group corresponding to the coordination polyhedron [65, 67]. Figure 1.6 schematically summarizes how the $4f^6$ configuration split up as a result from all interactions.

1.6.2 Radiative transitions and selection rules

Although the trivalent lanthanoids have numerous electronic microstates, as can be seen from Table 1.3, the number of possible transitions between them is restricted by selection rules. A photon can interact with the 4f electrons through its electric or magnetic component. Since a photon cannot change the spin of an electron, the spin selection rule

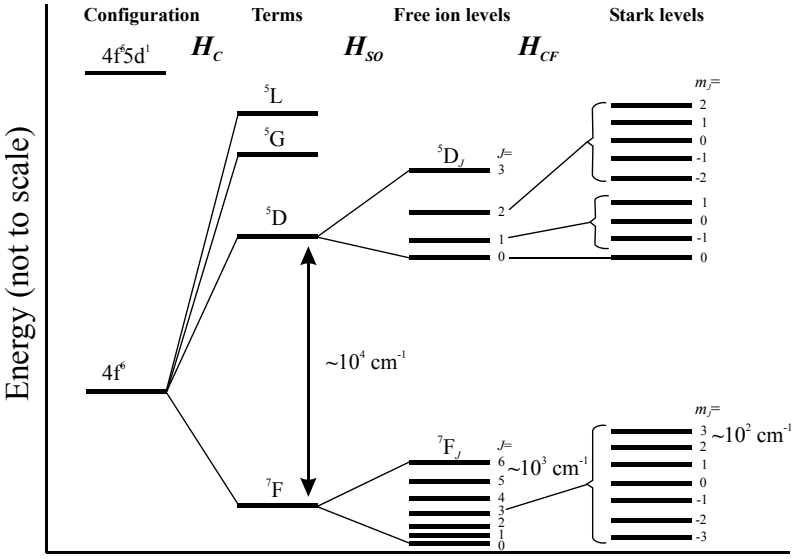

Figure 1.6: A schematic representation of the interactions that lead to splitting of the $4f^n$ configuration, here given (partially) for Eu^{3+}. From left to right: splitting due to Coulombic interactions (H_C), spin-orbit coupling (H_{SO}) and the crystal field (H_{CF}).

($\Delta S = 0$) easily follows. Interaction of the electron with the photon's electric-field component results in a net linear displacement of the electron. This phenomenon is known as an *electric dipole* (ED) transition, because there is dipole moment associated with this type of charge migration. Thus, transitions between s and p orbitals are allowed, because they involve a spatial redistribution of the charge, while transitions between s orbitals are forbidden. In the latter case, the charge shift has spherical symmetry and has no dipole moment associated. More formally, the ED operator has odd parity, the parity of the initial and final state of the electrons should be different. Hence, $4f^n \rightarrow 4f^n$ transitions are ED forbidden, as l for none of the electrons changes during such transition. The odd parity of the ED operator is illustrated schematically in Figure 1.7. The type of $4f^n - 4f^n$ transitions that are allowed are the *magnetic dipole* (MD) transitions. Interaction of the photon's magnetic-field component with the *trajectory* of the electron results in a rotational displacement of the entire trajectory. Transitions between s and p orbitals are MD forbidden, because this would involve a change in parity. A transition from a p_x orbital to a p_y orbital is MD allowed; a chemist will readily recognize that this can be seen as a rotation. Put more formally, the MD operator has even parity and it couples states of the same parity. Therefore it is the only type of allowed transition on an isolated *Ln*(III) ion. A pictorial representation of the effect of the MD operator and its even parity is given in Figure 1.7.

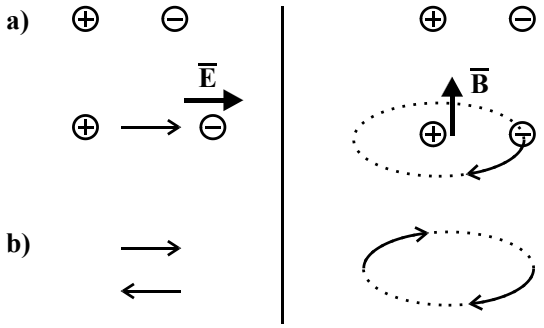

*Figure 1.7: a) A schematic representation of the effect of an ED (left) and MD (right) operator on an electron. The ED operator (thick arrow, **E**) results in a shift of the electron (thin arrow). The MD operator (thick arrow, **B**) results in shifting the electron over a circular trajectory. b) the effect of the inversion operation on the effect of the ED (left) and MD (right) operators. It can be seen that the effect of the ED operator changes sign, as the direction of the arrow is inversed. Thus, it has odd parity. For the MD operator, inversion does not invert the sense of rotation and so the MD operator has even parity.*

Lifting the selection rules: intermediate coupling

Following the above rules, only MD transitions would be allowed on an isolated lanthanoid ion. However, the large spin-orbit coupling constant of the heavy atomic nucleus of the lanthanoids also results in mixing of the free-ion levels for which $|\Delta L| = 1$ and $|\Delta S| = 1$ and $|\Delta J| = 0$. This phenomenon is known as *intermediate coupling* and as a result, L and S are only accurate quantum numbers to a certain extent. For instance, consider the $^5D_0 \rightarrow {}^7F_2$ transition of Eu(III), which is usually the strongest band in the emission spectrum. This spin forbidden transition should not occur according to the selection rules. The intermediate coupling scheme however enables a pathway for lifting the restrictions imposed by the parity and spin selection rules [68]. The $^5D_0$ level ($L = 2$, $S = 2$, $J = 0$) mixes with the $^7F_0$ level ($L = 3$, $S = 3$, $J = 0$) and the $^7F_2$ level ($L = 3$, $S = 3$, $J = 2$) mixes with the $^5D_2$ level ($L = 2$, $S = 2$, $J = 0$). Thus, although the $^5D_0$ level has still dominantly $^5D_0$ character, it also has some $^7F_0$ character, which helps alleviating the spin selection rule. The various types of transitions and the corresponding S, L, J selection rules are listed in Table 1.5.

Lifting the selection rules: crystal field

Another mechanism lifting the ED selection rule is the crystal field splitting, resulting from the electric field produced by the atoms surrounding the lanthanoid ion. If the crystal field symmetry is highly non-centrosymmetric, the crystal field helps mixing some opposite parity orbital character into the 4f orbitals. For example, some 5d character can be mixed into the 4f orbitals, similar to the formation of hybrid orbitals such as sp^3, sp^2 and sp on carbon atoms. As a result, the orbitals no longer are purely 4f-type, which enables a pathway for lifting the parity selection rule [68]. Transitions of this type are known as *forced ED* transitions, because they are 'forced' by the crystal field. Their intensity however is still only 10^{-4} times that of a fully allowed ED transition.

Table 1.5: Selection rules for several types of transitions and their properties [66, 68].

Type [a]	Parity	ΔS	ΔL	ΔJ	I_{rel} [b]
ED	Opposite	0	±1	0, ±1	1
Forced ED	Opposite	0	0, ±1, ±2, ±3, ±4, ±5, ±6; if L=0 or L'=0: ±2, ±4, ±6	0, ±1, ±2, ±3, ±4, ±5, ±6; if L=0 or L'=0: ±2, ±4, ±6	10^{-4}
MD	Same	0	0	0, ±1	10^{-6}
EQ	Same	0	0, ±1, ±2	0, ±1, ±2	10^{-10}

a) ED: Electric Dipole, MD: Magnetic Dipole, EQ: Electric Quadrupole. b) Typical intensity relative to a fully allowed ED transition.

Hypersensitivity

Because the 4f orbitals are shielded efficiently from the surroundings, the intensity of the majority of 4f – 4f transitions varies only within a factor of 2-3 in different host matrixes. However, the intensity of some transitions can increase by as much as a factor of 200 depending on the host environment of the ion [69, 70]. These so-called *hypersensitive transitions* obey the selection rules for electric quadrupole (EQ) transitions listed in Table 1.5, and are therefore also known as *pseudo-quadrupole* transitions [70]. An example of such transition is the $^5D_0 \rightarrow {}^7F_2$ transition on Eu(III). As of to date, there seems to be disagreement on whether the $^5D_4 \rightarrow {}^7F_6$ transition on Tb(III) exhibits hypersensitivity [69, 71].

1.6.3 Intensities of the transitions

Judd-Ofelt theory

A model for describing the intensities of the radiative 4f – 4f transitions of the lanthanoids has been developed independently by B.R. Judd and G.S. Ofelt in 1962 [72, 73]. This model is known as the *Judd-Ofelt theory* (JO theory), and it can be used to predict the intensity of a transition in absorption and emission spectra, the relative contribution of a transition to the luminescence spectrum and radiative lifetime of exited states [71, 74]. The model is semi-empirical and relies on only three parameters. In the JO theory, the dipole strength of a forced ED transition is expressed by equation 8.

$$D_{ED} = e^2 \sum_{\lambda=2,4,6} \Omega_\lambda |\langle J \left|\left| U^\lambda \right|\right| J' \rangle|^2 \qquad (8)$$

In equation 8, Ω_λ represents the JO-parameters that are dependent on the matrix surrounding the lanthanoid ion and the bracketed expressions are the squared reduced matrix elements of which the value is independent of the lanthanoid ion's host matrix. Furthermore, the matrix elements are dimensionless, and their values have been tabulated

[75]. In general, the rate A of a transition from an initial state of multiplicity J to a final state with multiplicity J' is given by equation 9.

$$A_{J-J'} = \frac{64\pi^4 \upsilon^3}{3h(2J+1)}\left[\frac{n(n^2+2)^2}{9} D_{ED} + n^3 D_{MD}\right] \quad (9)$$

In this equation, v represents the wavelength of the transition, J the multiplicity of the initial state, h Planck's constant and n the refractive index of the compound. The contributions of the electric and magnetic dipole strengths to the transition are indicated by D_{ED} and D_{MD}, respectively. The first can be calculated from equation 8, while MD components can be calculated and have been tabulated [71]. Typically, the calculations are performed in the centimeter-gram-second (cgs) system of units, using the appropriate values for h and e as listed in Table 1.6.

Table 1.6: conversion factors from cgs to SI and numerical values of useful constants [71].

Constant or unit	Value	Unit
h (Planck's constant)	$6.626 \cdot 10^{-27}$	erg · s
e (elementary charge)	$4.803 \cdot 10^{-10}$	esu
D_{MD} ($^5D_0 \rightarrow {}^7F_1$ on Eu(III))	$9.6 \cdot 10^{-42}$	$esu^2 \cdot cm^2$
esu (= 1 $erg^{1/2} \cdot cm^{1/2}$)	$3.336 \cdot 10^{-10}$	C
erg (= 1 $g \cdot cm^2 \cdot s^{-2}$)	$1 \cdot 10^{-7}$	J

JO theory applied to Eu(III) emission

A special case arises for Eu(III) emission spectra. Given the emission spectrum of an Eu(III) compound, calculation of the JO parameters is particularly straightforward. The transition from the $^5D_0$ resonance level to the $^7F_1$ level is purely of MD nature, while the $^5D_0 \rightarrow {}^7F_J$, $J = 2, 4, 6$ are purely of forced ED nature. Thus, based on equations 8 and 9, the theoretical intensities for those transitions are given by equations 10 and 11.

$$A_{0-1} = \frac{64\pi^4 \upsilon^3}{3h} n^3 D_{MD} \quad (10)$$

$$A_{0-2,4,6} = \frac{64\pi^4 \upsilon^3 e^2}{3h} \frac{n(n^2+2)^2}{9} \sum_{\lambda=2,4,6} \Omega_\lambda \left| \langle J \left| \left| U^\lambda \right| \right| J' \rangle \right|^2 \quad (11)$$

The remaining $^5D_0 \rightarrow {}^7F_J$, $J = 0, 3, 5$ transitions are forbidden in both ED and MD schemes and are not accounted for by JO-theory. In practice, these are indeed very weak. The squared reduced matrix elements required for evaluation of equation 11 can be found in literature and they are given in Table 1.7 [75, 76]. Since all non-diagonal matrix elements are zero, the sum in equation 11 reduces to a mere multiplication of the matrix element and the JO-parameter.

Table 1.7: Squared reduced matrix elements for analysis of the Eu(III) emission spectrum.

Transition	$\|\|U^{(2)}\|\|$	$\|\|U^{(4)}\|\|$	$\|\|U^{(6)}\|\|$
$^5D_0 \rightarrow {}^7F_2$	0.0032	0	0
$^5D_0 \rightarrow {}^7F_4$	0	0.0023	0
$^5D_0 \rightarrow {}^7F_6$	0	0	0.0002

The rate constant for the MD transition is readily calculated from equation 10, with D_{MD} given in Table 1.6, and equals approximately 49 s^{-1}. Provided that the spectrophotometer used to record the spectra has been corrected for the response of the detection system and calibrated to present the relative photon flow, experimental intensities can be found by integrating the corresponding lines in the spectrum [77]. The relative intensities of the $^5D_0 \rightarrow {}^7F_J$, $J = 0 - 6$ transitions with respect to the MD transition are easily found, and can be used to calculate the value of A_{0-6} using A_{0-1} as a yardstick. Summing these rates gives the total rate of radiative relaxation A_{rad} as shown in equation 12.

$$A_{rad} = \sum_J A_{0-J} \qquad (12)$$

1.6.4 Non-radiative relaxation

Decay of the excited state of the trivalent lanthanoid ions occurs not only *via* the radiative transitions described above; the energy can also be dissipated trough vibrations of the host lattice or complex in a process known as *multiphonon relaxation* [78]. The efficiency of this mode of relaxation depends on the size of the energy gap between the lowest lying excited state and the highest level of the ground state multiplet. A large gap requires more quanta to bridge it, making this mode of relaxation less favorable [51, 78]. A direct result of this *energy gap law* is the fact that *Ln*(III) luminescence occurs mostly from only one level, the *resonance level*, which is separated from the next lower lying level by a large energy gap. For Eu(III), this is the $^5D_0$ level, which is separated from the $^7F_6$ level by approximately 12,300 cm^{-1}, while for the Tb(III) ion the gap between the $^5D_4$ and $^7F_0$ levels is approximately 14,800 cm^{-1} [79]. Higher excited states such as $^5D_1$ and $^5D_2$ of Eu(III) are efficiently relaxed to the $^5D_0$ state by multiphonon relaxation, hence emission from these levels is rarely observed. It should be pointed out that certain selection rules apply to multiphonon relaxation processes, so the energy gap law cannot be used as an exclusive benchmark for judging the efficiency of multiphonon relaxation [80].

Intrinsic quantum yield

The lifetime of luminescence can be obtained experimentally (τ_{exp}); it contains contributions of both radiative and non radiative relaxation processes. With the rate of the radiative processes calculated using equation 12, the total rate of non-radiative relaxation processes can be calculated and expressed as A_{nrad}. Now, the total rate of depopulation of

the lanthanoid excited state, A_{tot}, can be expressed as $A_{tot} = A_{rad} + A_{nrad}$. The relation between τ_{exp} and A_{tot} is simply $A_{tot} = (\tau_{exp})^{-1}$, and equation 13 follows.

$$A_{tot} = \frac{1}{\tau_{exp}} = \frac{1}{\tau_{rad}} + \frac{1}{\tau_{nrad}} \quad (13)$$

The ratio between the rate of radiative relaxation and the total rate of relaxation is known as the *intrinsic quantum yield* Φ_{Ln} of the lanthanoid ion given by equation 14 [60, 81].

$$\Phi_{Ln} = \frac{A_{rad}}{A_{tot}} = \frac{\tau_{exp}}{\tau_{rad}} \quad (14)$$

1.7 Luminescent lanthanoid complexes

1.7.1 Historical notes

The study on luminescent lanthanoid complexes was initiated in 1942, when Weissman observed very intense luminescence characteristic for Eu(III) from crystals of europium salicylaldehyde when the compound was excited in the ligand-centered absorption band [82]. He realized that "excitation of the internal electronic system of the europium is provoked by light absorption in a region external to it". In 1957, Crosby observed similar behavior for an Yb(III) complex, and later also for complexes of Sm(III), Tb(III), Dy(III), Tm(III) and Yb(III) [83, 84]. In many cases, the luminescence that was observed upon ligand excitation was much brighter than that observed using direct excitation of the 4f manifold. The first extensive review on the subject was written by Crosby in 1966 [85]. In the early 1980s, research on luminescent lanthanoid complexes got a new impulse because it was realized that the compounds could be useful as medical imaging agent [86-88]. From that moment on, the photoluminescence of lanthanoid coordination compounds became a widely studied subject. The phenomenon of ligand-centered excitation of lanthanoid-centered luminescence became known as the *antenna effect* [88, 89].

1.7.2 Intramolecular energy transfer

Thanks to the ligand the lanthanoid center can be excited without having to rely on direct excitation using the forbidden 4f ← 4f transitions. The mechanism for this process is schematically shown in Figure 1.8 [51, 60, 90, 91]. It involves excitation of the ligand by means of an allowed transition. It is generally accepted that the ligand subsequently undergoes intersystem crossing (ISC) to an excited triplet state, followed by ligand-to-lanthanoid energy transfer. The lanthanoid ion will relax to its ground state as described in section 1.6, either radiatively or non-radiatively. At any stage of the transfer cascade, quenching may occur, reducing the luminescence efficiency. The overall quantum efficiency, Φ_{tot}, of this process is described by equation 15 [51, 60, 90].

$$\Phi_{tot} = \Phi_{ISC} \times \Phi_{ET} \times \Phi_{Ln} \quad (15)$$

In this equation, Φ_{ISC}, Φ_{ET} and Φ_{Ln}, represent the intersystem crossing, energy transfer and the lanthanoid ion's intrinsic quantum yields, respectively. The product of the first two is often referred to as the *sensitizer efficiency* $\eta_{sens} = \Phi_{ISC} \times \Phi_{ET}$, while Φ_{Ln} can be found from equation 14. Experimental evidence indicates that the energy transfer involves the triplet excited state of the ligand [83, 84, 88, 92, 93]. Although relaxation from the S* to the T* state of the ligand is spin-forbidden, the large spin-orbit coupling constant from the lanthanoid ion greatly aids in this process [51, 60, 91, 94]. Ligand to lanthanoid transfer directly from the singlet state cannot be ruled out completely, though, and has been reported [85, 88, 95, 96]. The ligand-centered energy levels in a lanthanoid complex can be determined by recording the absorption and emission spectrum for the Gd(III) analogs. As the first excited state of the Gd(III) ion, $^6P_{7/2}$ at 32,150 cm^{-1}, is generally much higher than the triplet state of a ligand, ET is not possible and the compound will exhibit ligand-centered phosphorescence from the T* state [60, 97-99].

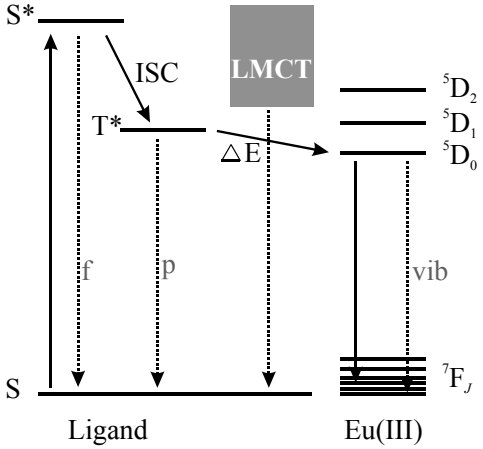

Figure 1.8: Jablonski diagram describing the energy transfer cascade in luminescent lanthanoid complexes. The preferred transfer pathway is indicated with uninterrupted arrows; quenching is indicated using dashed arrows. S/S: singlet ground- and excited state, T*: triplet excited state, ISC: intersystem crossing, LMCT: ligand-to-metal charge transfer band, ΔE: energy gap, f: fluorescence, p: phosphorescence, vib: vibrational quenching.*

Ligand to lanthanoid energy transfer

To describe energy transfer from the ligand to the lanthanoid ion, both Förster and Dexter type mechanisms can be invoked [51, 100-102]. Both transfer mechanisms are schematically shown in Figure 1.9. The Dexter mechanism involves a double electron transfer between the donor and acceptor and thus requires good overlap between the metal and ligand orbitals [103]. As a result, it is only efficient at very small distances between the ligand and the lanthanoid ion. In the Förster mechanism, the dipole moment of the ligand's excited state couples with that of the lanthanoid 4f levels [104]. For efficient Förster

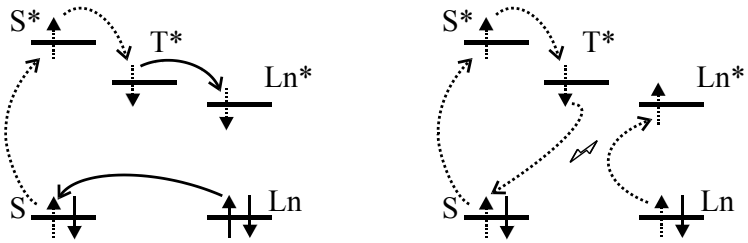

Figure 1.9: Schematic representation of Dexter (left) and Förster energy transfer mechanisms between the ligand and the lanthanoid ion. Transfer of electrons between the ligand and lanthanoid ion are indicated by solid arrows, dotted arrows indicate electronic processes within the ligand or lanthanoid ion.

transfer, large oscillator strengths are required. The group of Malta has derived a set of selection rules for Förster and Dexter type energy transfer mechanisms in luminescent lanthanoid complexes [97, 102]. Soon after the discovery of the antenna effect, it was realized that the level of the ligand-centered excited state with respect to the lanthanoid-centered resonance level plays an important role in the energy transfer process [84]. Systematic studies have shown that the energy gap between the T* state and the accepting level of the lanthanoid ion should be less than 1,850 cm^{-1} for efficient transfer [93]. That is, there should be a match between the ligand donor level and lanthanoid acceptor level. This match can be expressed as the *spectral overlap* in the Förster and Dexter transfer mechanisms [103-105]. If the gap is too small, thermally-assisted energy back-transfer may take place, providing a way of quenching the lanthanoid luminescence [51, 60, 86]. Another quenching pathway occurs in complexes based on lanthanoid ions having a low reduction potential, such as Eu(III) and Yb(III) (see 1.5.3) combined with a ligand that is easily oxidized [88]. In these compounds, ligand-to-metal charge transfer (LMCT) states may occur at levels sufficiently low to allow competition with L* → *Ln* energy transfer and thus cause quenching [51, 98, 106-108]. A theoretical framework describing energy transfer processes and the role of the LMCT state has been developed by Malta and co-workers [102, 106, 109-111].

Lanthanoid luminescence and quenching

Provided that the lanthanoid excited state is fed by the ligands, the complex should exhibit luminescence typical for the lanthanoid ion. As discussed in section 1.6.4, luminescence may be quenched by multiphonon quenching. In lanthanoid complexes, these phonons exist as high energy vibrational modes of C–H, O–H and N–H bonds [54, 86, 112]. As a rule of thumb, multiphonon relaxation is efficient if ΔE of the energy gap between two lanthanoid centered levels is equal to or smaller than six vibrational quanta [54, 113]. Considering C–H and O–H vibrations in the ligand, at 2,950 and 3,450 cm^{-1} respectively, it follows that these are efficient quenchers of Eu(III) and Tb(III) centered luminescence. Indeed, it is

known that water molecules in the first coordination sphere of Eu(III) are highly efficient luminescence quenchers. As the vibrational relaxation competes with the radiative route, its effectiveness may be assessed by recording the luminescence lifetime of the compound [112-114]. A suggested way of suppressing this mode of quenching is to replace the C–H and O–H bonds by C–D (ν = 2,100 cm^{-1}), C–F (ν = 1,200 cm^{-1}) and O–D (ν = 2,500 cm^{-1}) bonds [86, 115]. Meshkova *et al*. have demonstrated that substitution of the central C–H by a C–D bond in the β-diketone type ligand of a luminescent Yb(III) complex leads to an increase of the luminescence lifetime by 10 to 20% [112].

1.7.3 Examples of luminescent lanthanoid complexes

Several approaches have been taken to develop lanthanoid complexes showing highly efficient luminescence, and several reviews have been devoted to this subject in the past two decades [51, 60, 81, 86, 91, 97, 108, 115, 116]. The number of (potential) applications is large; besides use as phosphor materials (section 1.7.4) luminescent lanthanoid complexes can be used as, for example, imaging agents, biomarkers, immunoassays, pH sensors and O_2 sensors [81, 108, 117-119]. Suitable antenna ligands have hard donor atoms, and often have conjugated or aromatic systems to allow efficient light absorption at the desired wavelengths.

Complexes with β-diketonates

The β-diketonates constitute a very important class of ligands for luminescent complexes; the frequently used structures are shown in Figure 1.10. Several β-diketonates were used in the early studies by Weissman and have been the subject of several studies devoted to unraveling the energy transfer mechanism [82, 120-122]. Also in more recent studies β-diketonates continue to be used as ligands, and an extensive review on this class of compounds has been written by Binnemans [123]. Three β-diketonate ligands in their deprotonated form are required to counterbalance the positive charge on the lanthanoid ions. The coordination sphere is not saturated in such compounds, and solvent molecules will coordinate to the lanthanoid ion. To prevent this, a second ligand can be added to the reaction mixture to expel water and reduce quenching. If the ligand has an aromatic system, such as 1,10-phenanthroline, it may even act as an antenna. Examples of frequently used secondary ligands are shown in Figure 1.11. Homoleptic *tetrakis*-diketonato complexes can be prepared by employing a 1:4 metal-to-ligand ratio during synthesis. Depending on the synthetic strategy, the necessary cation can be provided by protonation of the base, e.g. the use of triethylamine gives $HNEt_3[EuL_4]$, or by using NaOH to deprotonate the β-diketone and addition of a chloride salt of the cation, such as NEt_4Cl [123, 124]. Alternatively, a quaternary ammonium hydroxide may be used as a base and source of the cation [125]. Other examples of counter ions used include the tetraphenylphosphonium, tetraphenylarsonium, 1,3-disubstitited imidazolium, morpholinium and

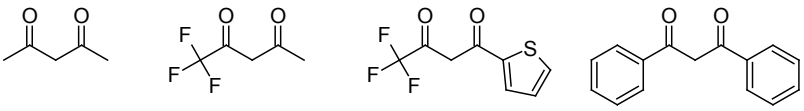

Figure 1.10: Examples of some widely used β-diketone ligands. From left to right: acetyl acetone (Hacac), trifluoroacetyl acetone (Htfac), 2-thenoyltrifluoroacetone (Httfa),dibenzoylmethane (Hdbm).

N-methylpyridinium ions [123, 124, 126-129].The β-diketonate ligands are highly efficient at sensitizing luminescence of the Eu(III) ion, because the triplet states closely match the ion's resonance level [97]. At approximately 21,000 cm^{-1}, the triplet state is too low for efficient population the $^5D_4$ level of the Tb(III) ion so that luminescence is rarely observed for Tb-dbm complexes, although exceptions have been reported [130]. Substituents on the ligand allow for tuning it to the metal, and can have a profound impact on its antenna properties [120]. In case of the tetrakis complexes, it was found that the cation provides additional handlebars for changing the luminescent properties of a given complex [124]. The highest luminescence quantum efficiency reported for a luminescent Eu(III) complex in the solid state is 85% for $[Eu(ttfa)_3(dbso)_2]$, (ttfa = trifluoroacetylacetonate; dbso = dibenzylsulfoxide) reported by Malta *et al.* [131]. For comparison, the quantum yield of $[Eu(ttfa)_3(H_2O)_2]$ is found to be only 23%, illustrating efficient quenching by the water molecules [132]. Very high photoluminescence quantum yields have also been reported for $HNEt_3[Eu(dbm)_4]$ at 75% [133]. Highly luminescent europium complexes can be obtained using this class of ligands; the compounds are however prone to photobleaching under UV radiation [123]. For example, Malta *et al.* have studied the temporal photoluminescence intensity of $[Eu(tta)_3(dbso)_2]$, and found that after 50 hours of irradiation at 400 nm, the luminescence intensity had dropped to 30% of its initial value [134].

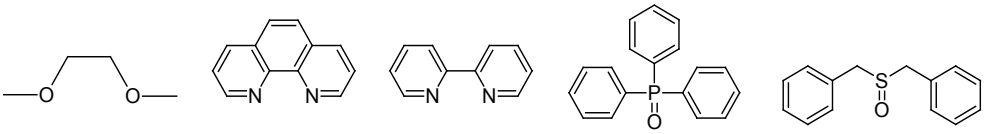

Figure 1.11:Examples of frequently used secondary ligands in lanthanoid(III) tris(dbm) complexes. From left to right: 1,2-dimethoxyethane (monoglyme), 1,10-phenanthroline (phen), 2,2'-bipyridine (bpy), triphenylphosphineoxide (tppo), dibenzylsulfoxide (dbso).

Small aromatic ligands

Many different and relatively small aromatic polydentate ligands can be successfully used to give photoluminescent lanthanoid complexes. For example, picolinates, salicylates, aromatic carboxylates and derived molecules have been used. Examples of such ligands are given in Figure 1.12. As with the β-diketonates, multiple ligands are required to saturate the coordination sphere around the central ion. Highly stable lanthanoid complexes showing very bright luminescence have been reported. For example, $[Eu(pbca)_3]$ (pbca = 4-phenyl-2,2'-bipyridine-5-carboxylate) has a luminescence quantum yield of 60%, while this figure for $[Tb(pbca)_3]$ is only 7% [135]. The complex $[Eu(bpc)_3]\cdot CH_3CN$ (bpc =

6-(1*H*-benzimidazol-2-yl)pyridine-2-carboxylate) is again very efficient at 61% quantum efficiency [136]. 2,6-Dipicolinic acid (H_2dpa) efficiently sensitizes both Eu(III) and Tb(III) centered luminescence, with quantum efficiencies of 72% and 68%, respectively [137]. Long luminescence lifetimes have been reported for complexes with the related amide ligand 2,6-pyridine-dicarboxamide (H_2pcam), shown in Figure 1.12b: 1.9 ms for $[Eu(pcam)_3](CF_3SO_3)_3$ and 2.2 ms for its Tb(III) analog [138]. While Eu(III) salicylates are often found to exhibit weak photoluminescence due to the presence of a low-lying LMCT state, the dinitro-substituted ligand (Figure 1.12c) is found to give Eu(III) complexes exhibiting very bright photoluminescence. This effect is explained by the increase of the energy of the LMCT state by the electron-withdrawing nitro group [139, 140].

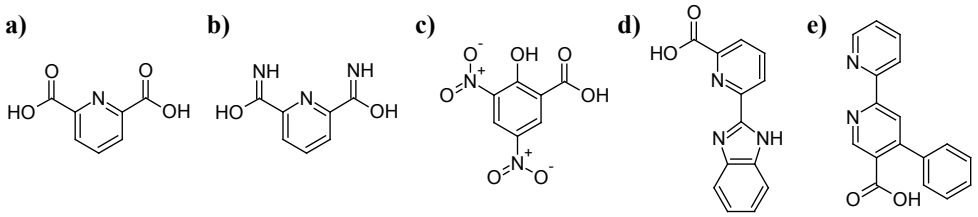

Figure 1.12: Overview of small aromatic ligands used in luminescent lanthanoid complexes. Shown are (a) 2,6-dipicolinic acid, H_2dpa, (b) 2,6-pyridine-dicarboxamide, H_2pcam, (c) 3,5-dinitrosalicylic acid, $H_2$3,5-NO_2-sal, (d) 6-(1H-benzimidazol-2-yl)pyridine-2-carboxylic acid, Hbpc, and (e) 4-phenyl-2,2'-bipyridine-5-carboxylic acid, Hpbca [135-138, 140-142].

Molecular cages

As complex formation is mostly entropy driven for lanthanoid ions, a successful strategy towards a stable complex is to use polydentate ligands that are able to fully encapsulate the lanthanoid ion. For luminescent complexes, one may distinguish ligands with chromophoric chelates and ligands with pendant chromophores [100]. The first have the antenna-part coordinating directly to the lanthanoid ion, while the latter have an antenna part that does not necessarily coordinate to the ion directly. Instead, the chromophore is attached to a ligand such as 1,4,7,10-tetraazacyclododecane (cyclen) (Figure 1.13b and c) or 1,4,7-triaza-cyclononane (TACN). When the antenna-part of the ligand is unable to coordinate to the lanthanoid ion, as for the ligand shown in Figure 1.13c, energy transfer is only possible via the through-space Förster-type mechanism [100, 104]. Ligands of the chromophoric chelate type bind to the lanthanoid ion through atoms that are part of the chromophore (Figure 1.13a, d and e) and allow both Förster and Dexter type energy transfer mechanisms [100, 103, 104]. Both the pendant chromophore and the chromophoric chelate approach towards cage-type ligands have led to lanthanoid complexes showing efficient photoluminescence. For example, the ligand in Figure 1.13d gives rise to Eu(III) and Tb(III) compounds that exhibit quantum yields in D_2O of 20% and 35%, respectively [89]. The ligand shown in Figure 1.13e forms a Tb(III) complex with a photoluminescence quantum yield of 61% in H_2O, while the analogous Eu(III) complex only manages to reach 6% [143].

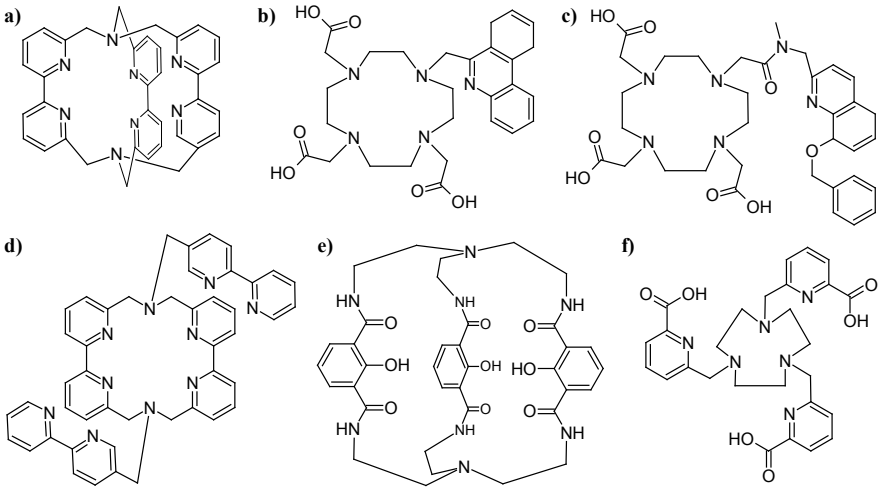

Figure 1.13: Examples of cage-type ligands used for photoluminescent Eu(III) and Tb(III) complexes. Ligands a, b, d and e and f belong to the chromophoric chelates category, while ligand c is an example of an antenna ligand with a pendant chromophore [89, 98, 143-146].

Metal organic frameworks

Thus far only isolated, mononuclear complexes have been considered. It is however perfectly possible to synthesize luminescent *metal organic frameworks*, or MOFs, using the lanthanoid ions. Typically, the ligands contain several groups that allow them to form bridges between the metal centers, thus forming an extended network of interlinked complexes. An overview of ligands that have been used in the preparation of photoluminescent lanthanoid(III) based MOFs is given in Figure 1.14. Synthesis of these compounds is usually performed under solvothermal conditions, that is, the reaction mixture is heated well above the solvent's boiling point in a pressure vessel. Alternative pathways, however, relying on a microwave or a carefully chosen mixture of solvents at room temperature have been reported [147-149]. An interesting feature of MOFs is demonstrated by Kerbellec and co-workers. They have reported luminescence for both $[Eu_2(bdc)_3]_n$ and $[Tb_2(bdc)_3]_n$ (bdc = 1,4-benzenedicarboxylate) with quantum efficiencies of 12% and 26%, respectively [150]. More recently, they found that it is possible to use a mixture of Eu(III) and Tb(III) ions in the reaction mixture, which allowed them to change the emission color from green to red by varying x in $[(Eu_{2-x}Tb_x)(bdc)_3]_n$ [151]. Inclusion of other metal ions such as Ca(II) and Na(I) to provide additional cross-links within the structure has proven to be successful, too [152, 153].

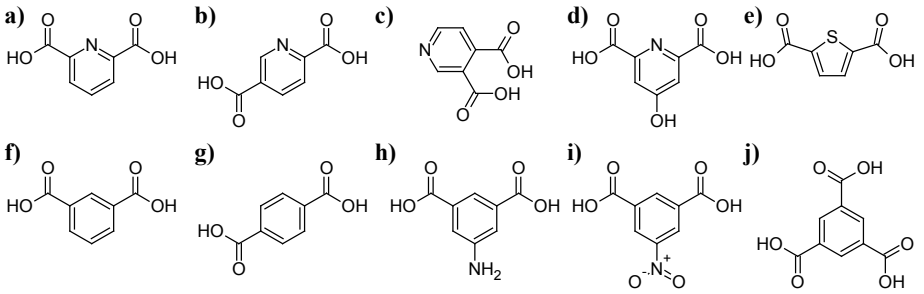

Figure 1.14: Overview of ligands that have been used for preparing MOFs with Ln(III) ions. (a) 2,6-dipicolinic acid, 2,6-H_2dpa, (b)2,5-H_2dpa, (c) 3,4-H_2dpa, (d) 4-hydroxylpyridine-2,6-dicarboxylic acid, H_3pdc, (e) thiophene-2,5-dicarboxylic acid, H_2tbc, (f)1,3-isophthalic acid, 1,3-H_2ipa, (g) 1,4-benzenedicarboxylic acid, H_2bdc, (h) 5-NH_2-1,3H_2ipa, (i) 5-NO_2-1,3H_2ipa, (j) 1,3,5-benzenetricarboxylic acid, H_3btc [149-152, 154-162].

1.7.4 Lanthanoid complexes as phosphor materials

The requirements for LED-phosphors listed in section 1.4.3 must be met before application in commercial LEDs can be considered. The use of europium(III) complexes as actual phosphors in LEDs has been demonstrated recently [163-166]. The complexes used are all of the β-diketonate type, and show quantum efficiencies ranging from 16% to 34% and in each case an LED emitting at 395 nm was used. Most of these investigations concern a single phosphor converted red In:GaN-based LED. Wang and co-workers have prepared a white LED using a europium complex as a red phosphor together with $BaMgA_{l1}O_{17}$:Eu(II) as a blue and ZnS:Cu(I):Al(III) as a green phosphor [166]. Still, the quantum yields of the complexes used were relatively low, and need to be improved. In addition, long term stability of the complexes must be ensured. The β-diketonate complexes are known to be prone to photobleaching, which may severely reduce the lifetime of the final SSL device [123, 134, 167].

Comparison with solid state phosphors

The phosphor materials that are widely used as of to date are typically based on inorganic oxides. As discussed in section 1.4.2, these materials are highly efficient and stable. However, they cannot be efficiently excited in the nUV range. Present research on developing new solid state phosphors appears to focus on Eu(II) based compounds [40, 41]. The emission color of these compounds is governed by the crystal field splitting of the excited $4f^6 5d^1$ configuration of the ion's excited state. While the broad band emission of the Eu(II) ion is not problematic for blue and green emitting phosphors, it is a problem for the red phosphor as deep-red emission contributes very little to the perceived light output (sections 1.3.1 and 1.4.3). Owing to its sharp emission line at 614 nm, the Eu(III) ion is a suitable emitter for creating an efficient phosphor. Recent investigations on suitable host materials for the Eu(III) ion focus on the use of molybdates and tungstates and are aimed at

shifting the lattice absorption into the nUV region. Generally, these compounds are claimed to be efficient red phosphors for nUV LEDs [168-171]. This is a doubtful statement, because excitation in the nUV region relies on the 4f ← 4f transitions on the Eu(III) ion centered at 395 nm [172]. Although these transitions usually appear to be strong in the excitation spectra, they are in fact weak due to their forbidden nature (section 1.6). This is illustrated by the diffuse reflectance spectra for $LiEu(WO_4)_{2-x}(MoO_4)_x$, in which the 4f – 4f transitions are weak compared to the allowed charge transfer band, although they are very intense in the excitation spectrum [171]. Other major drawbacks, making oxide type materials relatively expensive, are the synthesis temperatures and the required purity of the starting compounds. A typical synthesis of Ce:YAG involves temperatures in excess of 1500 °C [33]. High purity starting compounds (> 4N) are needed to avoid luminescence-quenching defects in the final phosphor material. For example, the photoluminescence quantum yield of Y_2O_3:Eu is reduced by as much as 7% in the presence of only 5 ppm Fe^{3+} impurity [20, 173]. Finally, a cost-effective method for recovery of the lanthanoids from oxides is still to be found [174-177]. Recycling of the lanthanoids has recently become attractive as China, which presently produces over 90% of all rare earths, has tightened its export quota [58, 176, 178]. Lanthanoid complexes are the class of compounds that can overcome these problems. Synthesis is typically performed at relatively low temperatures (< 200 °C) and owing to the molecular nature of lanthanoid complexes, there is no need for highly pure reactants. Both properties can substantially reduce production costs. In addition, the lanthanoids can be recovered by simply burning off the ligands. The absorption properties can be tuned to match the excitation source by making small modifications to the ligand, for instance by introducing substituents, while the favorable luminescent properties of the lanthanoid ion are retained. The main shortcomings that must be overcome before application of lanthanoid complexes as a phosphor material can be considered are the typically low quantum efficiency and poor long-term stability [123, 134, 165, 179, 180]. As described in section 1.7.3, exceptions to these general notions have been reported, justifying further research on the use of lanthanoid complexes as phosphor materials in LEDs.

1.8 Aim and scope of this thesis

Despite the many efforts to red-shift the excitation band of oxide-based phosphor materials to the nUV spectral region to allow for application in PC-WLEDs, no suitable material has been identified. The aim of the work described in this thesis is to synthesize complexes of Eu(III) and Tb(III) ions with ligands capable of efficient sensitization of luminescence of those ions upon excitation in the nUV region. In the present chapter, an introduction into the subject is given, as well as a description of the problems. In Chapter 2, the synthesis of derivatives of 1,10-phenanthroline as ligands to Eu(III), and the photophysical properties of the complexes with these ligands are described. In Chapter 3, the synthesis and photoluminescent properties of Eu(III) and Tb(III) compounds with novel small aromatic

ligands, giving rise to metal-organic frameworks (MOFs), are discussed. Another class of complexes using small ligands is discussed in Chapter 4, where phenol-type molecules are used to sensitize both Eu(III) and Tb(III) luminescence. In Chapter 5, the photoluminescence of Eu(III)-complexes with several substituted dibenzoylmethanates is discussed, and the influence of the counter ions is demonstrated. Chapter 6 concerns the photo and triboluminescent properties of the series $HNEt_3[Eu(dbm)_4]$. Chapter 7 contains a summary of this work, some concluding remarks and the future prospects. Appendix A deals with some details on photoluminescence quantum yield determinations.

Parts of this thesis are submitted for publication [181-185] or are in preparation.

1.9 References

[1] BP, *BP Statistical Review of World Energy*, 2012, Available from: www.bp.com/statisticalreview

[2] D. Pimentel, *Environ. Dev. Sustain.*, 14 (2012) 151-152.

[3] C. Pasten and J.C. Santamarina, *Energ. Policy*, 49 (2012) 468-476.

[4] P. Bertoldi and B. Atanasiu, *Electricity consumption and efficiëncy trends in the enlarged European union status report 2009*, 2009, Available from: http://iet.jrc.ec.europa.eu/energyefficiency/publication/electricity-consumption-and-efficiency-trends-european-union-status-report-2009

[5] B. Atanasiu and P. Bertoldi, *Int. J. Green Energy*, 7 (2010) 552-575.

[6] E.F. Schubert, J.K. Kim, H. Luo, and J.Q. Xi, *Rep. Prog. Phys.*, 69 (2006) 3069-3099.

[7] J.M. Phillips, M.E. Coltrin, M.H. Crawford, A.J. Fischer, M.R. Krames, R. Mueller-Mach, G.O. Mueller, Y. Ohno, L.E.S. Rohwer, J.A. Simmons, and J.Y. Tsao, *Laser Photonics Rev.*, 1 (2007) 307-333.

[8] E.F. Schubert and J.K. Kim, *Science*, 308 (2005) 1274-1278.

[9] Y. Narukawa, M. Ichikawa, D. Sanga, M. Sano, and T. Mukai, *J. Phys. D: Appl. Phys.*, 43 (2010) 354002.

[10] T.A. Edison, Electric lamp, Pat.no US223898, 1879.

[11] C.R. Ronda, *Luminescence - From Theory to Applications*, 2008: Wiley-VCH Verlag GmbH, Weinheim.

[12] E.F. Schubert, *Light-Emitting Diodes, 2nd edition*, 2006: Cambridge University Press, New York.

[13] P.W. Atkins and J. de Paula, *Atkins' Physical Chemistry, 8th edition*, 2006: W.H. Freeman and Company, New York.

[14] M. Csele, *Fundamentals of Light Souces and Lasers*, 2004: John Wiley & Sons, Hoboken, NJ, USA.

[15] *CRC Handbook of Chemistry and Physics, 85th edition*, 2005: CRC Press, Boca Raton.

[16] G.M. Neumann, *Thermochim. Acta*, 8 (1974) 369-379.

[17] F. Meyer, H.J. Spanner, and E. Germer, Metal vapor lamp, Pat.no US2182732, 1939.

[18] J.M. Anderson, Short arc fluorescent lamp, Pat.no US4093893, 1978.

[19] W.J. Roche, Single-base, self-igniting fluorescent lamp, Pat.no US3849699, 1974.

[20] G. Blasse and B.C. Grabmaier, *Luminescent Materials*, 1994: Springer Verlag, Berlin.
[21] R.N. Thayer and B.T. Barnes, *J. Opt. Soc. Am.*, 29 (1939) 131-134.
[22] T. Justel, H. Nikol, and C. Ronda, *Angew. Chem., Int. Ed.*, 37 (1998) 3085-3103.
[23] G. Blasse, *J. Alloy. Compd.*, 225 (1995) 529-533.
[24] F.A. Ponce and D.P. Bour, *Nature*, 386 (1997) 351-359.
[25] S. Nakamura, T. Mukai, and M. Senoh, *Appl. Phys. Lett.*, 64 (1994) 1687-1689.
[26] J. Wu, W. Walukiewicz, K.M. Yu, J.W. Ager III, E.E. Haller, H. Lu, W.J. Schaff, Y. Saito, and Y. Nanishi, *Appl. Phys. Lett.*, 80 (2002) 3967-3969.
[27] G. Chen, M. Craven, A. Kim, A. Munkholm, S. Watanabe, M. Camras, W. Götz, and F. Steranka, *Phys. Status Solidi A*, 205 (2008) 1086-1092.
[28] R. Mueller-Mach, G.O. Mueller, M.R. Krames, O.B. Shchekin, P.J. Schmidt, H. Bechtel, C.-H. Chen, and O. Steigelmann, *Phys. Status Solidi RRL*, 3 (2009) 215-217.
[29] J.R. Oh, S.-H. Cho, J.H. Oh, Y.-K. Kim, Y.-H. Lee, W. Kim, and Y.R. Do, *Opt. Express*, 19 (2011) 4188-4198.
[30] N. Kohei and K. Sueko, *Color vision*, in *Phosphor Handbook*, 2006, CRC Press, Boca Raton.
[31] L.E. Shea-Rohwer, J.E. Martin, X. Cai, and D.F. Kelley, *J. Solid State Sci. Technol.*, 2 (2013) R3112-R3118.
[32] C.R. Ronda, T. Justel, and H. Nikol, *J. Alloy. Compd.*, 277 (1998) 669-676.
[33] S. Ye, F. Xiao, Y.X. Pan, Y.Y. Ma, and Q.Y. Zhang, *Mater. Sci. Eng., R*, 71 (2010) 1-34.
[34] J.H. Oh, S.J. Yang, Y.-G. Sung, and Y.R. Do, *Opt. Express*, 20 (2012) 20276-20285.
[35] M. Raukas, J. Kelso, Y. Zheng, K. Bergenek, D. Eisert, A. Linkov, and F. Jermann, *J. Solid State Sci. Technol.*, 2 (2013) R3168-R3176.
[36] R.-J. Xie, N. Hirosaki, T. Takeda, and T. Suehiro, *J. Solid State Sci. Technol.*, 2 (2013) R3031-R3040.
[37] R.-J. Xie, N. Hirosaki, M. Mitomo, K. Sakuma, and N. Kimura, *Appl. Phys. Lett.*, 89 (2006) 241103.
[38] R.-J. Xie, N. Hirosaki, M. Mitomo, K. Takahashi, and K. Sakuma, *Appl. Phys. Lett.*, 88 (2006) 101104.
[39] R.-J. Xie and N. Hirosaki, *Sci. Technol. Adv. Mat.*, 8 (2007) 588-600.
[40] C.C. Lin and R.-S. Liu, *J. Phys. Chem. Lett.*, 2 (2011) 1268-1277.
[41] A. Zukauskas, R. Vaicekauskas, F. Ivanauskas, R. Gaska, and M.S. Shur, *Appl. Phys. Lett.*, 80 (2002) 234-236.
[42] E.N. Harvey, *A History of Luminescence*, 1957: American Philosophical Society, Philidelphia.
[43] S. Shigeo, *Introduction to the handbook*, in *Phosphor Handbook*, 2006, CRC Press, Boca Raton.
[44] C.R. Ronda, *J. Alloy. Compd.*, 225 (1995) 534-538.
[45] H.A. Höppe, *Angew. Chem., Int. Ed.*, 48 (2009) 3572-3582.
[46] R.-J. Xie, N. Hirosaki, N. Kimura, K. Sakuma, and M. Mitomo, *Appl. Phys. Lett.*, 90 (2007) 191101.
[47] K. Dowling, *Phys. Today*, 61 (2008) 74-75.
[48] U. Lafont, H. van Zeijl, and S. van der Zwaag, *Microelectron. Reliab.*, 52 (2012) 71-89.

[49] J. McKittrick, M.E. Hannah, A. Piquette, J.K. Han, J.I. Choi, M. Anc, M. Galvez, H. Lugauer, J.B. Talbot, and K.C. Mishra, *J. Solid State Sci. Technol.*, 2 (2013) R3119-R3131.
[50] N.G. Connelly, R.M. Hartshorn, T. Damhus, and A.T. Hutton, *Nomenclature of Inorganic-Chemistry (the Red Book) - IUPAC Recommendations*, 2005: Cambridge.
[51] J.-C.G. Bünzli and C. Piguet, *Chem. Soc. Rev.*, 34 (2005) 1048-1077.
[52] C. Huang, *Rare Earth Coordination Chemistry*, 2010: John Wiley & Sons, Singapore.
[53] F. Szabadvary, *The history of the discovery and separation of the rare earths*, in *Handbook on the Physics and Chemistry of Rare Earths*, 1988, Elsevier. 33-80.
[54] J.-C.G. Bünzli, S. Comby, A.-S. Chauvin, and C.D.B. Vandevyver, *J. Rare Earth.*, 25 (2007) 257-274.
[55] S. Cotton, *Lanthanide and Actinide Chemistry*, 2006: John Wiley & Sons, Chichester, UK.
[56] V.S. Sastri, J.-C.G. Bünzli, V. Ramachandra Rao, G.V.S. Rayudu, and J.R. Perumareddi, *Modern Aspects of Rare Earths and their Complexes*, 2003: Elsevier.
[57] S.R. Taylor, *Geochim. Cosmochim. Acta*, 28 (1964) 1273-1285.
[58] S. Massari and M. Ruberti, *Resour. Policy*, 38 (2013) 36-43.
[59] W.-K. Li, G.-d. Zhou, and T.C.W. Mak, *Advanced structural inorganic chemistry*, 2008: Oxford University Press, New York.
[60] L. Armelao, S. Quici, F. Barigelletti, G. Accorsi, G. Bottaro, M. Cavazzini, and E. Tondello, *Coord. Chem. Rev.*, 254 (2010) 487-505.
[61] R.E. Whan and G.A. Crosby, *J. Mol. Spectrosc.*, 8 (1962) 315-327.
[62] G.-Y. Adachi, K. Sorita, K. Kawata, K. Tomokiyo, and J. Shiokawa, *J. Less-common. Met.*, 93 (1983) 81-87.
[63] Y. Yao, Y. Zhang, Z. Zhang, Q. Shen, and K. Yu, *Organometallics*, 22 (2003) 2876-2882.
[64] J. Garcia and M.J. Allen, *Eur. J. Inorg. Chem.*, 2012 (2012) 4550-4563.
[65] B.M. Walsh, *Judd-Ofelt theory: principles and practices*, in *Advances in Spectroscopy for Lasers and Sensing*, 2006, Springer Netherlands. 403-433.
[66] J.-C.G. Bünzli and S.V. Eliseeva, *Basics of Lanthanide Photophysics*, in *Lanthanide Luminescence*, 2011, Springer Berlin Heidelberg. 1-45.
[67] C. Görller-Walrand and K. Binnemans, *Rationalization of crystal field parametrization*, in *Handbook on the physics and chemistry of the rare earths*, 1996, Elsevier. 121-284.
[68] P.A. Tanner and C.-K. Duan, *Coord. Chem. Rev.*, 254 (2010) 3026-3029.
[69] G. Ligner, R. Mohan, S. Knittel, and G. Duportail, *Spectrochim. Acta A*, 46 (1990) 797-802.
[70] C.K. Jørgensen and B.R. Judd, *Mol. Phys.*, 8 (1964) 281-290.
[71] C. Görller-Walrand and K. Binnemans, *Spectral intensities of f-f transitions*, in *Handbook on the Physics and Chemistry of Rare Earths*, 1998, Elsevier. 99-264.
[72] B.R. Judd, *Phys. Rev.*, 127 (1962) 750-761.
[73] G.S. Ofelt, *J. Chem. Phys.*, 37 (1962) 511-520.
[74] M.P. Hehlen, M.G. Brik, and K.W. Krämer, *J. Lumin.*, 136 (2013) 221-239.
[75] M.H.V. Werts, R.T.F. Jukes, and J.W. Verhoeven, *Phys. Chem. Chem. Phys.*, 4 (2002) 1542-1548.

[76] R. Reisfeld, E. Zigansky, and M. Gaft, *Mol. Phys.*, 102 (2004) 1319 - 1330.
[77] J.W. Verhoeven, *Pure Appl. Chem.*, 68 (1996) 2223-2286.
[78] M.H.V. Werts, *Sci. Prog.*, 88 (2005) 101-131.
[79] W.T. Carnall, P.R. Fields, and K. Rajnak, *J. Chem. Phys.*, 49 (1968) 4450-4455.
[80] M.J. Weber, *Phys. Rev. B*, 8 (1973) 54-64.
[81] J.-C.G. Bünzli, *Chem. Rev.*, 110 (2010) 2729-2755.
[82] S.I. Weissman, *J. Chem. Phys.*, 10 (1942) 214-217.
[83] G.A. Crosby and M. Kasha, *Spectrochim. Acta*, 10 (1958) 377-382.
[84] G.A. Crosby, R.E. Whan, and R.M. Alire, *J. Chem. Phys.*, 34 (1961) 743-748.
[85] G.A. Crosby, *Mol. Cryst.*, 1 (1966) 37-81.
[86] Y. Hasegawa, Y. Wada, and S. Yanagida, *J. Photochem. Photobiol., C*, 5 (2004) 183-202.
[87] H. Takalo, I. Hemmilä, T. Sutela, and M. Latva, *Helv. Chim. Acta*, 79 (1996) 789-802.
[88] G.E. Buono-core, H. Li, and B. Marciniak, *Coord. Chem. Rev.*, 99 (1990) 55-87.
[89] B. Alpha, R. Ballardini, V. Balzani, J.-M. Lehn, S. Perathoner, and N. Sabbatini, *Photochem. Photobiol.*, 52 (1990) 299-306.
[90] F. Gutierrez, C. Tedeschi, L. Maron, J.-P. Daudey, R. Poteau, J. Azema, P. Tisnès, and C. Picard, *Dalton Trans.*, (2004) 1334 -1347.
[91] K. Binnemans, *Chem. Rev.*, 109 (2009) 4283-4374.
[92] J.J. Freeman and G.A. Crosby, *J. Phys. Chem.*, 67 (1963) 2717-2723.
[93] M. Latva, H. Takalo, V.M. Mukkala, C. Matachescu, J.C. Rodriguez-Ubis, and J. Kankare, *J. Lumin.*, 75 (1997) 149-169.
[94] G.A. Hebbink, L. Grave, L.A. Woldering, D.N. Reinhoudt, and F.C.J.M. van Veggel, *J. Phys. Chem. A*, 107 (2003) 2483-2491.
[95] G.A. Hebbink, S.I. Klink, L. Grave, P.G.B.O. Alink, and F.C.J.M. van Veggel, *ChemPhysChem*, 3 (2002) 1014-1018.
[96] J.R.G. Thorne, J.M. Rey, R.G. Denning, S.E. Watkins, M. Etchells, M. Green, and V. Christou, *J. Phys. Chem. A*, 106 (2002) 4014-4021.
[97] G.F. de Sa, O.L. Malta, C.D. Donega, A.M. Simas, R.L. Longo, P.A. Santa-Cruz, and E.F. da Silva, *Coord. Chem. Rev.*, 196 (2000) 165-195.
[98] L. Prodi, M. Maestri, R. Ziessel, and V. Balzani, *Inorg. Chem.*, 30 (1991) 3798-3802.
[99] W.T. Carnall, P.R. Fields, and K. Rajnak, *J. Chem. Phys.*, 49 (1968) 4443-4446.
[100] E.G. Moore, A.P.S. Samuel, and K.N. Raymond, *Acc. Chem. Res.*, 42 (2009) 542-552.
[101] B. Yan, H. Zhang, S. Wang, and J. Ni, *J. Photochem. Photobiol., A*, 116 (1998) 209-214.
[102] F.R. Gonçalves e Silva, O.L. Malta, C. Reinhard, H.-U. Güdel, C. Piguet, J.E. Moser, and J.-C.G. Bünzli, *The Journal of Physical Chemistry A*, 106 (2002) 1670-1677.
[103] D.L. Dexter, *J. Chem. Phys.*, 21 (1953) 836-850.
[104] T. Förster, *Chem. Phys. Lett.*, 12 (1971) 422-424.
[105] L. Smentek and A. Kedziorski, *J. Lumin.*, 130 (2010) 1154-1159.
[106] W.M. Faustino, O.L. Malta, and G.F. de Sa, *J. Chem. Phys.*, 122 (2005) 054109.
[107] S. Petoud, J.-C.G. Bünzli, T. Glanzman, C. Piguet, Q. Xiang, and R.P. Thummel, *J. Lumin.*, 82 (1999) 69-79.

[108] N. Sabbatini, M. Guardigli, and J.M. Lehn, *Coord. Chem. Rev.*, 123 (1993) 201-228.
[109] F.R.G. e Silva and O.L. Malta, *J. Alloy. Compd.*, 250 (1997) 427-430.
[110] O.L. Malta, *J. Lumin.*, 71 (1997) 229-236.
[111] O.L. Malta and F.R. Gonçalves e Silva, *Spectrochim. Acta A*, 54 (1998) 1593-1599.
[112] S. Meshkova, Z. Topilova, M. Lozinskii, and D. Bol'shoi, *J. Appl. Spectrosc.*, 64 (1997) 229-233.
[113] G. Stein and E. Würzberg, *J. Chem. Phys.*, 62 (1975) 208-213.
[114] G.R. Choppin and D.R. Peterman, *Coord. Chem. Rev.*, 174 (1998) 283-299.
[115] S. Yanagida, Y. Hasegawa, K. Murakoshi, Y. Wada, N. Nakashima, and T. Yamanaka, *Coord. Chem. Rev.*, 171 (1998) 461-480.
[116] S. Faulkner, S.J.A. Pope, and B.P. Burton-Pye, *Appl. Spectrosc. Rev.*, 40 (2005) 1-31.
[117] D. Parker, P.K. Senanayake, and J.A.G. Williams, *J. Chem. Soc., Perkin Trans. 2*, (1998) 2129-2140.
[118] E. Pershagen, J. Nordholm, and K.E. Borbas, *J. Am. Chem. Soc.*, 134 (2012) 9832-9835.
[119] I. Hemmilä, *J. Alloy. Compd.*, 225 (1995) 480-485.
[120] N. Filipescu, W.F. Sager, and F.A. Serafin, *J. Phys. Chem.*, 68 (1964) 3324-3346.
[121] W.F. Sager, N. Filipescu, and F.A. Serafin, *J. Phys. Chem.*, 69 (1965) 1092-1100.
[122] L.R. Melby and N.J. Rose, Eight coordinate trivalent rare earth metal chelates with β-diketones, Pat.no US 3254103, 1966.
[123] K. Binnemans, *Rare earth beta-diketonates*, in *Handbook on the Physics and Chemistry of Rare Earths*, 2005, Elsevier. 107-272.
[124] A. Mech, M. Karbowiak, C. Görller-Walrand, and R. Van Deun, *J. Alloy. Compd.*, 451 (2008) 215-219.
[125] H. Bauer, J. Blanc, and D.L. Ross, *J. Am. Chem. Soc.*, 86 (1964) 5125-5131.
[126] X.-F. Chen, X.-H. Zhu, W. Chen, J.J. Vittal, G.-K. Tan, J. Wu, and X.-Z. You, *J. Coord. Chem.*, 52 (2000) 97-110.
[127] K. Goossens, P. Nockemann, K. Driesen, B. Goderis, C. Görller-Walrand, K. Van Hecke, L. Van Meervelt, E. Pouzet, K. Binnemans, and T. Cardinaels, *Chem. Mater.*, 20 (2007) 157-168.
[128] K. Lunstroot, K. Driesen, P. Nockemann, K. Van Hecke, L. Van Meervelt, C. Gorller-Walrand, K. Binnemans, S. Bellayer, L. Viau, J. Le Bideau, and A. Vioux, *Dalton Trans.*, (2009) 298-306.
[129] X.-R. Zeng, R.-G. Xiong, X.-Z. You, and K.-K. Cheung, *Inorg. Chem. Commun.*, 3 (2000) 341-344.
[130] H. Jiu, G. Liu, Z. Zhang, Y. Fu, J. Chen, T. Fan, and L. Zhang, *J. Rare Earth.*, 29 (2011) 741-745.
[131] O.L. Malta, H.F. Brito, J.F.S. Menezes, F.R. Gonçalves e Silva, C. de Mello Donegá, and S. Alves, *Chem. Phys. Lett.*, 282 (1998) 233-238.
[132] F.R.G. e Silva, J.F.S. Menezes, G.B. Rocha, S. Alves, H.F. Brito, R.L. Longo, and O.L. Malta, *J. Alloy. Compd.*, 303-304 (2000) 364-370.
[133] G. Bourhill, L.O. Pålsson, I.D.W. Samuel, I.C. Sage, I.D.H. Oswald, and J.P. Duignan, *Chem. Phys. Lett.*, 336 (2001) 234-241.
[134] L.D. Carlos, C.D.M. Donegá, R.Q. Albuquerque, S. Alves, J.F.S. Menezes, and O.L. Malta, *Mol. Phys.*, 101 (2003) 1037 - 1045.

[135] G.S. Kottas, M. Mehlstäubl, R. Fröhlich, and L. De Cola, *Eur. J. Inorg. Chem.*, 2007 (2007) 3465-3468.
[136] N.M. Shavaleev, S.V. Eliseeva, R. Scopelliti, and J.-C.G. Bünzli, *Chem.-Eur. J.*, 15 (2009) 10790-10802.
[137] T.J. Mooibroek, P. Gamez, A. Pevec, M. Kasunič, B. Kozlevčar, W.T. Fu, and J. Reedijk, *Dalton Trans.*, 39 (2010) 6483-6487.
[138] S. Tanase, P.M. Gallego, R. de Gelder, and W.T. Fu, *Inorg. Chim. Acta*, 360 (2007) 102-108.
[139] V. Tsaryuk, K. Zhuravlev, V. Zolin, P. Gawryszewska, J. Legendziewicz, V. Kudryashova, and I. Pekareva, *J. Photochem. Photobiol., A*, 177 (2006) 314-323.
[140] V. Tsaryuk, K. Zhuravlev, V. Kudryashova, V. Zolin, Y. Yakovlev, and J. Legendziewicz, *Spectrochim. Acta A*, 72 (2009) 1020-1025.
[141] K. Zhuravlev, V. Tsaryuk, J. Legendziewicz, V. Kudryashova, P. Gawryszewska, and V. Zolin, *Opt. Mater.*, 31 (2009) 1822-1824.
[142] P.A. Brayshaw, J.-C.G. Bünzli, P. Froidevaux, J.M. Harrowfield, Y. Kim, and A.N. Sobolev, *Inorg. Chem.*, 34 (1995) 2068-2076.
[143] S. Petoud, S.M. Cohen, J.-C.G. Bünzli, and K.N. Raymond, *J. Am. Chem. Soc.*, 125 (2003) 13324-13325.
[144] J.P. Cross, A. Dadabhoy, and P.G. Sammes, *J. Lumin.*, 110 (2004) 113-124.
[145] D. Maffeo and J.A.G. Williams, *Inorg. Chim. Acta*, 355 (2003) 127-136.
[146] J.W. Walton, R. Carr, N.H. Evans, A.M. Funk, A.M. Kenwright, D. Parker, D.S. Yufit, M. Botta, S. De Pinto, and K.L. Wong, *Inorg. Chem.*, 51 (2012) 8042-8056.
[147] N. Stock and S. Biswas, *Chem. Rev.*, 112 (2011) 933-969.
[148] Z.-J. Lin, Z. Yang, T.-F. Liu, Y.-B. Huang, and R. Cao, *Inorg. Chem.*, 51 (2012) 1813-1820.
[149] S.-P. Chen, Y.-X. Ren, W.-T. Wang, and S.-L. Gao, *Dalton Trans.*, 39 (2010) 1552-1557.
[150] C. Daiguebonne, N. Kerbellec, O. Guillou, J.-C.G. Bünzli, F. Gumy, L. Catala, T. Mallah, N. Audebrand, Y. Gérault, K. Bernot, and G. Calvez, *Inorg. Chem.*, 47 (2008) 3700-3708.
[151] N. Kerbellec, D. Kustaryono, V. Haquin, M. Etienne, C. Daiguebonne, and O. Guillou, *Inorg. Chem.*, 48 (2009) 2837-2843.
[152] M. Li, L. Yuan, H. Li, and J. Sun, *Inorg. Chem. Commun.*, 10 (2007) 1281-1284.
[153] T. Zhu, K. Ikarashi, T. Ishigaki, K. Uematsu, K. Toda, H. Okawa, and M. Sato, *Inorg. Chim. Acta*, 362 (2009) 3407-3414.
[154] C. Qin, X.-L. Wang, E.-B. Wang, and Z.-M. Su, *Inorg. Chem.*, 44 (2005) 7122-7129.
[155] Y.-g. Huang, B.-l. Wu, D.-q. Yuan, Y.-q. Xu, F.-l. Jiang, and M.-c. Hong, *Inorg. Chem.*, 46 (2007) 1171-1176.
[156] H.-H. Song and Y.-J. Li, *Inorg. Chim. Acta*, 361 (2008) 1421-1425.
[157] K. Liu, G. Jia, Y. Zheng, Y. Song, M. Yang, Y. Huang, L. Zhang, and H. You, *Inorg. Chem. Commun.*, 12 (2009) 1246-1249.
[158] D.-Y. Ma, H.-P. Zeng, Y.-W. Li, and J. Li, *Solid State Sci.*, 11 (2009) 1065-1070.
[159] X.-Q. Zhao, B. Zhao, S. Wei, and P. Cheng, *Inorg. Chem.*, 48 (2009) 11048-11057.
[160] F. Pellé, P. Aschehoug, S. Surblé, F. Millange, C. Serre, and G. Férey, *J. Solid State Chem.*, 183 (2010) 795-802.

[161] C.-H. Zhan, F. Wang, Y. Kang, and J. Zhang, *Inorg. Chem.*, 51 (2011) 523-530.
[162] X. Zhao, D.-X. Wang, Q. Chen, J.-B. Chen, G.-Y. Lin, S.-T. Yue, and Y.-P. Cai, *Inorg. Chem. Commun.*, 23 (2012) 127-131.
[163] G. Shao, Y. Li, K. Feng, F. Gan, and M. Gong, *Sens. Actuators, B*, 173 (2012) 692-697.
[164] P. He, H. Wang, S. Liu, J. Shi, and M. Gong, *Appl. Phys. B: Lasers Opt.*, 99 (2010) 757-762.
[165] H. Yan, H. Wang, P. He, J. Shi, and M. Gong, *Inorg. Chem. Commun.*, 14 (2011) 1065-1068.
[166] H. Wang, P. He, S. Liu, J. Shi, and M. Gong, *Appl. Phys. B: Lasers Opt.*, 97 (2009) 481-487.
[167] L. Armelao, G. Bottaro, S. Quici, M. Cavazzini, C. Scalera, and G. Accorsi, *Dalton Trans.*, 40 (2011) 11530-11538.
[168] J. Wang, X. Jing, C. Yan, J. Lin, and F. Liao, *J. Lumin.*, 121 (2006) 57-61.
[169] F. Mo, L. Zhou, Q. Pang, F. Gong, and Z. Liang, *Ceram. Int.*, 38 (2012) 6289-6294.
[170] W.Q. Yang, H.G. Liu, G.K. Liu, Y. Lin, M. Gao, X.Y. Zhao, W.C. Zheng, Y. Chen, J. Xu, and L.Z. Li, *Acta Mater.*, 60 (2012) 5399-5407.
[171] C.-H. Chiu, M.-F. Wang, C.-S. Lee, and T.-M. Chen, *J. Solid State Chem.*, 180 (2007) 619-627.
[172] J.M. Postema, W.T. Fu, and D.J.W. IJdo, *J. Solid State Chem.*, 184 (2011) 2004-2008.
[173] W. Van Schaik and G. Blasse, *Chem. Mater.*, 4 (1992) 410-415.
[174] T. Saito, H. Sato, and T. Motegi, *J. Alloy. Compd.*, 425 (2006) 145-147.
[175] M.A. Rabah, *Waste Manage.*, 28 (2008) 318-325.
[176] F. Yang, F. Kubota, Y. Baba, N. Kamiya, and M. Goto, *J. Hazard. Mater.*, 254–255 (2013) 79-88.
[177] I. De Michelis, F. Ferella, E.F. Varelli, and F. Vegliò, *Waste Manage.*, 31 (2011) 2559-2568.
[178] K. Binnemans, P.T. Jones, B. Blanpain, T. Van Gerven, Y. Yang, A. Walton, and M. Buchert, *J. Clean. Prod.*, 51 (2013) 1-22.
[179] X.-F. Qiao and B. Yan, *Inorg. Chem.*, 48 (2009) 4714-4723.
[180] B. Francis, D.B.A. Raj, and M.L.P. Reddy, *Dalton Trans.*, 39 (2010) 8084-8092.
[181] S. Akerboom, W.T. Fu, M. Lutz, and E. Bouwman, *Inorg. Chim. Acta*, 387 (2012) 289-293.
[182] S. Akerboom, X. Liu, S.H.C. Askes, I. Mutikainen, W.T. Fu, and E. Bouwman, Submitted (2013).
[183] S. Akerboom, J.J.M.H. van den Elshout, I. Mutikainen, W.T. Fu, and E. Bouwman, *Polyhedron*, In press (2013).
[184] S. Akerboom, J.J.M.H. Van den Elshout, I. Mutikainen, M.A. Siegler, W.T. Fu, and E. Bouwman, *Eur. J. Inorg. Chem.*, Submitted (2013).
[185] S. Akerboom, M.S. Meijer, M.A. Siegler, W.T. Fu, and E. Bouwman, *J. Lumin.*, 145 (2014) 278-282.

2 Substituted phenanthrolines as antennae in luminescent Eu(III) complexes

Eight novel europium(III)-based coordination compounds with 1,10-phenanthroline ligands with a chloro , methoxy-, ethoxy-, cyano-, carboxylic acid, methyl carboxylate-, ethyl carboxylate, and amino-substituent on the 2-position have been prepared in yields ranging from 43 to 89%. Additionally, one lanthanum(III) coordination compound of 2-amino-1,10-phenanthroline has been isolated. All compounds have the general formula $[Ln(L)_2(NO_3)_3]$, except for the compound with the carboxylate ligand, which has the formula $[Eu(O_2Cphen)_3]$. Of three of the Eu(III) complexes as well as the La(III) compound crystal structures have been determined, all showing similar N_4O_6 coordination spheres for the Ln(III) ion. Seven compounds exhibit bright luminescence characteristic of Eu(III) upon irradiation with near UV (nUV) radiation, indicating efficient ligand-to-metal energy transfer. The complex with 2-amino-1,10-phenanthroline is non-luminescent. The solid state photoluminescent quantum yields range from 10% to 79% and luminescence lifetimes vary from 0.43 to 1.57 ms. Analysis of the spectral intensities with the Judd-Ofelt theory shows a significant contribution of non-radiative processes that quench the luminescence of the $^5D_0$ level on Eu(III). In addition, 1-methyl-1,10-phenanthrolin-2(1H)-one has been used as a ligand for the first time, using Eu(III) as a central ion. The resulting complex exhibits moderately bright photoluminescence upon excitation with nUV radiation.

(Parts of this chapter have been published:
S. Akerboom, J.J.M.H. van den Elshout, I. Mutikainen, W.T. Fu, E. Bouwman, *Polyhedron* (2013), in press; S. Akerboom, J.J.M.H. van den Elshout, I. Mutikainen, M.A. Siegler, W.T. Fu, E. Bouwman, *Eur. J. Inorg. Chem.* (2013), in press)

2.1 Introduction

As discussed in Chapter 1, there is a need for highly efficient and stable red phosphor materials that can be efficiently excited in the nUV region. Complexes of Eu(III) ions with suitable antenna ligands are promising candidates for this purpose. A promising class of ligands comprises 1,10-phenanthrolines. Used either as a solitary sensitizer or as a neutral co-ligand to saturate the lanthanoid coordination sphere of complexes with anionic ligands, 1,10-phenanthrolines are capable of efficient sensitization of Eu(III)-centered luminescence [1-5]. The complex [Eu(1,10-phenanthroline)$_2$(NO$_3$)$_3$] is known to be highly luminescent, but efficient excitation at wavelengths above 355 nm is not possible [1, 6]. A redshift of the excitation maximum by at least 20 nm is required to allow for efficient excitation in the nUV range. To investigate the influence of substituents on 1,10-phenanthroline on the luminescence properties of complexes with Eu(III), a series of phenanthroline ligands with both electron-donating and electron-withdrawing substituents at the 2-position has been prepared. Coordination compounds with Eu(III) have been synthesized and their photophysical properties are reported. An overview of the compounds studied is given in Figure 2.1. During this study on the influence of substituents on 1,10-phenanthroline on the photoluminescent properties of the Eu(III) complexes, out of curiosity one of the synthetic intermediates, 1-methyl-1,10-phenanthrolin-2(1*H*)-one (**9**) shown in Figure 2.1, was used as a ligand for Eu(III). We were surprised by the relatively easy formation of a complex with a poor ketone-type ligand. Moreover, to the best of our knowledge, this molecule has never been used before as a ligand.

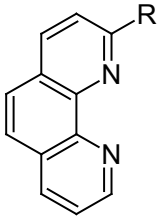

1-8

R	Ligand #	Complex #
CN	**1**	**Eu1**
COOH	**2**	**Eu2**
COOMe	**3**	**Eu3**
COOEt	**4**	**Eu4**
Cl	**5**	**Eu5**
OMe	**6**	**Eu6**
OEt	**7**	**Eu7**
NH_2	**8**	**Eu8**
		La8
	9	**Eu9**

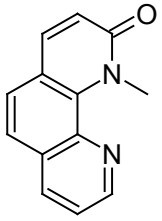

9

*Figure 2.1: An overview of the compounds described in this work. The complexes have the general formula [Ln(L)$_2$(NO$_3$)$_3$], Ln = Eu, La, except for Eu2 (see text).The complex synthesized with ligand **9** analyzes as [Eu(L)$_3$(NO$_3$)$_3$].*

2.2 Experimental

2.2.1 General

Phenanthroline was supplied by Merck, triethylamine was supplied by Acros and all other chemicals were purchased from Sigma–Aldrich and used as received.
NMR spectra were recorded on a Bruker DPX-300 spectrometer. Infrared spectra were recorded on a Perkin–Elmer Paragon 1000 FTIR spectrometer equipped with a Golden Gate ATR. Elemental analysis for C, H, N was performed on a Perkin–Elmer 2400 series II analyzer. Excitation and emission spectra were recorded on a Shimadzu RF–5301PC spectrofluoriphotometer equipped with a solid state sample holder and a UV-blocking filter. Photoluminescence quantum yields were determined using an Edinburgh Instruments FLS920 spectrofotometer equipped with an integrating sphere, following a modified version of the procedure reported by de Mello *et al*.[7]. All spectra were corrected for the response of the detection system and reflectivity of the integrating sphere. For lifetime measurements, a pulsed laser source at 355 nm was used as an excitation source on the same machine.
The nitrate salt of Eu(III) was obtained by dissolving Eu_2O_3 in hot concentrated nitric acid to give a clear solution. Subsequent evaporation of the solvent under reduced pressure gave the nitrate salt as a white crystalline compound, for which the composition $Eu(NO_3)_3 \cdot 5H_2O$ was assumed.

2.2.2 X-ray crystal structure determination

For the determination of the structures of **Eu6**, **Eu7** and **Eu9** a crystal was selected for the X-ray measurements and mounted to the glass fiber using the oil drop method. Data were collected at 173 K on a Nonius Kappa CCD diffractometer (Mo-Kα radiation, graphite monochromator, λ = 0.71073 Å) [8, 9]. The intensity data were corrected for Lorentz and polarization effects, and for absorption. The programs COLLECT, SHELXS–97 and SHELXL–97 were used for data reduction, structure solution and structure refinement, respectively [10, 11]. The non-hydrogen atoms were refined anisotropically. The H atoms were introduced in calculated positions and refined with fixed geometry with respect to their carrier atoms. In compound **Eu6** the solvent ethanol is disordered in two positions with population parameters 0.5.
For **Eu8** and **La8**, all reflection intensities were measured at 110(2) K using a KM4/Xcalibur (detector: Sapphire3) with enhanced graphite-monochromated Mo-Kα radiation (λ = 0.71073 Å) under the program CrysAlisPro (Version 1.171.35.11 for **Eu8**, Version 1.171.36.20 for **La8**, Oxford Diffraction Ltd., 2011). The program CrysAlisPro was used to refine the cell dimensions and for data reduction. The structure was solved with the program SHELXS–97 and was refined on F^2 with SHELXL–97 [10]. Analytical numeric absorption corrections based on a multifaceted crystal model were applied using

CrysAlisPro. The temperature of the data collection was controlled using the system Cryojet (manufactured by Oxford Instruments). The H atoms were placed at calculated positions using the instruction AFIX 43 or AFIX 93 with isotropic displacement parameters having values 1.2 times *U*eq of the attached C or N atoms.

2.2.3 Synthesis

*1,10-Phenanthroline-2-carbonitrile, CNphen (**1**)*

The compound was prepared following the procedures reported by Engbersen *et al*. and Corey *et al*. [12, 13]. ^{1}H NMR (300 MHz, MeOD) δ /ppm: 9.25 (dd, 1H), 9.06 (dd, 1H), 8.81 (d, 1H) 8.32-8.20 (m, 4H). IR (ν/cm^{-1}): 3068(br, m), 2230(m), 1584(m), 1506(s), 1486(s), 1417(m), 1403(m), 1390(s), 1296(m), 1313(m), 1135(m), 1098(s), 986(m), 961(w), 950(w), 899(m), 850(vs), 827(s), 816(m), 777(s), 737(vs), 717(s), 652(vs), 628(s), 578(m), 523(m), 461(m), 417(m).

*1,10-Phenanthroline-2-carboxylic acid, HO$_2$Cphen (**2**)*

Following the procedures described by Ten Brink *et al.*, **1** was hydrolyzed to the carboxylic acid [14]. ^{1}H NMR (300 MHz, $CDCl_3$) δ/ppm: 9.16 (d, 1H), 8.65 (d, 1H), 8.60 (dd, 1H), 8.49 (d, 1H), 8.12–8.04 (m, 2H), 7.91 (dd, 1H). IR (ν/cm^{-1}): 3468(m br), 3140(m br), 1700(vs), 1694(vs), 1652(s), 1616(m), 1564(m), 1456(s), 1424(s), 1358(vs br), 1294(s), 1204(s br), 1155(s), 861(vs), 834(s), 792(s), 770(s), 720(vs), 602(s), 536(s br), 419(s), 354(m), 338(m), 324(m).

*Methyl-1,10-phenanthroline-2-carboxylate, MeO$_2$Cphen (**3**)*

According to a procedure reported by Weijnen *et al*., **1** was converted to the methyl carboxylate [15]. ^{1}H NMR (300 MHz, MeOD) δ/ppm: 9.27 (dd, 1H), 8.44 (m, 2H), 8.29 (dd, 1H), 7.89 (m, 2H), 7.70 (dd, 1H), 4.12 (s, 3H). IR (ν/cm^{-1}): 3528(m br), 3410(m br), 1714(vs), 1668(s), 1651(s), 1616(s), 1558(s), 1506(s), 1496(s), 1398(s), 1364(m), 1304(s), 1282(vs br), 1172(s), 1141(s), 1087(s), 1019(s), 971(m), 861(vs), 832(s), 812(m), 772(m), 725(vs), 714(s), 668(s), 628(s), 419(s), 384(s), 374(s), 358(s).

*Ethyl-1,10-phenanthroline-2-carboxylate, EtO$_2$Cphen (**4**)*

A procedure similar to that described for **3** was adopted, except that 25 mL of ethanol was used instead of methanol. ^{1}H NMR (300 MHz, MeOD) δ/ppm: 9.12 (dd, 1H), 8.57 (d, 1H), 8.48 (dd, 1H), 8.39 (d, 1H), 8.00 (m, 2H) 7.81 (dd, 1H) 4.55 (q, 2H), 1.51 (t, 3H).
IR (ν/cm^{-1}): 3488(m br), 3182(m br), 1723(vs), 1684(m), 1616(s), 1507(m), 1456(m), 1442(s), 1404(s), 1302(s), 1278(vs br), 1196(m), 1157(s), 1141(vs), 1088(m), 970(s), 892(w), 861(s), 836(m), 828(m), 814(s), 762(s), 724(vs), 718(vs), 630(s), 492(m vbr), 448(vs), 344(s).

*2-Chloro-1,10-phenanthroline, Clphen (**5**)*

2-Chloro-1,10-phenanthroline was prepared from 1,10-phenanthroline N-oxide obtained from 1,10-phenanthroline as described for **9**, following literature procedures [12, 13]. The N-oxide was converted to 1-methyl-1,10-phenanthrolin-2(1*H*)-one following the procedure given by Kolling [16]. Subsequently, this compound was chlorinated following the procedure given by Halcrow *et al*. [17]. ^{1}H NMR (300 MHz, $CDCl_3$) δ/ppm: 9.06 (dd, 1H), 8.50 (dd, 1H), 8.45 (d, 1H), 7.98 (m, 2H), 7.82–7.75 (m, 2H). IR (ν/cm^{-1}): 3054 (w br), 1621(w), 1582(s), 1553(s), 1494(s), 1440(s), 1414(s), 1387(s), 1312(m), 1212(m), 1152(m), 1140(s), 1123(vs), 1071(s), 870(s), 839(vs), 824(s), 767(s), 730(vs), 711(s), 624(s), 611(s), 574(m), 514(m), 492(m), 420(s), 352(s), 321(m), 314(m).

*2-Methoxy-1,10-phenanthroline, MeOphen (**6**)*

This compound was synthesized from 5 following a procedure reported by Claus et al. [18]. ^{1}H NMR (300 MHz, MeOD) δ/ppm: 9.04 (dd, 1H), 8.44 (dd, 1H), 8.25 (d, 1H), 7.79 (m, 3H), 7.16 (d, 1H), 4.26 (s, 3H). IR (ν/cm^{-1}): 3372(m vbr), 3010(w), 2949(w), 1662(w), 1652(w), 1646(w), 1609(s), 1593(s), 1564(s), 1558(m), 1540(w), 1506(vs), 1464(vs), 1430(m), 1410(s), 1394(m), 1354(vs), 1303(m), 1266(vs), 1225(s), 1132(s), 1075(m), 1020(vs), 914(m), 876(m), 845(vs), 831(vs), 792(m), 770(s), 748(m), 732(s), 718(s), 683(vs), 655(s), 627(s), 569(m), 458(m), 437(s), 396(m), 375(m), 334(m), 316(m).

*2-Ethoxy-1,10-phenanthroline, EtOPhen (**7**)*

A procedure similar to that described for **6** was adopted, using ethanol instead of methanol. ^{1}H NMR (300 MHz, MeOD) δ/ppm: 9.01 (dd, 1H), 8.41 (dd, 1H), 8.22 (d, 1H), 7.75 (m, 3H), 7.12 (d, 1H), 4.76 (q, 2H), 1.48 (t, 3H). IR (ν/cm^{-1}): 3290(m vbr), 2978(m), 1684(m), 1652(m), 1622(s), 1612(s), 1594(s), 1560(s), 1506(s), 1499(s), 1457(vs), 1422(s), 1398(m), 1386(m), 1366(s), 1345(s), 1299(m), 1280(vs), 1226(m), 1139(s), 1098(m), 1076(m), 1043(s), 948(m), 882(m), 848(vs), 832(m), 804(m), 783(s), 740(vs), 718(s), 698(vs), 668(s), 660(s), 626(vs), 583(s), 564(s), 487(s), 429(m), 326(m), 322(m), 314(m).

*2-Amino-1,10-phenanthroline, NH_2Phen (**8**)*

Following the procedure reported by Engel, starting from **5** [19]. ^{1}H NMR (300 MHz, MeOD) δ/ppm: 8.99 (dd, 1H), 8.35 (dd, 1H), 8.06 (d, 1H), 8.74 (d, 1H) 7.65 (dd, 1H), 7.60 (d, 1H), 7.00 (d, 1H). IR (ν/cm^{-1}): 3320(m vbr), 1704(w), 1662(m), 1652(s), 1646(m), 1634(m), 1568(s), 1558(s), 1520(m), 1436(s), 1414(s), 1332(s), 1249(s), 1206(m), 1134(m), 1068(s), 840(s), 813(s), 709(vs), 680(s), 576(s), 552(vs), 403(s), 367(s), 364(s).

*1-Methyl-1,10-phenanthrolin-2(1H)-one, NMeOphen (**9**)*

Phenanthroline was oxidized to its N-oxide using dihydrogen peroxide following the methods reported by Engbersen and Corey [12, 13]. Subsequently, the N-oxide was converted to 1-methyl-1,10-phenanthrolin-2(1*H*)-one using dimethyl sulfate, following the procedure reported by Kolling [16]. ^{1}H NMR (300 MHz, $CDCl_3$) δ/ppm: 8.94 (dd, 1H),

8.18 (dd, 1H), 7.79 (d, 1H), 7.56 (m, 2H), 7.50 (dd, 1H), 6,91 (d, 1H), 4.49 (s, 3H). IR (ν/cm^{-1}): 1657(vs), 1646(vs), 1602(vs), 1539(s), 1505(s), 1468(s), 1418(m), 1271(m), 1196(m), 1166(w), 1128(s), 1035(m), 989(m), 911(m), 843(vs), 783(s), 732(s), 705(s), 656(s), 604(s), 577(m), 546(m), 463(vs).

$[Eu(CNphen)_2(NO_3)_3]\cdot 4H_2O$ ***(Eu1)***

A solution of 0.500 g (2.4 mmol) of **1** in 30 mL ethanol and a solution of 0.348 g (0.8 mmol) $Eu(NO_3)_3\cdot 5H_2O$ in 20 mL ethanol were heated to boiling for 15 minutes to ensure complete dissolution. The $Eu(NO_3)_3$ solution was added to the former slowly. Precipitate formed on cooling to room temperature. The solids was collected on a sintered glass funnel and dried in air to give 0.55 g of powder. Yield 84% based on Eu. IR (ν/cm^{-1}): 3351(m vbr), 3066(m br), 2240(m), 1635(m), 1616(s), 1594(s), 1538(m), 1506(m), 1472(m), 1432(s), 1393(vs), 1299(vs br), 1264(vs), 1232(s), 1214(s), 1152(m), 1040(m), 871(vs), 840(m), 818(m), 788(m), 760(m), 742(m), 730(s), 624(vs), 642(vs), 586(m), 462(vs), 418(s), 385(s), 328(s). Elemental analysis calcd (%) for $C_{26}H_{22}EuN_9O_{13}$ ($Eu(CNphen)_2(NO_3)_3\cdot 4H_2O$): C 38.06, H 2.70, N 15.36; found: C 38.07, H 2.37, N 15.13.

$[Eu(O_2Cphen)_3]\cdot H_2O$ ***(Eu2)***

To a solution of 37 mg (0.18 mmol) of **2** in 10 mL ethanol, 20 mg NEt_3 and 2 mL triethyl orthoformate (TEOF) were added. To a solution of 24 mg (0.06 mmol) $Eu(NO_3)_3\cdot 5H_2O$ in 10 mL ethanol, 4 mL TEOF was added. Both solutions were heated to 70 °C, after which the europium solution was added to the phenanthroline solution. A white precipitate appeared and heating was continued for 30 minutes. The solids were filtered over a paper filter, washed with 30 mL ether and dried in air. Yield 34 mg of microcrystalline powder, 61% based on Eu. IR (ν/cm^{-1}): 3420(m, vbr), 1658(m), 1652(s), 1622(vs), 1616(vs), 1568(vs), 1558(s), 1540(m), 1515(m), 1495(s), 1456(m), 1394(m), 1362(vs br), 1327(s), 1301(s), 1197(m), 1178(m), 1135(m), 1092(m), 1048(m), 910(m), 876(m), 839(m), 818(vs), 743(m), 721(vs), 641(s), 609(s), 421(s), 422(vs), 344(s). Elemental analysis calcd (%) for $C_{39}H_{23}EuN_6O_7$ + 0.1$Eu(NO_3)_3$ (Eu ($O_2Cphen)_3(H_2O)$ + 0.1$Eu(NO_3)_3$): C 53.61, H 2.69, N 10.10; found: C 53.76, H 2.81, N 10.05.

$[Eu(MeO_2Cphen)_2(NO_3)_3]$ ***(Eu3)***

A solution of 0.25 g (1 mmol) of **3** in 20 mL methanol and a solution of 0.15 g (0.33 mmol) $Eu(NO_3)_3\cdot 5H_2O$ in 20 mL methanol were heated to boiling. The $Eu(NO_3)_3$ solution was added to the ligand solution. After the mixture had cooled to room temperature, 20 mL ether was added to aid in precipitation of the complex. The white precipitate was collected by filtration and dried. Yield 64% based on Eu. IR (ν/cm^{-1}): 3400(m, br) 1674(m), 1622(m), 1575(m), 1464(vs, br), 1410(s), 1378(m), 1281(vs, br), 1187(m), 1143(m), 1096(m), 1028(m), 868(m), 840(s), 816(m), 738(m), 721(vs), 668(m), 642(s), 611(m), 472(m), 423(m), 398(m), 376(m), 352(m). Elemental analysis calcd (%) for $C_{28}H_{20}EuN_7O_{13}$

+ 0.14$Eu(NO_3)_3$ ($Eu(MeO_2Cphen)_2(NO_3)_3$ + 0.14$Eu(NO_3)_3$): C 39.02, H 2.34, N 12.06; found: C 39.03 H 2.50 N 11.60.

*[$Eu(EtO_2Cphen)_2(NO_3)_3$] (**Eu4**)*

A solution of 0.070 g (0.28 mmol) **4** in 5 mL ethanol and a solution of 0.059 g (0.14 mmol) $Eu(NO_3)_3 \cdot 5H_2O$ in 5 mL ethanol were heated to boiling. The former solution was slowly added to the latter. Upon cooling a very small amount of a yellowish precipitate formed, which was removed by filtration. Addition of diethyl ether to the filtrate caused a white powder to precipitate from the solution. This precipitate was collected on a Buchner funnel and air dried giving 0.107 g of powder. Yield 89% based on Eu. IR (ν/cm^{-1}): 3300(w br), 1684(m), 1616(m), 1569(m), 1558(w), 1516(m), 1496(s), 1464(s), 1456(s), 1436(s), 1404(s), 1286(vs br), 1096(m), 1029(m), 871(m), 826(s), 739(s), 721(vs), 668(s), 643(s), 610(s), 423(m), 398(m), 350(s), 328(m). Elemental analysis calcd (%) for $C_{30}H_{24}EuN_7O_{13}$ + 0.15$Eu(NO_3)_3$ ($Eu(EtO_2Cphen)_2(NO_3)_3$ + 0.15$Eu(NO_3)_3$): C 40.34, H 2.71, N 11.68; found: C 40.05, H 2.44, N 11.81.

*[$Eu(Clphen)_2(NO_3)_3$] (**Eu5**)*

A solution of 0.13 g (0.6 mmol) of **5** in 3 mL ethanol and a solution of 0.12 g (0.3 mmol) of $Eu(NO_3)_3 \cdot 5H_2O$ in 3 mL ethanol were heated to boiling. The Eu solution was slowly added to the phenanthroline solution. Heating and stirring was continued for 5 minutes. Upon cooling to room temperature, a precipitate formed. The precipitate was collected on a Buchner filter and washed with ethanol. The precipitate was allowed to dry in air. Yield 225 mg, 97% based on Eu. IR (ν/cm^{-1}): 1616(w), 1580(w), 1481(vs), 1424(s), 1374(w), 1294(vs), 1212(m), 1198(m), 1180(w), 1143(m), 1114(w), 1031(m), 995(w), 953(s), 886(s), 809(s), 780(w), 733(vs), 723(s), 638(s), 619(m), 576(w), 556(w), 522(w). Elemental analysis calcd (%) for $C_{24}H_{14}Cl_2EuN_7O_9$ ($Eu(Clphen)_2(NO_3)_3$): C 37.37, H 1.84, N 12.78; found: C 37.56, H 1.76, N 12.66.

*[$Eu(MeOphen)_2(NO_3)_3$] (**Eu6**)*

A solution of 600 mg (2.8 mmol) of **6** in 15 mL ethanol, and a solution of 375 mg (0.88 mmol) $Eu(NO_3)_3 \cdot 5H_2O$ in 10 mL ethanol were heated to boiling for 5 minutes. The salt solution was slowly added to the ligand solution. Precipitate appeared on cooling to room temperature and was collected on a sintered funnel. The precipitate was washed with 4 portions of 30 mL ethanol and dried in air. Yield 0.567 g, 85% based on Eu. IR (ν/cm^{-1}): 1610(m), 1594(m), 1575(m), 1516(s), 1496(s), 1471(vs), 1456(vs), 1436(s), 1418(vs), 1399(m), 1346(s), 1323(vs), 1287(vs), 1240(m), 1181(m), 1156(m), 1122(m), 1092(m), 1052(m), 1035(vs), 903(m), 848(vs), 814(m), 781(m), 740(vs), 728(s), 692(m), 659(m), 642(m), 586(m), 572(m), 490(m), 427(m), 398(m), 374(m), 344(m), 334(m), 327(m), 314(m). Elemental analysis calcd (%) for $C_{26}H_{20}EuN_7O_{11}$ ($Eu(MeOphen)_2(NO_3)_3$): C 41.17, H 2.66, N 12.93; found: C 40.64, H 2.70, N 12.66.

Single crystals were obtained from a diffusion experiment using a Y-tube. One leg of the tube was charged with 300 mg (1.4 mmol) of **6**, while the other was charged with 187 mg (0.44 mmol) of $Eu(NO_3)_3 \cdot 5H_2O$. The tube was filled with ethanol such that the solvent level was 4 mm above the intersection of both legs. After three weeks at room temperature, orange plate-like crystals had formed in the tube.

$[Eu(EtOphen)_2(NO_3)_3]$ ***(Eu7)***

A solution of 640 mg (2.85 mmol) of **7** in 15 mL ethanol and a solution of 407 mg (0.95 mmol) $Eu(NO_3)_3 \cdot 5H_2O$ in 10 mL ethanol were heated to boiling for five minutes. The salt solution was slowly added to the ligand solution. The precipitate that formed on cooling to room temperature was collected on a sintered glass funnel. The precipitate was washed with four portions of 30 mL ethanol and dried in air and in a desiccator. Yield 0.62 g, 64% based on Eu. IR (ν/cm^{-1}): 1612(m), 1593(m), 1575(m), 1512(s), 1472(s), 1456(vs), 1424(m), 1339(s), 1308(vs), 1286(br, vs), 1236(m), 1157(m), 1121(m), 1090(m), 1051(m), 1034(vs), 959(m), 878(m), 845(s), 813(m), 780(m), 739(vs), 727(s), 708(m), 668(m), 655(m), 642(s), 572(m), 510(m), 425(m), 375(m), 358(m), 324(m). Elemental analysis calcd (%) for $C_{28}H_{24}EuN_7O_{11}$ ($Eu(EtOphen)_2(NO_3)_3$): C 42.76, H 3.08, N 12.47; found: C 42.51, H 2.95, N 12.49.

Crystals were obtained as for **Eu6**, except that 25 mg (0.11 mmol) of **7** and 16 mg (0.04 mmol) of $Eu(NO_3)_3 \cdot 5H_2O$ were used. After three weeks at room temperature, yellow plate-like crystals had formed in the tube.

$[Eu(NH_2phen)_2(NO_3)_3]$ ***(Eu8)***

A solution of 0.32 g (1.6 mmol) of **8** in 20 mL ethanol and a solution of 0.23 g (0.54 mmol) $Eu(NO_3)_3 \cdot 5H_2O$ in 10 mL ethanol were heated and stirred at 60 °C for 10 minutes. The salt solution was added drop wise to the ligand solution. A yellow precipitate formed immediately. After cooling to room temperature the precipitate was collected on a sintered funnel and washed with three portions of 20 mL ethanol. The precipitate was allowed to dry in air, yielding 0.33 g (84% based on Eu). IR (ν/cm^{-1}): 3484(m), 3440(m), 3379(m), 3252(m), 1657(m), 1646(s), 1616(m), 1594(m), 1564(m), 1540(w), 1520(m), 1496(vs), 1472(vs), 1456(vs), 1436(s), 1423(s), 1385(vs), 1318(br, s), 1275(s), 1216(m), 1156(m), 1093(m), 1031(s), 841(vs), 811(s), 778(m), 732(s), 721(s), 702(s), 659(s), 643(s), 583(m), 518(m), 448(s), 433(s), 413(vs), 398(vs), 374(s), 349(m), 342(m), 328(s). Elemental analysis calcd (%) for $C_{24}H_{18}EuN_9O_9$ ($Eu(NH_2phen)_2(NO_3)_3$): C 39.57, H 2.49, N 17.31; found: C 39.45, H 2.80, N 16.72. Single crystals of **Eu8** were obtained using the procedure described for **Eu6**, but using 0.15 g (0.75 mmol) of **8** and 0.11 g (0.38 mmol) of $Eu(NO_3)_3 \cdot 5H_2O$ and slow cooling of the reaction mixture to room temperature.

*[La(NH$_2$phen)$_2$(NO$_3$)$_3$] (**La8**)*

The procedure for the synthesis of **Eu8** has been followed, except that 0.21 g (0.5 mmol) La(NO$_3$)$_3$·5H$_2$O was used instead of Eu(NO$_3$)$_3$·5H$_2$O and 0.29 g (1.5 mmol) of **8**. Yield 0.23 g (65% based on La). IR (ν/cm^{-1}): 3482(m), 3431(m), 3379(m), 3246(m), 1645(s), 1588(m), 1562(m), 1465(vs), 1438(vs), 1423(s), 1385(vs), 1317(br, s), 1269(s), 1215(m), 1031(s), 842(vs), 812(s), 775(m), 731(s), 719(s), 701(s), 659(m), 642(s), 582(w), 537(w), 514(w). Elemental analysis calcd (%) for C$_{24}$H$_{18}$LaN$_9$O$_9$ + 0.1La(NO$_3$)$_3$ (La(NH$_2$phen)$_2$(NO$_3$)$_3$ + 0.1La(NO$_3$)$_3$): C 38.55, H 2.43, N 17.42; found: C 38.03, H 2.32, N 17.41. Single crystals were obtained as for **Eu8**.

*[Eu(NMeOphen)$_3$(NO$_3$)$_3$] (**Eu9**)*

0.25 g (1.2 mmol) of **9** was dissolved in 15 mL of ethanol and heated to boiling for 15 minutes until complete dissolution of **9**. To this solution was slowly added a boiling solution of 0.17 g (0.4 mmol) Eu(NO$_3$)$_3$·5H$_2$O in 10 mL ethanol. The mixture was boiled and stirred for 15 more minutes and cooled down to room temperature. The resulting precipitate was collected by filtration, washed with ethanol and allowed to dry in air. Yield 200 mg, 50% based on Eu, of a light yellow powder. IR (ν/cm^{-1}): 1640(s), 1616(w), 1600(m), 1564(s), 1558(s), 1538(vs), 1496(s), 1472(vs), 1456(vs), 1436(m), 1424(s), 1404(s), 1291(br, vs), 1236(s), 1200(m), 1168(m), 1144(m), 1026(s), 989(m), 922(m), 848(vs), 831(m), 816(m), 780(s), 736(s), 708(vs), 668(m), 658(s), 604(s), 578(m), 547(m), 527(m), 478(vs), 398(w), 358(m), 336(w), 326(m), 318(m). Elemental analysis calcd (%) for C$_{39}$H$_{30}$EuN$_9$O$_{12}$ (Eu(NMeOphen)$_3$(NO$_3$)$_3$): C 48.36, H 3.12, N 13.01; found: C 48.88, H 3.18, N 13.26. Crystals suitable for single crystal X–ray diffraction were grown by slow diffusion of an ethanolic solution of 0.10 g (0.48 mmol) of ligand into an ethanolic solution of 0.067 g (0.16 mmol) of Eu(NO$_3$)$_3$·5H$_2$O in a Y-tube over a period of three weeks. Crystals appeared as large orange blocks of sizes up to 0.5 × 0.5 × 2.0 mm^3.

2.3 Results

2.3.1 Synthesis and characterization

All ligands were readily synthesized following procedures reported in literature and were analyzed using IR and NMR spectroscopy. Formation of the corresponding Eu(III) complexes was performed by addition of a hot ethanolic solution of Eu(NO$_3$)$_3$·5H$_2$O to a hot stirred solution of the ligand. The solutions were heated to boiling to ensure complete dissolution of the ligand and inorganic salt and to slow down precipitation of the product. In general, the lanthanoid complexes **Eu1-Eu9** are poorly soluble in ethanol and addition of the lanthanoid nitrate solution to the ligand solution at room temperature leads to the immediate formation of a fine precipitate. Unfortunately, the poor solubility of the compounds severely hampers proper analysis. Attempts were undertaken to analyze the lanthanoid coordination compounds with ESI-MS, but due to the poor solubility and

inherent high kinetic lability of the lanthanoid compounds only signals of the ligands were found in the mass spectra. Elemental analysis was performed to determine the composition of the complexes. All complexes analyze as $[Ln(L)_2(NO_3)_3]$, with the exception of **Eu2**, which analyzes as $[Eu(L)_3]$, and **Eu9**, which analyzes as $[Ln(L)_3(NO_3)_3]$. The deviation between the calculated and found values for the elemental analyses for compounds **Eu2**, **Eu3**, **Eu4** and **La8** are readily explained by the inclusion of minor quantities of $Eu(NO_3)_3$ in the samples, which cannot be removed by recrystallization. The molecular nature of these compounds ensures, however, that these minor impurities do not negatively affect their photoluminescent properties, in contrast to phosphor materials that are based on oxide type compounds. Compounds **Eu6** and **Eu7** were dried prior to elemental analysis and luminescence studies. As a result, the disordered solvent molecule that is observed in the crystal structure (*vide infra*) is not apparent from the elemental analysis. When exposed to air, the initially shiny crystals turn lusterless, indicating that solvent molecules are easily lost. TGA analysis showed that with the exception of **Eu3** and **Eu4**, the compounds are thermally stable to at least 200 °C.

The infrared spectra recorded for the ligands are complicated and show many bands, which makes full assignment of the signals difficult. Signals due to characteristic functional groups can be seen; for example, the signal at 2230 cm^{-1} cm can be attributed to the CN group of **1**, while strong bands around 1700 cm^{-1} recorded for ligands **2-4** is typical for the C=O stretch vibration. The strong band at 1650 cm^{-1} observed for **9** indicates the formation of the carbonyl group. NMR spectra recorded for the ligands agree with the literature, or can be readily assigned to the ligand structures. Comparing the IR spectra obtained for the coordination compounds **Eu1-La8** to those of the ligands reveals strong similarities between them, with minor peak shifts. Additional peaks are observed in the IR spectra of compounds **Eu1** and **Eu3-La8**: all show strong bands around 1030, 1290 and 1490 cm^{-1} that can be ascribed to vibrations of the nitrate ions [20]. Bands around 1650 cm^{-1} are observed for **Eu2-Eu4** due to the C=O stretch, which is slightly lower in energy than observed for the separate ligands, indicating that the carbonyl group is participating in a binding interaction in the complexes.

2.3.2 X-ray crystal structure determination

Projections of the structures of **Eu6-Eu8** are shown in Figure 2.2. Experimental data on the crystal structure determination are given in Table 2.1 for compounds **Eu6-La8** relevant bond lengths and angles are given in Table 2.2. Table 2.3 lists the experimental data, band distances and angles for **Eu9**.

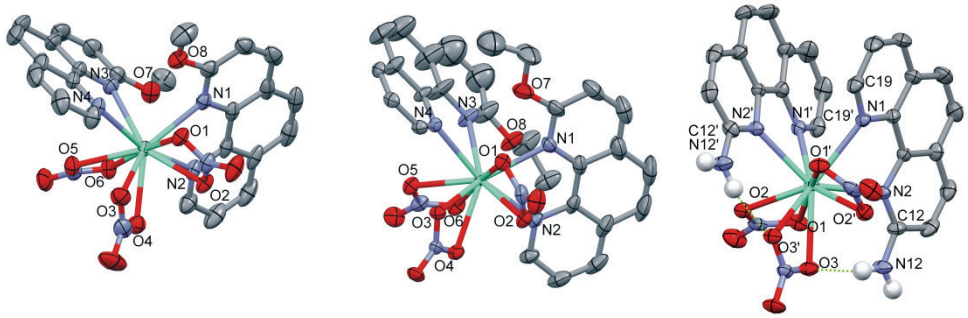

Figure 2.2: From left to right: thermal ellipsoid plots (50% probability contours) of the structures of ***Eu6****, [Eu(MeOphen)$_2$(NO$_3$)$_3$]·EtOH,* ***Eu7****, [Eu(EtOphen)$_2$(NO$_3$)$_3$]·EtOH and* ***Eu8****, [Eu(NH$_2$phen)$_2$(NO$_3$)$_3$] showing the relevant atomic numbering scheme. Only the major disorder component in* ***Eu8*** *and the amine hydrogens and the intramolecular hydrogen bonding interactions are shown; hydrogen atoms and lattice ethanol molecules have been omitted for clarity.*

Table 2.1: Details of the single crystal structure determination of complexes Eu6-La8.

	[Eu6]	**[Eu7]**	**[Eu8]**	**[La8]**
formula	$C_{28}H_{26}EuN_7O_{12}$	$C_{30}H_{30}EuN_7O_{12}$	$C_{24}H_{18}EuN_9O_9$	$C_{24}H_{18}LaN_9O_9$
fw	804.52	832.57	728.43	715.38
crystal size [mm^3]	0.07×0.15×0.20	0.08×0.10×0.10	0.09×0.18×0.37	0.07×0.19×0.23
crystal color	Orange	Yellow	Yellow	Pale yellow
crystal system	Orthorhombic	Triclinic	Monoclinic	Monoclinic
space group	Pbcn (no. 60)	P–1 (no. 2)	C2/c (no. 15)	C2/c (no. 15)
a [Å]	28.145(4)	10.231(1)	10.6715(3)	10.7600(4)
b [Å]	15.023(2)	10.266(1)	18.4251(4)	18.6250(5)
c [Å]	14.735(2)	17.648(1)	13.1230(2)	13.1289(4)
α [°]	90	105.03(5)	90	90
β [°]	90	97.04(5)	93.279(2)	92.011(3)
γ [°]	90	100.07(6)	90	90
V [Å^3]	6230.3(15)	1734.9(7)	2576.1(1)	2629.5(1)
Z	8	2	4	4
d_{calc} [g/cm^3]	1.715	1.594	1.878	1.807
μ [mm^{-1}]	2.089	1.878	2.509	1.697
refl. measured / unique	84459 / 7155	28296 / 7772	8625 / 2958	16280 / 2701
parameters	464	454	206	206
R1/wR2 [I>2σ(I)]	0.0314 / 0.0606	0.0556 / 0.1395	0.0196 / 0.0485	0.0224 / 0.0561
R1/wR2 [all refl.]	0.0531 / 0.0674	0.0657 / 0.1450	0.0221 / 0.0492	0.0253 / 0.0571
S	1.10	1.19	1.03	1.10
$\rho_{min/max}$ [e/Å^3]	–0. 60 / 0.60	–1.45 / 2.13	–0.68 / 0.91	–0.41 / 0.83

Table 2.2: Selected bond distances (Å) and angles (°) for complexes Eu6 - La8.

	[Eu6]	[Eu7]	[Eu8]	[La8]
Bond distance (Å)				
Ln-N1	2.574(3)	2.583(7)	2.600(2)	2.701(2)
Ln -N2	2.579(3)	2.583(6)	2.534(2)	2.622(2)
Ln -N3	2.572(3)	2.572(7)		
Ln -N4	2.590(3)	2.575(6)		
Ln -O1	2.555(2)	2.537(5)	2.528(2)	2.612(2)
Ln -O2	2.514(2)	2.547(5)	2.484(2)	2.585(2)
Ln -O3	2.502(3)	2.518(6)	2.577(2)	2.653(2)
Ln -O4	2.515(3)	2.548(6)		
Ln -O5	2.515(3)	2.545(6)		
Ln -O6	2.544(3)	2.514(5)		
Ln -O7	3.351(3)	3.375(6)		
Ln -O8	3.372(3)	3.411(5)		
Bond angle (°)				
N11-*Ln*-N110	63.65(9)	64.1(2)	64.92(6)	62.75(6)
N21-*Ln*-N210	63.48(9)	63.9(2)		
O31-*Ln*-O32	50.29(7)	50.2(2)	51.00(5)	49.23(6)
O41-*Ln*-O42	51.08(8)	50.5(2)	49.33(5)	48.17(5)
O51-*Ln*-O52	50.45(8)	50.5(2)		

Complexes **Eu6**-**La8** have a ten-fold coordination geometry around the central lanthanoid ion, as a result of two phenanthroline ligands binding in a bidentate mode and three bidentate nitrate ligands. The resulting coordination geometry around the Eu(III) ion is best described as a distorted sphenocorona. Compounds **Eu8** and **La8** are isostructural, with a C_2 axis passing through a nitrato N-O bond and the lanthanoid ion, whereas in **Eu6** and **Eu7** a pseudo C_2 axis is present. The coordination geometry of **Eu6** with the pseudo C_2 axis is shown in Figure 2.3.

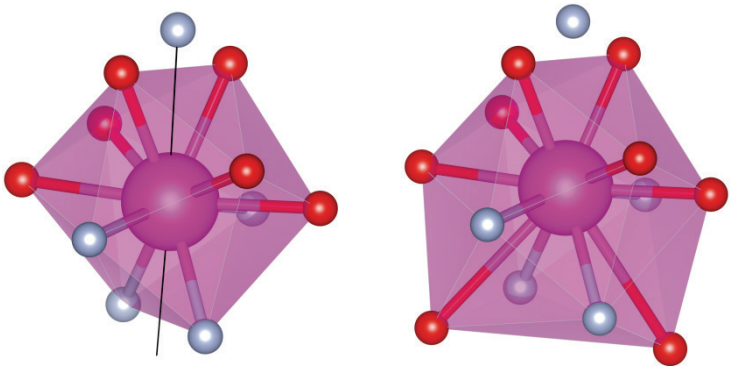

*Figure 2.3: Left: the sphenocorona geometry of **Eu6** with the pseudo C2-axis indicated as a black line passing through the nitrogen of the topmost nitrato ligand and the central Eu(III) ion. The lower two faces are approximately square. Right: expansion of the sphenocorona coordination sphere by inclusion of the second coordination sphere in **Eu6** and **Eu7**, showing additional interactions between the ether oxygen atoms and Eu(III) via the square faces.*

In both **Eu6** and **Eu7**, for each complex a disordered molecule of ethanol is present in the crystal lattice. In **Eu6** and **Eu7**, the Eu-O bond lengths range from 2.502(3) to 2.555(3) Å, while Eu-N bond lengths vary from 2.572(3) to 2.590(3) Å, which is in line with closely related compounds [1, 21]. The coordination angle of the nitrato ligands is around 50° whereas the phenanthroline N-Eu-N angles are around 63°.
The structures of **Eu8** and **La8** are mostly ordered, but the substituted carbon atom with the attached amine group of the phenanthroline ligands is located partially on C12 and partially on C19; the major component of the disordered C–NH_2 group is positioned on C12 (66.3% for **Eu8** and 60.1% for **La8**). In both positions the amine hydrogens form strong intramolecular H-bonding interactions with a coordinated nitrate oxygen atom, having an H···O distance of 1.96 Å in **Eu8** and 2.06 Å in **La8**. Intermolecular H-bonding interactions of the amine hydrogens with nitrate ions influence the packing of the molecules. The coordination bond lengths vary from 2.484(2) Å to 2.577(2) Å for Eu-O and from 2.534(2) Å to 2.600(2) Å for Eu-N. These values are in line with those found for **Eu6** and **Eu7**. In **La8**, the La-O bond distances range from 2.622(2) Å to 2.701(2) Å and from 2.585(2) Å to 2.653(2) Å for La-N. These values are slightly higher than those found for **Eu8** which is readily explained by lanthanoid contraction [21]. A projection of the crystal structure of **Eu9** is shown in Figure 2.4. The structure contains a single Eu(III) ion in the asymmetric unit, and has two molecules in the unit cell. The first coordination sphere of the complex contains three ligands bonded to Eu(III) through the carbonyl oxygen of **9** and three bidentate nitrate ions, resulting in a coordination number of nine around the central ion. Interestingly, all phenanthroline ligands are lying in approximately parallel planes. The geometry around the Eu(III) ion is best described as a highly distorted monocapped square antiprism with the top vertex and a corner of one of the squares being defined by nitrato oxygens, while the other three corners of this square are occupied by the carbonyl oxygens of the ligand. The other square face comprises four nitrato oxygen atoms. The Eu-O bond (Table 2.3) range from 2.322(1) to 2.360(2) Å for the Eu-carbonyl oxygens of the ligands, which can be considered as normal [21]. For the chelating nitrates, Eu-O bond lengths vary from 2.472(2) to 2.550(2) Å. The length of the C=O double bond varies from 1.258(3) to 1.268(4) Å, indicating a slight elongation as compared to C(sp^2)=O bonds that are around 1.20 Å on average [22]. The Eu-O-C bond angles vary markedly within the complex, as can be seen from Table 2.3. π-Stacking interactions play an important role in the crystal structure: the plane-to-plane distances between neighboring phenanthroline rings range from 3.227(1) to 4.097(1) Å. A number of these stacking interactions is shown in Figure 2.4; the distances between the centroids in this particular stacking interaction are 3.77 – 4.41 Å.

Table 2.3: Details of the single crystal structure determination, bond distances (Å) and angles (°) for Eu9.

Details of the experiment		**Bond distances and angles**			
formula	$C_{39}H_{30}EuN_9O_{12}$	*Bond distance* (Å)		*Bond Angle* (°)	
fw	968.68				
crystal size [mm^3]	0.20×0.20×0.10	Eu - O1	2.472(2)	O1 -Eu -O2	51.01(7)
crystal color	Orange	Eu - O2	2.516(2)	O3 -Eu -O4	51.17(6)
crystal system	Triclinic	Eu - O3	2.522(2)	O5 -Eu -O6	50.68(6)
space group	P–1 (no. 2)	Eu - O4	2.486(2)		
a [Å]	10.296(1)	Eu - O5	2.477(2)	C - O7 - Eu	143.8(2)
b [Å]	12.478(1)	Eu - O6	2.550(2)	C - O8 - Eu	152.0(2)
c [Å]	15.661(2)	Eu - O7	2.360(1)	C - O9 - Eu	134.4(2)
α [°]	77.45(1)	Eu - O8	2.322(1)		
β [°]	85.95(1)	Eu - O9	2.350(2)		
γ [°]	69.52(1)				
V [$Å^3$]	1839.8(4)	C - O7	1.265(3)		
Z	2	C - O8	1.258(3)		
d_{calc} [g/cm^3]	1.749	C - O9	1.286(4)		
μ [mm^{-1}]	1.786				
refl. measured / unique	29148 / 8357				
parameters	553				
R1/wR2 [I>2σ(I)]	0.0264 / 0.520				
R1/wR2 [all refl.]	0.0374 / 0.0555				
S	1.09				
$\rho_{min/max}$ [$e/Å^3$]	–0.50 / 0.69				

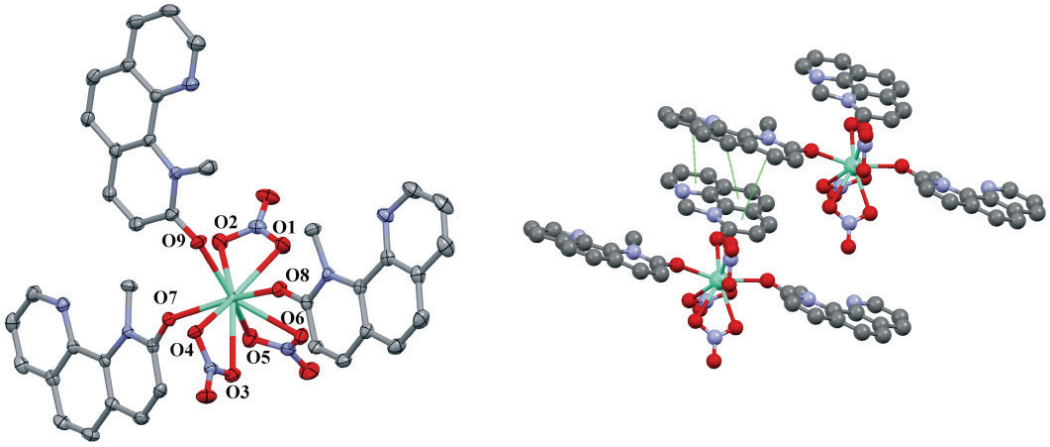

*Figure 2.4: Left: projection of the crystal structure of **Eu9** as thermal ellipsoid plot (50% probability) with the atom numbering scheme indicated. Hydrogen atoms have been omitted for clarity. Right: a projection of part of the structure of **Eu9**, showing the π-stacking interactions.*

2.3.3 Luminescence

The solid state photoluminescence spectra of complexes **Eu1-Eu9** and **La8** are shown in Figure 2.5. Excitation spectra were obtained by constantly monitoring the $^5D_0 \rightarrow {}^7F_2$ transition at 615 nm while scanning the excitation wavelength from 220 to 400 nm. All complexes feature a broad excitation band in the nUV region, originating from phenanthroline-centered excitation. The small spike on the shoulder of the broad band at 395 nm in the spectra of **Eu2**, **Eu5** and **Eu9** can be attributed to direct excitation of the Eu(III) ion *via* the ($^5L_6$, $^5G_2$, $^5L_7$, $^5G_3$) $\leftarrow {}^7F_0$ transition [23]. The excitation maxima for **Eu1**-**Eu8** are all fairly close, and range from 351 to 372 nm. For **Eu9**, the excitation maximum is at 275 nm. The absorption spectra recorded for **Eu1**-**Eu9** and **La8**, shown in Figure 2.6, indeed show broad and strong absorption bands in the near UV region. The emission spectra of **Eu1-Eu7** and **Eu9**, obtained by exciting the compounds in the ligand-centered excitation band, are characteristic for Eu(III) with lines at 580, 595, 615, 649 and 685 nm originating from the $^5D_0 \rightarrow {}^7F_J$ (J = 0, 1, 2, 3, 4) transitions. In all cases, the most dominant line corresponds to the $^5D_0 \rightarrow {}^7F_2$ transition. Different splitting patterns of the fundamental $^5D_0 \rightarrow {}^7F_J$ transition lines are the result from crystal field splitting by different coordination environments around the luminescent center. Photoluminescence quantum yields and lifetimes are listed in Table 2.4. The quantum yields range from 10% for **Eu1** to 79% for **Eu5**, and luminescence lifetimes vary from 0.43 for **Eu1** to 1.57 ms for **Eu2**. Equation 1 was used to fit the experimental decay curves using a least-squares fitting procedure with satisfactory results (R^2 > 99.7% in all cases).

$$I(t) = I(0) + A \cdot \exp\left(\frac{-t}{\tau}\right) \qquad (1)$$

Complex **Eu8**, with 2-aminophenanthroline as a ligand, shows no photoluminescence upon excitation in the (near-) UV region, while the analogous La(III) complex **La8** shows broad band luminescence from 400 to 600 nm.

Table 2.4. Photophysical properties of complexes Eu1-Eu9.

	Φ_{tot} (%)	Ω_2 (10^{-20} cm^2)	Ω_4 (10^{-20} cm^2)	τ_{exp} (ms)	τ_{rad} (ms)	Φ_{Ln} (%)	η_{sens} (%)
Eu1	10	8.82	5.25	0.43	2.56	17	61
Eu2	n.d.	n.d.	n.d.	1.57	n.d.	n.d.	n.d.
Eu3	27	9.75	4.53	0.66	2.37	28	98
Eu4	n.d.	n.d.	n.d.	0.57	n.d.	n.d.	n.d.
Eu5	79	11.93	5.98	1.00	1.94	52	~100
Eu6	20	10.29	4.92	1.04	2.20	47	43
Eu7	24	9.65	4.24	1.13	2.40	47	52
Eu9	22	11.66	0.61	0.74	1.47	50	44

Φ_{tot} (%): Overall photoluminescence quantum yield at 355 nm excitation, τ_{exp}: total lifetime of $^5D_0$ state, Ω_J: Intensity parameters, τ_{rad}: radiative lifetime, Φ_{Ln}: intrinsic quantum yield, η_{sens}: sensitizer efficiency.

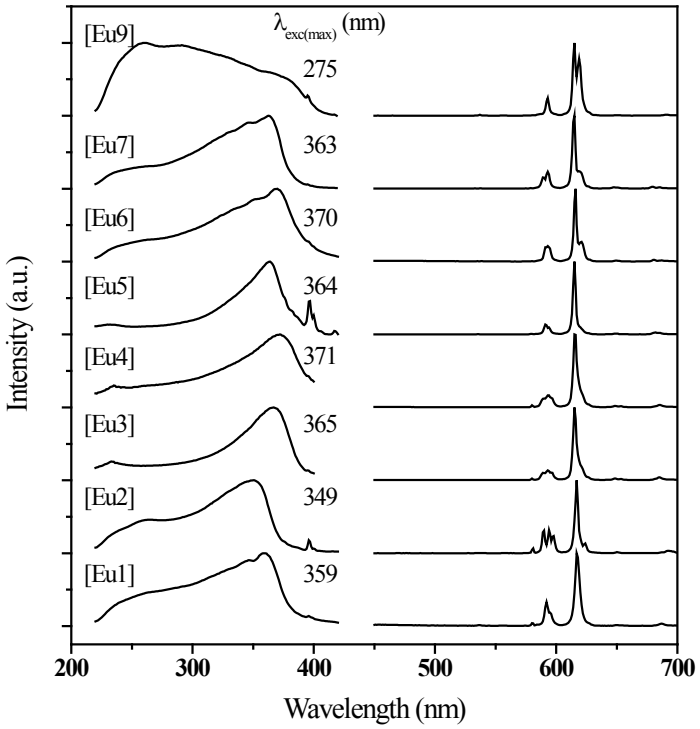

*Figure 2.5: Photoluminescence spectra of **Eu1-Eu9**. The excitation spectra (λ_{em} = 616 nm) are shown on the left hand side with the wavelength of maximum excitation intensity indicated. The right hand side shows the luminescence spectra of the compounds (λ_{exc} = 360 nm), characteristic of Eu(III) with lines at 595, 616, 5, 649 and 685 nm corresponding to $^5D_0 \rightarrow {}^7F_J$, J=1, 2, 3, 4 transitions.*

2.4 Discussion

2.4.1 X-ray crystal structure

The structures as determined for **Eu6**, **Eu7**, **Eu8** and **La8** are rather similar in that the coordination sphere comprises two substituted phenanthrolines binding in a bidentate mode, and three nitrato ligands binding in a bidentate mode. In all cases, the geometry around the *Ln*(III) center closely resembles a distorted sphenocorona. In **Eu6** and **Eu7**, a weak additional interaction between the Eu(III) center and the ether oxygens of the ligand appears to be present, each forming an apex on top of the square faces of the sphenocorona. These are the largest faces of the coordination polyhedron that offer a possibility for bonding to atoms in a second coordination sphere. Figure 2.3 illustrates how these two

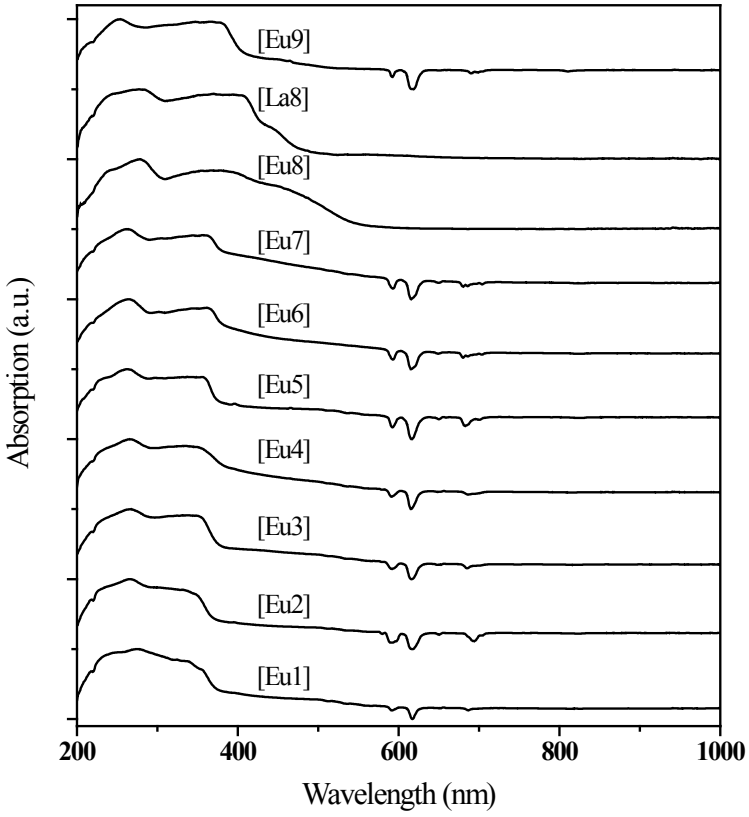

*Figure 2.6: Absorption spectra for compounds **Eu1-Eu9**, showing broad band absorption in the UV and nUV region. The peaks pointing downward are a result of Eu(III) centered emission.*

additional Eu-O bonds are oriented with respect to the polyhedron formed by the first coordination sphere. The bond lengths are 3.351(3) Å for Eu-O7 and 3.372(3) Å for Eu-O8 in **Eu6**. For **Eu7**, the bond lengths of Eu-O7 and Eu-O8 are 3.375(6) Å for Eu-O7 and 3.411(5) Å, respectively. These values are much larger than expected for a normal Eu-O bond, but within the reasonable range for an oxygen atom in the second coordination sphere of Eu(III) [24]. Although complexes **Eu6** and **Eu7** have very similar structures that closely resembles the structure of the Eu(III) complex with unsubstituted phenanthroline, the crystal packing is very different for both compounds [1, 6]. In the structure of **Eu6** and **Eu7**, π-stacking between the phenanthrolines of neighboring complexes with a interplanar distance of 3.400(1) Å and 3.408(6) Å, respectively, is observed, while the distance between two nearest neighbor Eu(III) ions is 9.632(1) Å and 9.440(2) Å, respectively. Compounds **Eu8** and **La8** are isostructural and adopt a structure that closely resembles that of $[Eu(phen)_2(NO_3)_3]$ [1, 6]. The most notable difference, as compared to the complexes **Eu6**, **Eu7** and the parent phenanthroline complex is the non-coplanarity of the *Ln*(III) ion

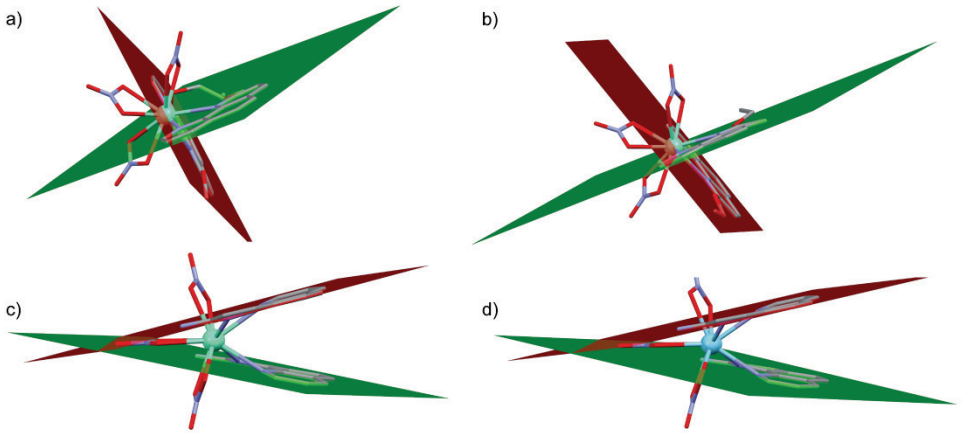

*Figure 2.7: Projections of **Eu6** (a), **Eu7** (b), **Eu8** (c) and **La8** (d) with planes defined by the phenanthroline moieties indicated as red and green surfaces. In **Eu6** and **Eu7**, the Eu(III) ion is in the red plane while in **Eu8** and **La8**, the Ln(III) ion is in neither of the planes.*

with the aromatic system of the phenanthroline ligands. As shown in Figure 2.7, in complexes **Eu8** and **La8**, the planes defined by the ligands do not contain the *Ln*(III) ion. In case of **Eu6** and **Eu7**, the *Ln*(III) ion is in the plane defined by one of the ligands and only slightly out of the plane defined by least-squares fitting to the second ligand. The structure of **Eu9** does not resemble that of **Eu6-La8** because a bidentate mode of coordination *via* the two phenanthroline nitrogens is impossible. Instead, **9** binds through the more available carbonyl oxygen.

2.4.2 Luminescence

Compared to the excitation spectrum of $[Eu(phen)_2(NO_3)_3]$, which has a maximum at 355 nm, the excitation maxima of **Eu1**-**Eu7** are slightly red-shifted, as shown in Figure 2.5. Of the entire series of complexes, **Eu3** and **Eu4** have the highest maximum excitation wavelength at around 370 nm. A slight shift of the maximum to shorter wavelengths is observed only for **Eu2**. At 275 nm, complex **Eu9** has the lowest excitation maximum of the compounds studied. The broad bands are due to the absorption by phenanthroline, indicating clearly that the ligands are acting as antennae. It seems that there is no simple correlation between the electronic properties of the substituent and the optimal excitation wavelength for **Eu1**-**Eu7**. Because in **Eu9** bonding of the ligand through its two nitrogen atoms is not possible, direct comparison of its luminescent properties to those determined for the other Eu(III)-phenanthroline complexes seems inappropriate. The methyl group at one of the nitrogen atoms prevents the bidentate coordination of the phenanthroline molecule, thus hindering the normal mode of coordination to the metal. Instead, the ligand

binds to the lanthanoid ion *via* its ketone moiety. While bèta-diketones have been widely studied as sensitizing ligand for lanthanoid compounds, ketones are generally considered to be poor ligands and thus seem to get less attention. However, complexes of Eu(III) with Michler's ketone, benzophenone and azaxanthones have been studied and are reported to exhibit bright photoluminescence, with quantum yields in solution ranging from 9 to 24% [25-27]. This is in line with the quantum yield determined for **Eu9**, which is 22%.
All compounds except for **Eu8** exhibit luminescence characteristic of Eu(III), with most of the emission intensity arising from the $^5D_0 \rightarrow {}^7F_2$ transition which is of a forced electric dipole (ED) nature. The fact that this transition is much stronger than the $^5D_0 \rightarrow {}^7F_1$ magnetic dipole (MD) transition is in agreement with the structures determined for **Eu6**, **Eu7** and **Eu9**, which show that the Eu ion is situated in a non-centrosymmetric coordination environment [28, 29]. Photoluminescence quantum yields and radiative lifetimes of complexes **Eu1** to **Eu9** are given in Table 2.4. Luminescence lifetimes are in the order of one millisecond, which is as expected for Eu(III) complexes. The most intense luminescence is observed for **Eu5**, which has a high quantum yield of 79%. Complexes **Eu1**, **Eu3**, **Eu5-Eu9** show moderately bright photoluminescence at quantum yields ranging from 10 to 27%; values that are comparable to those found for similar complexes in CH_3CN solution [1]. Complex **Eu8** does not exhibit detectable photoluminescence, which can be due to several reasons. Firstly, a spectral mismatch between the ligand's donor level and the Eu(III) ^5D_J acceptor levels can result in poor energy transfer between the ligand and the metal [30-34]. Since La(III), being a $4f^0$ ion, has no excited states below the ligand's excited states, La(III) complexes can be used to study the ligand-centered energy levels in the presence of a lanthanoid ion [35, 36]. Since no ligand-to-metal energy transfer can take place in these complexes, the ligand-centered triplet states can be determined from the phosphorescence spectrum. The room temperature emission spectrum recorded for **La8** (see supporting information) shows an emission band with a maximum at 488 nm (20,500 cm^{-1}), which is well above the $^5D_0$ resonance level of Eu(III) at 17,300 cm^{-1}, suggesting that energy transfer should be possible [37]. Secondly, the absence of photoluminescence in **Eu8** can be explained by the presence of a quenching mechanism, for example *via* a low-lying ligand to metal charge transfer (LMCT) state. The presence of a low lying LMCT state near the energy of the excited ^5D_J multiplet of Eu(III) is known to compete with the ligand to metal energy transfer, and can result in quenching of luminescence [33, 38]. A low energy LMCT state can be expected for lanthanoid complexes in which the ligands have a low oxidation potential and the lanthanoid ion a high electron affinity, as is the case for Eu(III) [34]. Unlike complex **La8**, which has a pale color, **Eu8** has a deep yellow color, which suggests that an LMCT transition might be present. As can be seen from Figure 2.6, the absorption spectra for compounds **Eu8** and **La8** are indeed different: both show a ligand-centered absorption band that extends to approximately 420 nm, but **Eu8** has an additional absorption that extends to almost 500 nm. As the compounds are the same except for the central ion, this difference can only be explained by the difference in chemical

nature of the lanthanoid ions. Finally, an explanation can be found from the crystal structure. It has been suggested that a rigid planar structure of the ligand within the complex is beneficial for energy transfer [39]. As the Eu(III) ion is not lying in the plane defined by the planar ligand molecule, ligand-to-metal energy transfer can be hampered.

2.4.3 Analysis of the emission spectra

The Judd-Ofelt theory (JO theory) provides a powerful framework for analysis of the intensities of the forced ED transitions in the lanthanoid ions [40, 41]. According to JO theory, the intensity of a forced ED transition depends on only three intensity parameters, Ω_λ, $\lambda = 2, 4, 6$, that contain information on the local structure around the lanthanoid ion, such as the symmetry and the degree of covalency of the bonds [42-45]. Details on the JO theory are outlined in section 1.6 of this thesis. Because for the Eu(III) ion, the transition $^5D_0 \rightarrow {}^7F_1$ has no electric dipole contribution so it can be considered practically insensitive to the surroundings of the Eu(III) ion. The strength of this transition has been derived theoretically ($D_{MD} = 9.6 \cdot 10^{-42}$ esu^{2}cm^2)[46] and can be used as an internal reference [44]. On the other hand, the transitions $^5D_0 \rightarrow {}^7F_{2,\,4,\,6}$, are of a purely forced electric dipole character and are described by JO theory. Using the $^5D_0 \rightarrow {}^7F_1$ as an internal reference and using equations 10 and 11 from Chapter 1, the JO parameters can be calculated from the emission spectrum. Relative intensities of the transitions are readily found from the spectrum by integration, provided that that the spectrum represents the relative photon flow [47]. Thus, equation 2 can be used as a theoretical expression for the intensity of the $^5D_0 \rightarrow {}^7F_{2,4,6}$ transitions. The values for the matrix elements used have been calculated and are listed in Table 1.7 [44, 48].

$$\frac{I_{J,exp}}{I_{1,exp}} \propto \frac{A_{0-J}}{A_{0-1}} = \left(\frac{\upsilon_J}{\upsilon_1}\right)^3 \cdot \frac{n\left(n^2+2\right)^2}{9n^3} \cdot \frac{e^2}{D_{MD}} \cdot \sum_{\lambda=2,4,6} \Omega_\lambda \langle J||U^\lambda||J'\rangle \qquad (2)$$

Here, $I_{J,exp}$ represents the experimentally observed intensity of a $^5D_0 \rightarrow {}^7F_J$ transition, υ_J and υ_1 the wavenumber of the $^5D_0 \rightarrow {}^7F_J$ and $^5D_0 \rightarrow {}^7F_1$ transitions, respectively and n the average refractive index of the medium around the Eu(III) ion. Since the $^5D_0 \rightarrow {}^7F_6$ transition was not detected, Ω_6 could not be determined [49, 50]. The Judd-Ofelt intensity parameters have been calculated for compounds **Eu1**-**Eu7**, and are given in Table 2.4. An average refractive index of 1.5 was used in the calculations [51, 52]. It is known that the intensity ratio $I(^5D_0 \rightarrow {}^7F_2) / I(^5D_0 \rightarrow {}^7F_1)$ of the ED vs. MD transitions is a measure of the site symmetry of Eu(III). The higher this ratio, the further the site symmetry departs from inversion symmetry [28]. From Eq. 2 it is obvious that the magnitude of Ω_2 directly depends on this ratio. In general a large Ω_2 is indicative of a low site symmetry and a covalent character of the chemical bonds to the *Ln*(III) ion [43, 53]. From the emission spectra shown in Figure 2.5, it is clear that the $^5D_0 \rightarrow {}^7F_2$ transition is much more intense than the $^5D_0 \rightarrow {}^7F_1$ transition, resulting in high Ω_2 parameters. There seems to be no well-

defined interpretation of the Ω_4 parameter [43]. From Chapter 1, Eq. 10 and 11, it is possible to estimate the radiative lifetime of the complexes. From Eq. 10 in Chapter 1, $A_{0\text{-}1}$ can be calculated (~49 s^{-1}), while the Einstein coefficients for the other transitions can be found from their intensities relative to that of the $^5D_0 \rightarrow {}^7F_1$ transition. The total emissive relaxation rate of the $^5D_0$ state, A_T, is found using equation 12 in Chapter 1. The radiative lifetime τ_{rad} of the emissive state is simply the reciprocal of A_T and is given in Table 2.4. From the experimentally obtained lifetime, τ_{exp} of the $^5D_0$ state and τ_{rad}, the intrinsic quantum yield Φ_{Ln} of the lanthanide ion can be calculated from τ_{exp} / τ_{rad}. The experimentally determined lifetime contains contributions of radiative and non-radiative decay processes of the emissive state, and Φ_{Ln} indicates the relative contribution of radiative transitions. The intrinsic quantum yields have been calculated and are given in Table 2.4. The values range from 17 to 52%, indicating that non-radiative decay processes contribute substantially to the depopulation of the $^5D_0$ state. From Φ_{Ln} and the overall photoluminescence quantum yield Φ_{tot} the efficiency of the sensitization process η_{sens} can be estimated from the relation $\Phi_{tot} = \eta_{sens} \times \Phi_{Ln}$ [54]. It indicates how effective the ligand is at transferring energy to the luminescent center. The ligands in **Eu3** and **Eu5** seem to be particularly effective at sensitizing Eu(III) luminescence, with the main quenching mechanism being non-radiative deactivation of the luminescent center.

2.5 Conclusion

Eight new europium(III) complexes with different 1,10-phenanthroline ligands substituted on the 2-position have been synthesized in yields ranging from 43% to 89%. One isostructural lanthanum(III) compound has been synthesized for the estimation of the ligand's triplet excited state. In addition, 1-methyl-1,10-phenanthrolin-2(1*H*)-one has been used as a ligand for the first time, using Eu(III) as a central ion. The resulting complex is described by $[Eu(L)_3(NO_3)_3]$ wherein the ligand is bound to Eu(III) in a monodentate fashion *via* its carbonyl oxygen. The other complexes all analyze as $[Eu(L)_2(NO_3)_3]$ except for $[Eu(O_2Cphen)_3]$. Solid state photoluminescence studies on the complexes reveal ligand centered excitation for all complexes except **Eu8**, which suggests that 2-amino-1,10-phenanthroline is unsuitable for sensitizing Eu(III) luminescence. A low lying charge-transfer band provides a means of non-radiative relaxation of the $^5D_0$ level on the Eu(III) ion. The luminescent complexes are efficiently excited in the near UV region and exhibit medium to high photoluminescence quantum yields. Compared to $[Eu(phen)_2(NO_3)_3]$, the excitation maximum of **Eu1**, **Eu3**, **Eu4**, **Eu6** and **Eu7** has shifted to longer wavelengths. There seems to be, however, no clear correlation between the electronic properties of the ligand substituent on the excitation maximum of the complex. Although the crystal structure determinations show similar coordination geometries for the lanthanoid ions, the crystal packings of **Eu6**, **Eu7** and **Eu8** are different. Notably, the Eu(III) ion in **Eu8** is not residing in the plane of the sensitizing ligand, which may be another cause of the ligand-to-metal energy transfer to be severely hampered. This suggests

that not only the electronic properties of the substituents should be considered when analyzing the antenna properties, but also the steric demands. The emission spectra are characteristic for Eu(III) centers in a non-centrosymmetric coordination site, which for **Eu6** and **Eu7** is confirmed by single crystal X-ray diffraction data. Analysis of the spectral intensities shows a significant contribution of non-radiative processes that quench the luminescence of the $^5D_0$ level on Eu(III), resulting in low intrinsic quantum yields. The nUV excitation properties and the highly monochromatic emission of **Eu4** and **Eu6** make these compounds suitable for application in nUV LED-chips, but the relatively low quantum yields limit their application as phosphor materials in PC-WLEDs.

2.6 References

[1] Z. Pan, G. Jia, C.-K. Duan, W.-Y. Wong, W.-T. Wong, and P.A. Tanner, *Eur. J. Inorg. Chem.*, 2011 (2011) 637-646.

[2] M.F. Belian, H.J. Batista, A.G.S. Bezerra, W.E. Silva, G.F. de Sá, and S. Alves Jr, *Chem. Phys.*, 381 (2011) 29-34.

[3] M.O. Ahmed, J.-L. Liao, X. Chen, S.-A. Chen, and J.H. Kaldis, *Acta Crystallogr., Sect. E: Struct. Rep. Online*, 59 (2003) m29-m32.

[4] C. Xu, *J. Rare Earth.*, 28 (2010) 854-857.

[5] B. Yan, H.-j. Zhang, S.-b. Wang, and J.-z. Ni, *Mater. Chem. Phys.*, 51 (1997) 92-96.

[6] A.G. Mirochnik, B.V. Bukvetskii, P.A. Zhikhareva, and V.E. Karasev, *Russ. J. Coord. Chem.*, 27 (2001) 443-448.

[7] J.C. de Mello, H.F. Wittmann, and R.H. Friend, *Adv. Mater.*, 9 (1997) 230-232.

[8] T. Kottke and D. Stalke, *J. Appl. Crystallogr.*, 26 (1993) 615-619.

[9] Nonius, *COLLECT*, *Nonius BV, Delft, The Netherlands*, 2002.

[10] G.M. Sheldrick, *Acta Crystallogr., Sect. A: Found. Crystallogr.*, 64 (2008) 112-122.

[11] G.M. Sheldrick, *SHELXS–97*, *Bruker AXS Inc., Madison, Wisconsin*, 1997.

[12] J.F.J. Engbersen, A. Koudijs, M.H.A. Joosten, and H.C. Vanderplas, *J. Heterocycl. Chem.*, 23 (1986) 989-990.

[13] E.J. Corey, A.L. Borror, and T. Foglia, *J. Org. Chem.*, 30 (1965) 288-290.

[14] G.J. ten Brink, I. Arends, M. Hoogenraad, G. Verspui, and R.A. Sheldon, *Adv. Synth. Catal.*, 345 (2003) 1341-1352.

[15] J.G.J. Weijnen, A. Koudijs, and J.F.J. Engbersen, *J. Chem. Soc., Perkin Trans. 2*, (1991) 1121-1126.

[16] L. Kolling, Phenanthroline-Comprising Complexes, Pat.no US2010/234548 A1k US2010/234548 A1, 2010.

[17] B.E. Halcrow and W.O. Kermack, *J. Chem. Soc.*, (1946) 155-157.

[18] K.G. Claus and J.V. Rund, *Inorg. Chem.*, 8 (1969) 59-63.

[19] Y. Engel, A. Dahan, E. Rozenshine-Kemelmakher, and M. Gozin, *J. Org. Chem.*, 72 (2007) 2318-2328.

[20] V. Tsaryuk, V. Zolin, L. Puntus, V. Savchenko, J. Legendziewicz, J. Sokolnicki, and R. Szostak, *J. Alloys Compd.*, 300–301 (2000) 184-192.

[21] A.G. Orpen, L. Brammer, F.H. Allen, O. Kennard, D.G. Watson, and R. Taylor, *J. Chem. Soc., Dalton Trans.*, (1989) S1-S83.

[22] *CRC Handbook of Chemistry and Physics, 85th edition*, 2005: CRC Press, Boca Raton.
[23] W.T. Carnall, P.R. Fields, and K. Rajnak, *J. Chem. Phys.*, 49 (1968) 4412-4423.
[24] D. Parker, R.S. Dickins, H. Puschmann, C. Crossland, and J.A.K. Howard, *Chem. Rev.*, 102 (2002) 1977-2010.
[25] M.H.V. Werts, M.A. Duin, J.W. Hofstraat, and J.W. Verhoeven, *Chem. Commun.*, (1999) 799-800.
[26] A. Beeby, L.M. Bushby, D. Maffeo, and J.A.G. Williams, *J. Chem. Soc., Perkin Trans. 2*, (2000) 1281-1283.
[27] P. Atkinson, K.S. Findlay, F. Kielar, R. Pal, D. Parker, R.A. Poole, H. Puschmann, S.L. Richardson, P.A. Stenson, A.L. Thompson, and J.H. Yu, *Org. Biomol. Chem.*, 4 (2006) 1707-1722.
[28] R. Reisfeld, E. Zigansky, and M. Gaft, *Mol. Phys.*, 102 (2004) 1319 - 1330.
[29] B. Francis, D.B.A. Raj, and M.L.P. Reddy, *Dalton Trans.*, 39 (2010) 8084-8092.
[30] J.-C.G. Bünzli, S. Comby, A.-S. Chauvin, and C.D.B. Vandevyver, *J. Rare Earth.*, 25 (2007) 257-274.
[31] M. Latva, H. Takalo, V.M. Mukkala, C. Matachescu, J.C. Rodriguez-Ubis, and J. Kankare, *J. Lumin.*, 75 (1997) 149-169.
[32] L. Armelao, S. Quici, F. Barigelletti, G. Accorsi, G. Bottaro, M. Cavazzini, and E. Tondello, *Coord. Chem. Rev.*, 254 (2010) 487-505.
[33] S. Petoud, J.-C.G. Bünzli, T. Glanzman, C. Piguet, Q. Xiang, and R.P. Thummel, *J. Lumin.*, 82 (1999) 69-79.
[34] W.M. Faustino, O.L. Malta, and G.F. de Sa, *J. Chem. Phys.*, 122 (2005) 054109.
[35] L. Prodi, M. Maestri, R. Ziessel, and V. Balzani, *Inorg. Chem.*, 30 (1991) 3798-3802.
[36] N.M. Shavaleev, S.V. Eliseeva, R. Scopelliti, and J.-C.G. Bünzli, *Chem.-Eur. J.*, 15 (2009) 10790-10802.
[37] W.T. Carnall, P.R. Fields, and K. Rajnak, *J. Chem. Phys.*, 49 (1968) 4450-4455.
[38] V. Tsaryuk, K. Zhuravlev, V. Kudryashova, V. Zolin, J. Legendziewicz, I. Pekareva, and P. Gawryszewska, *J. Photochem. Photobiol., A*, 197 (2008) 190-196.
[39] Y.S. Yang, M.L. Gong, Y.Y. Li, H.Y. Lei, and S.L. Wu, *J. Alloys Compd.*, 207–208 (1994) 112-114.
[40] B.R. Judd, *Phys. Rev.*, 127 (1962) 750-761.
[41] G.S. Ofelt, *J. Chem. Phys.*, 37 (1962) 511-520.
[42] J.H.S.K. Monteiro, I.O. Mazali, and F.A. Sigoli, *J. Fluoresc.*, 21 (2011) 2237-2243.
[43] H. Liang, Z. Zheng, Q. Zhang, H. Ming, B. Chen, J. Xu, and H. Zhao, *J. Mater. Res.*, 18 (2003) 1895-1899.
[44] M.H.V. Werts, R.T.F. Jukes, and J.W. Verhoeven, *Phys. Chem. Chem. Phys.*, 4 (2002) 1542-1548.
[45] C. Görller-Walrand and K. Binnemans, *Spectral intensities of f-f transitions*, in *Handbook on the Physics and Chemistry of Rare Earths*, 1998, Elsevier. 99-264.
[46] The dipole strength is expressed here in CGS units. As 1 esu ≈ 3.33564×10^{-10} C, one finds that 9.6×10^{-42} esu^{2}cm^2 equals 1.06814×10^{-64} C^{2}m^2 in SI units.
[47] J.W. Verhoeven, *Pure Appl. Chem.*, 68 (1996) 2223-2286.
[48] L. Huang, L. Cheng, H. Yu, L. Zhou, J. Sun, H. Zhong, X. Li, J. Zhang, Y. Tian, Y. Zheng, T. Yu, J. Wang, and B. Chen, *Physica B*, 406 (2011) 2745-2749.

[49] L. Đačanin, S.R. Lukić, D.M. Petrović, M. Nikolić, and M.D. Dramićanin, *Physica B*, 406 (2011) 2319-2322.
[50] R. Balakrishnaiah, R. Vijaya, P. Babu, C.K. Jayasankar, and M.L.P. Reddy, *J. Non-Cryst. Solids*, 353 (2007) 1397-1401.
[51] C.A. Kodaira, H.F. Brito, O.L. Malta, and O.A. Serra, *J. Lumin.*, 101 (2003) 11-21.
[52] M.E. de Mesquita, S.A. Júnior, F.R.G. e Silva, M.A. Couto dos Santos, R.O. Freire, N.B.C. Júnior, and G.F. de Sá, *J. Alloys Compd.*, 374 (2004) 320-324.
[53] H. Ebendorff-Heidepriem, D. Ehrt, M. Bettinelli, and A. Speghini, *J. Non-Cryst. Solids*, 240 (1998) 66-78.
[54] J.-C.G. Bünzli, *Chem. Rev.*, 110 (2010) 2729-2755.

3 Ln(III) complexes with small aromatic ligands

In this chapter, the synthesis of four new Ln(III) complexes (Ln = Eu, Tb) with furan-2,5-dicarboxylic acid (H_2fda) as a ligand, as well as the preparation of a metal organic framework of Tb(III) with 2-hydroxytrimesic acid (H_4tma) is described. The compounds have been synthesized and characterized in the solid state. Luminescence studies indicate that the compounds exhibit line-like luminescence characteristic of the lanthanoid ion upon excitation in the ligand absorption bands. Single crystal X-ray diffraction study of $([Eu(fda)(H_2O)_5]\cdot\frac{1}{2}(fda)\cdot 3H_2O)_n$ shows the formation of an inorganic polymer with infinite Eu-FDA chains. The structure of the metal organic framework of Tb(III) with H_4tma is described by the formula $[Tb(Htma)(H_2O)_2]$ and shows emission lines characteristic for Tb(III) when excited with near-UV radiation with a quantum yield of 67%, indicating that the ligand is acting as a highly efficient antenna for sensitizing Tb(III) emission.

(Parts of this chapter have been published:
S. Akerboom, W.T. Fu, M. Lutz and E. Bouwman, *Inorg. Chim. Acta* 387 (2012) 289; S. Akerboom, X. Liu, S.H.C. Askes, I. Mutikainen, W.T. Fu, E. Bouwman, manuscript submitted)

3.1 Introduction

As discussed in the first chapter of this thesis, LED-based solid state light sources have the potential to save substantial amounts of energy and reduce CO_2 emissions. For the approach relying on (partial) conversion of the emission of a blue or nUV emitting LED, phosphor materials are required [1, 2]. The phosphor materials that are currently applied in lighting technology are not suitable, as they cannot be efficiently excited by radiation in that spectral region [3-5]. Thus, new luminescent materials are needed, and complexes of the trivalent lanthanoid ions are promising candidates. As discovered in 1942 by Weissman, the ligands in these compounds can act as an antenna that absorbs incoming radiation and transfers it subsequently to the lanthanoid ion [6]. The favorable luminescent characteristics of the lanthanoids, such as millisecond lifetime and line like emission are, therefore, retained in these compounds [7]. Unlike the oxide-based phosphors, the preparation of complexes can be carried out at much lower temperatures, usually less than 200 °C. This can significantly reduce the production costs. In addition, complexes are molecule-based solid materials. They do not require highly pure rare earths as starting materials. Furthermore, recycling the expensive rare earths can be easily achieved from complexes, e.g. by dissolution in inorganic acids or by burning. Besides these advantages, the absorption properties of complexes can be, in principle, designed to match the excitation source by modifying the ligands. Ligands that are known to be good antennae for the lanthanoid ions are β-diketonates [8-10], Schiff bases [11, 12], macrocycles [13, 14] and aromatic carboxylates [15-17]. Recent work in our group has shown that pyridine-2,6-dicarboxamide is able to sensitize both Eu^{3+} and Tb^{3+} centered luminescence efficiently [18]. In subsequent work, it was found that the structurally similar pyridine-2,6-dicarboxylate is a suitable antenna for both Eu^{3+} and Tb^{3+} complexes with quantum yields as high as 72% and 68% respectively [19]. To continue on this line of research, the present study focuses on the structurally closely related furan-2,5-dicarboxylate (H_2fda) and 2-hydroxytrimesic acid (H_4tma) ligands as antennae for europium(III) and terbium(III).

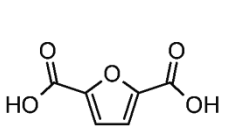

H_2fda

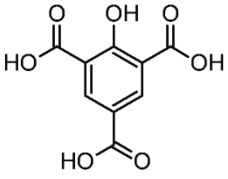

H_4tma

Ligand	Complex
H_2fda	Eufda1
	Tbfda1
	Eufda2
	Tbfda2
H_4tma	TbHtma

Figure 3.1: Overview of the ligands and complexes discussed in this chapter.

3.2 Experimental

3.2.1 General

Furan-2,5-dicarboxylic acid was purchased from Alfa-Aesar and was used as received. All other chemicals were purchased from Acros and used as-received. Pressure reaction vessels were purchased from Jinan Henghua Science & Technology Co., Ltd. To record NMR spectra, a Bruker DPX-300 spectrometer was used. Elemental analysis for C, H and N was performed on a Perkin-Elmer Paragon 2400 series II analyzer. Infrared spectra were recorded on a Perkin-Elmer Spectrum Two FTIR spectrometer equipped with the UATR Two accessory. Photoluminescence quantum yields were determined using the absolute method and an integrating sphere, following a modification of the procedure reported by de Mello et al. [20]. The integrating sphere (custom-made, based on the AvaSphere 30REFL) was connected to an irradiance calibrated CCD spectrometer (Avantes AvaSpec-2048UA). A 1000 Watt Xe-discharge lamp and a Spex monochromator were used as the excitation source. A Shimadzu RF-5301PC spectrofluoriphotometer was used to record excitation- and emission spectra. Luminescence lifetime was determined using an Edinburgh Instruments FLS920 spectrophotometer, using a pulsed laser as the excitation source. Stock solutions of europium chloride and terbium chloride were prepared by dissolving carefully weighed quantities of their respective oxides in a hot concentrated HCl solution followed by evaporation to dryness. The solids thus produced were dissolved in distilled water to yield 0.1 M solutions.

3.2.2 X-ray crystal structure determination

For **Eufda2** X-ray intensities were measured on a Bruker Kappa ApexII diffractometer with sealed tube and Triumph monochromator (λ = 0.71073 Å) up to a resolution of $(\sin\theta/\lambda)_{max}$ = 0.61 $Å^{-1}$ at a temperature of 150(2) K. The reflection profiles indicated a high mosaicity. Intensity integration was performed with the SAINT software [21]. An absorption correction based on multiple measured reflections was performed with SADABS [22] (0.56-0.75 correction range). The structure was solved with automated Patterson methods using the program DIRDIF [23] and refined with SHELXL-97 [24] against F^2 of all reflections. Hydrogen atoms were located in difference Fourier maps (hydrogen positions at O5W and O6W unreliable). C-H hydrogen atoms were refined with a riding model, O-H hydrogen atoms were kept fixed at their located positions. Geometry calculations and checking for higher symmetry was performed with the PLATON program [25]. For **TbHtma**, a crystal was selected for the X-ray measurements and mounted to the glass fiber using the oil drop method and data were collected at 173 K on a Nonius Kappa CCD diffractometer (Mo-Kα radiation, graphite monochromator, λ = 0.71073 Å) [26]. The intensity data were corrected for Lorentz and polarization effects, and for absorption. The programs COLLECT, SHELXS–97, SHELXL–97 were used for data reduction, structure

solution and structure refinement, respectively [24, 27, 28]. The nonhydrogen atoms were refined anisotropically. The hydrogen atoms were determined at the difference map and refined isotropically riding with the heavy atom connected except O2 hydrogen and water O8 hydrogens, which were refined isotropically. Further details on the crystal structure determination of **Eufda2** and **TbHtma** are given in Table 3.1.

3.2.3 Synthesis

2-hydroxy-trimesic acid (H_4tma)

Following literature procedures, 4-methylphenol (29 mmol, 3.0 g) was converted into 2-methoxy-trimesic acid [29-32]. Subsequently, this compound was converted into 2-hydroxy-trimesic acid by refluxing in 100 mL of 33% HBr in acetic acid for 120 minutes. The hot mixture was poured onto ice, after which the compound precipitated as a white microcrystalline solid. This was filtrated and dried in vacuo at 50 °C to give 2.7 g (12 mmol) of product in an overall yield of 43% based on 4-methyl-phenol. ^{1}H NMR (300 MHz, D_2O): δ 8.48 (s, 2H, H_{ar}), 8.04 (s, broad, 1H, OH). ^{13}C NMR (75 MHz, D_2O): δ 169.20 (-**C**OOH), 168.10 (-**C**OOH), 166.31 (**C**-OH), 136.85 (**C**-H), 118.12 (**C**-CO_2H), 117.44 (**C**-CO_2H). IR (ν, cm^{-1}): 2850(w, br), 1701(m), 1659(m), 1595(m), 1477(m), 1395(s), 1308(m), 1262(s), 1232(s), 1176(s), 1262(s), 1231(s), 1117(m), 891(m), 815(s), 767(m), 693(s), 652(m).

*$(H_2NMe_2)_5Ln_4Cl_3(fda)_7$ (Ln = Eu: **Eufda1**, Ln = Tb: **Tbfda1**)*

General procedure: 0.5 mmol of $LnCl_3{\cdot}xH_2O$, obtained by evaporation of 5 mL of the stock solutions, was dissolved in 10 mL of dmf. Next, 1.5 mmol of furan-2,5-dicarboxylic acid was added to this solution, which was then heated to reflux for 60 minutes. The suspension was cooled down to room temperature and the precipitates were collected by filtration and washed with ethanol. After drying the compounds were obtained in a yield of 59% (*Ln* = Eu) and 64% (*Ln* = Tb) as microcrystalline solids.

*$(H_2NMe_2)_5Eu_4Cl_3(fda)_7$ (**Eufda1**)*

Elemental analysis calculated for $C_{52}H_{54}Cl_3Eu_4N_5O_{35}$ (%): C 30.87, H 2.69, N 3.46, found (%) C 30.62, H 2.70, N 3.57. IR (ν/cm^{-1}): 1628(m), 1576(vs), 1539(s), 1362(vs), 1224(w), 1104(w), 1016(w), 780(vs), 676(m), 618(m), 494(s), 374(m).

*$(H2NMe_2)_6Tb_4Cl_4(fda)_7{\cdot}3H_2O$ (**Tbfda1**)*

Elemental analysis calculated for $C_{54}H_{60}Cl_3Tb_4N_5O_{38}$ (%): C 29.67, H 2.87, N 3.33, found (%) C 29.63, H 2.80, N 3.24. IR (ν/cm^{-1}): 1628(m), 1576(vs), 1538(s), 1362(vs), 1226(w), 1104(w), 1016(w), 780(vs), 678(m), 618(m), 496(s), 378(m).

$([Ln(fda)\cdot(H_2O)_5]\cdot\frac{1}{2}(fda)\cdot 3H_2O)_n$ (Ln = Eu: ***Eufda2****, Ln = Tb:* ***Tbfda2)***

In order to grow single crystals of $(H_2NMe_2)_6Ln_4Cl_4(fda)_7$, an attempt was made to recrystallize the solid. The compounds are insoluble in most common solvents such ethanol, methanol, chloroform, acetone, but are sparingly soluble in boiling water. **Eufda1** and **Tbfda1** were dissolved in the minimum amount of boiling water to yield clear solutions, which were slowly cooled to room temperature. The flasks with the solutions were then stored at 4 °C for several weeks, which resulted in the formation of colorless needle shaped crystals.

Eufda2 IR (ν/cm^{-1}): 3898(w, br), 1558(s), 1344(s), 1224(m), 1018(m), 966(m), 822(m), 778(s), 486(s). **Tbfda2** IR (ν_{max}/cm^{-1}): 3235(w, br), 1558(s), 1354(s), 1228(m), 1020(m), 968(m), 832(m), 782(m), 470(m).

$[Tb(Htma)(H_2O)_2]$ ***TbHtma***

A 20 mL teflon lined stainless steel pressure vessel was charged with 37 mg $TbCl_3\cdot 5H_2O$ (0.1 mmol), 67.8 mg (0.3 mmol) of H_4fda and 10 mL of demineralized water. The vessel was buried in a sand bath holding 14 kg of sand, which was then placed in an oven. The reaction mixture was reacted at 160 °C under autogenous pressure for three days. Then, the vessel was cooled down to 100 °C at a rate of 5 °C per hour, and to room temperature by natural cooling of the sand bath. The pale yellow crystals were filtered and washed with water and ethanol. Yield: 20 mg, 52% based on Tb(III). IR (ν/cm^{-1}): 3484(w, br), 1630(m), 1582(s), 1523(s), 1424(s), 1367(s), 1280(s), 1116(w), 838(w), 827(w), 787(s), 702(s), 560(s). Elemental analysis calcd (%) for $C_9H_5O_8Tb$, [Tb(Htma)(H_2O)]: C 27.02, H 1.26 found: C 26.72, H 1.22.

3.3 Results and discussion

3.3.1 Synthesis and characterization

Eufda1 and **Tbfda1** have been successfully synthesized following a method described by Mooibroek *et al.*, which relies on the thermal decomposition of dmf to carbon monoxide and dimethylamine during reflux [19]. The dimethylamine thus formed facilitates the deprotonation of furan-2,5-dicarboxylic acid, allowing complex formation with the lanthanoid ion present.

The ligand H_4tma was readily obtained from 4-methylphenol following literature procedures to 2-methoxy-trimesic acid, followed by ether hydrolysis catalyzed by HBr, in satisfactory yield. Complex synthesis of terbium salts with this ligand via conventional methods failed to give pure compounds; hydrothermal synthesis methods appeared to give better results. Although the final compound has a metal to ligand ratio of 1:1, the use of a metal to ligand ratio of 1:3 in the hydrothermal complex synthesis was found to produce the desired compound in highest yields. It was found that a concentration of 10^{-2} M of Tb(III)

ions resulted in the formation of the largest crystals, being suitable for X-ray diffraction. Experiments using M:L ratios of 1:1 and 1:2 were found to give comparatively low yields of luminescent material, while Tb(III) concentrations in excess of $2 \cdot 10^{-2}$ M resulted in formation of microcrystalline materials. Formation of a complex is evidenced by the IR spectra of H_4tma and **TbHtma**; the absorption bands from the free-ligand carbonyl groups around 1660 cm^{-1} are shifted to 1580 cm^{-1} in the complex. The **TbHtma** was dried in a vacuum oven at 60 °C prior to elemental analysis, which resulted in driving off one mole of water from the compound.

3.3.2 X-ray crystal structure determination

A projection of part of the single crystal structure of **Eufda2** is shown in Figure 3.2; experimental crystallographic data are given in Table 3.1. The crystal structure determination reveals infinite Eu-fda chains, a single non-coordinating doubly deprotonated ligand molecule for every two lanthanoid ions and non-coordinated lattice water molecules. Two independent europium ions are present in the asymmetric unit; both europium ions are nine-coordinated. The coordination sphere of each lanthanoid ion contains four oxygen atoms from the carboxylate moiety of the ligand and is further saturated by coordination of five water molecules. The coordination geometry can be described as a distorted monocapped square antiprism, with a water molecule as top vertex, three water molecules and one carboxylato oxygen atom in the top square and a lower square comprising a single water molecule and three carboxylato oxygen atoms. The Eu-O distances are given in Table 3.2; they range from 2.378(2) to 2.580(2) Å, which are as expected [33]. Unlike the complexes with

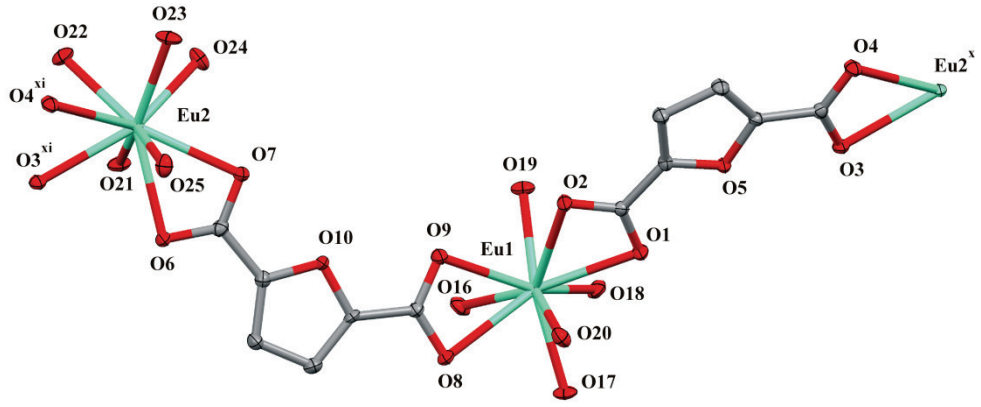

*Figure 3.2: projection of part of the crystal structure of **Eufda2**, showing the atom labeling scheme and the two Eu(III) sites. Atoms are shown as 50% displacement ellipsoids and hydrogen atoms are omitted for clarity. Symmetry operations: x (x, –1+y, 1+z); xi (x, 1+y, –1+z).*

pyridine-2,6-dicarboxylate and pyridine-2,6-dicarboxamide ligands reported before, the aromatic heteroatom is not coordinated to the lanthanoid. This is readily explained by the low basicity of the furan oxygen compared to the pyridine nitrogen. Perhaps the most striking feature is the presence of non-coordinating ligand molecules in the crystal structure. These ligands are stacked between the relatively flat Eu-fda chains and stabilize the crystal structure further by extensive hydrogen bonding involving nearby water molecules; hydrogen bond distances are given in Table 3.3. The coordinated ligand molecules also accept hydrogen bonds from non-coordinating water molecules, resulting in a 3-dimensional hydrogen bonding network. The presence of lattice water molecules is in agreement with the observation that the crystals rapidly decompose when removed from the mother liquor.

A projection of the crystal structure of **TbHtma** is given in Figure 3.3 and crystallographic data are summarized in Table 3.1. The asymmetric unit of **TbHtma** contains a single Tb(III) ion, one ligand and two molecules of water. The Tb ion has a coordination number of eight and the geometry around the Tb(III) ion can be described as a distorted biaugmented triangular prism. The two triangular faces of the prism are defined

Table 3.1: Details on the single crystal structure determination of complexes Eufda2 and TbHtma.

	Eufda2	**TbHtma**
formula	$C_{18}H_{38}Eu_2O_{31}$	$C_9H_7O_9Tb$
fw	1054.40	418.08
crystal size [mm^3]	0.56 × 0.13 × 0.05	0.02 × 0.04 × 0.28
crystal color	colorless	colorless
crystal system	triclinic	monoclinic
space group	$P\bar{1}$ (no. 2)	$P2_1/c$ (no.14)
a [Å]	10.7780(11)	9.402(1)
b [Å]	10.8948(11)	6.5399(5)
c [Å]	15.1161(15)	16.147(1)
α [°]	83.552(4)	90
β [°]	85.476(4)	110.95(1)
γ [°]	84.133(4)	90
V [$Å^3$]	1750.4(3)	927.2(2)
Z	2	4
d_{calc} [g/cm^3]	2.000	2.995
μ [mm^{-1}]	3.661	7.680
refl. measured / unique	51429 / 6461	13479 / 1636
parameters / restraints	460 / 0	193 / 3
R1/wR2 [I>2σ(I)]	0.0226 / 0.0569	0.0174 / 0.0424
R1/wR2 [all refl.]	0.0248 / 0.0585	0.0178 / 0.0427
S	1.111	1.17
$\rho_{min/max}$ [$e/Å^3$]	–1.05 / 2.08	–0.93 / 0.69

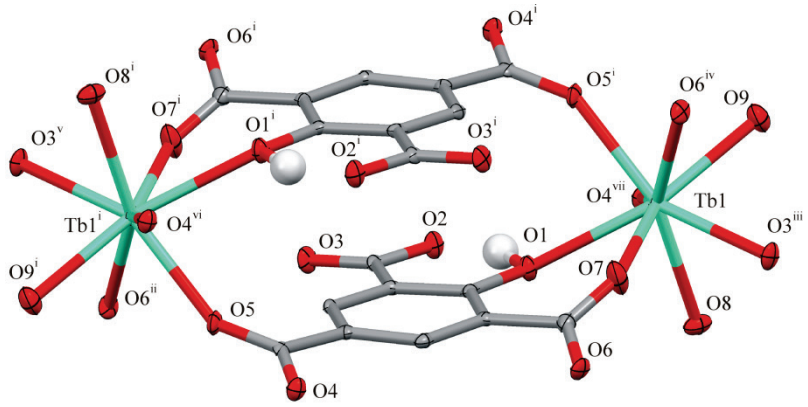

*Figure 3.3: Projection of part of the structure of **TbHtma** showing the labeling scheme and two sites for Tb(III). Atoms are shown as 30% displacement ellipsoids and hydrogen atoms except for H1 are omitted for clarity. Symmetry operations: i (2 – x, 1 – y, z); ii (x, 3/2 – y, – 1/2 + z); iii (x, 3/2 – y, 1/2 + z); iv (2 – x, – 1/2 + y, 1/2 – z); v (2 – x, – 1/2 + y, – 1/2 – z); vi (3 – x, 1 – y, – z); vii (– 1 + x, y, z).*

by (O1, O7, O8) and ($O5^{i}$, $O6^{iv}$, O9); the apexes of the square pyramids formed at two of the faces of this prism are defined by $O3^{iii}$ and $O4^{vii}$. Tb-O bond lengths are listed in Table 3.4; they range from 2.255(2) to 2.435(3) Å, which is normal for this type of bonds [18, 19, 33, 34]. Of interest is the mode of coordination of the ligand to the Tb(III) ion.The ligand provides four end-on bonds *via* its carboxylate groups and a bidentate chelating mode of bonding through the phenol oxygen and one of its neighboring carboxylate groups. The binding modes of the ligand in **TbHtma** are illustrated in Figure 3.4. Noteworthy is the strong intramolecular hydrogen bond between the phenolic proton and the carboxylate O2, with a H···O2 bond distance of 1.403(2) Å. No further hydrogen bonds can be identified in the structure.

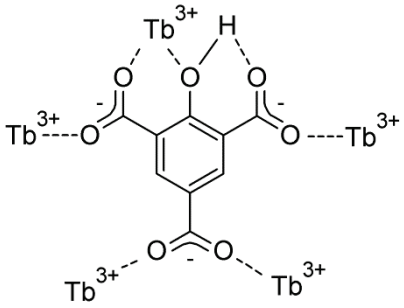

*Figure 3.4: schematic representation of the binding modes in **TbHtma**.*

The three dimensional structure of the network consists of puckered layers of ligand molecules, interacting by π-stacking with a perpendicular plane-to-plane distance of 3.265(1) Å, as is shown in Figure 3.5. The ligands of adjacent layers are connected by Tb(III) centers, and each Tb ion forms a node that connects five ligands, as is shown in Figure 3.6. All together, the three dimensional structure results in a highly dense packing with a calculated density as high as 2.995 g·cm^{-3}.

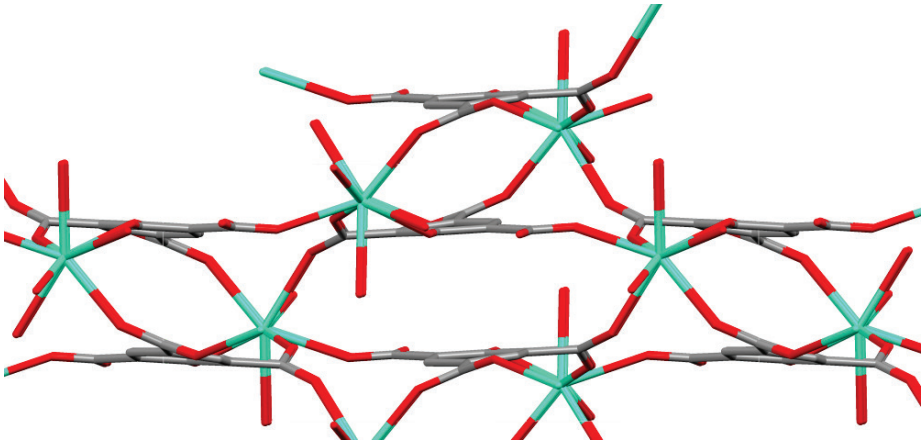

*Figure 3.5: Projection of the packing in **TbHtma** along the crystallographic a-axis, showing extensive pi-stacking in the structure.*

Table 3.2: selected bond distances (Å) and angles (°) for Eufda2. Atom labeling is shown in Figure 3.2.

Bond distance (Å)				Bond angle (°)	
Eu1-O1	2.483(2)	Eu2-O3	2.473(2)	O1-Eu1-O2	51.96(7)
Eu1-O2	2.544(2)	Eu2-O4	2.572(2)	O8-Eu1-O9	51.84(7)
Eu1-O8	2.580(2)	Eu2-O6	2.521(2)		
Eu1-O9	2.459(2)	Eu2-O7	2.499(2)		
Eu1-O16	2.409(2)	Eu2-O21	2.438(2)		
Eu1-O17	2.399(2)	Eu2-O22	2.413(2)		
Eu1-O18	2.434(2)	Eu2-O23	2.378(2)	O3-Eu2-O4	51.92(7)
Eu1-O19	2.442(2)	Eu2-O24	2.424(2)	O6-Eu2-O7	51.99(7)
Eu1-O20	2.417(2)	Eu2-O25	2.432(2)		

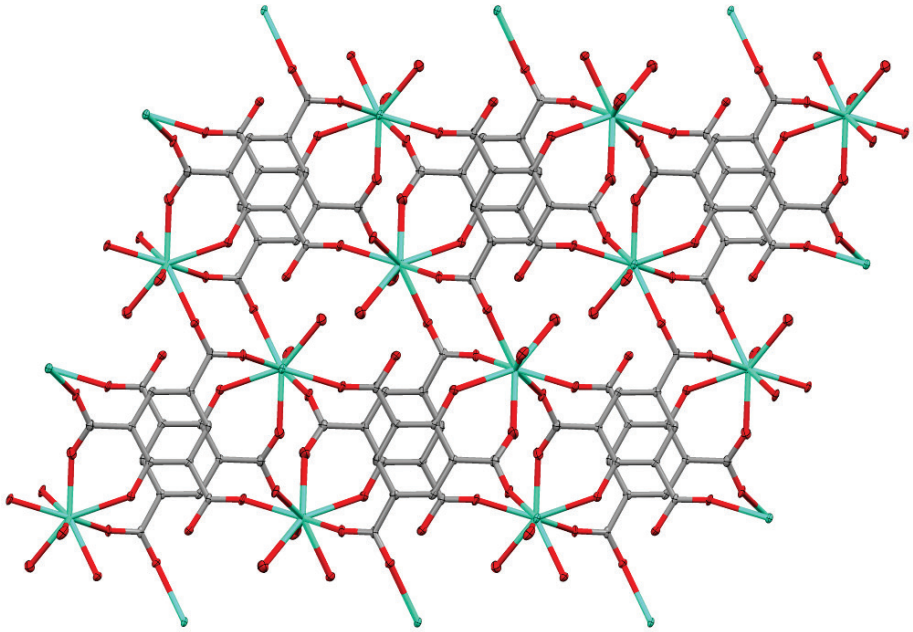

*Figure 3.6: A projection of the packing of **TbHtma** along the crystallographic y-axis, showing connectivity of the ligands and Tb(III) centers.*

Table 3.3: Hydrogen bonding geometries in Eufda2 with coordinated water as donor

D-H···A [Å]	D-H [Å]	H···A [Å]	D···A [Å]	D-H···A [°]
O16-H16A···O6^{i}	0.85	1.86	2.700(3)	173
O16-H16B···O5W^{ii}	0.92	1.85	2.759(3)	173
O17-H17A···O2W^{iii}	0.84	1.96	2.798(3)	175
O17-H17B···O3^{iv}	0.93	1.88	2.744(3)	154
O17-H17B···O5^{iv}	0.93	2.48	3.174(3)	131
O18-H18A···O1^{iv}	0.66	2.15	2.779(3)	160
O18-H18B···O3W^{ii}	0.95	1.83	2.763(3)	166
O19-H19A···O4W^{ii}	0.86	1.95	2.805(3)	172
O19-H19B···O4^{v}	0.80	1.98	2.781(3)	171
O20-H20A···O14^{i}	0.83	2.02	2.820(3)	162
O20-H20B···O14^{iii}	0.86	1.92	2.770(3)	169
O21-H21A···O8^{i}	0.74	2.02	2.728(3)	161
O21-H21B···O13	0.80	2.27	2.957(3)	144
O22-H22A···O1W^{vi}	0.81	2.00	2.783(3)	165
O22-H22B···O2^{vii}	0.92	1.77	2.688(3)	174
O23-H23A···O6W^{viii}	0.85	1.88	2.731(5)	177
O23-H23B···O9^{vii}	0.94	1.87	2.739(3)	153
O23-H23B···O10^{vii}	0.94	2.50	3.206(3)	132
O24-H24A···O7^{vii}	0.81	2.01	2.777(3)	160
O24-H24B···O11	0.85	1.94	2.781(3)	165
O25-H25A···O12^{ix}	0.88	1.87	2.730(3)	167
O25-H25B···O12^{vii}	0.88	1.99	2.805(4)	153

Symmetry operations: i (1 – x, 1 – y, 1 – z); ii (1 – x, – y, 1 – z); iii (x, y, z + 1); iv (1 – x, – y, 2 – z); v (2 – x, – y, 2 – z); vi (x + 1, y, z); vii (2 – x, 1 – y, 1 – z); viii (x + 1, y + 1, z); ix (x, y + 1, z).

Table 3.4: selected bond distances (Å) and angles (°) for TbHtma. Atom labeling is shown in Figure 3.3.

Bond distance		Bond angle	
Tb1-O1	2.403(3)	O3^{iii}-Tb1-O4^{vii}	121.40(9)
Tb1-O3^{iii}	2.287(2)	O5^{i}-Tb1-O6^{iv}	71.03(9)
Tb1-O4^{vii}	2.354(2)	O5^{i}-Tb1-O9	85.76(9)
Tb1-O5^{i}	2.255(2)	O6^{iv}-Tb1-O9	75.25(9)
Tb1-O6^{iv}	2.353(2)	O1-Tb1-O7	66.2(1)
Tb1-O7	2.274(3)	O1-Tb1-O8	79.38(9)
Tb1-O8	2.435(3)	O7-Tb1-O8	90.8(1)
Tb1-O9	2.336(3)		
Hydrogen bond			
O2···H1	1.403(2)		

Symmetry operations: i (2 – x, 1 – y, z); iii (x, 3/2 – y, 1/2 + z); iv (2 – x, – 1/2 + y, 1/2 – z); vii (– 1 + x, y, z).

3.3.3 Photoluminescence

*Complexes with the **fda** ligand*

The room temperature luminescence spectra were recorded for all four compounds, and are shown in Figure 3.7. All compounds exhibit luminescence spectra characteristic of the respective *Ln*(III) ions upon excitation in the ligand absorption band.

The emission spectrum of **Eufda1** shows lines at 591, 614, 651 and 698 nm, corresponding to the $^5D_0 \rightarrow {}^7F_1$, $^5D_0 \rightarrow {}^7F_2$ and $^5D_0 \rightarrow {}^7F_4$ transitions, respectively. The $^5D_0 \rightarrow {}^7F_1$ transition is a magnetic dipole (MD) transition and as such virtually insensitive to the crystal field around the Eu(III) ion, while the forced electric dipole (ED) transitions $^5D_0 \rightarrow {}^7F_2$ and $^5D_0 \rightarrow {}^7F_4$ are [35]. The fact that the $^5D_0 \rightarrow {}^7F_2$ ED transition is much stronger than the MD transition indicates a low symmetry Eu^{3+} site, lacking an inversion centre [36]. Apart from the lanthanoid-centered emission, a weak broad emission band around 450 nm is present. This feature is likely due to some residual ligand emission, resulting from incomplete energy transfer of the ligand to the lanthanoid ion. The excitation spectrum features two broad bands centered on 230 nm and 320 nm, which is typical for ligand-centered transitions. In addition, the strong line around 395 nm can be attributed to the ($^5L_6$, $^5G_2$, $^5L_7$, $^5G_3$) $\leftarrow {}^7F_0$ transitions of Eu^{3+} [37]. The emission spectrum of **Eufda2** shows features similar to that of the **Eufda1** compound, with no significant shift of the emission lines. The broad ligand-centered emission is completely absent, indicating more complete ligand to lanthanoid energy transfer. Judged by the naked eye, the luminescence intensity of **Eufda2** is weak compared to **Eufda1** upon excitation by a standard UV lamp at 254 nm.

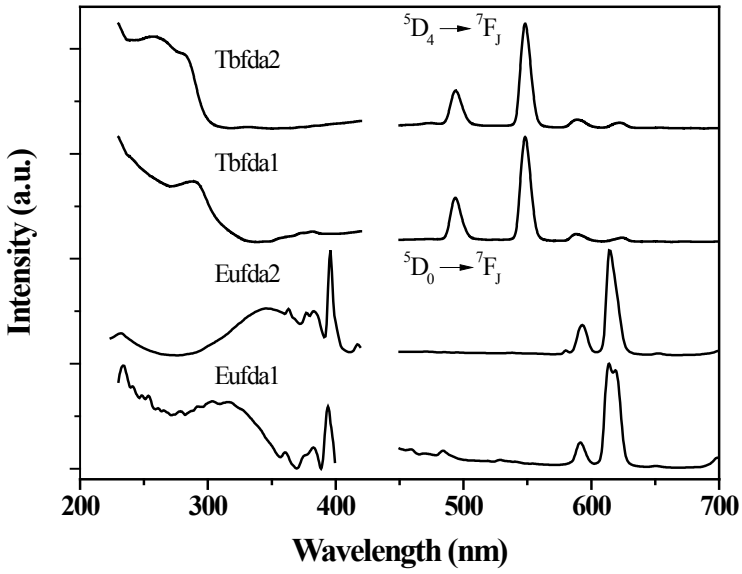

*Figure 3.7: From bottom to top: excitation (left) and emission (right) spectra for **Eufda1**, **Eufda2**, **Tbfda1** and **Tbfda2** recorded at room temperature in the solid state. The emission spectra are characteristic of the lanthanoid ion.*

This difference in intensity could not be quantified due to limitations of the equipment used to record the spectra. The excitation spectrum features a broad band around 340 nm that corresponds to a ligand-centered transition, and again a strong line around 395 nm due to direct excitation into the Eu^{3+} 4f manifold. Compared to the excitation spectrum of **Eufda1**, the excitation band of **Eufda2** is shifted to longer wavelengths, which is likely due to structural differences between **Eufda1** and **Eufda2**. Because of the forbidden nature of the 4f – 4f transitions, direct excitation into the 4f manifold is inefficient. Yet the intensity of this line is higher than the ligand-centered excitation band, indicating that ligand centered excitation is comparatively weak. When excited in the ligand-centered excitation band, the complex **Tbfda1** exhibits luminescence characteristic of Tb(III), with sharp lines at 494, 549, 589, and 624 nm. These are readily assigned to transitions from the $^5D_4$-state to $^7F_6$, $^7F_5$, $^7F_4$ and $^7F_3$ states, respectively. The excitation spectrum shows a broad band with a maximum at 289 nm, originating from the ligand centered $\pi^* \leftarrow \pi$ transition. This band extends to 320 nm, making it blue shifted compared to the excitation spectrum of **Eufda1**. In addition, a very weak band between 350 and 400 nm can be observed, resulting from excitations from the $^7F_6$ state to the $^5D_3$, $^5G_6$, $^5L_{10}$, $^5G_5$, $^5D_2$, $^5G_4$ and $^5L_9$ levels [37]. Comparing the **Tbfda2** emission spectrum with the one obtained for **Tbfda1**, no significant shift can be observed in the emission lines. The luminescence intensity of **Tbfda2** is weak compared to **Tbfda1** upon excitation by a standard UV lamp at 254 nm, as judged by the

eye. The excitation spectrum is somewhat blue shifted, featuring a single broad band with a maximum around 256 nm.
The furan-dicarboxylate ligand thus appears to be able to sensitize both Eu(III) and Tb(III) centered luminescence. The typical sensitization mechanism involves excitation of the ligand to an excited singlet state, S* ← S, followed by intersystem crossing to a triplet state S* → T* which is promoted by the heavy atom effect due to the lanthanoid ion. Subsequently, energy transfer from ligand to lanthanoid occurs, which is followed by lanthanoid-centered emission [38]. To avoid thermal repopulation of the ligand's triplet state, it must be at least 1,850 cm^{-1} higher in energy than the emissive level of the lanthanoid ion [39]. For Tb(III) complexes, this suggests a triplet state of at least 22,350 cm^{-1}, whereas for Eu(III) complexes the energetic requirements are less clear cut because of its multiple acceptor levels [40].
In both **Eufda2** and **Tbfda2**, the lanthanoid ion is surrounded by five molecules of water. It is known that water molecules present in the first coordination sphere of a lanthanoid ion are efficient luminescence quenchers [41, 42]. This is a result of energy transfer from the lanthanoid ion's excited state to O-H oscillators provided by the coordinated water molecules. Although the coordinated water does not fully quench the luminescence of the lanthanoid ion, it most certainly lowers both luminescence lifetime and intensity of **Eufda2** and **Tbfda2**. This may explain why **Eufda2** and **Tbfda2** give relatively weak luminescence compared to **Eufda1** and **Tbfda1**, respectively.

*Complex with the **Htma** ligand*

Upon illumination of **TbHtma** by a standard laboratory UV lamp emitting at 366 nm, the compound exhibits bright green emission. Photoluminescence spectra recorded in the solid-state for **TbHtma** are shown in Figure 3.8. The excitation spectrum shows a broad band in the nUV region with a maximum at 378 nm, which is typical for ligand-centered excitation. The emission spectrum is characteristic of the Tb(III)-ion, with transitions from the $^5D_4$ level to the ^7F_J manifold appearing as emission lines at 492 nm ($J = 6$), 549 nm ($J = 5$), 588 nm ($J = 4$) and 622 nm ($J = 3$). The $^5D_4 \rightarrow {}^7F_5$ transition dominates the emission spectrum, contributing over 70% to the total emission intensity. The emission lines are visibly split as a result of crystal field splitting. The photoluminescence quantum yield determined for this compound is 67% upon excitation at 380 nm. This is a remarkably high value, even higher than the value reported for the Tb(III) complex with 5-*tert*-butyl-2-hydroxy-isophthalate as a ligand (52%) or the Tb(III) complexes with 2-hydroxyphthalimide ligands (59 and 61%) [43, 44]. The luminescence decay curve is shown in Figure 3.9, and a single exponential function was fitted to it, yielding a lifetime of 0.50 ms. This is as expected for a Tb(III) compound with a single luminescent center.

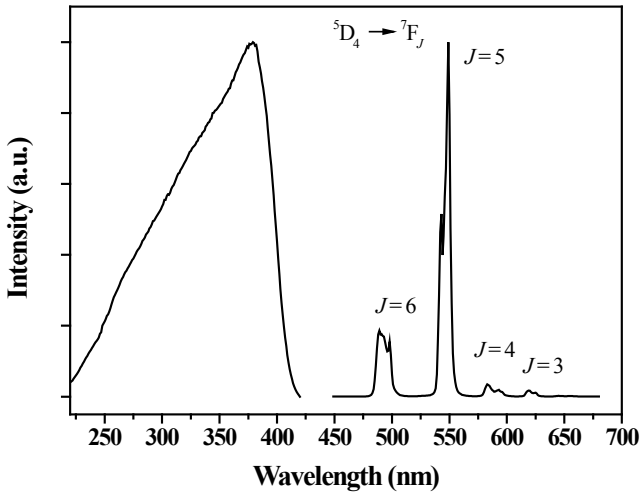

*Figure 3.8: Excitation (left, λ_{em} = 549 nm) and emission (right, λ_{exc} = 360 nm) spectra recorded for **TbHtma** in the solid state at room temperature. The emission spectrum is characteristic for the Tb(III) ion.*

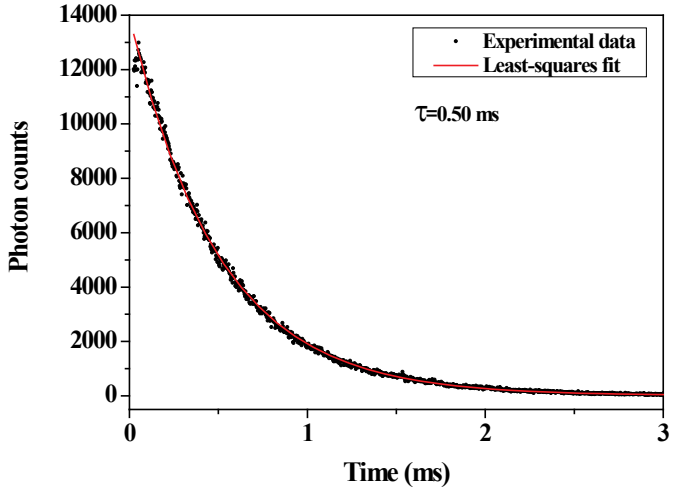

*Figure 3.9: The luminescence decay curve obtained for **TbHtma** in the solid state at room temperature (black line) and the least squares fit of a single-exponential decay-curve (red line).*

3.4 Conclusion

Four new Eu(III) and Tb(III) complexes have been synthesized using the furan-2,5-dicarboxylate ligand. Synthesis in dmf provides the anhydrous compounds described by the general formula $(H_2NMe_2)_6Ln_4Cl_4(fda)_7$ (*Ln* = Eu, Tb). Both compounds exhibit luminescence characteristic of the lanthanoid upon ligand centered excitation,

showing that in both cases the ligand acts as an antenna. Due to their low efficiency, neither compound is suitable for application as a phosphor material in LEDs. Recrystallisation from water results in the formation of $([Ln(fda)\cdot(H_2O)_5]\cdot\frac{1}{2}(fda)\cdot 3H_2O)_n$ (*Ln* = Eu, Tb) that also show lanthanoid-centered emission. The crystal structure of the latter compound reveals two low-symmetry *Ln*-sites, which is consistent with the luminescence spectra. 2-Hydroxy-trimesic acid has been synthesized from 4-methylphenol using standard literature procedures in non-optimized yields. It has been reacted with $TbCl_3$ under hydrothermal conditions, giving a novel metal-organic framework type compound with the formula $[Tb(Htma)(H_2O)_2]$. This compound exhibits very efficient photoluminescence characteristic for the Tb(III)-ion upon excitation of the ligand-centered absorption band by near-UV radiation. The quantum yield for this process is 67%, indicating that 2-hydroxytrimesic acid is a highly efficient antenna for the sensitization of Tb(III) emission. Owing to its high quantum yield and long excitation wavelength, this compound is an ideal candidate green phosphor material for application in LEDs.

3.5 References

[1] J.M. Phillips, M.E. Coltrin, M.H. Crawford, A.J. Fischer, M.R. Krames, R. Mueller-Mach, G.O. Mueller, Y. Ohno, L.E.S. Rohwer, J.A. Simmons, and J.Y. Tsao, *Laser Photonics Rev.*, 1 (2007) 307-333.

[2] R.-J. Xie and N. Hirosaki, *Sci. Technol. Adv. Mat.*, 8 (2007) 588-600.

[3] H.A. Höppe, *Angew. Chem., Int. Ed.*, 48 (2009) 3572-3582.

[4] A.A. Setlur, *Electrochem. Soc. Interface*, 18 (2009) 32-36.

[5] C.C. Lin and R.-S. Liu, *J. Phys. Chem. Lett.*, 2 (2011) 1268-1277.

[6] S.I. Weissman, *J. Chem. Phys.*, 10 (1942) 214-217.

[7] R.E. Whan and G.A. Crosby, *J. Mol. Spectrosc.*, 8 (1962) 315-327.

[8] K. Binnemans, *Chem. Rev.*, 109 (2009) 4283-4374.

[9] P. He, H.H. Wang, S.G. Liu, J.X. Shi, G. Wang, and M.L. Gong, *Inorg. Chem.*, 48 (2009) 11382-11387.

[10] C.R. De Silva, J.R. Maeyer, R. Wang, G.S. Nichol, and Z. Zheng, *Inorg. Chim. Acta*, 360 (2007) 3543-3552.

[11] R.D. Archer, H. Chen, and L.C. Thompson, *Inorg. Chem.*, 37 (1998) 2089-2095.

[12] H. Chen and R.D. Archer, *Inorg. Chem.*, 33 (1994) 5195-5202.

[13] D. Parker, P.K. Senanayake, and J.A.G. Williams, *J. Chem. Soc., Perkin Trans. 2*, (1998) 2129-2140.

[14] J.-C.G. Bünzli, *J. Alloys Compd.*, 408-412 (2006) 934-944.

[15] V. Tsaryuk, K. Zhuravlev, V. Zolin, P. Gawryszewska, J. Legendziewicz, V. Kudryashova, and I. Pekareva, *J. Photochem. Photobiol., A*, 177 (2006) 314-323.

[16] K. Liu, G. Jia, Y. Zheng, Y. Song, M. Yang, Y. Huang, L. Zhang, and H. You, *Inorg. Chem. Commun.*, 12 (2009) 1246-1249.

[17] T. Zhu, K. Ikarashi, T. Ishigaki, K. Uematsu, K. Toda, H. Okawa, and M. Sato, *Inorg. Chim. Acta*, 362 (2009) 3407-3414.

[18] S. Tanase, P.M. Gallego, R. de Gelder, and W.T. Fu, *Inorg. Chim. Acta*, 360 (2007) 102-108.

[19] T.J. Mooibroek, P. Gamez, A. Pevec, M. Kasunič, B. Kozlevčar, W.T. Fu, and J. Reedijk, *Dalton Trans.*, 39 (2010) 6483-6487.
[20] J.C. de Mello, H.F. Wittmann, and R.H. Friend, *Adv. Mater.*, 9 (1997) 230-232.
[21] Bruker, *SAINT-plus*, 2001. Bruker AXS Inc: Madison, Wisconsin, USA. p.
[22] G.M. Sheldrick, *SADABS: Area-Detector Absorption Correction*, 1999. Universität Göttingen: Göttingen, Germany. p.
[23] P.T. Beurskens, G. Beurskens, R. de Gelder, S. Garcia-Granda, R.O. Gould, and J.M.M. Smits, *The DIRDIF2008 program system*, 2008. Crystallography Laboratory, University of Nijmegen: Nijmegen, The Netherlands. p.
[24] G.M. Sheldrick, *Acta Crystallogr., Sect. A: Found. Crystallogr.*, 64 (2008) 112-122.
[25] A.L. Spek, *Acta Crystallogr., Sect. D: Biol. Crystallogr.*, 65 (2009) 148-155.
[26] T. Kottke and D. Stalke, *J. Appl. Crystallogr.*, 26 (1993) 615-619.
[27] G.M. Sheldrick, *SHELXS–97*, *Bruker AXS Inc., Madison, Wisconsin*, 1997.
[28] Nonius, *COLLECT*, *Nonius BV, Delft, The Netherlands*, 2002.
[29] F. Ullmann and K. Brittner, *Ber. Dtsch. Chem. Ges.*, 42 (1909) 2539-2548.
[30] H.T. Openshaw and R. Robinson, *J. Chem. Soc.*, (1946) 912-918.
[31] R. Gupta, S. Mukherjee, and R. Mukherjee, *J. Chem. Soc., Dalton Trans.*, (1999) 4025-4030.
[32] K.N. Raymond, S. Petoud, and J. Xu, Aromatic Triamide-Lanthanide Complexes, Pat.no 20090036537, 2009.
[33] A.G. Orpen, L. Brammer, F.H. Allen, O. Kennard, D.G. Watson, and R. Taylor, *J. Chem. Soc., Dalton Trans.*, (1989) S1-S83.
[34] X.-Q. Zhao, B. Zhao, S. Wei, and P. Cheng, *Inorg. Chem.*, 48 (2009) 11048-11057.
[35] C. Görller-Walrand and K. Binnemans, *Spectral intensities of f-f transitions*, in *Handbook on the Physics and Chemistry of Rare Earths*, 1998, Elsevier. 99-264.
[36] R. Reisfeld, E. Zigansky, and M. Gaft, *Mol. Phys.*, 102 (2004) 1319 - 1330.
[37] W.T. Carnall, P.R. Fields, and K. Rajnak, *J. Chem. Phys.*, 49 (1968) 4412-4423.
[38] W.F. Sager, N. Filipescu, and F.A. Serafin, *J. Phys. Chem.*, 69 (1965) 1092-1100.
[39] M. Latva, H. Takalo, V.M. Mukkala, C. Matachescu, J.C. Rodriguez-Ubis, and J. Kankare, *J. Lumin.*, 75 (1997) 149-169.
[40] W.T. Carnall, P.R. Fields, and K. Rajnak, *J. Chem. Phys.*, 49 (1968) 4447-4449.
[41] S. Meshkova, Z. Topilova, M. Lozinskii, and D. Bol'shoi, *J. Appl. Spectrosc.*, 64 (1997) 229-233.
[42] Y. Hasegawa, Y. Wada, and S. Yanagida, *J. Photochem. Photobiol., C*, 5 (2004) 183-202.
[43] L. Benisvy, P. Gamez, W.T. Fu, H. Kooijman, A.L. Spek, A. Meijerink, and J. Reedijk, *Dalton Trans.*, (2008) 3147-3149.
[44] S. Petoud, S.M. Cohen, J.-C.G. Bünzli, and K.N. Raymond, *J. Am. Chem. Soc.*, 125 (2003) 13324-13325.

4 Phenol-type ligands as sensitizers

*Eight new complexes of europium(III) and terbium(III) using 2-(4,5-dihydro-1,3-oxazol-2-yl)phenol (H**L1**) and 2-(4,5-dihydro-1,3-thiazol-2-yl)phenol (H**L2**) as ligands have been prepared in yields ranging between 74 and 100%. Depending on the synthetic strategy employed, ligand-to-metal ratios of 1:3 and 1:4 can be achieved, giving rise to compounds with the formulae $[Ln_2(L)_6]$ and $NR_4[Ln(L)_4]$, Ln = Eu, Tb and R = ethyl, n-butyl. An attempt at recrystallisation of the complexes from dmso resulted in the formation of an octanuclear complex held tightly together by carbonate ions that have been formed from CO_2 captured from the atmosphere. Those compounds are described by the general formula $[Na_2(Ln(\mathbf{L1})_3)_2(CO_3)(dmso)_2]_2$. Of five compounds, the crystal structures have been determined, all showing a bidentate mode of binding of the ligand via the phenolate oxygen and the nitrogen atom of the five-membered ring. The compounds $[Tb_2(\mathbf{L1})_6]$, $NBu_4[Tb(\mathbf{L1})_4]$, $[Tb_2(\mathbf{L2})_6]$ and $[Na_2(Tb(\mathbf{L1})_3)_2(CO_3)(dmso)_2]_2$ show bright luminescence characteristic for the Tb(III) ion upon excitation with near-UV radiation, with quantum yields ranging from 16% to 79%. Strong emission typical for the Eu(III) ion is observed for $NBu_4[Eu(\mathbf{L1})_4]$ and $NEt_4[Eu(\mathbf{L2})_4]$ with quantum yields of 43% and 20%, respectively. The other compounds are only very weakly luminescent.*

(This Chapter will be published: S. Akerboom, E. Tom Hazenberg, I. Schrader, S.F. Verbeek, I. Mutikainen, W. T. Fu, E. Bouwman, manuscript in preparation)

4.1 Introduction

In Chapter 1 of this thesis, it is discussed how highly energy efficient LED-based Solid State Lighting (SSL) sources have the potential to replace the conventional light bulbs [1]. This in turn would save large amounts of energy and reduce CO_2 emissions [2]. New phosphor materials that can efficiently convert nUV or blue radiation into visible light are required for the development of highly efficient SSLs [3-6]. Although phosphor materials are widely used in today's lighting and display technologies, they have been designed for high energy excitation sources and cannot be efficiently excited in the nUV of blue spectral region [7]. Complexes of the trivalent lanthanoid ions are attractive candidate phosphor materials because of their broad, ligand centered excitation bands and line like emission spectra characteristic of the lanthanoid ion [8]. Ligands that are currently known to efficiently sensitize luminescence of the lanthanoids include beta-diketonates, aromatic carboxylates, salicylates and polycyclic heteroaromatic ligands such as 1,10-phenanthroline and 2,2'-bipyridine [9-16]. Previous work on the use of benzoxazole and benzothiazole substituted pyridine-2-carboxylate as a ligand to the lanthanoids has demonstrated these ligands to be highly capable of sensitizing lanthanoid-centered luminescence, in particular that of Eu(III) [17]. Salicylate-type ligands are found to be highly efficient at sensitizing luminescence by the Tb(III) ion, while they generally fail to excite Eu(III) luminescence [14, 18]. In view of this, oxazoline and thiazoline substituted phenols seem attractive antenna ligands for enhancing luminescence of Eu(III) and Tb(III) ions. This Chapter reports on the synthesis, characterization, structure and photophysical properties of a family of Eu(III) and Tb(III) complexes with 2-(4,5-dihydro-1,3-oxazol-2-yl) phenol (H**L1**) and 2-(4,5-dihydro-1,3-thiazol-2-yl)phenol (H**L2**) as ligands. The compounds discussed are shown in Figure 4.1.

H**L1**	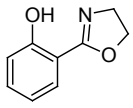	$NBu_4[Tb(\mathbf{L1})_4]$	Tb**L1**_4
		$NBu_4[Eu(\mathbf{L1})_4]$	Eu**L1**_4
		$[Tb(\mathbf{L1})_3]_2$	Tb**L1**_3
		$[Eu(\mathbf{L1})_3]_2$	Eu**L1**_3
		$[Na_2(Tb(\mathbf{L1})_3)_2(CO_3)(dmso)_2]_2$	Tb**L1**_CO_3
		$[Na_2(Eu(\mathbf{L1})_3)_2(CO_3)(dmso)_2]_2$	Eu**L1**_CO_3
H**L2**	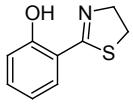	$NEt_4[Tb(\mathbf{L2})_4]$	Tb**L2**_4
		$NEt_4[Eu(\mathbf{L2})_4]$	Eu**L2**_4
		$[Tb(\mathbf{L2})_3]$	Tb**L2**_3
		$[Eu(\mathbf{L2})_3]$	Eu**L2**_3

Figure 4.1: Schematic overview of the ligands and coordination compounds discussed in this chapter. The rightmost column indicates the designations used.

4.2 Experimental

4.2.1 General

NMR spectra were recorded on a Bruker DPX-300 spectrometer. Infrared spectra were recorded on a Perkin-Elmer Paragon 1000 FTIR spectrometer equipped with a Golden Gate ATR. Elemental analysis for C, H, N and S was performed on a Perkin-Elmer 2400 series II analyzer. Excitation and emission spectra were recorded on a Shimadzu RF–5301PC spectrofluoriphotometer equipped with a solid state sample holder and a UV-blocking filter. Photoluminescence quantum yields were recorded on an Avantes AvaSpec-2048 CCD spectrometer connected to a custom made integrating sphere, based on the AvaSphere 30REFL, using a modification of the absolute method reported by De Mello [19]. A 1000 Watt Xe-discharge lamp and a SPEX monochromator were used as the excitation source. UV-Vis absorption spectra were measured with the same spectrometer, connected to a solid state reflection probe and using an AvaLight DH-S-BAL light source. For determination of luminescence lifetime, an Edinburgh Instruments FLS920 spectrophotometer was used together with a pulsed laser excitation source.

4.2.2 X-ray crystallography

Crystals of Tb**L1**_3, Eu**L1**_4, Eu**L1**_CO_3 and Tb**L1**_CO_3 selected for the X–ray measurements were mounted to the glass fiber using the oil drop method and data were collected at 173 K on a Nonius Kappa CCD diffractometer (Mo-Kα radiation, graphite monochromator, λ = 0.71073 Å) [20]. The intensity data were corrected for Lorentz and polarization effects, and for absorption. The programs COLLECT, SHELXS–97, SHELXL–97 were used for data reduction, structure solution and structure refinement, respectively [21-23]. The non-hydrogen atoms were refined anisotropically. The hydrogen atoms were situated at the calculated positions and refined isotropically riding with the heavy atom connected. Eu**L1**_CO_3 and Tb**L1**_CO_3 are isomorphic with one coordinating dmso disordered over two positions with population parameters 0.75 and 0.25. The population parameters of the disordered dmso molecules were fixed during the final least-square cycles. Single crystal structure determination of Eu**L2**_4 was performed on a STOE IPDS 2T diffractometer, equipped with a Mo-anode (Mo-Kα radiation, λ = 0.71073 Å) as X-ray source, a graphite monochromator and an imaging plate as detector. The data was corrected for Lorentz and polarization effects and for absorption. The programs WinGX and SHELXS-97 were used for crystal structure determination and SHELXL-97 was used for structure refinement [21, 22, 24]. All atomic positions were restrained during refinement and hydrogen atoms were calculated for ideal positions due to the poor crystallininty of the compound.

4.2.3 Synthesis

*2-(4,5-dihydro-1,3-oxazol-2-yl)phenol (H**L1**)*

Following a modification of the procedure reported in [25]. Methyl salicylate (9.13 g, 60 mmol) and 2-aminoethanol (3.62 mL, 60 mmol) were refluxed under argon in a round-bottomed flask for one hour. The methanol that had formed was removed *in vacuo*, leaving the 2-aminoethyl salicylate as highly viscous oil. Subsequently, the oil was dissolved in 150 mL of dichloromethane. The resulting solution was cooled on ice and $SOCl_2$ (3.8 mL, 63 mmol) was added drop-wise under stirring. The flask was allowed to warm up to room temperature and stirred for 18 hours, resulting in the formation of a white precipitate. The solid compound was separated by filtration and air-dried after which it was taken up in 60 mL of 0.6 M aqueous sodium hydrogen carbonate. The product was extracted with diethyl ether (3 × 90 mL) and obtained as a crystalline solid after drying over magnesium sulfate and evaporation of the solvent. Yield: 5.2 g (32 mmol, 53%). ^{1}H NMR (300 MHz, dmso) δ /ppm: 7.64 (dd, J = 7.8, 1.8 Hz, 1H), 7.45 (m, 1H), 7.00 (dd, J = 8.4, 1.1 Hz, 1H) 6.94 (td, J = 7.5, 1.2 Hz, 1H), 4.48 (t, J = 9.3 Hz, 2H), 4.07 (t, J = 9.3 Hz, 2H). IR (ν/cm^{-1}): 2954(w), 2888(w), 1636(m), 1494(m), 1370(m), 1312(m), 1256(m), 1232(m), 1068(m), 938(m), 798(m), 754(s), 678(m), 536(m).

*2-(4,5-dihydro-1,3-thiazol-2-yl)phenol (H**L2**)*

Following a procedure reported by Minkkilä *et al.* [26]. A neat mixture of 2-hydroxybenzonitrile (2.32 g, 19.5 mmol) and 2-aminoethanethiol (2.26 g, 29.3 mmol) was stirred under heating to 100 °C for one hour After cooling, the mixture was treated with 1.0 M HCl (20 mL) and water (50 mL) and the resulting suspension was extracted with dichloromethane (4 × 70 mL). After drying the organic fraction over magnesium sulfate, the solvent was removed *in vacuo*, leaving the product as yellow needles. Yield, 2.6 g (14 mmol, 73%). ^{1}H NMR (300 MHz, $CDCl_3$) δ /ppm: 7.37 (m, 2H), 6.93 (m, 2H), 4.45 (t, J = 8.3 Hz, 2H), 3.34 (t, J = 8.3 Hz, 2H). IR (ν/cm^{-1}): 2932(w), 2860(w), 1623(w), 1593(s), 1573(m), 1488(s), 1455(m), 1408(m), 1330(m), 1256(m), 1223(s), 1154(m), 1122(m), 1118(m), 1040(m), 1013(s), 956(m), 932(s), 804(s), 754(s), 680(m), 665(m), 613(m), 566(m), 537(w).

*[Tb(**L1**)$_3$]$_2$ (Tb**L1**_3)*

H**L1** (0.16 g, 1.0 mmol) was dissolved in 20 mL of methanol and 0.50 mL of methanolic NaOH solution (2.0 M) was added. The solution was heated to just below its boiling point, after which a $TbCl_3$ solution (3.3 mL 0.1 M in methanol) was added. The resulting suspension was refluxed for one hour. The precipitate was filtered and dried *in vacuo* at 60 °C. Yield: 0.19 g (0.29 mmol, 87%) of a white solid. IR (ν/cm^{-1}): 2888(w), 1616(m), 1472(s), 1444(m), 1378(m), 1344(m), 1256(m), 1228(m), 1058(m), 856(m), 754(m),

686(m). Elemental analysis calculated (%) for $C_{27}H_{24}N_3O_6Tb$ ([Tb(**L1**)$_3$]): C, 50.25; H, 3.75; N, 6.51. Found (%): C, 50.04; H, 3.44; N 6.61.

*[Eu(**L1**)$_3$]$_2$ (Eu**L1**_3)*

Following the procedure described for Tb**L1**_3, but with a 0.1 M methanolic solution of $EuCl_3$ instead. Yield: 182 mg (0.29 mmol, 86%) of a white solid. IR (ν/cm^{-1}): 2888(w), 1616(m), 1472(s), 1444(m), 1378(m), 1344(m), 1256(m), 1228(m), 1058(m), 856(m), 754(m), 686(m). Elemental analysis calculated (%) for $C_{27}H_{24}EuN_3O_6$ ([Eu(**L1**)$_3$]): C, 50.79; H, 3.79; N, 6.58. Found (%): C, 49.46; H, 3.64; N 6.42.

*NBu$_4$[Tb(**L1**)$_4$] (Tb**L1**_4)*

H**L1** (0.16 g, 1.0 mmol) and tetra-n-butylammonium hydroxide (1.2 mL 1 M in methanol) were dissolved in methanol (20 mL) and the solution was heated to just below its boiling point. Next, 2.5 mL of a $TbCl_3$ solution (0.1 M in methanol) was added and the resulting suspension was refluxed for one hour. The solvent was removed using a rotary evaporator and the remaining solids were rinsed onto a glass filter using demineralized water and dried *in vacuo* at 60 °C. Yield: 0.22 g (0.21 mmol, 83%) of a white solid. IR (ν/cm^{-1}): 2958(w), 2892(w), 1622(s), 1540(w), 1472(s), 1446(m), 1346(s), 1258(m), 1228(m), 754(m). Elemental analysis calculated (%) for $C_{52}H_{74}N_5O_{11}Tb$ (NBu_4[Tb(**L1**)$_4$]·3H_2O): C, 56.57; H, 6.76; N, 6.34. Found (%): C, 55.64; H, 6.62; N 6.25.

*NBu$_4$[Eu(**L1**)$_4$] (Eu**L1**_4)*

Following the procedure described for Tb**L1**_4, but with a 0.1 M methanolic solution of $EuCl_3$ instead and starting from 6 mmol (0.98 g) of H**L1**. Yield 1.04 g (1.31 mmol, 88%) of a white powder. IR (ν/cm^{-1}): 2958(w), 1622(s), 1540(m), 1472(s), 1444(s), 1346(s), 1260(m), 1230(m), 1150w, 754(s). Elemental analysis calculated (%) for $C_{52}H_{68}N_5O_8Tb$ (NBu_4[Eu(**L1**)$_4$]·3H_2O): C, 56.93; H, 6.80; N, 6.38. Found (%): C, 56.61; H, 6.88; N 6.29.

*[Tb(**L2**)$_3$] (Tb**L2**_3)*

Using the procedure for Tb**L1**_3, starting from 0.60 mmol (107 mg) of H**L2** and 0.20 mmol of $TbCl_3$. Yield: 0.10 g (0.074 mmol, 74%) of a white solid. IR (ν/cm^{-1}): 2850(w), 1595(s), 1566(s), 1538(s), 1464(s), 1440(s), 1428(s), 1336(s), 1327(w), 1304(w), 1277(w), 1253(m), 1215(s), 1186(m), 1151(m), 1119(w), 1015(s), 945(m), 853(w), 829(m), 755(s), 744(s), 689(m), 658(m), 624(m), 590(m), 577(m), 530(m), 512(m), 504(m). Elemental analysis calculated (%) for $C_{27}H_{24}N_3O_3TbS_3$ ([Tb(**L2**)$_3$]): C, 46.75; H, 3.49; N, 6.06; S, 13.87. Found (%): C, 46.05; H, 3.67; N 6.01; S, 13.40.

*[Eu(**L2**)$_3$] (Eu**L2**_3)*

Using the procedure reported for Tb**L1**_3. Yield: 0.10 g (0.074 mmol, 74%) of a yellow powder. IR (ν/cm^{-1}): 2850(w), 1595(s), 1566(s), 1538(s), 1464(s), 1440(s), 1428(s), 1336(s), 1327(w), 1304(w), 1277(w), 1253(m), 1215(s), 1186(m), 1151(m), 1119(w),

1036(w), 1015(s), 945(m), 853(w), 829(m), 755(s), 744(s), 689(m), 658(m), 624(m), 590(m), 577(m). Elemental analysis calculated (%) for $C_{27}H_{24}EuN_3O_3S_3$ ([Eu(**L2**)$_3$]): C, 47.23; H, 3.52; N, 6.12; S, 14.01. Found (%): C, 46.34; H, 3.70; N 6.01; S, 13.58.

*NEt_4[Tb(**L2**)$_4$] (Tb**L2**_4)*

H**L2** (0.106 mg, 0.6 mmol) and tetra-ethylammonium hydroxide (0.42 mL 1.5 M in methanol) were dissolved in methanol (8 mL) and the solution was heated to just below its boiling point. Next, 1.5 mL of a $TbCl_3$ solution (0.1 M in methanol) was added and the resulting suspension was refluxed for one hour. The solvent was removed using a rotary evaporator and the solids were rinsed onto a glass filter using demineralized water and dried *in vacuo* at 60 °C. Yield: 144 mg (0.14 mmol, 96%) of a white solid. IR (ν/cm^{-1}): 2850(w), 1595(s), 1575(s), 1532(m), 1464(s), 1442(s), 1428(s), 1392(w), 1343(s), 1325(w), 1257(m), 1210(m), 1178(w), 1148(s), 1122(w), 1036(w), 1005(m), 937(m), 853(w), 829(s), 742(s), 673(m), 652(m), 624(m), 580(m), 530(m), 509(m). Elemental analysis calculated (%) for $C_{44}H_{52}N_5O_4S_4Tb$ (NEt_4[Tb(**L2**)$_4$]): C, 52.74; H, 5.23; N, 6.99. Found (%): C, 50.68; H, 5.23; N 6.99.

*NEt_4[Eu(**L2**)$_4$] (Eu**L2**_4)*

Following the procedure reported for Tb**L2**_4. Yield: 149 mg (0.15 mmol, 100%) of a yellow solid. IR (ν/cm^{-1}): 2850(w), 1595(s), 1575(s), 1532(m), 1464(s), 1442(s), 1428(s), 1392(w), 1343(s), 1325(w), 1257(m), 1210(m), 1178(w), 1148(s), 1122(w), 1036(w), 1005(m), 937(m), 853(w), 829(s), 742(s), 673(m), 652(m), 624(m), 580(m), 530(m), 509(m). Elemental analysis calculated (%) for $C_{44}H_{52}EuN_5O_4S_4$ (NEt_4[Eu(**L2**)$_4$]): C, 53.11; H, 5.27; N, 7.04. Found (%): C, 51.43; H, 4.78; N 6.86.

*[Na_2(Tb(**L1**)$_3$)$_2$(CO_3)(dmso)$_2$]$_2$ (Tb**L1**_CO_3)*

A reaction tube was charged with NaOH (50 mg, 1.25 mmol) and H**L1** (163 mg, 1.0 mmol) and 10 mL of dimethylsulfoxide (dmso) was added. On top of the dmso layer was added a layer of methanolic solution of $TbCl_3$ (3.3 mL 0.1 M). The tube was left open to the air and kept undisturbed. Within three weeks, crystals appeared at the interface of the solution. The methanol had evaporated over this period. IR (ν/cm^{-1}): 3380(w, br), 2973(w), 2902(w), 1622(vs), 1546(m), 1506(m), 1473(vs), 1445(s), 1415(m), 1373(m), 1343(s), 1327(m), 1285(w), 1258(m), 1231(s), 1154(m), 1134(w), 1054(vs), 1036(s), 1013(w), 949(s), 918(w), 850(s), 760(vs), 733(m), 688(s), 659(m), 581(s), 547(w), 535(m). Elemental analysis calculated (%) for $C_{59}H_{60}N_6Na_2O_{17}S_2Tb_2$ (Na_2[Tb(**L1**)$_3$]$_2$(CO_3)(dmso)$_2$): C, 45.63; H, 3.89; N, 5.41. Found (%): C, 43.79; H, 3.64; N 5.12.

*[Na_2(Eu(**L1**)$_3$)$_2$(CO_3)(dmso)$_2$]$_2$ (Eu**L1**_CO_3)*

Following the procedure reported for Tb**L1**_CO_3, using a methanolic solution of $EuCl_3$ (0.1 M) instead of the $TbCl_3$ solution. IR (ν/cm^{-1}): 3390(w, br), 2973(w), 2902(w), 1621(vs), 1545(m), 1504(m), 1473(vs), 1444(s), 1409(m), 1372(m), 1341(s), 1284(w), 1257(m),

1230(s), 1214(m), 1153(m), 1128(w), 1053(vs), 1036(s), 948(s), 918(w), 850(s), 760(vs), 730(m), 688(s), 659(m), 580(s), 545(w), 535(m). Elemental analysis calculated (%) for $C_{59}H_{60}Eu_2N_6Na_2O_{17}S_2$ ($Na_2(Eu(\mathbf{L1})_3)_2(CO_3)(dmso)_2$): C, 46.04; H, 3.93; N, 5.46. Found (%): C, 44.17; H, 3.45; N 5.25.

4.3 Results

4.3.1 Synthesis and characterization

The ligands H**L1** and H**L2** were readily obtained in acceptable yields following literature procedures. Several peaks in the IR spectrum of H**L1** are assigned as follows: the signal at 1643 cm^{-1} (C=N stretch), 1232 cm^{-1} (C-O stretch phenol) and 754 cm^{-1} (out of plane C-H bending in 1,2-disubstituted benzene ring). Likewise, the IR spectrum of H**L2** contains signals that are readily assigned to the molecule: 1593 cm^{-1} (C=N stretch), 1223 cm^{-1} (C-O stretch phenol) and 754 cm^{-1} (1,2-disubstituted benzene ring).

The complexes were typically synthesized by refluxing methanolic solutions of the lanthanoid salt, ligand and base mixed in the appropriate ratio. The solutions were heated to ensure complete dissolution of the ligands and to slow down the precipitation of the product. In general, the formation of precipitate was observed when the addition of lanthanoid solution was nearly complete. In general, the synthetic procedures offered the complexes in high yields, ranging between 74% for Eu**L2**_3 and Tb**L2**_3 to 100% for Eu**L2**_4.

The infrared spectra for the complexes with **L1** show bands due to ligand vibrations. Coordination of the ligand to the metal is evident from the red-shift of several peaks. The free-ligand C=N stretch at 1643 cm^{-1} for H**L1** is shifted to 1616 cm^{-1} in the complexes and also the phenol C-O stretch is shifted to a lower frequency in the complexes (1228 vs. 1232 cm^{-1}). The IR spectra for Tb**L1**_CO_3 and Eu**L1**_CO_3 are similar to of the other complexes with **L1**. The additional strong absorption at 1050 cm^{-1} can be assigned to the S=O stretching mode of the dmso molecules. For the complexes with **L2**, a shift of the phenol C-O vibration is observed from 1223 cm^{-1} in the free ligand to 1215 cm^{-1} in the 1:3 complexes and 1222 cm^{-1} in the 1:4 complexes. Interestingly, washing of the 1:4 complexes with **L1** and **L2** with demineralized water was found to be the best procedure for removing unreacted materials. Use of cold ethanol gave rise to the formation of complexes with a M:L ratio of 1:3, as found from elemental analysis. Apparently, the tetra-alkyl ammonium salt of the ligand is relatively easily washed out of the 1:4 complexes. Several approaches were undertaken to obtain single crystals of the compounds. Compounds Eu**L1**_CO_3 and Tb**L1**_CO_3 were obtained in an attempt to grow single crystals of Eu**L1**_3 and Tb**L2**_3. The crystals that have formed indeed show a lanthanoid-to-**L1** ratio of 1:3, but are in fact bimetallic octanuclear compounds containing Na(I) and *Ln*(III) ions that are tightly bridged by carbonate anions. The only possible source of those carbonate ions is CO_2 captured from the air by the basic solution.

4.3.2 Single crystal structure determinations

Experimental data on the crystal structure determination are given in Table 4.1 for compounds Tb**L1**_3, Eu**L1**_4, Eu**L2**_4, Eu**L1**_CO_3 and Tb**L1**_CO_3. Relevant bond lengths and angles for Tb**L1**_3, Eu**L1**_4 and Eu**L2**_4 are given in Table 4.2 and in those for Eu**L1**_CO_3 and Tb**L1**_CO_3 are listed in Table 4.3. Note that the quality of the structure determined for Eu**L2**_4 is low. Hence, it is shown for comparison with Eu**L1**_4 only. In all compounds, the ligand binds in a bidentate mode to the lanthanoid ion through its phenolate oxygen and the nitrogen atom of the five-membered ring. A projection of the structure of Tb**L1**_3 is shown in Figure 4.2. It is a dimeric complex in which the Tb(III) ion has a N_3O_4 coordination sphere. Each Tb ion is surrounded by three chelating ligands; one phenolate oxygen atom of each Tb center forms a bridge between the two metal centers that are related by an inversion center. The coordination geometry around Tb can be described as a distorted pentagonal bipyramid with N1 and O3i on the axial positions. The bond lengths range from 2.445(2) to 2.537(2) Å for Tb-N and from 2.188(1) to 2.369(1) for Tb-O, which is normal for this type of bonds [27]. The distance between the two Tb-centers is 3.7061(6) Å. Projections of the structures of Eu**L1**_4 and Eu**L2**_4 are shown in Figure 4.3. The environment around the Eu(III) ion in Eu**L1**_4 and Eu**L2**_4 is comprised of four phenolate oxygen atoms and four nitrogen atoms, resulting in an N_4O_4 coordination sphere. For both compounds, the geometry of the coordination sphere is best described as a distorted trigonal dodecahedron.

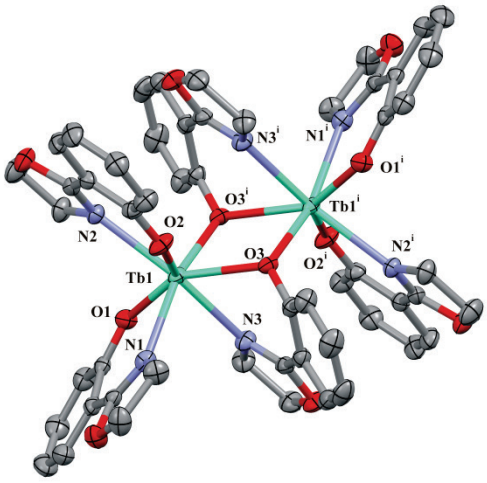

*Figure 4.2: Projection of part of the structure of Tb**L1**_3, shown as 50% probability ellipsoids, with the atom labeling scheme indicated. Hydrogen atoms have been omitted for clarity. The complex is binuclear, with an inversion centre relating the two metal centers. Symmetry operation: i: –x, 1 – y , 1 – z.*

Table 4.1: Details on the X-ray structure determination of complexes TbL1_3, EuL1_4, EuL2_4, EuL1_CO_3 and TbL1_CO_3.

	TbL1_3	**EuL1_4**	**EuL2_4**	**EuL1_CO_3**	**TbL1_CO_3**
formula	$C_{54}H_{48}EuN_6O_{12}$	$C_{52}H_{68}EuN_5O_8$	$C_{44}H_{52}EuN_5O_4S_4$	$C_{59}H_{60}Eu_2N_6Na_2O_{17}S_2$	$C_{59}H_{60}N_6Na_2O_{17}S_2Tb_2$
fw	1290.82	1043.07	995.11	1539.17	1553.11
crystal size [mm^3]	0.20×0.20×0.15	0.20×0.20×0.17	n.d.	0.15×0.15×0.10	0.25×0.25×0.20
crystal color	Colorless	Colorless	Colorless	Colorless	Colorless
crystal system	Triclinic	Monoclinic	Monoclinic	Monoclinic	Monoclinic
space group	P–1 (# 2)	$P2_1/c$ (# 14)	$P2_1/c$ (# 14)	$P2_1/n$ (# 14)	$P2_1/n$ (# 14)
a [Å]	10.142(1)	13.818(2)	10.888(3)	13.631(5)	13.613(2)
b [Å]	15.445(1)	19.342(5)	24.875(8)	25.174(6)	25.110(5)
c [Å]	11.644(2)	19.720(3)	17.698(4)	18.252(5)	18.264(2)
α [°]	85.44(1)	90	90	90	90
β [°]	89.43(1)	108.04(3)	106.85(2)	99.31(3)	99.69(1)
γ [°]	82.26(1)	90	90	90	90
V [$Å^3$]	1218.4(3)	5011.4(19)	4588(2)	6181(3)	6154.0(2)
Z	1	4	4	4	4
d_{calc} [g/cm^3]	1.759	1.383	1.441	1.654	1.676
μ [mm^{-1}]	2.951	1.309	1.595	2.167	2.436
refl. measured / unique	20239/5560	64982/8814	16846/7864	97939/14138	68166/10746
parameters	334	599	239	835	835
R1/wR2 [I>2σ(I)]	0.0165/0.0415	0.0378/0.0829	0.1608/ 0.3868	0.0457/0.0707	0.0370/0.0687
R1/wR2 [all refl.]	0.0191/0.0428	0.0597/0.0977	0.2259/0.4243	0.0753/0.0779	0.0473/0.0717
S	1.08	1.11	1.27	1.10	1.21
$\rho_{min/max}$ [$e/Å^3$]	–0.53/0.62	–0.55/2.75	4.00/–3.30	–0.59/1.54	–0.62/1.52

For Eu**L1**_4, the bond lengths range from 2.575(4) to 2.620(3) Å for Eu-N and from 2.311(3) to 2.337(3) Å for Eu-O. For The Eu-N bond lengths in Eu**L2**_4 range from 2.50(3) to 2.68(3) Å while the Eu-O bonds vary between 2.24(3) and 2.28(1) Å. The latter bond lengths are substantially shorter than the Eu-O bonds in Eu**L1**_4, which might be due to the strong compression of the $[Eu(\mathbf{L2})_4]^-$ complex ion along the crystallographic a-axis. Otherwise, comparable values are known in literature [27]. In both compounds, the alkyl groups of the tetraalkyl-ammonium cation occupy the interspace between two ligands coordinated to the Eu(III) ion.

Compounds Tb**L1**_CO_3 and Eu**L1**_CO_3 are isostructural, and are both described as bimetallic octanuclear complexes. The structures contain two independent sodium ions and two independent lanthanoid ions; the other four metal ions are related by an inversion center. A projection of the symmetry-independent part of Tb**L1**_CO_3 is shown in

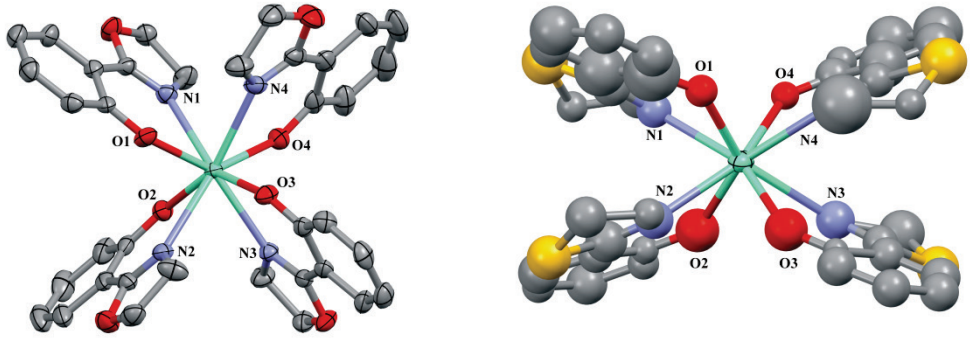

*Figure 4.3: Projections of the structures of Eu**L1**_4 (left) and Eu**L2**_4 (right), with the atom labeling schemes indicated. Hydrogen atoms have been omitted for clarity. The structure of Eu**L1**_4 is shown as 50% probability ellipsoids; the structure of Eu**L2**_4 is shown as 30% probability ellipsoids. In both compounds, the geometry around the central ion is best described as a distorted trigonal dodecahedron.*

Figure 4.4. A wireframe diagram showing the connectivity of the metal centers is given in Figure 4.5. In Tb**L1**_CO_3 and Eu**L1**_CO_3, each *Ln* ion is surrounded by three ligands **L1** binding in a bidentate mode. The two independent *Ln* centers (*Ln*1 and *Ln*2) are bridged by O91 of the carbonate ion. The resulting bond is almost linear (*Ln*1-O91-*Ln*2 = 172.7(1)° and 172.1(1)° for Tb**L1**_CO_3 and Eu**L1**_CO_3). The Na1 ion connects through a third bond of O91. The carbonate ion chelates each *Ln* ion; the resulting *Ln*1-CO_3-*Ln*2 moiety is quasi-planar. The remaining edge of the carbonate ion chelates the Na2 ion through O92 and O93. Two phenol oxygen atoms of each *Ln* center bridge to the Na1 ion, while only one phenol oxygen (O312) bridges the *Ln*1 and Na2 ions. The O93 atom forms a bridge between Na2 and the symmetry related $Na2^i$ ion at a nearly right angle (Na2-O93-$Na2^i$ = 88.8(1)° and 89.9(1)° for Tb**L1**_CO_3 and Eu**L1**_CO_3). Thus, Na2-O93-$Na2^i$-$O93^i$ defines a slightly distorted rectangle with an inversion center at its midpoint generating the other half of the molecule. Both lanthanoid sites have an N_3O_5 coordination sphere that can be described as a distorted trigonal dodecahedron. *Ln*-N distances range from 2.522(4) to 2.560(4) Å for Eu**L1**_CO_3 and from 2.483(4) to 2.538(4) Å for Tb**L1**_CO_3; *Ln*-O bond distances vary from 2.257(3) to 2.544(3) Å and from 2.237(3) to 2.483(3) Å for Eu**L1**_CO_3 and Tb**L1**_CO_3, respectively. In both compounds, the bonds between the lanthanoid ion and the carbonate oxygen atoms are substantially longer than the bonds to the phenolate oxygens. In addition, the Na1 ion resides in a six coordinated site, with the geometry resembling a distorted octahedron. The Na2 ion resides in a five-fold coordination site, which is best described as a distorted trigonal bipyramid. Na-O bond lengths in Eu**L1**_CO_3 range from 2.279(4) to 2.759(4) Å and from 2.287(4) to 2.792(4) Å in Tb**L1**_CO_3. In both Eu**L1**_CO_3 and Tb**L1**_CO_3, disorder is found for the dmso attached to Na2. In both cases, the molecule is disordered over two positions, with relative occupancies of 0.75 and 0.25.

Table 4.2: Selected bond distances (Å) and angles (°) for TbL1_3, EuL1_4 and EuL2_4. Atom labeling is shown in Figure 4.2 for TbL1_3 and in Figure 4.3 for EuL1_4 and EuL2_4.

	TbL1_3	EuL1_4	EuL2_4
Bond distance (Å)			
Ln-N1	2.445(2)	2.597(4)	2.50(3)
Ln -N2	2.468(2)	2.620(3)	2.59(2)
Ln -N3	2.537(2)	2.575(4)	2.69(3)
Ln -N4		2.611(4)	2.67(3)
Ln -O1	2.188(1)	2.311(3)	2.26(2)
Ln -O2	2.194(1)	2.337(3)	2.24(3)
Ln -O3	2.369(1)	2.331(3)	2.26(3)
Ln -O3^{i}	2.300(1)		
Ln -O4		2.316(3)	2.28(1)
C15-C16	1.453(3)	1.479(6)	1.46(4)
C25-C26	1.444(3)	1.467(8)	1.48(4)
C35-C36	1.453(3)	1.473(6)	1.48(5)
C45-C46		1.458(8)	1.47(3)
Bond angle (°)			
N1-*Ln*-O1	73.54(5)	70.6(1)	65(1)
N2-*Ln*-O2	72.27(5)	69.5(1)	64.5(8)
N3-*Ln*-O3	67.32(5)	70.2(1)	68.5(8)
O4-*Ln*-N4		69.9(1)	63(1)
Tb-O3-Tb^{i}	105.08(5)		
O3-Tb-O3^{i}	74.92(5)		

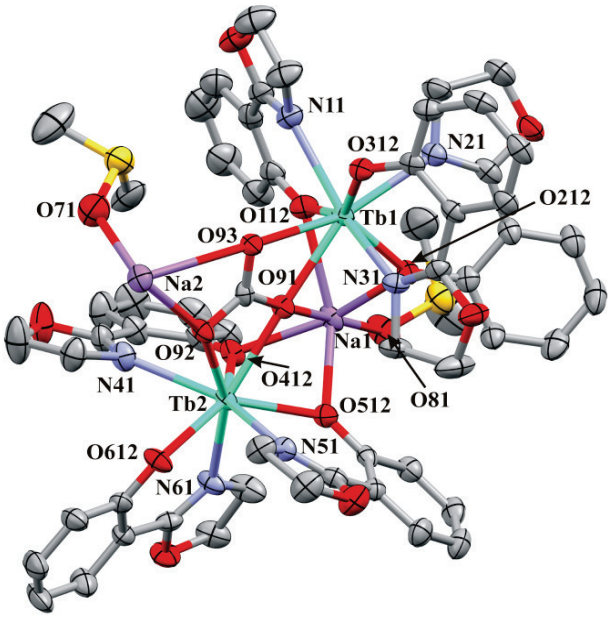

*Figure 4.4: Projection of half a molecule of Tb**L1**_CO_3 shown as 50% probability ellipsoids, with the atom labeling scheme indicated. Hydrogen atoms have been removed for clarity, and only the major component of the disordered dmso molecule is shown.*

Table 4.3: Selected bond distances (Å) and angles (°) for EuL1_CO_3 and TbL1_CO_3. Atom labeling is shown in Figure 4.4.

	EuL1_CO_3	TbL1_CO_3		EuL1_CO_3	TbL1_CO_3
Bond distance (Å)			*Bond angle* (°)		
*Ln*1-N1	2.560(4)	2.538(4)	O1-*Ln*1-N1	70.6(1)	71.3(1)
*Ln*1-N2	2.522(4)	2.500(4)	O2-*Ln*1-N2	71.4(1)	71.8(1)
*Ln*1-N3	2.546(4)	2.513(4)	O3-*Ln*1-N3	68.0(1)	68.6(1)
*Ln*1-O1	2.296(3)	2.277(3)	O4-*Ln*2-N4	69.5(1)	70.3(1)
*Ln*1-O2	2.301(3)	2.285(3)	O5-*Ln*2-N5	69.6(1)	70.3(1)
*Ln*1-O3	2.344(3)	2.318(3)	O6-*Ln*2-N6	71.9(1)	72.7(1)
*Ln*1-O91	2.493(3)	2.483(3)			
*Ln*1-O93	2.498(3)	2.470(3)	*Ln*1-O3-Na2^{i}	97.6(1)	98.2(1)
*Ln*2-N4	2.536(4)	2.514(4)	*Ln*1-O93-Na2^{i}	97.8(1)	98.5(1)
*Ln*2-N5	2.543(4)	2.513(4)	O93-*Ln*1-O3	78.95(9)	79.0(1)
*Ln*2-N6	2.514(4)	2.483(4)	O93-Na2^{i}-O3	81.3(1)	80.3(1)
*Ln*2-O4	2.311(3)	2.281(3)	Na2-O93-Na2^{i}	89.9(1)	88.8(1)
*Ln*2-O5	2.329(3)	2.308(3)	O93-Na2-O93^{i}	90.1(1)	91.2(1)
*Ln*2-O6	2.257(3)	2.237(3)			
*Ln*2-O91	2.544(3)	2.516(3)	*Ln*1-O91-C91	94.4(2)	93.6(2)
*Ln*2-O92	2.484(3)	2.465(3)	*Ln*2-O91-C91	92.8(2)	92.8(2)
Na1-O81	2.473(3)	2.287(4)	*Ln*1-O91-*Ln*2	172.1(1)	172.7(1)
Na1-O91	2.279(4)	2.464(3)	Na1-O91-*Ln*1	88.0(1)	88.0(1)
Na1-O1	2.657(3)	2.630(4)	Na1-O91-*Ln*2	84.12(9)	84.8(1)
Na1-O2	2.356(3)	2.345(3)			
Na1-O4	2.346(3)	2.337(4)			
Na1-O5	2.422(3)	2.412(3)			
Na2-O92	2.316(3)	2.325(4)			
Na2-O93	2.759(4)	2.792(4)			
Na2-O71	2.37(4)	2.37(4)			

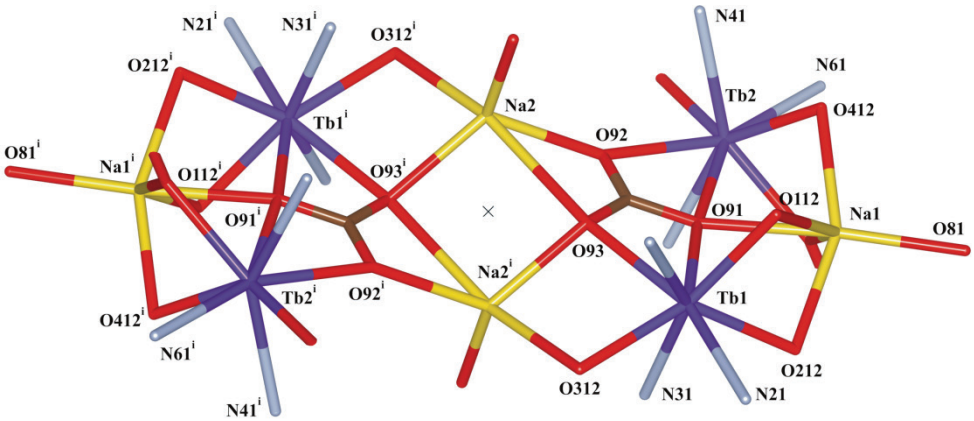

*Figure 4.5: Wireframe representation of the structure of Tb**L1**_CO_3 showing the connectivity of the metal centers. The position of the inversion center is indicated by a cross. Symmetry operation: i) 1 – x, – y, –z.*

4.3.3 Luminescence

All compounds show photoluminescence upon excitation in the near-UV region. Photoluminescence emission and excitation spectra are shown in Figure 4.6. Excitation spectra were obtained by constantly monitoring the intensity of the strongest emission line, i.e. the $^5D_0 \rightarrow {}^7F_2$ transition for Eu(III) compounds and the $^5D_4 \rightarrow {}^7F_5$ transition for Tb(III) compounds, while scanning the excitation wavelength from 220 to 420 nm. The Eu(III) complexes all exhibit luminescence characteristic for the Eu(III) ion, with transitions from the $^5D_0$ resonance level to the ^7F_J manifold around 590, 614, 650 and 700 nm for $J = 1$, 2, 3 and 4, respectively [28]. In all cases, the most dominant line is the $^5D_0 \rightarrow {}^7F_2$ transition. Only weak luminescence is observed for Eu**L1**_CO_3; luminescence intensities of Eu**L1**_3, Eu**L2**_3 are even lower and their spectra are not included. The excitation spectra show broad bands extending into the near-UV region. All three Eu compounds have an excitation band at 290 nm and a second distinct band at 370 nm. In the excitation spectrum of Eu**L2**_3, a band appears around 340 nm, while Eu**L1**_CO_3 has an additional band centered at 396 nm.

The emission spectra recorded for the Tb(III) compounds all show lines characteristic for transitions from the $^5D_4$ level of Tb(III) to the ^7F_J manifold, at 488, 545, 585 and 627 nm for $J = 6$, 5, 4 and 3 [29]. In all cases, the strongest line corresponds to the $^5D_4 \rightarrow {}^7F_5$ transition. The excitation spectra for the Tb(III) complexes with **L1** appear to be composed of three distinct bands of roughly equal intensity centered at 295, 325 and 370 nm. The excitation spectrum of Tb**L1**_CO_3 is similar to the one recorded for Tb**L1**_3 and has nearly constant intensity between 295 and 375 nm, whereas the 370 nm band for Tb**L1**_4 is slightly more intense. The photoluminescence quantum yields and experimental luminescence lifetimes of the complexes are given in Table 4.4.

Table 4.4: Photophysical properties of the Eu(III) and Tb(III) complexes.

Compound	Φ_{tot} (%)	Ω_2 (10^{-20} cm^2)	Ω_4 (10^{-20} cm^2)	τ_{exp} (ms)	τ_{rad} (ms)	Φ_{Ln} (%)	η_{sens} (%)
Eu**L1**_3	n.d.	n.d.	n.d.	n.d.	n.d.	n.d.	n.d.
Tb**L1**_3	38	n.d.	n.d.	0.47	n.d.	n.d.	n.d.
Eu**L1**_4	43	20.7	2.57	0.67	1.40	48	90
Tb**L1**_4	79	n.d.	n.d.	0.66	n.d.	n.d.	n.d.
Eu**L2**_3	n.d.	n.d.	n.d.	n.d.	n.d.	n.d.	n.d.
Tb**L2**_3	16	n.d.	n.d.	0.03	n.d.	n.d.	n.d.
Eu**L2**_4	20	17.5	5.1	0.33	1.51	22	91
Tb**L2**_4	3	n.d.	n.d.	n.d.	n.d.	n.d.	n.d.
Eu**L1**_CO_3	n.d.	n.d.	n.d.	n.d.	n.d.	n.d.	n.d.
Tb**L1**_CO_3	51	n.d.	n.d.	n.d.	n.d.	n.d.	n.d.

Φ_{tot}: Overall photoluminescence quantum yield at 360 nm excitation, τ_{exp}: experimental lifetime of the emissive state of the Ln(III) ion, Ω_J intensity parameters, τ_{rad}: radiative lifetime of the $^5D_0$ state of Eu(III), Φ_{Ln}: intrinsic quantum yield, η_{sens}: sensitizer efficiency.

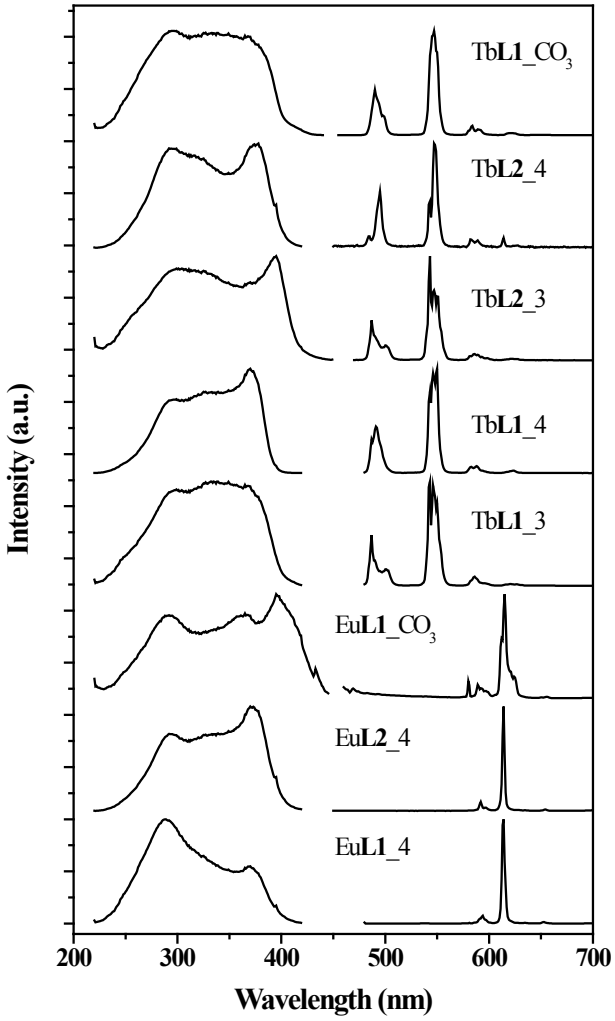

*Figure 4.6: Photoluminescence spectra of the Eu(III) compounds Eu**L1**_4, Eu**L2**_4 and Eu**L1**_CO3 (bottom) and of the Tb(III) compounds Tb**L1**_3, Tb**L1**_4, Tb**L2**_3, Tb**L2**_4 and Tb**L1**_CO$_3$ (top). The excitation spectra (λem = 614 nm for Eu(III) compounds and λem = 545 nm for Tb(III) compounds) are shown on the left hand side while the right hand side shows the emission spectra (λexc = 360 nm) of the compounds. The emission lines at 595, 614, 649 and 685 nm correspond to the $^5D_0 \rightarrow {}^7F_J$, J = 1, 2, 3, 4 transitions of the Eu(III) ion. The emission lines at 495, 545, 580 and 625 nm are characteristic of the Tb(III) ion, corresponding to the $^5D_4 \rightarrow {}^7F_J$, J = 6, 5, 4, 3 transitions.*

For the Eu-complexes, the luminescence intensity of Eu**L1**_3, Eu**L2**_3 and Eu**L1**_CO$_3$ was too weak to allow for reliable determination of quantum yields. For Eu**L1**_4, a quantum yield of 43% and a lifetime of 0.67 ms were recorded. For the Tb(III) complexes, solid state photoluminescence quantum yields range from 3% for Tb**L2**_3 to 79% for Tb**L1**_4. The luminescence lifetimes for these complexes are 0.33 and 0.66 ms, respectively.

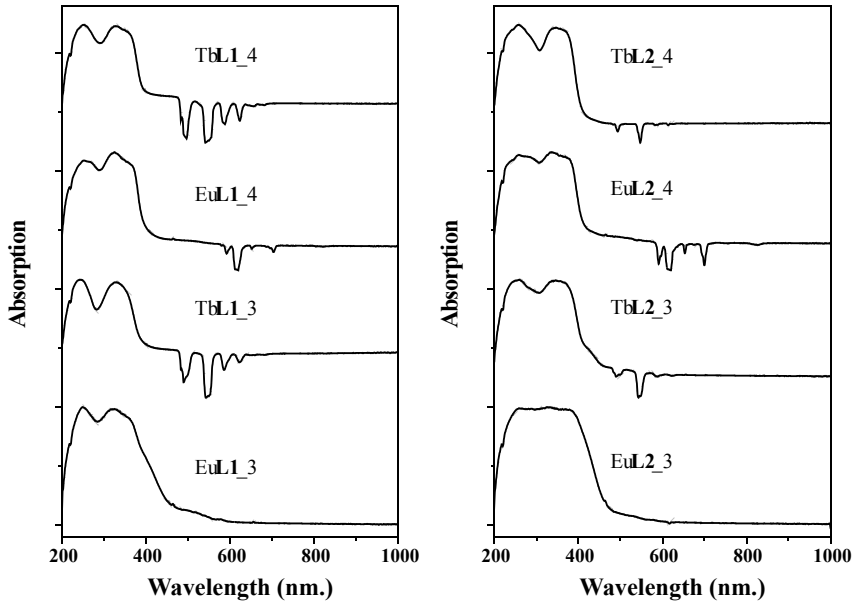

*Figure 4.7: Absorption spectra recorded for Ln**L1**_x compounds (left) and Ln**L2**_x compounds (right). The downward pointing peaks result from luminescence of the compounds upon excitation in the nUV.*

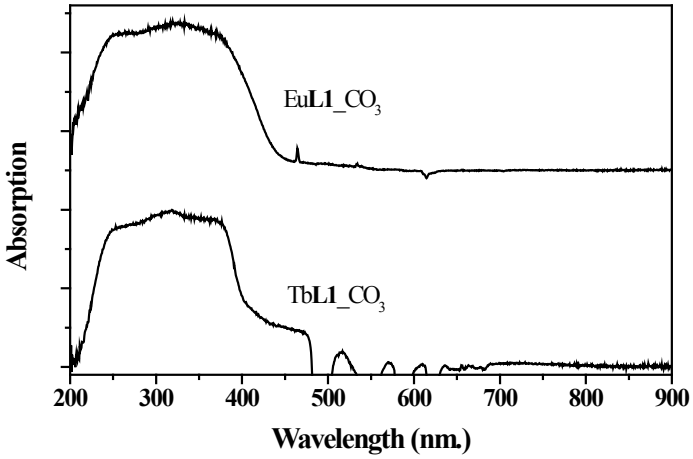

*Figure 4.8: Absorption spectra recorded for Ln**L1**_CO_3 compounds. The downward pointing peaks result from luminescence of the compounds upon excitation in the nUV.*

4.3.4 Absorption spectra

The absorption spectra of the compounds are given in Figure 4.7 and Figure 4.8.The absorption spectra all feature broad absorption bands in the nUV region, and two bands

may be distinguished; one centered at 250 nm and one around 330 nm. The shapes of absorption bands are roughly the same as observed in the excitation spectra, indicating ligand sensitization of the lanthanoid emission in these complexes.

4.4 Discussion

4.4.1 Single crystal structure determinations

In the compounds with a *Ln*(III) to ligand ratio of 1:4, the ligand is able to saturate the coordination sphere around the lanthanoid ion. In the Tb**L1**_3 complex with a 1:3 *Ln*(III)-to-ligand ratio, the coordination sphere of the Tb(III) ion is saturated by forming a di-μ-phenolato bridge between two adjacent Tb(III) ions, which results in an increased coordination number. The formation of bridges between two lanthanoid ions is not uncommon, and has been reported for phenolates, chlorides, acetates and benzoates [30-35]. Interestingly, there is a significant difference between the Tb-O bond lengths of the bridging phenolate. Both bonds are somewhat longer than the Tb-O bonds to the non-bridging phenolates, but the bridging Tb-O3^{i} bond (2.300(1) Å) is actually shorter than the chelating Tb-O3 bond (2.369(1) Å). The asymmetry of the μ-phenolato bridge is larger than reported in previous studies [30, 34].

The structures of compounds Eu**L1**_4 and Eu**L2**_4 are highly similar, although the structure of the latter complex is compressed along the crystallographic a-axis. The packing is similar in both cases, involving packing along the crystallographic y-axis of alternating $[EuL_4]^-$ ions and NR_4^+ ions. In Eu**L2**_4, CH-π stacking appears to be present between the terminal methyl groups of the cation and the benzene rings of the ligands with an average carbon-π-plane distance of approximately 3.6 Å [36]. Such interactions appear to be present as well in between the NBu_4^+ cations and the $[EuL_4]^-$ complexes in Eu**L1**_4.

In Eu**L1**_CO_3 and Tb**L1**_CO_3, the phenol-oxygens O112-O512 form a bridge between the *Ln*(III) and Na centers. In all cases, the Ln-O bond is shorter than the Na-O bond, due to the slightly larger ionic radius of the sodium ion. As can be seen from Figure 4.5, the slightly distorted rectangle defined by Na2, O93 and the equivalent Na2^{i} and O93^{i} atoms is at the center of the structure. Attached on two opposing sides of this rectangle is a distorted rhombus defined by Tb1, O3, Na2^{i} and O93, with O-M-O, (M = Na, *Ln*) angles < 90° and obtuse *Ln*-O-Na angles. The carbonate ions form an important center in the structure, connecting all metal centers in the asymmetric unit of the molecule as well as connecting the asymmetric units leading to the formation of an octanuclear complex. The capture of CO_2 from the air resulting in the formation of a bridging carbonate ion has been reported before for the synthesis of *Ln*(III) compounds [37-40]. Also in other reports, where the carbonate ion is purposely added [41, 42] or formed upon decomposition of one of the reagents [43-45], the CO_3^{2-} ion acts as an important linker in the structure.

4.4.2 Luminescence

Photoluminescence spectra

The broad excitation bands recorded for all luminescent compounds clearly indicate that both **L1** and **L2** are acting as antennae that sensitize the lanthanoid-centered emission. The emission spectra of the Eu(III) compounds are all dominated by the $^5D_0 \rightarrow ^7F_2$ transition around 614 nm. The fact that the intensity of the $^5D_0 \rightarrow ^7F_2$ transition, which is of forced electric dipole (ED) nature, is much higher than that of the $^5D_0 \rightarrow ^7F_1$ magnetic dipole (MD) transition indicates that the Eu(III) ion is situated in a non-centrosymmetric environment [46-48]. This is in agreement with the structures determined for Eu**L1**_4, Eu**L2**_4 and Eu**L1**_CO_3. For the Eu(III) complexes, the excitation spectra appear to vary markedly between the compounds. For Eu**L1**_4, the band around 370 nm is the weakest, while it is the strongest band in the excitation spectrum of Eu**L2**_4. For Eu**L1**_CO_3, an additional strong band centered at 395 nm appears. Because ligand-centered excitation in this compound is only very weak, direct excitation of the Eu(III) ion is comparatively strong. Consequently, this band may arise from the overlap of the ($^5L_6$, $^5G_2$, $^5L_7$, $^5G_3$) $\leftarrow ^7F_0$ transitions of Eu(III) around 395 nm, with a weak ligand-centered band. The emission spectra of Tb**L1**_3, Tb**L1**_4, Tb**L2**_3, Tb**L2**_4 and Tb**L1**_CO_3 are similar and are dominated by the Tb(III) $^5D_4 \rightarrow ^7F_5$ transition around 546 nm. The different splitting patterns of the emission lines are a result of crystal field splitting of the free ion ^7F_J level. Comparing the excitation spectra for the Tb(III) complexes sensitized by the **L1** ligand shows that those for Tb**L1**_3 and Tb**L1**_CO_3 are highly similar, while for Tb**L1**_4 the intensity of the band at 374 nm is slightly enhanced. The enhanced long-wavelength band is also seen for Tb**L2**_3 and Tb**L2**_4, for which the excitation spectra are nearly identical. Similar appearances of excitation spectra for a given ligand are as expected, because they depend on the ligand-centered energy levels. These, in turn, can vary slightly between complexes as a result of slight differences in structure.

Luminescence efficiency

In this study, the metal-to-ligand ratio is found to have a strong impact on the luminescence efficiency of the complexes. For example Eu**L1**_3 and Eu**L1**_CO_3 are practically non-luminescent while Eu**L1**_4 shows relatively bright luminescence with a quantum yield of 43%. Similarly, Eu**L2**_3 is not luminescent while Eu**L2**_4 shows moderately bright luminescence with a quantum efficiency of 20%. Thus, only the Eu(III) complexes with a 1:4 lanthanoid-to-ligand ratio show visible luminescence. The Tb**L1**_3, Tb**L1**_4 and Tb**L1**_CO_3 complexes all show moderate to strong photoluminescence, with the quantum efficiency for Tb**L1**_4 compound being as high as 79%. The improved efficiency of Tb**L1**_4 as compared to Tb**L1**_3 is also reflected in the increased lifetime, indicating that the contribution of non-radiative processes has decreased. For Tb(III) compounds with the ligand **L2**, the behavior with respect to changes in the M:L ratio is reversed compared to

those with **L1**. Thus, Tb**L2**_3 shows moderately intense luminescence with a quantum yield of 16%, while Tb**L2**_4 shows only very weak luminescence. Overall, the ligand **L2** is not as good an antenna for Tb(III) as is the **L1** ligand.
In general, the luminescence lifetime is shorter for complexes with lower overall luminescence quantum yields. This is readily explained by the larger relative contribution of non-radiative pathways depopulating the *Ln*(III) excited state, resulting in lowering of the intrinsic quantum yield of the ion [49, 50]. For compounds based on the Eu(III) ion, the intrinsic quantum yield is readily calculated if the experimental lifetime is known and an emission spectrum representing the relative photon flow is available [51, 52]. With A_{rad} and A_{nrad} representing the radiative and non-radiative depopulation rate constants, respectively, the intrinsic quantum yield Φ_{Ln} is given by equation 1.

$$\Phi_{Ln} = \frac{A_{rad}}{A_{rad}+A_{nrad}} \qquad (1)$$

The intrinsic quantum yields for the Eu(III) ion in Eu**L1**_4 and Eu**L2**_4 are given in Table 4.4. It appears that the main difference in overall quantum yield is largely the result of different intrinsic quantum yields of the Eu(III) ion among the two compounds; the quantum efficiency for Eu**L2**_4 is half that of Eu**L1**_4, and so is its luminescence lifetime: 0.33 ms vs. 0.67 ms. An expression for the overall photoluminescence quantum yield Φ_{tot} may be written as equation 2.

$$\Phi_{tot} = \eta_{sens} \times \Phi_{Ln} \qquad (2)$$

With Φ_{Ln} representing the intrinsic quantum yield given in equation 1 and η_{sens} representing the sensitizer efficiency, which contains contributions of the ligand-centered intersystem crossing efficiency and ligand-to-metal energy transfer energy, this equation can be used to assess the antenna efficiency of the ligands. From Table 4.4 it can be seen that for Eu**L1**_4 and Eu**L2**_4, the sensitizer efficiency is practically the same for both ligands. Because the 1:4 M:L Eu(III) complexes both show intense luminescence, the lack of efficient metal-centered photoluminescence for Eu**L1**_3, Eu**L2**_3 and Eu**L1**_CO_3 cannot be attributed to the ligand-centered triplet excited state being too low in energy. In addition, no residual ligand-centered phosphorescence is observed. It is known that in Eu(III) complexes a low-lying ligand-to-metal charge transfer band can be present. The charge transfer band in turn can compete with the ligand-to-metal energy transfer, thereby effectively quenching lanthanoid-centered luminescence [53-56]. The presence of such state can be identified from absorption spectra, which are shown in Figure 4.7 for the *Ln***L1**_*x* and *Ln***L2**_*x*, (*x* = 1, 2) complexes and in Figure 4.8 for the *Ln***L1**_CO_3 compounds [57]. Superficially, all absorption spectra look highly similar, with equal-intensity bands around 250 nm and 350 nm. Indeed, compared to the Tb(III) complexes, the long wavelength absorption band for the 1:3 Eu(III) complexes extends slightly further into the blue spectral region. This

additional band around 400 nm indicates the presence of a charge transfer band for Eu**L1**_3 and Eu**L2**_3. Also, comparing the absorption spectra of Eu**L1**_CO_3 and Tb**L1**_CO_3 reveals that the absorption spectrum of Eu**L1**_CO_3 extends further into the visible region. It seems that the structure of the 1:3-compounds is better capable of stabilizing the divalent state of the Eu-ion than the 1:4 structure. Lowering of the LMCT state in an Eu(III) complex as a result of a different M:L ratio has been reported before and appears to be responsible for quenching the Eu(III)-centered emission in the 1:3 complexes [53]. It appears that generally, phenol-type ligands fail to excite luminescence of the Eu(III) ion. For example, 4-hydroxyisophthalate is able to sensitize emission of the Tb(III) ion, while the analogous Eu(III) complex is non luminescent [58]. Similarly, complexes of Eu(III) with salicylate-type ligands were found to be weakly or even non-luminescent, while their Tb(III) analogues show bright luminescence [18]. This is readily understood from the ability of phenolates to form phenoxyl radicals upon oxidation [59]. Because the Eu ion has a stable divalent state, a low lying charge transfer band may occur in such compounds, quenching the luminescence [54]. Indeed, it is found that 3,5-dinitrosalicylate is an efficient sensitizer for Eu(III) luminescence [13, 60]. In this ligand, the two strongly electron-withdrawing groups raise the level of the LMCT state sufficiently to prevent competition between the LMCT state and L* → Eu(III) energy transfer. Although **L1** and **L2** described in this chapter do not bear such strongly electron-withdrawing groups, luminescence of the complexes with the 1:4 Eu:L ratio is not hindered by a low energy LMCT state. This mechanism of quenching is usually not present in Tb(III) complexes as the Tb ion has no stable divalent state, and as a result, all Tb(III) complexes show photoluminescence. The weak emission intensity of the Tb**L2** complexes compared to the Tb**L1** complexes might be due to a poor spectral match between the ligand **L2** and the Tb(III) ion.

4.5 Conclusion

Ten new complexes of Eu(III) and Tb(III) ions, using phenol oxazoline or phenol thiazoline in M:L ratios of 1:3 and 1:4 have been synthesized in yields ranging from 74% to 100%. The complexes show luminescence characteristic of the lanthanoid ion upon excitation in the nUV spectral region, the intensity of which is strongly influenced by the M:L ratio. Solid state photoluminescence studies on the complexes indicate that **L1** can sensitize luminescence of the Tb(III) ion in both 1:3 and 1:4 M:L ratios, with the 1:4 ratio giving the most intense photoluminescence. The same ligand only sensitizes Eu(III) centered luminescence in a M:L ratio of 1:4. The presence of an LMCT state in the 1:3 complexes appears to be responsible for quenching the luminescence. The ligand **L2** is a less effective antenna for sensitizing Eu(III) and Tb(III) luminescence; the 1:4 M:L Eu(III) complex shows moderately intense luminescence, whereas the 1:3 complex does not. The 1:3 M:L ratio appears to stabilize an LMCT state in the Eu(III) complexes, which in turn quenches Eu-centered luminescence. This shows that not only the ligand centered energy levels determine the photoluminescence efficiency of the complex, but also the M:L ratio should

be taken into consideration. The long-wavelength excitation maximum of Eu**L1**_4 combined with a moderately high quantum yield show that this class of ligands is promising as sensitizer for Eu(III) and Tb(III) ions. Due to its long-wavelength excitation maximum and high photoluminescence quantum efficiency of 80%, Tb**L1**_4 is an interesting candidate material for a new green phosphor in LEDs.

4.6 References

[1] R. Haitz and J.Y. Tsao, *Optik & Photonik*, 6 (2011) 26-30.
[2] E.F. Schubert, J.K. Kim, H. Luo, and J.Q. Xi, *Rep. Prog. Phys.*, 69 (2006) 3069-3099.
[3] C.C. Lin and R.-S. Liu, *J. Phys. Chem. Lett.*, 2 (2011) 1268-1277.
[4] A.A. Setlur, *Electrochem. Soc. Interface*, 18 (2009) 32-36.
[5] S. Ye, F. Xiao, Y.X. Pan, Y.Y. Ma, and Q.Y. Zhang, *Mater. Sci. Eng., R*, 71 (2010) 1-34.
[6] H.A. Höppe, *Angew. Chem., Int. Ed.*, 48 (2009) 3572-3582.
[7] M. Raukas, J. Kelso, Y. Zheng, K. Bergenek, D. Eisert, A. Linkov, and F. Jermann, *J. Solid State Sci. Technol.*, 2 (2013) R3168-R3176.
[8] K. Binnemans, *Chem. Rev.*, 109 (2009) 4283-4374.
[9] K. Binnemans, *Rare earth beta-diketonates*, in *Handbook on the Physics and Chemistry of Rare Earths*, 2005, Elsevier. 107-272.
[10] M.L.P. Reddy, V. Divya, and R.O. Freire, *Dalton Trans.*, 40 (2011) 3257-3268.
[11] T.J. Mooibroek, P. Gamez, A. Pevec, M. Kasunič, B. Kozlevčar, W.T. Fu, and J. Reedijk, *Dalton Trans.*, 39 (2010) 6483-6487.
[12] K.P. Zhuravlev, V.I. Tsaryuk, I.S. Pekareva, J. Sokolnicki, and Z.S. Klemenkova, *J. Photochem. Photobiol., A*, 219 (2011) 139-147.
[13] K. Zhuravlev, V. Tsaryuk, J. Legendziewicz, V. Kudryashova, P. Gawryszewska, and V. Zolin, *Opt. Mater.*, 31 (2009) 1822-1824.
[14] K. Manseki and S. Yanagida, *Chem. Commun.*, (2007) 1242-1244.
[15] M. Latva, H. Takalo, V.M. Mukkala, C. Matachescu, J.C. Rodriguez-Ubis, and J. Kankare, *J. Lumin.*, 75 (1997) 149-169.
[16] Z. Pan, G. Jia, C.-K. Duan, W.-Y. Wong, W.-T. Wong, and P.A. Tanner, *Eur. J. Inorg. Chem.*, 2011 (2011) 637-646.
[17] N.M. Shavaleev, R. Scopelliti, F. Gumy, and J.-Claude G. Bünzli, *Inorg. Chem.*, 48 (2009) 6178-6191.
[18] V. Tsaryuk, K. Zhuravlev, V. Zolin, P. Gawryszewska, J. Legendziewicz, V. Kudryashova, and I. Pekareva, *J. Photochem. Photobiol., A*, 177 (2006) 314-323.
[19] J.C. de Mello, H.F. Wittmann, and R.H. Friend, *Adv. Mater.*, 9 (1997) 230-232.
[20] T. Kottke and D. Stalke, *J. Appl. Crystallogr.*, 26 (1993) 615-619.
[21] G.M. Sheldrick, *Acta Crystallogr., Sect. A: Found. Crystallogr.*, 64 (2008) 112-122.
[22] G.M. Sheldrick, *SHELXS–97*, *Bruker AXS Inc., Madison, Wisconsin*, 1997.
[23] Nonius, *COLLECT*, *Nonius BV, Delft, The Netherlands*, 2002.
[24] L. Farrugia, *J. Appl. Crystallogr.*, 32 (1999) 837-838.
[25] H.R. Hoveyda, V. Karunaratne, S.J. Rettig, and C. Orvig, *Inorg. Chem.*, 31 (1992) 5408-5416.

[26] A. Minkkilä, M.J. Myllymäki, S.M. Saario, J.A. Castillo-Melendez, A.M.P. Koskinen, C.J. Fowler, J. Leppänen, and T. Nevalainen, *Eur. J. Med. Chem.*, 44 (2009) 2994-3008.
[27] A.G. Orpen, L. Brammer, F.H. Allen, O. Kennard, D.G. Watson, and R. Taylor, *J. Chem. Soc., Dalton Trans.*, (1989) S1-S83.
[28] W.T. Carnall, P.R. Fields, and K. Rajnak, *J. Chem. Phys.*, 49 (1968) 4450-4455.
[29] W.T. Carnall, P.R. Fields, and K. Rajnak, *J. Chem. Phys.*, 49 (1968) 4447-4449.
[30] L. Zhang, Y. Ji, X. Xu, Z. Liu, and J. Tang, *J. Lumin.*, 132 (2012) 1906-1909.
[31] U. Baisch, D.B. Dell`Amico, F. Calderazzo, R. Conti, L. Labella, F. Marchetti, and E.A. Quadrelli, *Inorg. Chim. Acta*, 357 (2004) 1538-1548.
[32] Q. Yu, X. Zhou, M. Liu, J. Chen, Z. Zhou, X. Yin, and Y. Cai, *J. Rare Earth.*, 26 (2008) 178-184.
[33] X. Qiu, Y. Zhang, and X. Li, *J. Rare Earth.*, 27 (2009) 797-800.
[34] S. Liu, L. Gelmini, S.J. Rettig, R.C. Thompson, and C. Orvig, *J. Am. Chem. Soc.*, 114 (1992) 6081-6087.
[35] Z. Wang, J. Reibenspies, and A.E. Martell, *Inorg. Chem.*, 36 (1997) 629-636.
[36] M. Nishio, *CrystEngComm*, 6 (2004) 130-158.
[37] P. Bag, S. Dutta, P. Biswas, S.K. Maji, U. Florke, and K. Nag, *Dalton Trans.*, 41 (2012) 3414-3423.
[38] G. Bombieri, F. Benetollo, A. Polo, K.K. Fonda, and L.M. Vallarino, *Polyhedron*, 10 (1991) 1385-1394.
[39] S. Fleming, C.D. Gutsche, J.M. Harrowfield, M.I. Ogden, B.W. Skelton, D.F. Stewart, and A.H. White, *Dalton Trans.*, (2003) 3319-3327.
[40] S.K. Langley, B. Moubaraki, and K.S. Murray, *Inorg. Chem.*, 51 (2012) 3947-3949.
[41] G.B. Deacon, C.M. Forsyth, P.C. Junk, and A. Urbatsch, *Eur. J. Inorg. Chem.*, 2010 (2010) 2787-2797.
[42] K. Xiong, X. Wang, F. Jiang, Y. Gai, W. Xu, K. Su, X. Li, D. Yuan, and M. Hong, *Chem. Commun.*, 48 (2012) 7456-7458.
[43] L. Huang, L. Han, D. Zhu, L. Chen, and Y. Xu, *Inorg. Chem. Commun.*, 21 (2012) 80-83.
[44] S. Romero, A. Mosset, and J.C. Trombe, *J. Solid State Chem.*, 127 (1996) 256-266.
[45] C. Serre, J. Marrot, and G. Férey, *Inorg. Chem.*, 44 (2005) 654-657.
[46] R. Reisfeld, E. Zigansky, and M. Gaft, *Mol. Phys.*, 102 (2004) 1319 - 1330.
[47] B. Francis, D.B.A. Raj, and M.L.P. Reddy, *Dalton Trans.*, 39 (2010) 8084-8092.
[48] R.J. Wiglusz, T. Grzyb, A. Lukowiak, P. Głuchowski, S. Lis, and W. Strek, *Opt. Mater.*, 35 (2012) 130-135.
[49] L. Armelao, S. Quici, F. Barigelletti, G. Accorsi, G. Bottaro, M. Cavazzini, and E. Tondello, *Coord. Chem. Rev.*, 254 (2010) 487-505.
[50] J.-C.G. Bünzli, *Chem. Rev.*, 110 (2010) 2729-2755.
[51] M.H.V. Werts, R.T.F. Jukes, and J.W. Verhoeven, *Phys. Chem. Chem. Phys.*, 4 (2002) 1542-1548.
[52] J.W. Verhoeven, *Pure Appl. Chem.*, 68 (1996) 2223-2286.
[53] S. Petoud, J.-C.G. Bünzli, T. Glanzman, C. Piguet, Q. Xiang, and R.P. Thummel, *J. Lumin.*, 82 (1999) 69-79.
[54] W.M. Faustino, O.L. Malta, and G.F. de Sa, *J. Chem. Phys.*, 122 (2005) 054109.

[55] V. Tsaryuk, K. Zhuravlev, V. Kudryashova, V. Zolin, J. Legendziewicz, I. Pekareva, and P. Gawryszewska, *J. Photochem. Photobiol., A*, 197 (2008) 190-196.
[56] G. Blasse, *Mater. Chem. Phys.*, 16 (1987) 201-236.
[57] G.K. Liu, M.P. Jensen, and P.M. Almond, *J. Phys. Chem. A*, 110 (2006) 2081-2088.
[58] L. Benisvy, P. Gamez, W.T. Fu, H. Kooijman, A.L. Spek, A. Meijerink, and J. Reedijk, *Dalton Trans.*, (2008) 3147-3149.
[59] C. Li and M.Z. Hoffman, *J. Phys. Chem. B*, 103 (1999) 6653-6656.
[60] V. Tsaryuk, K. Zhuravlev, V. Kudryashova, V. Zolin, Y. Yakovlev, and J. Legendziewicz, *Spectrochim. Acta A*, 72 (2009) 1020-1025.

5 Tuning Eu(III) complexes with dibenzoylmethanates

Seven novel Eu(III)-based coordination compounds with dibenzoylmethanate-type ligands bearing methyl, fluoro, chloro, bromo and iodo substituents on various positions of the phenyl groups have been prepared in yields ranging from 46% to 100%. All compounds have the general formula $HNEt_3[Eu(L)_4]$. In addition, two novel compounds that are described by the general formula $A[Eu(dbm)_4]$ ($A = Li^+$, NBu_4^+) have been synthesized and the structures have been determined using X-ray crystallography. All compounds show bright photoluminescence characteristic of the Eu(III) ion when excited in the ligand-centered absorption band using near-UV radiation. Overall photoluminescence quantum yields range from 13% to 57%, and luminescence lifetimes vary from 0.19 ms to 0.89 ms. The effects of the substituents on the efficiency of the sensitization process have been studied using luminescence lifetime measurements and Judd-Ofelt analysis of the corrected emission spectra. The differences in sensitization efficiency of the ligands can be explained by the different electronic properties of the substituents. The counter ion is found to have a large impact on the luminescent properties of the $[Eu(dbm)_4]^-$ complex ion.

(This Chapter will be published: S. Akerboom, W.T. Fu and E. Bouwman, manuscript in preparation)

5.1 Introduction

Amongst the ligands that are known to efficiently sensitize luminescence of Eu(III) ions, the β-diketones have been the most widely studied class. The early paper by Weissman already concerns the use of *inter alia* benzoylacetonate (bzac), m-nitrobenzoylacetonate and dibenzoylmethanate (dbm) as antenna ligands. In the work that followed, complexes based on β-diketone type ligands were widely investigated [1-5]. Lanthanoid complexes with β-diketones continue to be widely studied as of to date, and have been the subject of an extensive review by Binnemans recently [6]. However, systematic studies on the influence of substituents on dbm molecules on the luminescent properties of the resulting *Ln*(III) complexes appear to be scarce. Systematic investigation to the influence of substitution on the absorption spectra of dibenzoylmethane molecules has been performed in 1955 [7]. In the mid 1960s, Sager *et al.* have investigated the influence of several substituents on the dbm and acac ligands on the luminescence of Eu(III) complexes [2, 3]. More recent systematic investigations on the spectroscopic properties of substituted Hdbm-type molecules mainly focus on their use in sunscreen agents [8-11]. In 2011, the group of Reddy prepared several acetylacetone complexes with highly conjugated substituents, shifting the excitation maximum into the visible part of the spectrum [12]. The aim of this work is to provide a systematic understanding of the photoluminescence properties of the Eu(III) complexes with some novel substituted dibenzoylmethanate ligands. The influence of the substituents on the antenna properties of the ligand is interpreted using the Hammett equation for the electronic properties of the substituents. Judd-Ofelt theory is used to analyze the emission spectra in order to gain more insight in the processes that influence the overall photoluminescence quantum yield of the complexes. Because the photophysical properties of the compounds in the solid state are of interest, the influence of the counter ions should be considered. As was already shown by Mech *et al.*, the counter ions influence the packing of the $[Eu(dbm)_4]^-$ complex ions in the solid state [13]. In turn, this is shown to have a strong impact on the photoluminescent properties of the resulting compounds in. Similar observations were made for tetrakis(naphthoyltrifluoroacetonato)europate(III) complexes with different counter ions [14]. In this chapter, the synthesis of seven Hdbm-type ligands and their Eu(III) complexes is reported; the numbering scheme used throughout this chapter and the composition of the ligands is shown in Figure 5.1. In addition, the photoluminescent properties and structures of two compounds comprising the $[Eu(dbm)_4]^-$ complex ion and a Li^+ or NBu_4^+ cation are compared to assess the influence of the counter ions on the luminescent properties.

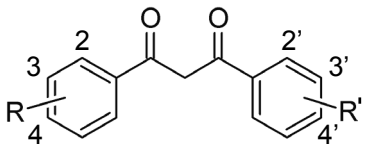

Ligand	R	R'	Complex
H**L1**	4-F	4'-Me	**Eu1**
H**L2**	4-Br	4'-Me	**Eu2**
H**L3**	3-F	4'-Me	**Eu3**
H**L4**	3-Cl	4'-Me	**Eu4**
H**L5**	3-Br	4'-H	**Eu5**
H**L6**	3-I	4'-Me	**Eu6**
H**L7**	2-Cl	4'-Me	**Eu7**

Figure 5.1: An overview of the ligands described in this chapter, showing the numbering scheme used. All complexes are described by the general formula $HNEt_3[Eu(L)_4]$.

5.2 Experimental

5.2.1 General

NMR spectra were recorded on a Bruker DPX-300 spectrometer. Infrared spectra were recorded on a Perkin–Elmer Spectrum Two FTIR spectrometer equipped with the UATR Two accessory. Elemental analysis for C, H, N was performed on a Perkin–Elmer 2400 series II analyzer. Excitation and emission spectra were recorded on a Shimadzu RF–5301PC spectrofluoriphotometer equipped with a solid state sample holder and a UV-blocking filter. Photoluminescence quantum yields were recorded on an Avantes AvaSpec-2048 CCD spectrometer connected to a custom-made integrating sphere, based on the AvaSphere 30REFL, using a modification of the absolute method reported by De Mello [15]. A 1000 Watt Xe-discharge lamp and a SPEX monochromator were used as the excitation source. UV-Vis absorption spectra were measured with the same spectrometer, connected to a solid state reflection probe and using an AvaLight DH-S-BAL light source. For determination of luminescence lifetime, an Edinburgh Instruments FLS920 spectrophotometer was used together with a pulsed laser excitation source.

5.2.2 X-ray crystal structure determination

A crystal was selected for the X–ray measurements and mounted to the glass fiber using the oil drop method and data were collected at 173 K on a Nonius Kappa CCD diffractometer (Mo-Kα radiation, graphite monochromator, $\lambda = 0.71073$ Å)[16]. The intensity data were corrected for Lorentz and polarization effects and for absorption. The programs COLLECT, SHELXS–97, SHELXL–97 were used for data reduction, structure solution and structure refinement, respectively [17-19]. The nonhydrogen atoms were refined anisotropically. The H atoms were geometrically fixed and allowed to ride on the attached atoms. For $Li[Eu(dbm)_4]\cdot H_2O$, the H atoms of the water molecules were not located. For $NBu_4[Eu(dbm)_4]$, the measured crystal was pseudo merohedrally twinned and the refinement was made using twin matrix (–1 0 0 0 –1 0 0 0 1) and BASF parameter 0.53767. The carbon chains of the tetrabutylammonium molecule were refined isotropically. The H atoms were geometrically fixed and allowed to ride on the attached atoms.

5.2.3 General procedure for esterification of benzoic acids

A typical procedure for the synthesis of methyl benzoate esters: 10 mmol of the substituted benzoic acid was converted to the methyl ester by refluxing overnight in 50 mL of absolute methanol in the presence of 1 mL of concentrated sulfuric acid. The resulting mixture was concentrated *in vacuo*, and the resulting oil was dissolved in 50 mL of diethyl ether. The ether solution was transferred to a separatory funnel and washed with saturated sodium hydrogen carbonate (2 × 50 mL) solution and with 30 mL of brine. The combined aqueous layers were extracted with a single portion of 50 mL diethyl ether and the extract was added to the other ether solution. The combined organic layers were dried over magnesium sulfate and concentrated *in vacuo* to give the methyl ester as an oil or solid.

5.2.4 General procedure for the synthesis of dibenzoylmethanates

To a flame dried reflux setup under Ar was added NaH (0.44 g, 11 mmol of a 60% w/w suspension in mineral oil), which was washed with 20 mL of petroleum ether. This was suspended in 50 mL of dry toluene, and the substituted methyl benzoate (10 mmol) was added. To the resulting suspension, a solution of the substituted acetophenone (10 mmol) was added dropwise under stirring. After completing the addition, the mixture was brought to a reflux and left to react overnight. After cooling down to room temperature, the mixture was concentrated *in vacuo* and the resulting residue was taken up in 50 mL of water and acidified to pH ~ 6 using a 1 M solution of HCl. The resulting solution was extracted with ethyl acetate (2 × 50 mL), and the combined organic layers were dried over $MgSO_4$ and concentrated. The residue was recrystallized from hot hexane-ethanol mixtures to yield yellow microcrystalline product. Typically, more product could be obtained by further cooling the mother liquor.

*1-(4-fluorophenyl)-3-(4-methylphenyl)propane-1,3-dione (H**L1**)*

Starting from methyl (4-fluorobenzoate) and 4-methylacetophenone; yield 0.83 g, 32% of a yellow microcrystalline powder. ^{1}H NMR (300 MHz, $CDCl_3$): δ 8.01 (dd, J = 8.9, 5.3 Hz, 1H), 7.92 – 7.85 (m, 2H), 7.33 – 7.27 (m, 2H), 7.17 (dd, J = 8.9, 8.3 Hz, 1H), 6.78 (s, 1H), 2.44 (s, 3H). IR (ν/cm^{-1}): 3073(w), 3031(w), 2916(w), 2859(w), 1599(s), 1531(s), 1492(s), 1400(w), 1378(w), 1297(s), 1219(s), 1185(s), 1155(s), 1123(m), 1104(m), 1086(w), 1054(m), 1011(m), 967(w), 918(w), 847(s), 836(s), 779(vs), 740(m), 695(w), 666(w), 638(w), 632(w), 611(m), 566(m), 506(s), 495(s), 464(m).

*1-(4-bromophenyl)-3-(4-methylphenyl)propane-1,3-dione (H**L2**)*

Starting from 19 mmol methyl (4-methylbenzoate) and 19 mmol 4-bromoacetophenone; yield 0.64 g, 11% of a yellow microcrystalline powder. ^{1}H NMR (300 MHz, $CDCl_3$): δ 7.92 – 7.82 (m, 4H), 7.66 – 7.59 (m, 2H), 7.33 – 7.27 (m, 2H), 6.79 (s, 1H), 2.44 (s, 3H). IR (ν/cm^{-1}): 3028(vw), 2963(vw), 1581(m), 1516(m), 1479(m), 1295(m), 1277(m), 1225(m), 1207(m), 1006(m), 968(m), 916(m), 841(s), 694(m), 663(w), 542(m), 492(s), 468(s).

*1-(3-fluorophenyl)-3-(4-methylphenyl)propane-1,3-dione (H**L3**)*

Starting from methyl (3-fluorobenzoate) and 4-methylacetophenone; yield 1.1 g, 42% of a yellow microcrystalline powder. ^{1}H NMR (300 MHz, $CDCl_3$): δ 7.91 – 7.88 (m, 2H), 7.78 – 7.73 (m, 1H), 7.70 – 7.65 (m, 1H), 7.50 – 7.42 (m, 1H), 7.32 – 7.29 (m, 1H), 7.28 – 7.21 (m, 1H), 6.80 (s, 1H), 2.44 (s, 3H). IR (ν/cm^{-1}): 3075(w), 2988(w), 1685(w), 1610(m), 1526(m), 1504(m), 1474(m), 1440(m), 1302(m), 1246(s), 1210(w), 1179(s), 1123(w), 1076(w), 1057(w), 1017(w), 1000(w), 978(w), 936(w), 909(m), 884(w), 847(w), 829(w), 800(w), 769(vs), 735(s), 684(w), 666(m), 649(w), 577(m), 534(m), 498(m), 460(m).

*1-(3-chlorophenyl)-3-(4-methylphenyl)propane-1,3-dione (H**L4**)*

Starting from methyl (3-chlorobenzoate) and 4-methylacetophenone; yield 0.11 g, 4% of a yellow microcrystalline powder after 3 recrystallisations from hexane-ethanol. ^{1}H NMR (300 MHz, $CDCl_3$): δ 7.95 (t, J = 1.9 Hz, 1H), δ 7.90 (d, J = 8.3 Hz, 2H), δ 7.86 (dt, J = 7.5 Hz, 1.5 Hz, 1H), δ 7.52 (m, J = 8.1 Hz, 1.2 Hz 1H), δ 7.43 (t, J = 8.1 Hz, 1H), δ 7.31 (d, J = 8.1 Hz, 2H), δ 6.79 (s, 1H), 2.44 (s, 3H).

*1-(3-bromophenyl)-3-phenylpropane-1,3-dione (H**L5**)*

Starting from methyl (3-bromobenzoate) and acetophenone; yield 0.93 g, 30% of a yellow microcrystalline powder. ^{1}H NMR (300 MHz, $CDCl_3$): δ 8.12 (t, J = 1.8 Hz, 1H), 8.02 – 7.97 (m, 2H), 7.93 – 7.87 (m, 1H), 7.71 – 7.66 (m, 1H), 7.62 – 7.46 (m, 3H), 8.12 (t, J = 7.9 Hz, 1H). IR (ν/cm^{-1}): 1591(w), 1513(m), 1485(m), 1454(m), 1290(m), 1264(w), 1222(s), 1175(m), 1160(w), 1100(w), 1054(m), 1022(w), 998(w), 911(w), 892(w), 794(w), 757(vs), 704(w), 691(m), 679(s), 655(s), 607(s), 504(w), 451(w).

*1-(3-iodophenyl)-3-(4-methylphenyl)propane-1,3-dione (H**L6**)*

Starting from methyl (3-iodobenzoate) and 4-methylacetophenone; yield 2.13 g, 59% of a yellow microcrystalline powder. ^{1}H NMR (300 MHz, $CDCl_3$): δ 8.21 – 8.29 (m, 1H), 7.95 – 7.85 (m, 4H), 7.32 – 7.25 (m, 2H), 7.23 – 7.20 (d, J = 7.9 Hz, 1H), 6.77 (s, 1H), 2.44 (s, 3H). IR (ν/cm^{-1}): 3065(w), 2996(w), 2950(w), 1711(vs), 1589(w), 1564(m), 1472(w), 1436(s), 1411(m), 1370(w), 1329(w), 1293(s), 1278(s), 1254(vs), 1193(m), 1120(s), 1098(m), 1080(m), 1060(m), 996(m), 963(m), 925(w), 890(m), 839(w), 811(m), 738(vs), 708(vs), 670(s), 645(m), 478(m).

*1-(2-chlorophenyl)-3-(4-methylphenyl)propane-1,3-dione (H**L7**)*

Starting from methyl (2-chlorobenzoate) and 4-methylacetophenone; yield 1.22 g, 45% of a yellow microcrystalline powder. ^{1}H NMR (300 MHz, $CDCl_3$): δ 7.87 – 7.84 (m, 2H), 7.69 – 7.66 (m, 1H), 7.49 – 7.36 (m, 3H), 7.29 – 7.33 (m, 1H), 7.27 – 7.28 (1H), 6.71 (s, 1H), 2.43 (s, 3H). IR (ν/cm^{-1}): 1592(m), 1493(s), 1430(m), 1308(m), 1258(m), 1223(w), 1209(w), 1187(m), 1162(w), 1125(w), 1104(w), 1068(w), 1040(m), 1018(w), 966(w), 830(m), 789(s), 759(vs), 735(s), 712(m), 689(m), 666(w), 638(m), 582(w), 538(w), 468(s).

5.2.5 Complex synthesis

In a typical procedure, 0.5 mmol of the ligand was dissolved in 3 mL of hot ethanol (65 °C) and 0.125 mmol of $EuCl_3 \cdot 6H_2O$ was dissolved in 1 mL of hot ethanol. Then, 0.5 mmol (0.07 mL) of triethylamine was added to the ligand solution and while swirling the resulting solution, the europium solution was added dropwise. The hot mixture was left on the hot plate for 10 minutes, after which it was allowed to cool down to room temperature. The product precipitated as a yellow compound which was collected by filtration, washed with cold ethanol and diethyl ether and dried *in vacuo*. All attempts to grow single crystals of sufficient size for single crystal XRD failed.

*$HNEt_3[Eu(\mathbf{L1})_4]$ (**Eu1**)*

Starting from 0.25 mmol of $EuCl_3$ and 1 mmol of ligand; yield 255 mg, 80% based on Eu, of a light yellow powder. IR (ν/cm^{-1}): 3061(w), 3030(w), 2985(w), 1670(m), 1601(s), 1584(m), 1547(s), 1525(s), 1487(vs), 1418(s), 1380(s), 1295(m), 1219(s), 1207(m), 1180(m), 1154(s), 1128(w), 1114(w), 1093(m), 1056(m), 1013(m), 968(w), 938(w), 886(w), 849(s), 838(m), 774(vs), 741(m), 696(m), 672(w), 638(w), 616(s), 598(m), 582(m), 499(s), 479(s). Elemental analysis calcd (%) for $C_{70}H_{64}EuF_4NO_8$ ($HNEt_3[Eu(\mathbf{L1})_4]$): C 66.35, H 5.09, N 1.11; found: C 65.70, H 4.59, N 1.10.

*$HNEt_3[Eu(\mathbf{L2})_4]$ (**Eu2**)*

Yield 96 mg, 51% based on Eu, of a light yellow powder. IR (ν/cm^{-1}): 1659(w), 1592(m), 1543(m), 1521(s), 1497(m), 1477(m), 1424(s), 1398(m), 1379(m), 1290(m), 1224(w), 1206(w), 1182(w), 1098(w), 1070(m), 1008(s), 951(m), 843(s), 807(w), 769(vs), 722(w), 593(m), 494(m), 469(m). Elemental analysis calcd (%) for $C_{70}H_{64}Br_4EuNO_8$ ($HNEt_3[Eu(\mathbf{L2})_4]$): C 55.36, H 4.25, N 0.92; found: C 55.33, H 3.38, N 0.86.

*$HNEt_3[Eu(\mathbf{L3})_4]$ (**Eu3**)*

Starting from 0.25 mmol of $EuCl_3$ and 1 mmol of ligand; yield 148 mg, 46% based on Eu, of a light yellow powder. IR (ν/cm^{-1}): 1597(m), 1582(m), 1558(s), 1520(s), 1495(s), 1472(s), 1456(s), 1386(m), 1294(w), 1233(m), 1175(m), 1118(w), 952(m), 889(m), 834(w), 800(w), 768(vs), 726(s), 673(w), 561(w), 456(m), 421(m). Elemental analysis calcd (%) for $C_{70}H_{64}EuF_4NO_8$ ($HNEt_3[Eu(\mathbf{L3})_4]$): C 66.35, H 5.09, N 1.11; found: C 65.11, H 4.81, N 1.15.

*$HNEt_3[Eu(\mathbf{L4})_4]$ (**Eu4**)*

Yield 170 mg, 100% based on Eu, of a light yellow powder. IR (ν/cm^{-1}): 3061(w), 3027(w), 2985(w), 1595(s), 1554(s), 1520(s), 1493(s), 1465(s), 1434(m), 1384(m), 1311(w), 1279(m), 1266(m), 1221(m), 1205(m), 1183(m), 1130(w), 1112(w), 1077(w), 1061(m), 1019(w), 942(w), 905(w), 833(w), 790(w), 765(vs), 732(m), 689(s), 672(w), 648(w), 594(w), 544(m), 497(w), 462(s). Elemental analysis calcd (%) for $C_{70}H_{64}Cl_4EuNO_8$ ($HNEt_3[Eu(\mathbf{L4})_4]$): C 62.70, H 4.81, N 1.04; found: C 60.74, H 4.23, N 1.04.

*$HNEt_3[Eu(\mathbf{L5})_4]$ (**Eu5**)*

Yield 120 mg, 66% based on Eu, of a light yellow powder. IR (ν/cm^{-1}): 3061(w), 2985(w), 1731(w), 1704(w), 1671(w), 1592(s), 1573(w), 1547(vs), 1511(vs), 1484(m), 1450(s), 1419(s), 1381(vs), 1304(m), 1282(m), 1266(m), 1214(m), 1178(w), 1127(w), 1059(m), 1024(m), 998(w), 943(w), 900(w), 805(w), 795(w), 750(vs), 704(vs), 686(s), 670(m), 655(s), 638(w), 609(m), 516(m), 467(m). Elemental analysis calcd (%) for $C_{66}H_{60}Br_4EuNO_8$ ($HNEt_3[Eu(\mathbf{L5})_4]$): C 54.19, H 3.86, N 0.96; found: C 52.81, H 3.44, N 0.96.

$HNEt_3[Eu(\mathbf{L6})_4]$ ($HNEt_3[\mathbf{Eu6}]$)

Starting from 0.25 mmol of $EuCl_3$ and 1 mmol of ligand; yield 360 mg, 84% based on Eu, of a light yellow powder. IR (ν/cm^{-1}): 1592(s), 1549(s), 1516(s), 1490(s), 1456(s), 1380(s), 1279(m), 1220(m), 1182(m), 1112(w), 1053(m), 1018(m), 995(w), 940(w), 834(w), 762(vs), 729(m), 668(s), 592(w), 456(m), 418(w). Elemental analysis calcd (%) for $C_{70}H_{64}EuI_4NO_8$ ($HNEt_3[Eu(\mathbf{L6})_4]$): C 49.26, H 3.78, N 0.82; found: C 48.11, H 3.15, N 0.83.

*$HNEt_3[Eu(\mathbf{L7})_4]$ (**Eu7**)*

Yield 130 mg, 78% based on Eu, of a light yellow powder. IR (ν/cm^{-1}): 3057(w), 2980(w), 2605(w), 2498(w), 1672(w), 1591(vs), 1552(s), 1519(s), 1494(s), 1437(vs), 1422(s), 1397(s), 1295(m), 1254(m), 1220(w), 1205(w), 1180(m), 1111(w), 1073(w), 1040(s), 1019(m), 939(w), 834(w), 809(w), 785(m), 754(vs), 737(s), 690(m), 640(m), 595(m), 542(m), 506(m), 453(s). Elemental analysis calcd (%) for $C_{70}H_{64}Cl_4EuNO_8$ ($HNEt_3[Eu(\mathbf{L7})_4]$): C 62.70, H 4.81, N 1.04; found: C 61.07, H 4.70, N 1.36.

*$NBu_4[Eu(dbm)_4]$ (**Eu8**)*

In 5 mL of ethanol was dissolved 2.1 mmol of Hdbm (0.5 g) and 2.1 mmol of NBu_4OH and the mixture was heated to 60 °C. Then, slowly a hot solution of 0.53 mmol of $EuCl_3$ in 5 mL ethanol was added. The mixture was stirred for 15 more minutes and allowed to cool to room temperature, yielding needle shaped crystals. Yield 0.59 g, 86% based on Eu. IR (ν/cm^{-1}): 3351(w, br), 3061(w), 2959(w), 2873(w), 1595(s), 1549(s), 1508(vs), 1463(vs), 1416(vs), 1307(m), 1279(m), 1213(m), 1179(w), 1156(w), 1066(m), 1023(m), 1000(w), 940(w), 925(w), 807(w), 781(m), 738(s), 717(vs), 688(vs), 607(s), 517(m), 502(m). Elemental analysis calcd (%) for $C_{76}H_{84}EuNO_8$ ($NBu_4[Eu(dbm)_4]$): C 70.90, H 6.26, N 1.09; found: C 70.50, H 6.54, N 1.13.

*$Li[Eu(dbm)_4]\cdot H_2O$ (**Eu9**)*

In 5 mL of ethanol was dissolved 0.53 mmol of $EuCl_3\cdot 6H_2O$, and the solution was heated to 60 °C. To another flask with 15 mL of ethanol was added 2.1 mmol of Hdbm (0.5 g), 2.1 mmol of NaOH (90 mg) and 3.75 mmol (0.26 g) of $LiNO_3\cdot 6H_2O$ and heated to 60 °C. The latter solution was added dropwise to the $EuCl_3$ solution with gentle stirring. Upon cooling,

the mixture yielded needle shaped crystals. Yield 0.39 g, 68% based on Eu. IR (ν/cm^{-1}): 3629(w), 3425(w, br), 3058(w), 1594(s), 1547(s), 1509(vs), 1476(s), 1454(s), 1389(s), 1308(m), 1279(m), 1218(m), 1178(w), 1155(w), 1058(m), 1022(m), 999(w), 939(w), 781(w), 744(m), 718(vs), 684(vs), 607(s), 519(s), 502(s).

$HNEt_3[Eu(dbm)_4]$

The synthesis of this compound is described in Chapter 6.

5.3 Results

5.3.1 Synthesis and Characterization

All Hdbm derivatives were synthesized in non-optimized yields following the same basic procedure for Claisen condensation reactions, and were analyzed using IR and NMR spectroscopy. Complex formation was performed by mixing of hot ethanolic solutions of the europium salt and ligand to ensure their complete dissolution and to slow down the precipitation of the product upon addition of the $EuCl_3$ solution. In general it was found that precipitation only starts after nearly complete addition of the $EuCl_3$ solution. The complexes with the substituted dbm ligands all analyze as $HNEt_3[EuL_4]$. The infrared spectra of the compounds are all similar and contain features as expected for these compounds, with aromatic C-H stretching around 3000 cm^{-1}, C=O stretching vibrations around 1590 cm^{-1} and strong bands in the 700-800 cm^{-1} region as a result of out-of-plane bending of the aromatic C-H groups. Unfortunately, all attempts to grow single crystals for structure determination have failed. However, based on the composition, it is assumed that the coordination environment of the Eu(III) ion in these compounds is similar to that of the parent compound, $HNEt_3[Eu(dbm)_4]$ [20-22]. The IR spectra of the two compounds $A[Eu(dbm)_4]$ (A = NBu_4^+ and Li^+) are very similar, the main difference is the absorption at 2873 cm^{-1}, which is characteristic for the NBu_4^+ cation.

5.3.2 X-ray crystal structure

Single crystals of **Eu8**, $NBu_4[Eu(dbm)_4]$ and **Eu9**, $Li[Eu(dbm)_4]\cdot H_2O$, were obtained by direct crystallization from the reaction mixture. Their crystal structures were determined using single crystal X-ray diffraction. Crystallographic data for of **Eu8** and **Eu9** are given in Table 5.1 and some selected bond distances and angles are listed in Table 5.2. Both compounds crystallize in the monoclinic *C*2/*c* space group. However, the structure of **Eu9** has a single crystallographically independent Eu(III) site, whereas **Eu8** has three, referred to as Eu-a, Eu-b and Eu-c hereafter. Furthermore, in **Eu9** a twofold rotation axis passes through the Eu(III) ion, and as a result there are just four independent Eu-O distances in this complex. In **Eu8**, a twofold rotation axis passes through the center of Eu-b and Eu-c, while the Eu-a site is surrounded by four crystallographically independent ligands. Because the coordination geometry of the Eu(III) sites in **Eu8** resemble each other, the data for only one

site are given in Table 5.2. In both **Eu8** and **Eu9**, the Eu(III) ion is surrounded by four dbm^- ligands binding in a bidentate mode and the geometry of $[Eu(dbm)_4]^-$ complex ion is best described as a distorted square antiprism, as shown in Figure 5.2. For **Eu9**, the Eu-O bond lengths range from 2.352(5) to 2.390(6) Å, for **Eu8** they range from 2.34(1) to 2.428(7) Å, which is normal for this type of bonds [23]. It should be noted that the packing in the structures of **Eu8** and **Eu9** differs substantially. In the latter structure, the alkyl groups of the tetrabutylammonium ions occupy the interspace between two of the ligands coordinated to Eu(III). In **Eu9**, the Li^+ ion resides in the cavities between the complexes and the molecule of water is coordinated to the Li^+ ion.

Table 5.1: Crystallographic data for compounds Eu8 and Eu9.

	Eu8	**Eu9**
formula	$C_{304}H_{326}Eu_4N_4O_{32}$	$C_{60}H_{44}EuLiO_9$
fw	5155.53	2139.74
crystal size [mm^3]	0.10 × 0.25 × 0.25	0.20 × 0.20 × 0.30
crystal color	colorless	colorless
crystal system	monoclinic	monoclinic
space group	*C*2/*c* (no. 15)	*C*2/*c* (no. 15)
a [Å]	28.220(4)	27.348(2)
b [Å]	42.970(6)	8.535(1)
c [Å]	21.415(4)	24.994(2)
α [°]	90	90
β [°]	90.05(3)	108.70(2)
γ [°]	90	90
V [$Å^3$]	25968(7)	5526.0(11)
Z	4	2
d_{calc} [g/cm^3]	1.319	1.284
μ [mm^{-1}]	1.023	1.188
refl. measured / unique	166900 / 22949	27693 / 4760
parameters / restraints	1392 / 18	339 / 24
R1/wR2 [I>2σ(I)]	0.0833 / 0.1177	0.0678 / 0.1828
R1/wR2 [all refl.]	0.1791 / 0.1327	0.0835 / 0.2033
S	1.63	1.09
$\rho_{min/max}$ [$e/Å^3$]	–1.49 / 2.24	–1.44 / 2.02

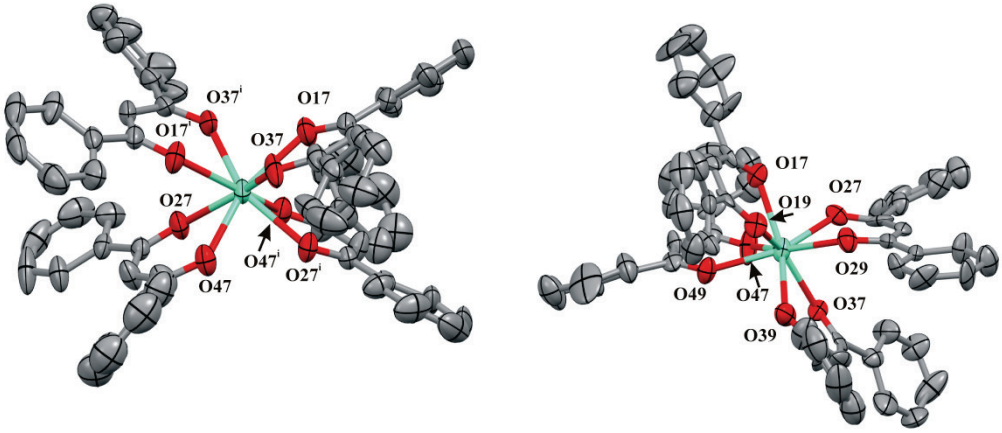

*Figure 5.2: Thermal ellipsoid plot (50% probability contours) of the $[Eu(dbm)_4]^-$ complex ions in **Eu9** ($Li[Eu(dbm)_4]$, left) and one of the three complex ions in **Eu8** ($NBu_4[Eu(dbm)_4]$, right). In both cases, the geometry resembles a distorted square antiprism. Hydrogen atoms have been omitted for clarity and the numbering scheme for O atoms is indicated.*

Table 5.2: Selected bond distances and angles for Eu8 and Eu9.

	Eu8	**Eu9**	
Bond distance (Å)			
Eu1–O17	2.390(8)	Eu1–O17	2.375(5)
Eu1–O27	2.399(9)	Eu1–O27	2.352(5)
Eu1–O37	2.428(7)	Eu1–O37	2.390(6)
Eu1–O47	2.34(1)	Eu1–O47	2.385(5)
Eu1–O19	2.388(9)		
Eu1–O29	2.352(9)		
Eu1–O39	2.41(1)		
Eu1–O49	2.368(8)		
Bond angle (°)			
O17-Eu1-O19	70.2(3)	O17-Eu1-O37	71.8(2)
O27-Eu1-O29	69.2(3)	O27-Eu1-O47	71.1(2)
O37-Eu1-O39	68.6(3)	O27-Eu1-O37	74.0(2)
O47-Eu1-O49	68.8(3)	O17-Eu1-O47	74.5(2)
O17-Eu1-O47	75.6(3)		
O19-Eu1-O49	74.1(3)		
O27-Eu1-O37	75.5(3)		
O29-Eu1-O39	76.7(3)		

5.3.3 Luminescent properties and lifetime

The solid state photoluminescence spectra recorded at room temperature for **Eu1 - Eu9** are shown in Figure 5.3. Excitation spectra were obtained by constantly monitoring the intensity of the Eu(III) $^5D_0 \rightarrow {}^7F_2$ hypersensitive transition at 614 nm while scanning the excitation wavelength. All complexes show two broad excitation bands in the UV and near-

UV (400 nm) region as a result of ligand-centered excitation [3, 4]. With the exception of **Eu7**, the excitation band in the UV region, around 290 nm, is slightly more intense than the second band at 400 nm. These bands also appear in the solid state UV-Vis absorption spectra that are shown in Figure 5.4. The emission spectra obtained by ligand-centered excitation all show lines at 595, 614, 650 and 720 nm. These are characteristic for the Eu(III) ion as a result of transitions from the $^5D_0$ resonance level to the ^7F_J manifold. All emission spectra are dominated by the $^5D_0 \rightarrow {}^7F_2$ transition at 614 nm. Table 5.3 lists the photoluminescence properties for all coordination compounds. The overall quantum yields, upon excitation with 360 nm radiation, range from 13% for **Eu2** to 57% for **Eu8**. The luminescence decay curves measured for **Eu1 - Eu7** could be satisfactorily fitted with a single exponential function, indicating the presence of a single luminescent Eu(III) center in the complexes. Experimental luminescence lifetimes range from 0.19 ms for **Eu2** to 0.89 ms for **Eu7**.

Table 5.3: Photophysical properties of the coordination compounds.

Complex	Φ_{tot} (%)	Ω_2 (10^{-20} cm^2)	Ω_4 (10^{-20} cm^2)	Ω_6 (10^{-20} cm^2)	τ_{exp} (ms)	τ_{rad} (ms)	Φ_{Ln} (%)	η_{sens} (%)
Eu1	24	23.96	2.96	0*	0.31	1.19	26	92
Eu2	13	21.70	2.68	0*	0.19	1.30	15	88
Eu3	27	22.20	4.09	11.47	0.54	1.23	44	62
Eu4	31	21.72	4.85	17.58	0.57	1.22	47	66
Eu5	35	21.53	4.97	20.27	0.55	1.23	45	78
Eu6	22	19.46	4.86	18.91	0.53	1.34	40	54
Eu7	24	9.47	5.73	8.61	0.89	2.18	41	59
Eu8	57	24.03$^{\pm}$	3.87$^{\pm}$	15.76$^{\pm}$	n.d.	1.14$^{\pm}$	n.d.	n.d.
Eu9	42	11.47	3.87	10.77	n.d.	2.18	n.d.	n.d.
$NEt_3[Eu(dbm)_4]$**	27	19.94$^{\pm}$	4.50$^{\pm}$	16.44$^{\pm}$	n.d.	1.32$^{\pm}$	n.d.	n.d.

*Notes: *: $^5D_0 \rightarrow {}^7F_6$ transition was too weak to be observed, **: for comparison, compound reported in Chapter 7; $^{\pm}$: average value for multiple Eu(III) sites ; Φ_{tot} (%): Overall photoluminescence quantum yield at 360 nm excitation, τ_{exp}: experimental lifetime of $^5D_0$ state, Ω_J: Intensity parameters, τ_{rad}: radiative lifetime, Φ_{Ln}: intrinsic quantum yield, η_{sens}: sensitizer efficiency.*

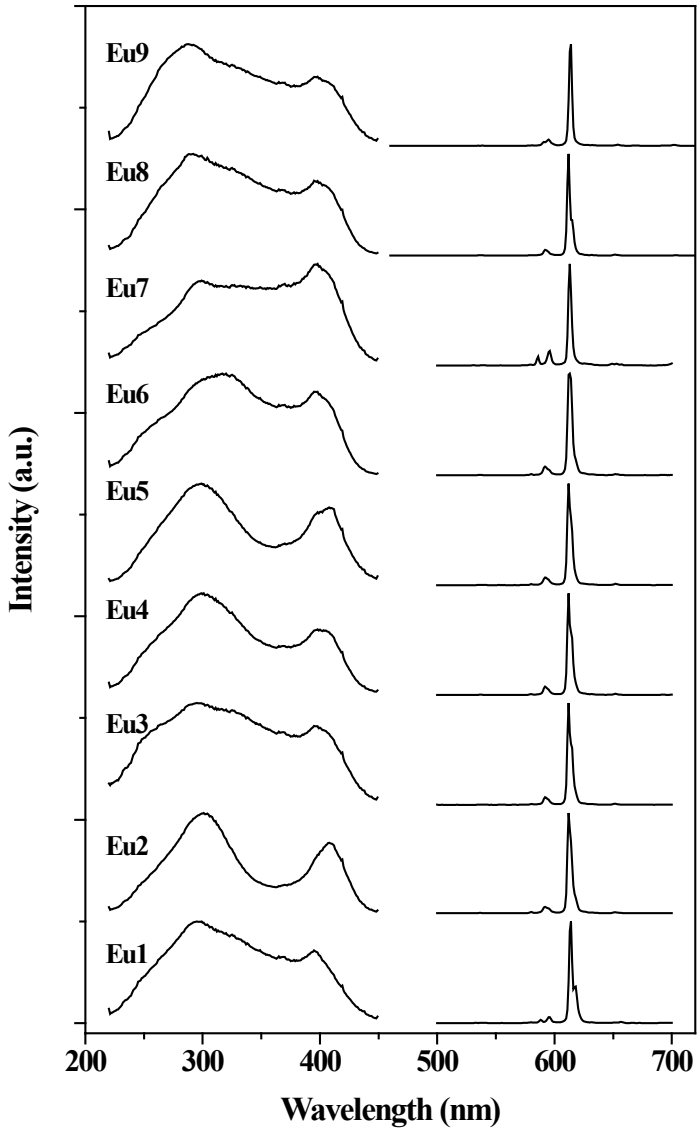

*Figure 5.3: Photoluminescence spectra for **Eu1 - Eu9**. Excitation spectra, shown on the left hand side, are recorded while monitoring the intensity of the strongest emission line at 614 nm. The right hand side shows the emission spectra of the compounds obtained upon excitation at 360 nm. The emission spectra are characteristic for the Eu(III) ion, with lines at 595, 614, 650 and 720 nm, corresponding to the $^5D_0 \rightarrow {}^7F_J$, J =1, 2, 3, 4 transitions.*

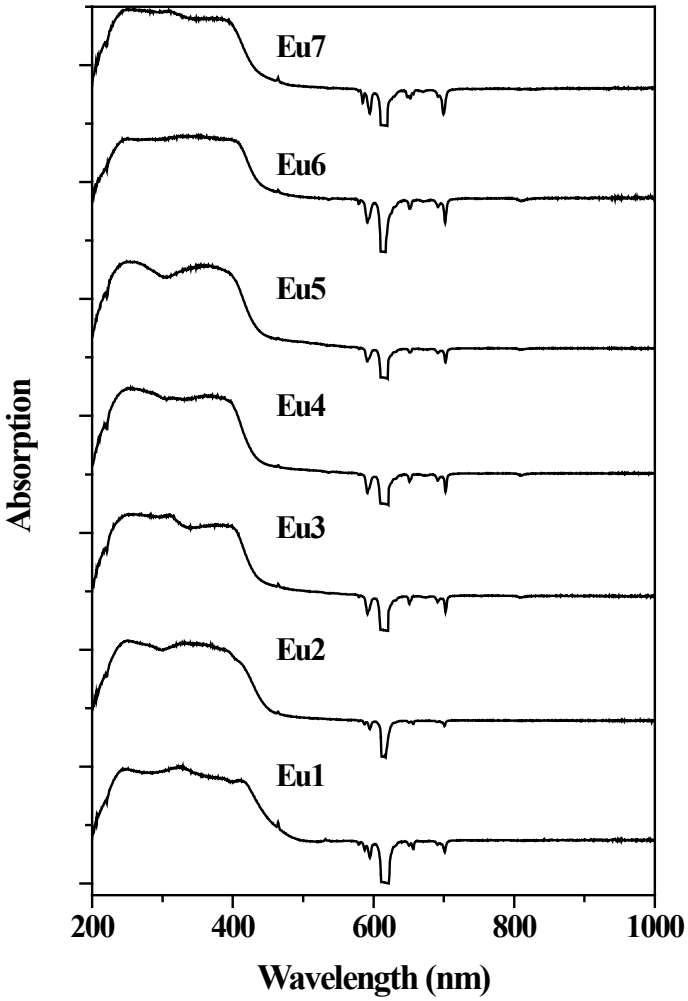

*Figure 5.4: Absorption spectra recorded for the Eu(III) complexes **Eu1** - **Eu7** in the solid state. The downward pointing peaks are due to Eu(III)-centered photoluminescence.*

5.4 Discussion

5.4.1 General remarks on the luminescent properties

The photoluminescence excitation spectra for all complexes show two bands, one centered around 290 nm and 400 nm, respectively. The absorption spectra show similar features and appear to be composed of two broad bands in the UV and nUV region. The emission that results upon excitation in the ligand-centered bands is typical for the Eu(III) ion in a non-centrosymmetric environment. The relatively high intensity of the $^5D_0 \rightarrow {}^7F_2$ electric dipole

(ED) transition with respect to the $^5D_0 \rightarrow {}^7F_1$ magnetic dipole (MD) transition is indicative of a low symmetry coordination site of the Eu(III) ion in all complexes [24].

5.4.2 Influence of the counter ions

The excitation spectra of the compounds with the unsubstituted ligand, $HNEt_3[Eu(dbm)_4]$, **Eu8** and **Eu9**, are highly similar. This is to be expected, because the antenna ligand is the same in all three compounds. However, the counter ion otherwise has a significant influence on the photophysical properties of the $[Eu(dbm)_4]^-$ complex ion. The structure of **Eu8** has three different sites for the Eu(III) ion, while the structure of **Eu9** has just one Eu(III) site. Due to the broad ligand centered absorption bands, it was impossible to selectively excite individual Eu(III) sites in $HNEt_3[Eu(dbm)_4]$ and **Eu8**. In related work, using low temperature spectroscopy, Mech and co-workers have shown that the properties of the various Eu(III) sites can be indeed very different [13]. Thus, only average values could be calculated for the intensity parameters and radiative lifetime, using the overall integrated intensity of the $^5D_0 \rightarrow {}^7F_J$ transitions. The intensity parameters Ω_λ are highly sensitive to the coordination sphere of the Eu(III) ion. From Table 5.3, it can be seen that there are significant differences amongst the three compounds with different counter ions. The observed differences are most likely the result from different packing arrangements of the $[Eu(dbm)_4]^-$ complex ions in those complexes, as different arrangements affect the Eu-O bond distances and angles. Worth noting is the increase in overall quantum yield on going from the $HNEt_3^+$ to Li^+ to NBu_4^+ counter ions, which is most likely due to higher energy transfer efficiency and / or less contributions of non-radiative quenching processes in the latter compounds.

5.4.3 Influence of the substituents

The emission spectra of Eu(III) compounds have been analyzed by using the Judd-Ofelt (JO) theory [25, 26]. According to JO theory, the intensities of a forced electric dipole transition depends only on three parameters (Ω_λ, $\lambda = 2, 4, 6$), which are dependent on the surroundings of the lanthanoid ion. Properties such as the symmetry of the coordination sphere, the nature of the bonds and the basicity of the coordinating atoms are reflected in the parameters [27-31]. The calculated JO parameters for **Eu1 - Eu9** are listed in Table 5.3. All compounds have a high Ω_2, indicating low site symmetry and a relatively covalent bond between Eu(III) and the ligands [32, 33]. Based on the JO parameters, compounds **Eu1**-**Eu7** may be divided into three groups. The first comprises **Eu1** and **Eu2**, and is characterized by $\Omega_2 > 21 \cdot 10^{-20}$ cm^2 and $\Omega_4 < 3 \cdot 10^{-20}$ cm^2. For the compounds in this group the value of the Ω_6 parameter could not be determined because emission of the corresponding $^5D_0 \rightarrow {}^7F_6$ transition was absent. The second group, covering the compounds **Eu3** to **Eu6** has a comparable Ω_2 ($\sim 21 \cdot 10^{-20}$ cm^2) but with $4 \cdot 10^{-20}$ cm$^2 < \Omega_4 < 5 \cdot 10^{-20}$ cm^2. The Ω_6 parameter increases steadily from 11.5 for **Eu3** to 20.3 for **Eu5** and drops slightly to 18.9 for **Eu6**. Compound **Eu7** forms the last 'group' because its JO parameters differ

substantially from all other compounds. The Ω_2 parameter is about half that of all other compounds, while its Ω_4 is the highest of the entire series. The value of the Ω_6 parameter is in between those found for the other two groups. These differences reflect the different coordination environments in the complexes. A large Ω_2 is associated with a highly asymmetric coordination environment and / or covalency of the M-L bonds [31-33]. Its value is similar for the first two groups, indicating a low symmetry coordination sphere and similar nature of the M-O bonds in these compounds. For compound **Eu7** the low Ω_2 suggests substantially different coordination geometry in this compound, as can be expected from the steric demands of the 2-Cl substituent on the ligand. Since the meaning of the Ω_4 parameter is ill-defined it is not appropriate to draw any conclusions from its values [34]. The Ω_6 parameter is linked to the electron density on the donor atoms and to the Coulomb interaction between the lanthanoid ion and the donor atoms [31, 33, 35]. Its value increases when the electron density on the coordinating atoms decreases and when the M-L distance increases or with decreasing covalency [35]. The value of this parameter is negligible in the first group, which indicates a covalent character of the M-O bond. In the second group of compounds, the value of the Ω_6 parameter is fairly large, suggesting a less covalent nature of the M-L bonds compared to the first group. In addition, the trend of Ω_6 for the second group of complexes reflects a decreasing electron density on the ligands on going from **L3** to **L5** and a slight increase for **L6**, which correlates with the electron withdrawing character of the substituent halogen atoms. For the last compound, **Eu7**, Ω_6 takes an intermediate value compared to the other two groups of complexes. This suggests that the nature of the M-L bonds is not as covalent as in **Eu1** and **Eu2**, but more covalent than in **Eu3** - **Eu6**.

5.4.4 Luminescent lifetime and intrinsic quantum yield

The $^5D_0 \rightarrow {}^7F_1$ transition of the Eu(III) ion is of purely MD nature and as such insensitive to the ion's coordination environment. As a result, the radiative lifetime of Eu(III) can be calculated from its emission spectrum, provided that the spectra are corrected for the response of the spectrometer [29]. In that case, the intensity of the MD transition can be used as an internal benchmark and its relaxation (A_{0-1}) rate can be calculated (49 s^{-1}) [29]. The relaxation rate of the other transitions can be found from their intensities I_{0-J} using equation 1.

$$A_{0-J} = A_{0-1}\frac{I_{0-J}}{I_{0-1}} \qquad (1)$$

The total radiative relaxation rate A_{rad} is the sum of all A_{0-J}'s and the radiative lifetime τ_{rad} is the reciprocal of A_{rad}. The radiative lifetimes for **Eu1 - Eu9** have been calculated and are listed in Table 5.3. The excited $^5D_0$ state of Eu(III) is not only depopulated by radiative processes, but also by non-radiative processes such as multiphonon quenching [36]. This is reflected in the experimental lifetime, which is usually shorter than the radiative lifetime. If

the rate of such non-radiative processes is given by A_{nrad}, the sum of A_{rad} and A_{nrad} results in the total relaxation rate A_{tot}, which is in turn the reciprocal of the experimental lifetime τ_{exp}, as shown in equation 2.

$$A_{tot} = \frac{1}{\tau_{exp}} = \frac{1}{\tau_{rad}} + \frac{1}{\tau_{nrad}} \quad (2)$$

The relative contribution of the radiative process to the relaxation of the excited state is known as the intrinsic quantum yield, Φ_{Ln} of the lanthanoid ion [37, 38]. Its value can be calculated from equation 3.

$$\Phi_{Ln} = \frac{A_{rad}}{A_{tot}} = \frac{\tau_{exp}}{\tau_{rad}} \quad (3)$$

The intrinsic quantum yields for **Eu1 - Eu7** are listed in Table 5.3. The lowest value is obtained for **Eu2** at 15%, indicating that the non-radiative processes are mainly responsible for relaxation of the $^5D_0$ state of Eu(III). For the other compounds, the values range from 26% to 47%, which shows that non-radiative decay processes contribute substantially to the depopulation of the Eu(III) $^5D_0$ state in all compounds. As a result, the overall quantum yields are limited.

5.4.5 Antenna efficiency

Using the intrinsic quantum yield and the overall photoluminescence quantum yield Φ_{tot}, the efficiency of the sensitization process η_{sens} can be estimated from the relation $\Phi_{tot} = \eta_{sens} \cdot \Phi_{Ln}$ [37, 39]. The sensitization efficiency is a measure of how effective an antenna the ligand is, and can be used to compare the antenna potential of the ligands. For compounds **Eu1 - Eu7**, the values for sensitization efficiency have been calculated and are listed in Table 5.3. The values range from 54% for **Eu6** to 92% for **Eu1**, indicating moderate to highly efficient ligand-to-metal energy transfer. The sensitization efficiency is determined by the efficiency of the intersystem crossing and ligand to metal energy transfer processes [37]. The efficiency of the energy transfer process depends on the energy gap between the ligand excited triplet state and the accepting level on the lanthanoid ion [40, 41]. In general, the introduction of substituents on the dibenzoylmethane molecule can be expected to affect the following properties:

- The energy levels of the excited singlet and triplet states;
- The intersystem crossing efficiency;
- The orbital overlap between ligand orbitals and metal orbitals.

For ortho-substitution, steric effects may play a role, and in case of meta-substitution, only inductive effects can occur, while both resonance and inductive effects of the substituents

may influence the properties of para-substituted molecules. The excited triplet state of the dbm^- ligands is associated with a double-radical structure resulting from the separation of two electrons of a double bond. Owing to their parallel spin, a strong repulsion exists between these electrons, resulting in the largest possible spatial separation [2]. As a result, the excited triplet state is stabilized by substituents that allow such separation. This stabilizing effect of the ligand T*-state is expected to be the largest for the first group of complexes, consisting of **Eu1** and **Eu2**, with a 4-Me, 4'-F and 4-Me, 4'-Br substitution pattern. Indeed, these compounds show relatively high sensitizer efficiencies around 90%. However, the luminescent centers in these compounds have the lowest intrinsic quantum yields of the series studied, resulting in low overall quantum yields. This indicates that non-radiative processes depopulating the Eu(III) $^5D_0$ state are the limiting factor. Comparison of the compounds **Eu3 - Eu6**, with F, Cl, Br and I as substituents, respectively, shows that the overall quantum yield increases slightly from 27% for **Eu3** to 35% for **Eu5**, and drops to 22% for **Eu6**. The intrinsic quantum yields for all complexes are roughly the same and vary from 40% to 47%. Indeed, the main difference in overall quantum yield is the result from differences in sensitizer efficiency, which show the same trend as the overall quantum efficiency. This can be understood from the ability of the different halogen substituents to lower the energy of the T*-state, that is, the ability to separate the two electrons of the T*-state. The inductive electron-withdrawing power of the halogens increases on going from F to I, lowering the triplet state and thereby facilitating ligand-to-metal energy transfer. This in turn increases sensitizer efficiency. In case of **Eu6**, the ligand T*-state may be too close to the $^5D_0$ level of Eu(III), which allows for thermal assisted back-transfer of energy thus lowering the sensitizer efficiency [41]. Compared to the first group of complexes, the ligands with the halogens on the 3'-position are less efficient antennae.

It has been reported that ortho substitution with F and Cl results in decreased absorption intensity with respect to the unsubstituted dbm molecule, because the conjugation between the benzene ring and the chelate ring is disturbed [11]. Nevertheless, the quantum yield of $HNEt_3$[**Eu7**] with a 2-chloro substituent on the ligand, is still moderate with 24%. This complex has the longest experimental and radiative lifetimes, suggesting that the ligands provide a rigid environment for the luminescent center. Although the coordination sphere around the metal ion may differ substantially from the other complexes, the ability of the ligand $\mathbf{L7}^-$ to sensitize Eu(III) emission is average in the series **Eu1 - Eu7**.

It appears that the classification of the compounds **Eu1 - Eu7** into three groups based on the Judd-Ofelt parameters can be extended to include sensitizer efficiency of the ligand and the intrinsic quantum yield of the luminescent center. For the first group, the sensitizer efficiency is the highest of the entire series of complexes studied, but the intrinsic quantum yields are the lowest. The Ω_6 parameter could not be determined owing to the low intensity of the corresponding $^5D_0 \rightarrow {}^7F_6$ transition in the emission spectra. This is indicative of a relatively covalent nature of the Eu-O bonds in the complex. Because of the 4,4'-substitution pattern, both resonance and inductive effects play a role. Although the

halogens are electron-withdrawing, resonance structures that increase the electron density at the donor atoms are present. This nature is reflected in the Hammett σ constants for the halogens, which have a more chemical background [42]. Some relevant Hammett parameters are given in Table 5.4. The halogens have positive σ_p, indicating their overall electron-withdrawing nature, but negative σ_R, indicating electron donation by resonance. This electron donating resonance effect is not possible in the ligands of the second group, with the halogen on the 3-position. Hence, only the withdrawing inductive effect remains, which is indicated by the positive values for σ_m of the halogens in Table 5.4. In turn, this results in a less covalent Eu-O bond, which is reflected by increased Ω_6 parameters. The slightly increased values for the Ω_4 and the nonzero values for the Ω_6 parameters are the main differences comparing the second group to the first. It should be noted here that the slightly electron donating 4'-Me substituent is not present in **Eu5**. This might partially explain the increased Ω_2 and η_{sens} parameters in Table 5.3 for this compound. The last group, compound **Eu7**, is characterized by the lowest Ω_2 parameter and the longest radiative and experimental lifetimes of the entire series. In this compound, an electron donation by resonance of the chloride p orbitals with the aromatic system is possible. However, unfortunately no reliable σ_o parameters exist as steric effects play a major role on the ortho position.

Table 5.4: Selected Hammett σ constants, compiled from ref [42].

Substituent	σ_m	σ_p	σ_I	σ_R
CH_3	– 0.07	– 0.17	–0.04	–0.11
F	0.34	0.06	0.52	–0.34
Cl	0.37	0.23	0.47	–0.23
Br	0.39	0.23	0.44	–0.19
I	0.35	0.18	0.39	–0.16

Notes: Hammett σ parameters reflect the electron withdrawing (positive values) and electron donating (negative values) properties of substituents on a phenyl ring with respect to hydrogen. σ_m: overall σ parameter for the meta position, σ_p: overall σ parameter for the para position, $\sigma_{I/R}$: parameter describing just inductive/resonance effects.

5.5 Conclusion

Seven new Eu(III) complexes with various substituted dibenzoylmethane ligands have been synthesized in yields ranging from 46% to 100%. In addition, two new compounds of the $[Eu(dbm)_4]^-$ complex ion with NBu_4^+ and Li^+ have been prepared. Photoluminescence studies indicate that ligand-centered excitation in the near-UV spectral region results in emission from the Eu(III) center for all complexes. Analysis of the corrected emission spectra reveals the effects of the ligand substituents on the environment of the Eu(III) ion, as well as the effect on the antenna efficiency of the ligands. These effects can be at least qualitatively understood by the electron-withdrawing and donating properties of the

substituents. Substitution with F and Br on the para position gives rise to highly efficient sensitization of Eu(III) luminescence, but results in a coordination sphere around Eu(III) that gives rise to efficient non-radiative quenching. This severely limits the overall photoluminescence quantum yield of the compounds. Substitution on the meta position of the phenyl ring gives results in lower sensitizer efficiencies but higher intrinsic quantum yields of the luminescent center. In addition, there appears to be a minor improvement in sensitizer efficiency when the substituent's abilities to stabilize the ligand T*-state increases. Ortho substitution leads to important changes in the coordination environment of the Eu(III) ion, as evidenced by the intensity parameters. In addition to the substituents, the counter ion has a substantial influence on the photophysical properties of the compounds.

5.6 References

[1] J.J. Freeman and G.A. Crosby, *J. Phys. Chem.*, 67 (1963) 2717-2723.

[2] N. Filipescu, W.F. Sager, and F.A. Serafin, *J. Phys. Chem.*, 68 (1964) 3324-3346.

[3] W.F. Sager, N. Filipescu, and F.A. Serafin, *J. Phys. Chem.*, 69 (1965) 1092-1100.

[4] R.G. Charles and E.P. Riedel, *J. Inorg. Nucl. Chem.*, 28 (1966) 3005-3018.

[5] L.R. Melby and N.J. Rose, Eight coordinate trivalent rare earth metal chelates with β-diketones, Pat.no US 3254103, 1966.

[6] K. Binnemans, *Rare earth beta-diketonates*, in *Handbook on the Physics and Chemistry of Rare Earths*, 2005, Elsevier. 107-272.

[7] G.S. Hammond, W.G. Borduin, and G.A. Guter, *J. Am. Chem. Soc.*, 81 (1959) 4682-4686.

[8] W. Schwack and T. Rudolph, *J. Photochem. Photobiol., B*, 28 (1995) 229-234.

[9] J.-C. Hubaud, I. Bombarda, L. Decome, J.-C. Wallet, and E.M. Gaydou, *J. Photochem. Photobiol., B*, 92 (2008) 103-109.

[10] I. Karlsson, L. Hillerstrom, A.L. Stenfeldt, J. Martensson, and A. Borje, *Chem. Res. Toxicol.*, 22 (2009) 1881-1892.

[11] J. Zawadiak and M. Mrzyczek, *Spectrochim. Acta A*, 96 (2012) 815-819.

[12] M.L.P. Reddy, V. Divya, and R.O. Freire, *Dalton Trans.*, 40 (2011) 3257-3268.

[13] A. Mech, M. Karbowiak, C. Görller-Walrand, and R. Van Deun, *J. Alloy. Compd.*, 451 (2008) 215-219.

[14] S.M. Bruno, R.A.S. Ferreira, F.A. Almeida Paz, L.s.D. Carlos, M. Pillinger, P. Ribeiro-Claro, and I.S. Gonçalves, *Inorg. Chem.*, 48 (2009) 4882-4895.

[15] J.C. de Mello, H.F. Wittmann, and R.H. Friend, *Adv. Mater.*, 9 (1997) 230-232.

[16] T. Kottke and D. Stalke, *J. Appl. Crystallogr.*, 26 (1993) 615-619.

[17] G.M. Sheldrick, *Acta Crystallogr., Sect. A. Found. Crystallogr.*, 64 (2008) 112-122.

[18] G.M. Sheldrick, *SHELXS–97*, *Bruker AXS Inc., Madison, Wisconsin*, 1997.

[19] Nonius, *COLLECT*, *Nonius BV, Delft, The Netherlands*, 2002.

[20] L.M. Sweeting and A.L. Rheingold, *J. Am. Chem. Soc.*, 109 (1987) 2652-2658.

[21] F.A. Cotton, L.M. Daniels, and P. Huang, *Inorg. Chem. Commun.*, 4 (2001) 319-321.

[22] S. Akerboom, M.S. Meijer, M.A. Siegler, W.T. Fu, and E. Bouwman, *J. Lumin.*, 145 (2014) 278-282.

[23] A.G. Orpen, L. Brammer, F.H. Allen, O. Kennard, D.G. Watson, and R. Taylor, *J. Chem. Soc. Dalton Trans.*, (1989) S1-S83.
[24] R. Reisfeld, E. Zigansky, and M. Gaft, *Mol. Phys.*, 102 (2004) 1319 - 1330.
[25] B.R. Judd, *Phys. Rev.*, 127 (1962) 750-761.
[26] G.S. Ofelt, *J. Chem. Phys.*, 37 (1962) 511-520.
[27] J.H.S.K. Monteiro, I.O. Mazali, and F.A. Sigoli, *J. Fluoresc.*, 21 (2011) 2237-2243.
[28] H. Liang, Z. Zheng, Q. Zhang, H. Ming, B. Chen, J. Xu, and H. Zhao, *J. Mater. Res.*, 18 (2003) 1895-1899.
[29] M.H.V. Werts, R.T.F. Jukes, and J.W. Verhoeven, *Phys. Chem. Chem. Phys.*, 4 (2002) 1542-1548.
[30] C. Görller-Walrand and K. Binnemans, *Spectral intensities of f-f transitions*, in *Handbook on the Physics and Chemistry of Rare Earths*, 1998, Elsevier. 99-264.
[31] S. Tanabe, T. Ohyagi, N. Soga, and T. Hanada, *Phys. Rev. B*, 46 (1992) 3305-3310.
[32] C.K. Jørgensen and R. Reisfeld, *J. Less-common. Met.*, 93 (1983) 107-112.
[33] H. Ebendorff-Heidepriem, D. Ehrt, M. Bettinelli, and A. Speghini, *J. Non-Cryst. Solids*, 240 (1998) 66-78.
[34] M.P. Hehlen, M.G. Brik, and K.W. Krämer, *J. Lumin.*, 136 (2013) 221-239.
[35] S. Tanabe, K. Takahara, M. Takahashi, and Y. Kawamoto, *J. Opt. Soc. Am. B*, 12 (1995) 786-793.
[36] M.H.V. Werts, *Sci. Prog.*, 88 (2005) 101-131.
[37] J.-C.G. Bünzli, *Chem. Rev.*, 110 (2010) 2729-2755.
[38] L. Armelao, S. Quici, F. Barigelletti, G. Accorsi, G. Bottaro, M. Cavazzini, and E. Tondello, *Coord. Chem. Rev.*, 254 (2010) 487-505.
[39] B. Francis, D.B.A. Raj, and M.L.P. Reddy, *Dalton Trans.*, 39 (2010) 8084-8092.
[40] S. Faulkner, S.J.A. Pope, and B.P. Burton-Pye, *Appl. Spectrosc. Rev.*, 40 (2005) 1-31.
[41] M. Latva, H. Takalo, V.M. Mukkala, C. Matachescu, J.C. Rodriguez-Ubis, and J. Kankare, *J. Lumin.*, 75 (1997) 149-169.
[42] M. Montalti, A. Credi, L. Prodi, and M.T. Gandolfi, *Handbook of Photochemistry 3rd edition*, 2006, Boca Raton, Florida: CRC Press.

6 Triboluminescence of lanthanoid dibenzoylmethanates

A series of lanthanoid coordination compounds with the general formula $HNEt_3[Ln(dbm)_4]$ (Ln = La, Nd, Sm, Eu, Tb, Dy, Ho, Er, Tm, Yb; dbm = dibenzoylmethanate) has been prepared and characterized. Single crystals with Ln = La, Nd and Sm were obtained. Single crystal X-ray diffraction studies reveal that the compounds with Ln = La, Nd crystallize in the space group $P2_1/c$, while the Sm-compound crystallizes in the space group Pc. Based on powder XRD data, the compounds with Ln = Eu - Yb can be described with a monoclinic cell. Photoluminescence studies show that compounds with Ln = Sm, Eu exhibit bright photoluminescence characteristic of the lanthanoid ion upon excitation in the near UV range. Furthermore, $HNEt_3[Sm(dbm)_4]$ has been identified as a novel triboluminescent compound.

(The work in this chapter has been published:
S. Akerboom, M. Meijer, M.A. Siegler, W.T. Fu, E. Bouwman, *J. Lumin.* 145 (2014) 278).

6.1 Introduction

Since the 1950s, molecules based on the beta-diketone structural motif have been found to be good ligands for *Ln*(III) ions, giving rise to stable complexes [1]. The chemical and physical properties of these complexes have been reviewed extensively by Binnemans [2]. When deprotonated, the beta-diketone molecules are monoanionic and, in principle, three ligands are needed to compensate for the charge of the *Ln*(III) ion, giving rise to a neutral complex. In such complexes, the coordination number of the metal is 6, while the lanthanoids normally prefer a higher coordination number, typically 8 or 9 [3, 4]. As a result, the coordination sphere in these complexes is usually saturated by coordination of solvent molecules to the lanthanoid ion, examples include $[Eu(ttfa)_3(H_2O)_2]$, $[Eu(aftfbd)_3(H_2O)_2]$ and $[Eu(ttfa)_3(DMSO)_2]$ (Httfa = 1-(2-thienyl)-4,4,4-trifluoro-1,3-butanedione, Haftbd = (2-acetylfluorene)-4,4,4-trifluoro-1,3-butanedione) [5-7]. These solvent molecules can be replaced by another chelating neutral ligand, such as 1,10-phenanthroline or 2,2'-bipyridine [6, 8, 9]. It is however possible to prepare homoleptic *Ln*(III) complexes with four beta-diketone type ligands when the appropriate conditions are employed during synthesis. As the resulting complex will be monoanionic, a counter ion is needed. Lanthanoid complexes with beta-diketones have interesting photophysical properties, including photoluminescence, laser action and electroluminescence [7, 8, 10-14]. These are a result of the so-called 'antenna-effect', in which the ligand is capable of transferring energy of its excited state to an excited state of the lanthanoid ion. This mechanism provides efficient sensitization of the lanthanoid ion, as direct intra-4f transitions are parity- and often spin forbidden. In 1966, Hurt *et al.* reported that $HNEt_3[Eu(dbm)_4]$ (Hdbm = dibenzoylmethane) exhibits intense luminescence, characteristic of Eu(III), upon fracture of the crystals, a phenomenon known as *triboluminescence* (TrL) [15]. The word derives from the Greek *tribein*, meaning 'to rub' [16]. For the analogous Tb(III) complex, only very weak triboluminescence was observed. Triboluminescence has also been reported for (2-hydroxyethylammonium)$[Eu(dbm)_4]$ and (pyrrolidinium)$[Eu(dbm)_4]$ by Xiong *et al.*[17] and for $[Tb(tmhd)_3$(4-(dimethylamino)pyridine)] (Htmhd = 2,2,6,6-tetramethyl-3,5-heptanedione) and its Sm(III) analog [18]. In these compounds, the luminescence spectrum is characteristic for the lanthanoid ion in the complex. Bulgakov and co-workers have studied triboluminescence for the entire series $[Ln(acac)_3(H_2O)]$, *Ln* = Ce, Pr, Eu, Gd, Tb, but only for the Eu and Tb compounds the TrL spectrum shows emission by the lanthanoid ion [19]. For the other compounds, the TrL-spectra correspond to the $^3\Pi_u$-$^3\Pi_g$ transitions of N_2*. The authors explain the TrL phenomenon as arising from adsorbed molecules of dinitrogen. Excitation of adsorbed dinitrogen molecules can in turn be explained by the generation of an electric field upon fracture of the crystals [18, 19]. In the past, it has often been claimed that noncentrosymmetric crystals are a prerequisite for TrL to occur [20]. Cracking such materials would lead to the buildup of opposite charge on the opposing crystal faces at

voltages high enough to allow for gas discharge. In triboluminescent lanthanoid complexes, the resulting emission can be absorbed by the ligands. Indeed, experiments with Gd(III) complexes show TrL characteristic for the ligand, suggesting that the ligand is acting as an energy-harvesting antenna [21]. As of to date, the compound described by Hurt is still the compound with highest TrL intensity [22]. The present Chapter concerns a systematic investigation of the photo- and triboluminescent properties of some lanthanoid analogues of $HNEt_3[Eu(dbm)_4]$.

6.2 Experimental

6.2.1 General

C, H, N analysis was performed using a Perkin-Elmer 2400 series II analyzer. X–ray powder diffraction was performed on a Philips X'pert diffractometer equipped with an X'cellerator detector. A Perkin-Elmer Spectrum Two FTIR spectrometer equipped with the UATR Two accessory was used to record IR spectra. Photoluminescence spectra were recorded on a Shimadzu RF-5301PC spectrofluoriphotometer. Triboluminescence spectra were recorded using an irradiance calibrated Avantes AvaSpec ULS2048L CCD spectrometer connected to a quartz cuvette holder. The spectrometer was controlled by the AvaSoft 7.7 software, which was programmed to record and save a spectrum every 40 ms while the sample was being crushed in the cuvette using a stainless steel spatula.

6.2.2 Crystal structure determination

Single crystal X-ray diffraction measurements were performed on crystals of [**1**], [**2**] and [**3**]. All reflection intensities were measured at 110(2) K ([**1**] and [**2**]) or 190(2) K ([**3**]) using a SuperNova diffractometer equipped with Atlas detector with Mo-Kα ([**1**], λ = 0.71073 Å) or Cu-Kα ([**2**] and [**3**], λ = 1.5418 Å) radiation (mirror optics) under the program CrysAlisPro (Version 1.171.36.24 Agilent Technologies, 2012). The program CrysAlisPro was used to refine the cell dimensions and for data reduction. The structure was solved with the program SHELXS-97 and was refined on F^2 with SHELXL-97 [23, 24]. Analytical numeric absorption corrections based on a multifaceted crystal model were applied using CrysAlisPro. The temperature of the data collection was controlled using the system Cryojet, manufactured by Oxford Instruments. The H atoms, unless otherwise specified, were placed at calculated positions with isotropic displacement parameters having values 1.2 or 1.5 times *U*eq of the attached C atoms. The H atoms attached to the N atoms of the triethylammonium cations were found from Fourier difference maps, and their atomic coordinates and isotropic thermal factors were refined freely.

Unit cell dimensions of compounds [**4**] - [**10**] have been determined using the Le Bail extraction routine implemented in the Rietica program (version 1.77) [25, 26]. A six term polynomial was used to fit the background, and the peak profile was described by a pseudo-

Voigt function. Lattice refinements of compounds [**4**] - [**10**] were carried out in the space group *I2/a* that has been reported for [**4**] by Sweeting *et al.* in 1987 [20]. Note that the *I2/a* cell can be transformed to a *C2/c* cell, which is the standard setting for space group no. 15.

6.2.3 Synthesis

Lanthanoid chlorides were synthesized by stirring the respective oxides in an excess of concentrated hydrochloric acid at 90 °C in a round bottom flask equipped with a reflux condenser until clear solutions were obtained. Subsequently, the solutions were concentrated to a volume of approximately 10 mL by rotary evaporation, 35 mL of water was added and the resulting mixtures were concentrated *in vacuo* to give the salts as fine powders.

Compounds [**1**] to [**10**] were synthesized according to a general procedure. Hdbm (897 mg, 4.0 mmol) was dissolved in EtOH (10 mL) and NEt_3 (0.56 mL, 4.0 mmol) was added. The yellow solution was heated to 60 °C. The lanthanoid salt $Ln Cl_3 \cdot n H_2O$, assuming $n = 7$ for *Ln* = La, Pr and $n = 6$ for *Ln* = Nd - Yb, (1.0 mmol) was also dissolved in 10 mL EtOH and heated to 60 °C. The lanthanoid salt solution was added slowly to the solution containing the ligand, resulting in a suspension. The suspension was stirred at 60 °C for 2 hours, causing it to redissolve. The erlenmeyer flasks containing the mixtures were closed with a stopper and placed on a bench. Crystals began to appear within a few hours. After 1 day the crystals were collected on a P3 glass frit, washed with cold EtOH and dried in a vacuum oven at 40 °C for one day.

*$HNEt_3[La(dbm)_4]$ ([**1**])*

Starting from $LaCl_3 \cdot 7H_2O$ (371 mg, 1.00 mmol). This reaction mixture was stored at –20 °C for 10 days to promote crystal growth. The product is a pale yellow crystalline solid. Yield: 328 mg (0.29 mmol, 29%). Elemental analysis calcd (%) for $C_{66}H_{60}LaNO_8$ ($HNEt_3[La(dbm)_4]$): C 69.90, H 5.33, N 1.24; found: C 69.98, H 5.75, N 1.25.

*$HNEt_3[Nd(dbm)_4]$ ([**2**])*

Starting from $NdCl_3 \cdot 6H_2O$ (359 mg, 1.00 mmol); product is an orange crystalline solid. Yield: 730 mg (0.64 mmol, 64%). Elemental analysis calcd (%) for $C_{66}H_{60}NNdO_8$ ($HNEt_3[Nd(dbm)_4]$): C 69.56, H 5.31, N 1.23; found: C 69.51, H 5.67, N 1.55.

*$HNEt_3[Sm(dbm)_4]$ ([**3**])*

Starting from $SmCl_3 \cdot 6H_2O$ (365 mg, 1.00 mmol); product is a yellow crystalline solid. Yield: 584 mg (0.51 mmol, 51%). Elemental analysis calcd (%) for $C_{66}H_{60}NO_8Sm$ ($HNEt_3[Sm(dbm)_4]$): C 69.20, H 5.28, N 1.22; found: C 68.87, H 4.94, N 1.27.

*$HNEt_3[Eu(dbm)_4]$ ([**4**])*

Starting from $EuCl_3 \cdot 6H_2O$ (366 mg, 1.00 mmol); product is a yellow crystalline solid. Yield: 901 mg (0.79 mmol, 79%). Elemental analysis calcd (%) for $C_{66}H_{60}EuNO_8$ ($HNEt_3[Eu(dbm)_4]$): C 69.10, H 5.27, N 1.22; found: C 68.80, H 5.88, N 1.20.

*$HNEt_3[Tb(dbm)_4]$ ([**5**])*

Starting from $TbCl_3 \cdot 6H_2O$ (10 mL of a 0.1 M stock solution in ethanol); product is a yellow crystalline solid. Yield: 779 mg (0.67 mmol, 67%). Elemental analysis calcd (%) for $C_{66}H_{60}NO_8Tb$ ($HNEt_3[Tb(dbm)_4]$): C 68.69, H 5.24, N 1.21; found: C 68.67, H 5.66, N 1.23.

*$HNEt_3[Dy(dbm)_4]$ ([**6**])*

Starting from $DyCl_3 \cdot 6H_2O$ (377 mg, 1.00 mmol); product is a pale yellow crystalline solid. Yield: 774 mg (0.81 mmol, 81%). Elemental analysis calcd (%) for $C_{66}H_{60}DyNO_8$ ($HNEt_3[Dy(dbm)_4]$): C 68.47, H 5.22, N 1.21; found: C 68.51, H 5.66, N 1.28.

*$HNEt_3[Ho(dbm)_4]$ ([**7**])*

Starting from $HoCl_3 \cdot 6H_2O$ (379 mg, 1.00 mmol); product is a yellow crystalline solid in daylight and an orange-pink crystalline solid under fluorescent lighting. Yield: 811 mg (0.70 mmol, 70%). Elemental analysis calcd (%) for $C_{66}H_{60}HoNO_8$ ($HNEt_3[Ho(dbm)_4]$): C 68.33, H 5.21, N 1.21; found: C 68.06, H 5.63, N 1.23.

*$HNEt_3[Er(dbm)_4]$ ([**8**])*

Starting from $ErCl_3 \cdot 6H_2O$ (382 mg, 1.00 mmol); product is a pale orange crystalline solid. Yield: 702 mg (0.60 mmol, 60%). Elemental analysis calcd (%) for $C_{66}H_{60}ErNO_8$ ($HNEt_3[Er(dbm)_4]$): C 68.19, H 5.20, N 1.20; found: C 67.98, H 5.67, N 1.26.

*$HNEt_3[Tm(dbm)_4]$ ([**9**])*

Starting from $TmCl_3 \cdot 7H_2O$ (401 mg, 1.00 mmol); product is a yellow crystalline solid. Yield: 561 mg (0.48 mmol, 48%). Elemental analysis calcd (%) for $C_{66}H_{60}NO_8Tm$ ($HNEt_3[Tm(dbm)_4]$): C 68.10, H 5.19, N 1.20; found: C 67.13, H 6.12, N 1.24.

*$HNEt_3[Yb(dbm)_4]$ ([**10**])*

Starting from $YbCl_3 \cdot 6H_2O$ (387 mg, 1.00 mmol); product is a yellow crystalline solid. Yield: 654 mg (0.56 mmol, 56%). Elemental analysis calcd (%) for $C_{66}H_{60}NO_8Yb$ ($HNEt_3[Yb(dbm)_4]$): C 67.86, H 5.18, N 1.20; found: C 67.75, H 5.55, N 1.19.

6.3 Results and discussion

6.3.1 Synthesis

All *Ln*(III) complexes have been synthesized in yields ranging from 29% for the La(III) compound to 83% for the Eu(III) compound. The reactions were performed in hot ethanolic solution to ensure complete dissolution of the lanthanoid salt and ligand and allow for crystallization upon cooling to room temperature. The results of elemental analysis show that all compounds are described by the general formula $HNEt_3[Ln(dbm)_4]$. In addition, the IR spectra obtained for [**1**]- [**10**] are highly similar and resemble the IR spectrum of Hdbm. The strong bands in the 1600 cm^{-1} region are readily assigned to the carbonyl bands of the ligand, while the two bands at 743 and 689 cm^{-1} can be assigned to the out of plane C-H bending of the phenyl groups of the ligand. Compound [**1**] is highly soluble in ethanol, as compared to the other lanthanoid compound; cooling of its reaction mixture did not lead to the formation of a crystalline compound or a precipitate even after several days. Concentration of the mixture to approximately half its initial value eventually led to the formation of a crystalline solid in a low yield relative to the other compounds. The color that is observed for compound [**7**] is strongly dependent on the light source used to illuminate the compound. This is not uncommon for Ho(III) compounds and it is a result of the interplay between the absorption spectrum of the compound and the emission spectrum of the light source [27].

*Structure of **[1], [2] and [3]***

Single crystals of compounds [**1**] ($HNEt_3[La(dbm)_4]$), [**2**] ($HNEt_3[Nd(dbm)_4]$) and [**3**] ($HNEt_3[Sm(dbm)_4]$) were obtained by direct crystallization from the reaction mixture. Their solid-state structures were determined *via* single crystal X-ray crystallography. Crystallographic data for compounds [**1**], [**2**] and [**3**] are given in Table 6.1; selected bond distances and angles are given in Table 6.2. All three compounds crystallize in a monoclinic space group with two crystallographically independent lanthanoid ion sites in the asymmetric unit. As the differences in bond distances and angles of the two independent molecules are negligible, the data for only one of each are provided in Table 6.2. The structure of the $[Ln(dbm)_4]^-$ complex ion is highly similar for all three compounds, with four dbm^- ligands binding in a bidentate mode. The coordination geometry around the central ion is best described as a distorted square antiprism. For [**1**], the La-O bond lengths range from 2.444(2) to 2.556(2) Å, while the Nd-O bond lengths in [**2**] vary between 2.389(2) to 2.503(2) Å. In compound [**3**], Sm-O bond lengths range from 2.358(4) to 2.421(3) Å. These values can be considered normal for this type of bonds [28]. The decrease of the average bond lengths on going from [**1**] to [**3**] are a result of lanthanoid contraction.

Table 6.1: Crystallographic data for compounds [1], [2] and [3].

	[**1**]	[**2**]	[**3**]
formula	$C_{66}H_{60}LaNO_8$	$C_{66}H_{60}NNdO_8$	$C_{66}H_{60}NO_8Sm$
fw	1134.06	1139.39	1145.50
crystal size [mm^3]	0.18 × 0.23 × 0.27	0.24 × 0.26 × 0.33	0.20 × 0.24 × 0.37
crystal color	colorless	colorless	colorless
crystal system	monoclinic	monoclinic	monoclinic
space group	$P2_1/c$ (# 14)	$P2_1/c$ (# 14)	Pc (# 7)
a [Å]	19.0448(3)	19.14645(15)	25.3006(2)
b [Å]	22.2878(2)	22.30120(16)	9.02328(7)
c [Å]	28.0866(4)	27.8550(2)	27.4737(2)
β [°]	109.6946(15)	110.0750(9)	112.5634(11)
V [$Å^3$]	11225.2(3)	11171.15(14)	5792.00(8)
Z	8	8	4
d_{calc} [g/cm^3]	1.342	1.355	1.314
μ [mm^{-1}]	0.818	7.546	8.051
refl. measured / unique	131872 / 22962	87068 / 21347	35745 / 16830
parameters	1383	1383	1523
R1/wR2 [I>2σ(I)]	0.0271 / 0.0656	0.0287 / 0.0794	0.0297 / 0.0714
R1/wR2 [all refl.]	0.0358 / 0.0710	0.0301 / 0.0804	0.0343 / 0.0725
S	1.040	1.080	0.990
$\rho_{min/max}$ [$e/Å^3$]	–1.17 / 0.78	–2.11 / 1.82	–0.82 / 1.53

Table 6.2: Selected bond distances and angles for compounds [1], [2], and [3].

	[**1**]	[**2**]	[**3**]
Bond distance (Å)			
Ln1–O1A	2.4646(18)	2.4088(19)	2.4084(28)
Ln1–O2A	2.5111(17)	2.4512(18)	2.3695(31)
Ln1–O3A	2.4931(22)	2.4307(24)	2.4105(25)
Ln1 -O4A	2.4526(22)	2.4028(23)	2.3582(41)
Ln1 –O5A	2.4586(20)	2.4045(20)	2.4207(32)
Ln1 –O6A	2.5559(19)	2.5028(21)	2.4066(32)
Ln1 –O7A	2.5397(16)	2.4822(16)	2.4051(34)
Ln1 –O8A	2.4589(18)	2.4025(18)	2.3856(30)
Bond angle (°)			
O1A-*Ln1*-O2A	68.948(64)	70.295(72)	71.096(98)
O3A-*Ln1*-O4A	68.500(66)	70.069(73)	70.575(112)
O5A-*Ln1*-O6A	68.489(60)	69.865(63)	70.012(108)
O7A-*Ln1*-O8A	68.459(63)	69.638(65)	70.763(112)
O1A-*Ln1*-O6A	81.986(62)	79.999(67)	76.114(95)
O2A-*Ln1*-O5A	73.274(62)	72.645(66)	72.014(104)
O3A-*Ln1*-O8A	71.252(63)	71.164(68)	79.977(97) (O4A-O8A)
O4A-*Ln1*-O7A	77.639(63)	76.643(69)	72.670(115) (O3A-O7A)
Hydrogen bond distances			
N–H···O	(O5A) 1.91(3)	(O5A) 1.91(3)	(O6A) 1.972(3)
N–H···O	(O8A) 1.92(4)	(O8A) 1.92(4)	(O3B) 1.976(3)

Despite the similar coordination geometries of the lanthanoid ions in structures [**1**] - [**3**], the packing of [**3**] is different from that of [**1**] and [**2**]. In addition, in [**3**] disorder is found for two phenyl groups on one of the independent molecules and for one phenyl group on the other molecule. In all cases the phenyl groups are disordered over two orientations, with relative occupancies of 0.627(5) and 0.373(5), 0.581(6) and 0.419(6) for the first independent molecule and 0.633(15) and 0.367(15) for the second independent molecule. The triethylammonium ion fits in the cavities formed by the packed complexes, as is illustrated in Figure 6.1. In [**1**] and [**2**], hydrogen bonds exist between the triethylammonium hydrogen and O5A and O8A of the ligands of one of the symmetry independent molecules. In [**3**], the ammonium hydrogen forms a hydrogen bond to O6A and O3B; hydrogen bond lengths are given in Table 6.2.

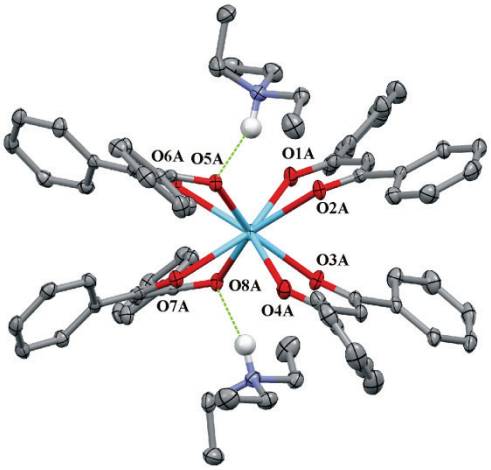

*Figure 6.1: Thermal ellipsoid plot (50% probability contours) of [**1**], ($HNEt_3[La(dbm)_4]$), showing one of the two crystallographically independent La(III) complex anions and two hydrogen bonded $HNEt_3$ cations, as well as the distorted square antiprismatic coordination sphere. Hydrogen bonds between the ammonium hydrogen and the ligands are indicated by a dashed line and the numbering scheme for O atoms is indicated. Other hydrogen atoms have been omitted for clarity.*

Structure of [4] - [10]

X-ray powder diffraction patterns recorded for compounds [**4**] - [**10**] at room temperature appear to be highly similar, and could be indexed with a monoclinic cell in the space group *I2/a* [20]. The room temperature powder XRD patterns for compounds [**1**] - [**2**] could not be indexed in *I2/a*, while this was possible for the pattern recorded for [**3**]. The difference is most likely a result from lanthanoid contraction. Results of the LeBail extraction are given in Table 6.3.

Table 6.3: Results of the LeBail extraction of unit cell dimensions of room temperature powder XRD data.

	S.G.	a (Å)	b (Å)	c (Å)	β (°)	V (Å^3)	Rp	χ^2
[**1**]*	*P2$_1$/c*	19.0448(3)	22.2878(2)	28.0866(4)	109.695(2)	5613	–	–
[**2**]*	*P2$_1$/c*	19.1465(2)	22.3012(2)	27.8550(2)	110.075(1)	5586	–	–
[**3**]	*I2/a*	25.344(5)	9.154(1)	27.618(3)	112.31(1)	5928(2)	3.15	1.53
[**4**]	*I2/a*	25.340(2)	9.1553(6)	27.640(1)	112.210(6)	5936.6(7)	2.90	1.67
[**5**]	*I2/a*	25.171(7)	9.140(1)	27.621(2)	112.100(8)	5901(2)	3.61	3.53
[**6**]	*I2/a*	25.152(3)	9.121(1)	27.642(2)	111.900(8)	5884(1)	3.04	2.26
[**7**]	*I2/a*	25.138(3)	9.1431(6)	27.652(3)	112.000(7)	5892.7(9)	2.59	1.49
[**8**]	*I2/a*	25.129(4)	9.154(1)	27.603(4)	111.80(1)	5896(2)	2.51	1.43
[**9**]	*I2/a*	25.116(4)	9.167(1)	27.640(3)	111.74(1)	5911(1)	2.56	1.53
[**10**]	*I2/a*	25.047(3)	9.1627(8)	27.616(3)	111.560(8)	5894(1)	2.68	1.82

*Notes: * Unit cell dimensions acquired from single crystal measurements; the unit cell volume for these compounds (Z = 8) is divided by 2 for comparison with the data for [**3**] - [**4**] (Z = 4).*

Luminescent properties

When compounds [**1**] - [**10**] are illuminated by a standard laboratory UV lamp at 366 nm, only compounds [**3**] (*Ln* = Sm) and [**4**] (*Ln* = Eu) clearly show visible luminescence. Indeed, room temperature photoluminescence (PL) could only be detected for [**3**] and [**4**]. The photoluminescence spectra for these compounds are given in Figure 6.2 and Figure 6.3. Both compounds show broad excitation bands in the UV to nUV region of the spectrum, indicating ligand-centered excitation. Superimposed on the broad bands, narrow lines corresponding to direct excitation of the luminescent centre can be distinguished. For [**3**], a narrow line at 420 nm ($[^6P_{5/2}, {}^4P_{5/2}] \leftarrow {}^6H_{5/2}$) can be seen, which is characteristic for the Sm(III) ion [29]. The emission spectrum of [**3**] shows lines characteristic for the $^4G_{5/2} \rightarrow {}^6H_J$ transitions of Sm(III) at 565 nm (J = 5/2), 610 nm (J = 7/2), 650 nm (J = 9/2), and 700 nm (J = 11/2). The most intense transition in the emission spectrum is the $^4G_{5/2} \rightarrow {}^6H_{9/2}$ transition, which is mainly of electric dipole (ED) nature. The $^4G_{5/2} \rightarrow {}^6H_{5/2}$ transition in contrast is mainly of magnetic dipole (MD) nature. As a result, its intensity is relatively insensitive to the environment of the Sm(III) ion and can therefore be taken as an internal reference. The fact that the intensity of the $^4G_{5/2} \rightarrow {}^6H_{9/2}$ transition is larger than the intensity of the $^4G_{5/2} \rightarrow {}^6H_{5/2}$ transition indicates that the Sm(III) ion occupies a non-centrosymmetric coordination site, which is in agreement with the structure determined by single X-ray crystallography [2, 30, 31]. The excitation spectrum recorded for [**4**] is similar to that of [**3**], showing an additional narrow line at 395 nm ($[^5L_6, {}^5G_2, {}^5L_7, {}^5G_3] \leftarrow {}^7F_0$) characteristic for direct excitation of the Eu(III) ion [32]. In the emission spectrum, four lines can be seen corresponding to the $^5D_0 \rightarrow {}^7F_J$ transitions of Eu(III) at 595 nm (J = 1), 615 nm (J = 2), 650 nm (J = 3) and 700 nm (J = 4).

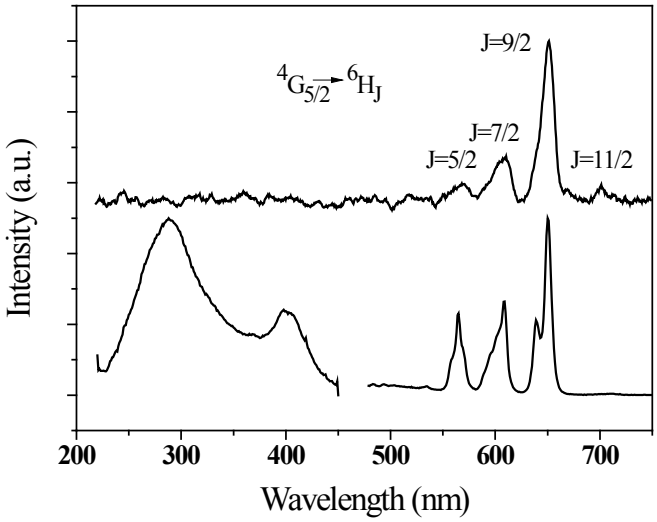

*Figure 6.2: Triboluminescence emission (top) and photoluminescence (bottom) spectra for [**3**] ($HNEt_3[Sm(dbm)_4]$). The excitation spectrum on the bottom left was recorded monitoring the intensity of the $^4G_{5/2} \rightarrow {}^6H_{9/2}$ transition, while the emission spectrum on the bottom right was obtained using an excitation wavelength of 298 nm.*

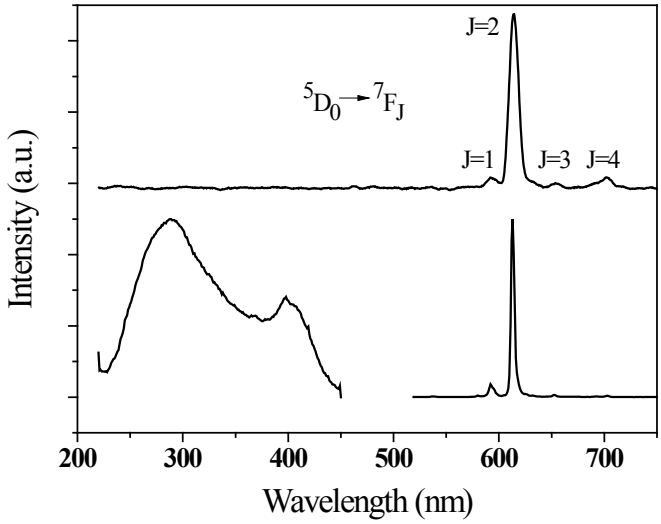

*Figure 6.3: Triboluminescence emission (top) and photoluminescence (bottom) spectra for [**4**] ($HNEt_3[Eu(dbm)_4]$). The excitation spectrum on the bottom left was recorded monitoring the intensity of the $^5D_0 \rightarrow {}^7F_2$ transition, while the emission spectrum on the bottom right was obtained using an excitation wavelength of 380 nm.*

Most of the emission intensity comes from the $^5D_0 \rightarrow {}^7F_2$ ED transition while the $^5D_0 \rightarrow {}^7F_1$ MD transition is weak, which is indicative of the lack of an inversion center on Eu(III). Although visible luminescence is also expected from [**5**] as a result of the Tb(III) $^5D_4 \rightarrow {}^7F_5$ transition at 545 nm, and from [**6**] due to the Dy(III) $^4F_{9/2} \rightarrow {}^6H_{13/2}$ transition at 570 nm, no photoluminescence emission could be detected within the sensitivity of the instrument being used. This observation is readily explained by the fact that the triplet level of the dbm ligands, which is around 20,500 cm^{-1} is too close to or below the resonance levels of Tb(III) ($^5D_4$ at 20,500 cm^{-1}) and Dy(III) ($^4F_{9/2}$ at 21,000 cm^{-1}) [2, 29, 33, 34]. Because of the $4f_0$ configuration of La(III), no luminescence is expected from [**1**], while complexes [**2**] and [**7**] to [**10**] are expected to give luminescence only in the nIR region [2]. Photoluminescence emission spectra were recorded up to the longest possible wavelength of the spectrometer (900 nm), but no emission was detected for [**1**], [**2**] and [**5**] - [**10**]. Triboluminescence (TrL) has also been detected for [**3**] and [**4**], with the TrL spectra showing the same emission lines as the corresponding PL spectra. The TrL spectra for [**3**] and [**4**] are shown in Figure 6.2 and Figure 6.3, respectively. Compound [**4**] is one of the best triboluminescent compounds known, and a TrL spectrum was readily obtained. Compound [**3**] shows fairly bright orange flashes visible to the naked eye upon crushing. The intensity is, however, much lower than that of [**4**]. To our knowledge, triboluminescence has not been reported for compound [**3**]. Differences between the PL and TrL emission spectra in Figure 6.2 and Figure 6.3 mainly result from the differences in resolution and spectral sensitivity of the spectrophotometers used. Interestingly, the only complex to show TrL besides [**4**] is also the only photoluminescent compound. This supports the hypothesis involving excitation of the luminescent center *via* the ligand. Fascinatingly, the ability of [**4**] to show triboluminescence has been linked to the structural disorder of the ligand's phenyl groups by Sweeting *et al.* [20]. Because the structure they report for [**4**] is centrosymmetric, this compound has been the counterexample against the requirement for a non-centrosymmetric space group for TrL to occur for a long time. However, Cotton *et al.* have reinvestigated the structure of [**4**] and found the non-centrosymmetric space group *Ia* [35]. In the structure they describe, disorder is also present for four of the ligand phenyl groups. Compound [**3]** also crystallizes in a non-centrosymmetric space group and has disordered phenyl groups. Thus, as of yet it is unclear whether the relation between TrL and a non-centrosymmetric space group really exists, or if the presence of disorder within the structure provides another pathway to enable TrL.
It is worth mentioning that Fontenot *et al.* have studied the same series of compounds for their triboluminescent properties and published their results roughly simultaneously with the publication of the work described in this Chapter [16, 36]. In their work, they report that the Eu(III) compound shows by far the strongest TrL, followed by the Sm(III) compound. The latter is found to give only 1.8% of the intensity of the Eu(III) compound. This is in qualitative agreement with our observations. However, the authors also report TrL for the Gd(III), Nd(III), Pr(III), Tb(III) and Yb(III) compounds, of which the relative TrL emission

intensity compared to the Eu(III) compound is in between 0.1 and 1%. Our equipment is probably not sufficiently sensitive to detect such weak TrL emissions.

6.4 Conclusion

A series of compounds described by the general formula $HNEt_3[Ln(dbm)_4]$, *Ln* = La, Nd, Sm, Eu, Tb, Dy, Ho, Er, Tm, Yb has been prepared. Single crystal X-ray diffraction studies show that the compounds with *Ln* = La, Nd are isostructural and crystallize in the $P2_1/c$ space group. The Sm-compound on the other hand crystallizes in the *Pc* space group. Bright triboluminescence was detected for this compound, in analogy with the Eu-compound. Because this compound is found to crystallize in a non-centrosymmetric space group, it cannot settle the debate on whether or not centrosymmetry is a prerequisite for TrL to occur.

6.5 References

[1] S.I. Weissman, *J. Chem. Phys.*, 10 (1942) 214-217.

[2] K. Binnemans, *Rare earth beta-diketonates*, in *Handbook on the Physics and Chemistry of Rare Earths*, 2005, Elsevier. 107-272.

[3] L. Armelao, S. Quici, F. Barigelletti, G. Accorsi, G. Bottaro, M. Cavazzini, and E. Tondello, *Coord. Chem. Rev.*, 254 (2010) 487-505.

[4] G. Vicentini, L.B. Zinner, J. Zukerman-Schpector, and K. Zinner, *Coord. Chem. Rev.*, 196 (2000) 353-382.

[5] J.G. White, *Inorg. Chim. Acta*, 16 (1976) 159-162.

[6] H. Wang, P. He, S. Liu, J. Shi, and M. Gong, *Appl. Phys. B: Lasers Opt.*, 97 (2009) 481-487.

[7] H.F. Brito, O.L. Malta, and J.F.S. Menezes, *J. Alloy. Compd.*, 303-304 (2000) 336-339.

[8] L. Huang, L. Cheng, H. Yu, L. Zhou, J. Sun, H. Zhong, X. Li, J. Zhang, Y. Tian, Y. Zheng, T. Yu, J. Wang, and B. Chen, *Physica B*, 406 (2011) 2745-2749.

[9] J.-C.G. Bünzli, E. Moret, V. Foiret, K.J. Schenk, M. Wang, and L. Jin, *J. Alloy. Compd.*, 207-208 (1994) 107-111.

[10] A. Mech, M. Karbowiak, C. Görller-Walrand, and R. Van Deun, *J. Alloy. Compd.*, 451 (2008) 215-219.

[11] R.G. Charles and E.P. Riedel, *J. Inorg. Nucl. Chem.*, 28 (1966) 3005-3018.

[12] Y. Hasegawa, Y. Wada, and S. Yanagida, *J. Photochem. Photobiol., C*, 5 (2004) 183-202.

[13] Y.-g. Lü, G. Li, C.-h. Shi, L.-s. Yu, F. Luan, and F.-j. Zhang, *T. Nonferr. Metal. Soc.*, 20 (2010) 2336-2339.

[14] F. Chen, Z. Bian, and C. Huang, *J. Rare Earth.*, 27 (2009) 345-355.

[15] C.R. Hurt, N. McAvoy, S. Bjorklund, and N. Filipescu, *Nature*, 212 (1966) 179-180.

[16] R. Fontenot, W. Hollerman, K. Bhat, S. Allison, and M. Aggarwal, *Journal of Theoretical and Applied Physics*, 7 (2013) 30.

[17] R.-G. Xiong and X.-Z. You, *Inorg. Chem. Commun.*, 5 (2002) 677-681.

[18] W. Clegg, I. Sage, I. Oswald, P. Brough, and G. Bourhill, *Acta Crystallogr., Sect. C. Cryst. Struct. Commun.*, 56 (2000) 1323-1325.
[19] R.G. Bulgakov, S.P. Kuleshov, A.N. Zuzlov, and R.R. Vafin, *Russ. Chem. Bull.*, 53 (2004) 2712-2714.
[20] L.M. Sweeting and A.L. Rheingold, *J. Am. Chem. Soc.*, 109 (1987) 2652-2658.
[21] E.E.S. Teotonio, G.M. Fett, H.F. Brito, W.M. Faustino, G.F. de Sá, M.C.F.C. Felinto, and R.H.A. Santos, *J. Lumin.*, 128 (2008) 190-198.
[22] R.S. Fontenot, K.N. Bhat, W.A. Hollerman, M.D. Aggarwal, and K.M. Nguyen, *CrystEngComm*, 14 (2012) 1382-1386.
[23] G.M. Sheldrick, *SHELXS–97*, *Bruker AXS Inc., Madison, Wisconsin*, 1997.
[24] G.M. Sheldrick, *Acta Crystallogr., Sect. A. Found. Crystallogr.*, 64 (2008) 112-122.
[25] B.A. Hunter, *Rietica*, *IUCR Powder Diffraction*, 1997.
[26] A. Le Bail, H. Duroy, and J.L. Fourquet, *Mater. Res. Bull.*, 23 (1988) 447-452.
[27] K. Binnemans and C. Görller-Walrand, *Chem. Phys. Lett.*, 235 (1995) 163-174.
[28] A.G. Orpen, L. Brammer, F.H. Allen, O. Kennard, D.G. Watson, and R. Taylor, *J. Chem. Soc. Dalton Trans.*, (1989) S1-S83.
[29] W.T. Carnall, P.R. Fields, and K. Rajnak, *J. Chem. Phys.*, 49 (1968) 4424-4442.
[30] J.H.S.K. Monteiro, I.O. Mazali, and F.A. Sigoli, *J. Fluoresc.*, 21 (2011) 2237-2243.
[31] H.F. Brito, O.L. Malta, M.C.F.C. Felinto, E.E.S. Teotonio, J.F.S. Menezes, C.F.B. Silva, C.S. Tomiyama, and C.A.A. Carvalho, *J. Alloy. Compd.*, 344 (2002) 293-297.
[32] W.T. Carnall, P.R. Fields, and K. Rajnak, *J. Chem. Phys.*, 49 (1968) 4450-4455.
[33] E.E.S. Teotonio, H.F. Brito, G.F. de Sá, M.C.F.C. Felinto, R.H.A. Santos, R.M. Fuquen, I.F. Costa, A.R. Kennedy, D. Gilmore, and W.M. Faustino, *Polyhedron*, 38 (2012) 58-67.
[34] W.T. Carnall, P.R. Fields, and K. Rajnak, *J. Chem. Phys.*, 49 (1968) 4447-4449.
[35] F.A. Cotton, L.M. Daniels, and P. Huang, *Inorg. Chem. Commun.*, 4 (2001) 319-321.
[36] S. Akerboom, M.S. Meijer, M.A. Siegler, W.T. Fu, and E. Bouwman, *J. Lumin.*, 145 (2014) 278-282.

7 Summary, general discussion and outlook

7.1 Summary

7.1.1 Introduction

In the Chapter 1 of this thesis, a general introduction into energy requirements of artificial light sources, light source principles and color vision is given. It is shown that a substantial amount of energy can be saved when current lamps are replaced by more efficient light sources. A discussion of several approaches towards highly efficient solid state light sources (SSLs) based on light emitting diodes (LEDs) is given. Although white light emitting SSLs already exist, their properties such as efficiency and emission spectrum can be improved significantly. The approach of using an LED emitting in the near-UV region combined with a layer of down-conversion phosphors shows potential. However, the required phosphor materials that can be efficiently excited in the near-UV are lacking. In this respect, complexes of the trivalent lanthanoid ions are promising. In such compounds, the line-like emission of the lanthanoid ion can be efficiently excited via the ligand centered absorption bands. The ligands in turn can be tuned to match the excitation source, for instance by introduction of substituents. Details on the energy transfer mechanisms in these complexes and the photophysics of the trivalent lanthanoid ions are given, as well as some basic lanthanoid coordination chemistry. The final section of the chapter deals with various approaches towards highly efficient photoluminescent complexes described in this thesis.

7.1.2 Substituted phenanthrolines as antennae

1,10-Phenanthroline is known to be an efficient sensitizer of Eu(III)-centered luminescence. Unfortunately, the maximum excitation wavelength of this compound occurs at 355 nm. For this reason, the ligand 1,10-phenanthroline cannot be used to excite Eu(III) emission with a In:GaN based LED emitting in the near-UV. To investigate whether it is possible to shift this excitation maximum to longer wavelengths, a series of eight new Eu(III)-based coordination compounds with 1,10-phenanthroline bearing a chloro-, methoxy-, ethoxy-, cyano-, carboxylic acid, methyl carboxylate-, ethyl carboxylate, and amino-substituent on the 2-position have been prepared. This work is described in Chapter 2. It was found that all compounds except for [Eu(2-amino-1,10-phenanthroline)$_2$(NO$_3$)$_3$] show photoluminescence characteristic of the Eu(III) ion upon excitation with nUV radiation. It was established that in [Eu(2-chloro-1,10-phenanthroline)$_2$(NO$_3$)$_3$], the luminescence apparently is quenched by a low-lying LMCT-band. A high quantum yield of 78% is found for [Eu(2-chloro-1,10-phenanthroline)$_2$(NO$_3$)$_3$], but its excitation maximum is incompatible with the emission of a near UV LED. The excitation maximum of the compounds [Eu(2-(ethylcarboxylate)-1,10-phenanthroline)$_2$(NO$_3$)$_3$] and [Eu(2-methoxy-1,10-phenanthroline)$_2$(NO$_3$)$_3$] is at 370 nm, but the low quantum efficiency limits their application as a phosphor. In all cases, the overall quantum yield of the compounds is limited by the low intrinsic quantum yield of the Eu(III) ion (17-52%). Also in Chapter 2, the first-time use of 1-methyl-1,10-phenanthrolin-

2(1*H*)-one, a synthetic intermediate, as a ligand is reported, using Eu(III) as central ion. Using X-ray crystallography, the ligand is found to bind to the metal *via* its carbonyl oxygen, resulting in a compound that shows moderately efficient luminescence with a quantum yield of 22% at 355 nm excitation.

7.1.3 Ln(III) complexes with small aromatic ligands

As described in Chapter 1 of this thesis, small aromatic molecules can be used as efficient antennae for sensitizing emission of the lanthanoid ions. Both mononuclear complexes and metal organic frameworks can be formed with these ligands and the lanthanoid ions. In Chapter 3, the synthesis of compounds of Eu(III) and Tb(III) with furan-2,5-dicarboxylic acid (H_2fda) and a compounds of Tb(III) with 2-hydroxytrimesic acid (H_4tma) are described. It is found that refluxing the ligand H_2fda with lanthanoid salts in N,N-dimethylformamide (dmf) gives rise to coordination compounds that analyze as $(H_2NMe_2)_6Ln_4(fda)_7Cl_4$. Recrystallisation of these compounds from water results in the formation of a one-dimensional coordination polymer. Both the dmf compounds and the coordination polymer of Eu(III) and Tb(III) show photoluminescence characteristic of the lanthanoid ion. In general, the emission intensity of the compounds is weak. The emission intensity of the recrystallized compounds is even lower. This is readily understood, as the *Ln*(III) ion is surrounded by five molecules of water that can quench luminescence by vibronic coupling. The ligand H_4tma is found to give rise to a rigid three-dimensional metal-organic framework with a high density when reacted with $TbCl_3$ in water under hydrothermal conditions. Moreover, this compound shows bright luminescence with a photoluminescence quantum yield of 67%. This high efficiency, combined with an excitation maximum of 378 nm, make this compound an ideal candidate green phosphor material for application in LEDs.

7.1.4 Phenol-type ligands as sensitizers

In Chapter 4, the synthesis of ten novel Eu(III) and Tb(III) complexes with 2-(4,5-dihydro-1,3-oxazol-2-yl)phenol (**L1**) and its thiazolyl analog (**L2**) as ligands is described. It is found that these phenol-type ligands are suitable for sensitization of luminescence of both Eu(III) and Tb(III) ions. The luminescence intensity of in particular the Eu(III) complexes is found to be highly sensitive to the metal-to-ligand (M:L) ratio; Eu(III) complexes with a M:L ratio of 1:3 practically do not exhibit photoluminescence, while those with a 1:4 ratio show fairly bright photoluminescence with quantum yields of 20% (Eu**L2**_4) and 43% (Eu**L1**_4). The antenna efficiency is found to be around 90% in both complexes but the overall quantum yield appears to be limited by the low intrinsic quantum yields of the Eu(III) ion. The 1:3 complexes are not luminescent, which is readily explained by the presence of a low-lying LMCT state. The presence of such state is evidenced from an additional band in the absorption spectra of the Eu(III) compounds when compared to their Tb(III) analogs. In general, the Tb(III) complexes show

photoluminescence regardless of the M:L ratio, and the luminescence efficiencies of the Tb(III) complexes with **L2** as a ligand are comparatively low. The compound Tb**L1**_4 shows very intense photoluminescence with a quantum efficiency as high as 79% upon excitation at 360 nm while Tb**L2**_4 on the contrary shows faint luminescence. This is explained by a poor spectral match between the **L2** T* state and the Tb(III) $^5D_4$ state. Overall, **L1** appears to be a better antenna than **L2** for both Eu(III) and Tb(III) ions. An attempt at recrystallisation of Eu**L1**_3 and Tb**L1**_3 from DMSO gave rise to the formation of an octanuclear complex in which the metal centers are tightly linked together by carbonate ions that have formed from CO_2 captured from the atmosphere. The Eu(III) complex shows very faint luminescence upon excitation with nUV radiation, while the Tb(III) complex has a fairly high quantum efficiency of 51%.

7.1.5 Tuning Eu(III) complexes with dibenzoyl methanates

Dibenzoylmethane (Hdbm) is a molecule that can highly efficiently sensitize luminescence of the Eu(III) ion. Presently, studies on the effect of the introduction of substituents on dbm^- on its ability to sensitize Eu(III) luminescence are scarce. Also, the influence of the cations on the luminescence of anionic complexes of formula $[Eu(dbm)_4]^-$ is poorly investigated. In Chapter 5, the synthesis of seven complexes of Eu(III) with halogen-substituted dbm ligands is described. Based on the position of the substituents on the phenyl groups with respect to the chelating 1,3-diketo moiety (ortho, meta or para), the compounds are classified into three groups. The emission spectra of the complexes are analyzed using JO theory, and differences between the ligand substitution patterns are apparent from the intensity parameters $\Omega_{2,4,6}$. The ligands with a 4-Br and a 4-F substituent are found to have high antenna efficiencies of around 90%, but the intrinsic quantum yield of the Eu(III) ion is very low in these compounds. The compounds with a 3-F, 3-Cl, 3-Br and 3-I substituent show lower antenna efficiencies (54 to 62%). The intrinsic quantum yield of the Eu(III) ion is increased in these compounds, resulting in overall photoluminescence quantum yields of 22-35%. The compound with the 2-Cl substituent on the ligand shows by far the longest experimental lifetime (0.89 ms) and the lowest Ω_2 parameter of the series. In Chapter 5, it is shown that these properties can be at least qualitatively understood by considering the electron-withdrawing properties of the substituents. The strong influence of the counter ion on the luminescent properties of $[Eu(dbm)_4]^-$ is demonstrated by the comparison of the luminescent properties of the compounds with $HNEt_3^+$, Li^+, and NBu_4^+ counter ions. Moreover, the crystal structures of the two latter compounds have been determined and are reported.

7.1.6 Triboluminescence

Some complexes of the trivalent lanthanoid ions are found to exhibit luminescence upon fracture of the crystallites in a phenomenon known as triboluminescence (TrL). Although not yet fully resolved, it appears that the TrL mechanism involves energy transfer from the

ligand-centered excited state to the lanthanoid excited state, similar to the mechanism for photoluminescence of such compounds. In addition, there is still disagreement on whether only compounds with structures with a non-centrosymmetric space group can exhibit TrL [1]. One of the compounds that shows the brightest TrL is the Eu(III) coordination compound $HNEt_3$[Eu(dibenzoylmethanate)$_4$], which is closely related to the compounds discussed in Chapter 5. For these reasons series of lanthanoid coordination compounds with the general formula $HNEt_3$[*Ln*(dibenzoylmethanate)$_4$] (*Ln* = La, Nd, Sm, Eu, Tb, Dy, Ho, Er, Tm, Yb) has been synthesized. Crystal structures of the compounds with *Ln* = La, Nd and Sm are described, and photo- and triboluminescence studies indicate that the only compounds to exhibit visible photoluminescence, those with *Ln* = Sm, Eu, are also the only ones to exhibit detectable TrL. This is in agreement with the mechanism of ligand mediated excitation of the *Ln*(III) ion. The Sm-compound is identified as a novel triboluminescent compound; because it crystallizes in a non-centrosymmetric space group the compound does not disprove the relation between TrL and a non-centrosymmetric space group.

7.2 General discussion and outlook

The aim of the research described in this thesis was to investigate the potential of photoluminescent *Ln*(III) complexes as future phosphor materials for In:GaN light emitting diode based solid state light sources. Many requirements have to be met before such application can be considered, i.e. a high lumen-equivalent emission spectrum, a high absorption coefficient at the LED emission maximum, high quantum efficiency, a high stability and low thermal quenching. In this work, focus was put on shifting the wavelength of most efficient excitation towards 400 nm, whilst maintaining a high photoluminescence quantum yield. Many different kinds of ligands were investigated for their ability to sensitize luminescence of the Eu(III) and Tb(III) ions.

It is shown that indeed Eu(III) complexes with high photoluminescence quantum yields and long-wavelength excitation maxima can be obtained. It is shown that derivatives of dibenzoylmethane give rise to Eu(III) complexes with those desirable photophysical properties. In addition, it is demonstrated that substituting the dibenzoylmethane ligands has a profound impact on the quantum efficiency, and in addition that the counter ions provide valuable handlebars for further improving the emission quantum yield. However, Eu(III) complexes with closely related ligands have been demonstrated to exhibit poor photostability [2]. It would be valuable to investigate the influence the substituents on the dbm-ligands have on the photostability of their Eu(III) complexes. Elucidation of the decomposition products could give useful information on the mechanism of the decomposition pathway. For example, from research on the photostability of Hdbm-type molecules for application in sunscreen agents, these molecules are found to show higher photostability when in their ‘keto-enol’-form compared to their ‘diketo’-form [3, 4]. When

coordinated to Eu(III) in complexes, the tautomeric form of the ligands resembles that of the keto-enol form more closely than that of the diketo-form.

The Eu(III) complexes with derivatives of 1,10-phenanthroline are promising in terms of their efficiency, but the excitation maximum needs to be shifted further towards the visible part of the electromagnetic spectrum. It is shown that indeed substitution on the 2-position can establish a slight shift of the excitation maximum. In this research, only substitution on the 2-position of the aromatic system of the phenanthroline molecule was investigated. It would be of great interest to see the influence of substitution on other positions on the antenna properties. Extension of the aromatic system of 1,10-phenanthroline has been demonstrated to not give the desired shift [5]. The excitation maximum should be shifted at least 10 more nanometers before excitation with In:GaN based LEDs becomes possible, and photoluminescence quantum yields should be increased. It was shown that for the Eu(III) complexes with phenanthroline-based ligands, the low intrinsic quantum yield (Φ_{Ln}) of the Eu(III) ion was severely limiting the overall quantum yield. As the intrinsic quantum yield is often lowered by coupling of the *Ln*(III) excited state to vibrational modes of the ligand, it is quite possible that a different ligand substitution pattern will influence Φ_{Ln}. It would be interesting to find if there is a relation between the substitution pattern of the ligand and Φ_{Ln}. In the present study, only complexes with nitrato ligands besides the substituted phenanthrolines were studied. It would be interesting to study the influence of other anionic ligands on the luminescent properties of the Eu(III) complexes.

As shown in Chapter 3, an interesting class of coordination compounds is formed by the metal organic frameworks. Although the compounds with furan-2,5-dicarboxylic acid have photophysical properties that make them unsuitable for application as a phosphor, the metal organic framework of Tb(III) with 2-hydroxytrimesic acid has potential. Its high quantum efficiency of 67% combined with an excitation maximum at 378 nm make this compound a good candidate material for a new phosphor. The use of ligands with slightly different arrangements of functional groups around the benzene ring would be highly interesting, as this will most likely give rise to compounds with a very different structure. If a ligand can be found that is able to efficiently sensitize luminescence by both Eu(III) and Tb(III) ions, it would be possible to make a metal organic framework of which the emission spectrum can be tuned during synthesis by varying the Eu:Tb ratio.

In this work, it is shown that Tb(III) based coordination compounds with high photoluminescence quantum efficiency and long wavelength excitation maxima can be obtained. Most notably, the complex with the phenol-oxazoline ligand in Chapter 4 stands out, with a quantum yield of 79% and an excitation maximum of 370 nm. In case of the latter compound, it would be worthwhile to investigate the photoluminescence properties of neutral heteroleptic coordination compounds, e.g. those described by the general formula [*Ln*(III)(**L1**$^-$)$_3$(**L2**)], H**L1** being the phenol-oxazoline ligand and **L2** a neutral ligand such as

1,10-phenanthroline or 2,2'-bipyridine. Because it is shown that not only the ligand, but also the M:L ratio is an important parameter determining the photophysical properties of the complex, this offers an interesting way for tuning the properties. In addition, it would be fascinating to see what luminescent behavior such Eu(III) complexes would exhibit.

In this thesis, it is shown that *Ln*(III) coordination compounds with their excitation maximum and a strong absorption in the nUV region ($\lambda_{exc} > 360$ nm) and a high photoluminescence quantum yield ($\Phi > 70\%$) can be synthesized. In addition, the luminescence of these compounds is purely due to the 4f–4f transitions of the *Ln*(III) ion and therefore is well suitable for application as a phosphor for lighting technology. With these highly desirable photophysical properties in mind, it can be concluded that further investigations on the potential of this class of compounds as a phosphor material is at least as useful as the work that is currently being widely performed on the improvement of oxide-type phosphors.

7.3 References

[1] F.A. Cotton, L.M. Daniels, and P. Huang, *Inorg. Chem. Commun.*, 4 (2001) 319-321.

[2] L.D. Carlos, C.D.M. Donegá, R.Q. Albuquerque, S. Alves, J.F.S. Menezes, and O.L. Malta, *Mol. Phys.*, 101 (2003) 1037 - 1045.

[3] W. Schwack and T. Rudolph, *J. Photochem. Photobiol., B*, 28 (1995) 229-234.

[4] I. Karlsson, L. Hillerstrom, A.L. Stenfeldt, J. Martensson, and A. Borje, *Chem. Res. Toxicol.*, 22 (2009) 1881-1892.

[5] J.W. Verhoeven, E.B. Van Der Tol, F.J. Steemers, W. Verboom, D. Reinhoudt, Nicolaas, and J.W. Hofstraat, Complex comprising a rare-earth metal ion and a complexing moiety, Pat.no WO 1998/049163k 1998.

Appendix A

The determination of photoluminescence quantum yields is of importance when studying luminescent compounds intended for use as a phosphor material. It is a measure of how efficient a compound is at converting light from one wavelength to another. In order to assess the quantum yields of many of the compounds described in this work, a setup based on an integrating sphere was built. This appendix gives a justification of the measurements, as well as a brief description of the required measurements.

Remarks on quantum yield determination

The photoluminescence quantum yield (PLQY) is an important performance benchmark for phosphor materials. It expresses how efficiently the phosphor can convert light to a different wavelength. Provided that the absorption at the excitation wavelength is high, a high PLQY phosphor material gives intense luminescence. The determination of the quantum yield requires only two quantities to be measured: the number of absorbed photons and the number of emitted photons per unit of time. Two principle methods for determining the PLQY exist: the *relative method* and the *absolute method* [1-3]. Both methods will be discussed below, with the focus on the second method.

The relative method for determination of PLQY

The relative method can be performed using standard emission and absorption spectrometers, but requires the use of a standard sample with a known quantum yied Φ_{Ref}. The absorption spectrometer is used for determining the absorption factors f_S and f_{Ref} of the sample and reference, respectively. The luminescence spectrometer is used to record emission spectra. The integrated intensities of the emission spectra, F_S and F_{Ref}, are readily obtained, and the PLQY of the sample, Φ_S, is obtained with equation A1.

$$\Phi_S = \frac{f_{Ref}}{f_S} \cdot \frac{F_S}{F_{Ref}} \cdot \Phi_{Ref} \qquad \text{(A1)}$$

This method is easily executed and provides a quick way for PLQY determination. Importantly, the emission spectrometer should be calibrated in such way that the intensity is proportional to the *photon flow*, i.e., $I(\lambda) \propto [mole\ of\ photons \cdot nm^{-1} \cdot s^{-1}]$ [3, 4]. Preferably, the excitation wavelength of the reference and sample is the same, otherwise an additional factor, correcting for the spectral intensity of the excitation source and differences in photon energy, is required in A1.The requirement for a standard sample with a known PLQY greatly limits the applicability of this method, especially when proper standards for the excitation wavelength of interest are lacking [3]. In addition, the method assumes an isotropic distribution of the emission intensity, which limits its usefulness for PLQY determination of, for example, luminescent films [1, 5, 6].

The absolute method for determination of PLQY

The absolute method does not rely on a reference sample with a known quantum yield, but on a spectrometer coupled to an *integrating sphere*. Also in this case, the setup must be calibrated to give intensities proportional to the photon flow. A detailed procedure for measuring absolute fluorescence quantum yields using a combination of an integrating sphere and a CCD spectrometer is given by De Mello *et al.* [1]. Using their method, three experiments as shown in Figure A1 are required for determining the PLQY of a compound. However, performing only two of the measurements can give the information needed for

determining the photoluminescence quantum yield, as will be demonstrated below. As in the original paper, it is assumed that the integrating sphere behaves as an ideal scatterer and does not absorb radiation. In addition, it is assumed that the compound under investigation has a large Stokes shift, so that it will not re-absorb its own emission. For the complexes described in this thesis, the Stokes shift is sufficiently large to make this a valid method of quantum yield determination. The three experiments are briefly described below and the following definitions will be used:

- L_x: relative number of unabsorbed excitation photons in experiment x.
- P_x: relative number of photoluminescence photons in experiment x.
- Φ: photoluminescence quantum yield of the sample under investigation.
- Abs_x: relative number of photons absorbed by the sample in experiment x.

The expressions for L_x, P_x and Abs_x for each experiment are listed in Table A1. Note that $L_x+Abs_x=L_a$ for all experiments.

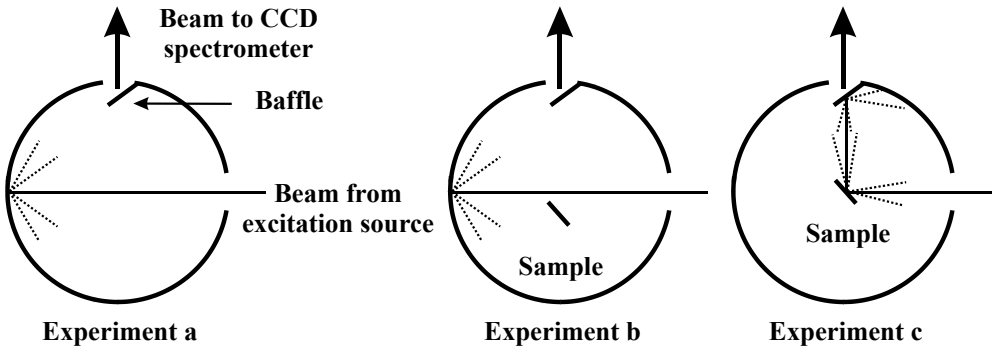

Figure A1: the three experiments described by De Mello for the determination of the PLQY of a luminescent sample [1].

Because of the way the spectrometer is calibrated, the relative number of photons is found by integrating the appropriate part of the spectrum.

Experiment a: The excitation beam is aimed at the wall of the empty integrating sphere. Only excitation source emission is measured by the CCD, its intensity is L_a.

Experiment b: The integrating sphere is loaded with a photoluminescent sample; the excitation beam is aimed at the sphere wall. A fraction μ of the excitation light scattered by the sphere wall is absorbed by the sample. With Φ as the photoluminescence quantum yield, the emission of the sample is given by $\Phi\mu L_a$. The intensity of the excitation signal is decreased to L_b.

Experiment c: The integrating sphere is loaded with a photoluminescent sample; the excitation beam is aimed directly at the sample. The sample absorbs a fraction A of the

incident light directly, a fraction (1–A) is transmitted or reflected into the integrating sphere. Of the latter fraction, a fraction μ is absorbed by the sample. Hence, the intensity of the excitation source is given by equation A2.

$$L_c = (1-\mu)(1-A)L_a = (1-A)L_b \quad \text{(A2)}$$

The number of absorbed photons in this experiment is determined by the number of photons absorbed at the first strike of the excitation beam with the sample (AL_a) and that fraction of excitation light that has not been absorbed at the first strike, but is scattered or transmitted into the sphere and absorbed at a later stage, resulting in equations A3.

$$Abs_c = AL_a + (1-A)Abs_b = AL_a + (1-A)\mu L_a \quad \text{(A3a)}$$

$$Abs_c = L_a\big(A + \mu(1-A)\big) \quad \text{(A3b)}$$

The sample emits light as a result from direct excitation (ΦAL_a) and as a result from excitation by the scattered or transmitted fraction of excitation light that has not been absorbed at the first strike ($\Phi\mu(1-A)L_a$), which results in equation A4 for P_c.

$$P_c = \Phi AL_a + \Phi\mu(1-A)L_a = \Phi AL_a + (1-A)P_b \quad \text{(A4)}$$

A summary of the experiments and the corresponding expressions is given in Table A1.

Table A1: Details of the luminescence experiments.

Experiment	a	b	c
Description	Empty I.S., exc. source on	Loaded I.S., exc. beam aimed at sphere wall	Loaded I.S., exc. beam aimed at sample
L	L_a	$L_b = (1-\mu)L_a$	$L_c = (1-A)L_b$
P	–	$P_b = \Phi\mu L_a$	$P_c = \Phi AL_a + (1-A)P_b$
Abs	–	$Abs_b = \mu L_a$	$Abs_c = \big(A + \mu(1-A)\big)L_a$

Calculation of the PLQY

From (A4), an expression for the photoluminescence quantum yield (A5) can be derived.

$$\Phi = \frac{P_c - (1-A)P_b}{AL_a} \quad \text{(A5)}$$

This expression is the same as equation 7 in De Mello's paper. However, on noting that P_c can be expressed as a function of L_a only, using $P_b = \Phi\mu L_a$, one finds equation A6.

$$P_c = \Phi AL_a + \Phi\mu(1-A)L_a = \Phi(AL_a + \mu(1-A)L_a) \quad \text{(A6)}$$

Equation A6 can be rearranged to give an expression for the quantum yield: equation A7.

$$\Phi = \frac{P_c}{L_a\left(A+\mu(1-A)\right)} \quad \text{(A7)}$$

Using this expression, the quantum yield can be determined from parameters measured in experiments a and c. The denominator of equation A7 can be recognized as the right-hand side of equation A3b: the absorbed light from the excitation source in experiment c. Intuitively, Abs_c is just the difference between L_a and L_c. Using the relations from Table A1 indeed it can be shown that $Abs_c = L_a - L_c$, see equations A8.

$$L_a - L_c = L_a - (1-\mu)(1-A)L_a \quad \text{(A8a)}$$

$$L_a - L_c = (\mu + A - \mu A)L_a = L_a\left(A + \mu(1-A)\right) \quad \text{(A8b)}$$

As a result, equation A7 simplifies to equation A9.

$$\Phi = \frac{P_c}{L_a - L_c} \quad \text{(A9)}$$

The three parameters in equation A9 are readily found from integrating the appropriate signals in the spectra resulting from experiments a and c.

Measurements in practice

In practice, experiment a is performed using a sample holder with optical grade $BaSO_4$ installed inside the integrating sphere as a white reference. This experiment results in the lower curve in Figure A2; its surface area is a direct measure of the number of excitation source photons that enter the integrating sphere over the integration time of the detector (L_a).

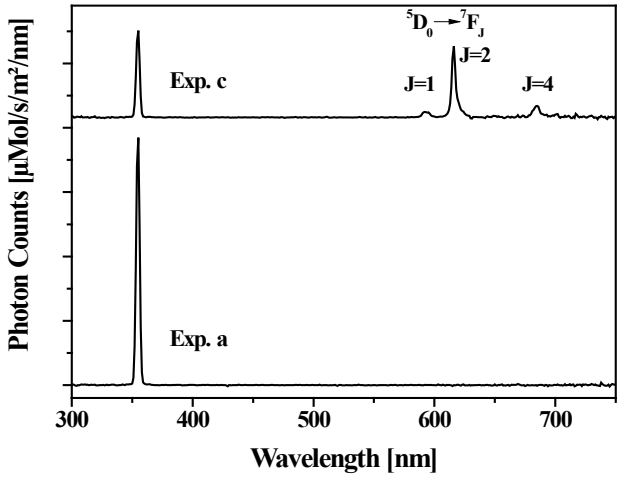

Figure A2: Spectra obtained with $BaSO_4$ (exp. a, bottom) and $[Eu(phen)_2(NO_3)_3]$ (exp. c, top) placed in the sample holder of the integrating sphere.

For experiment c, the sample holder is loaded with the compound of interest. The resulting spectrum contains a signal resulting from unabsorbed excitation photons and a signal from the luminescent compound. Integrating these curves gives L_c and P_c, respectively. A typical curve for experiment c performed on a luminescent Eu(III) complex, $[Eu(phen)_2(NO_3)_3]$ *in casu*, is shown on top in Figure A2.

Non-ideal behavior of the integrating sphere

Up until here, ideal behavior of the IS was assumed and it was assumed that its surface does not absorb radiation at any wavelength. In practice, integrating spheres tend to absorb radiation at shorter wavelengths. In view of the compounds described in this thesis, this means that short wavelength excitation photons are absorbed by the IS, which leads to an error in the PLQY determination. As the intensity of the excitation beam will be underestimated, an overestimation of the PLQY will result. To treat this problem, an additional absorption coefficient, *f*, has to be taken into account. Furthermore, it will be assumed that the excitation beam entering the IS has an intensity of L_i. A new set of equations, taking the additional absorption factor into account has been derived and is listed in Table A2. Not that the relation $L'_x+Abs'_x=L_i$ holds for each experiment.

Table A2: Set of equations describing the intensity of the excitation and emission signals.

Exp.	a	b	c
L'	$L'_a = (1-f)L_i$	$L'_b = (1-\mu)(1-f)L_i$	$L'_c = (1-A)(1-\mu)(1-f)L_i$
P'	$P'_a = 0$	$P'_b = \Phi\mu(1-f)L_i$	$P'_c = \Phi AL_i + (1-A)\Phi\mu(1-f)L_i$
Abs'	$Abs'_a = fL_i$	$Abs'_b = fL_i + \mu(1-f)L_i$	$Abs'_c = AL_i + (1-A)L_i\big(f+\mu(1-f)\big)$

From the expression for P'_c, in Table A2 an expression for the PLQY can be derived (A10).

$$\Phi = \frac{P'_c}{AL_i+(1-A)(1-f)\mu L_i} \qquad \text{(A10)}$$

Since $L'_c = (1-A)(1-\mu)(1-f)L_i$, one may write
$L'_c = (1-A)(1-f)L_i - \mu(1-A)(1-f)L_i$. This may be rearranged to give equation A11.

$$\mu(1-A)(1-f)L_i = (1-A)(1-f)L_i - L'_c \qquad \text{(A11)}$$

The left hand side of equation A11 can be recognized as the right part of the denominator in equation A10; substitution yields equation A12.

$$\Phi = \frac{P'_c}{AL_i+(1-A)(1-f)L_i-L'_c} \qquad \text{(A12)}$$

Equation A12 can be rearranged to give equation A13.

$$\Phi = \frac{P'_c}{L_i(1-f+Af)-L'_c} = \frac{P'_c}{L'_a-L'_c+AfL_i} \quad \text{(A13)}$$

This expression is similar to A9, but it contains an additional term in the denominator as a result from the absorption by the IS. This phenomenon can be corrected for only if the absorption coefficients of both the IS surface (*f*) and the sample (*A*) at the excitation wavelength of interest are known, as well as the intensity of the excitation beam.

References

[1]. J.C. de Mello, H.F. Wittmann, and R.H. Friend, *Adv. Mater.*, 9 (1997) p. 230-232.

[2]. G. Bourhill, L.O. Pålsson, I.D.W. Samuel, I.C. Sage, I.D.H. Oswald, and J.P. Duignan, *Chem. Phys. Lett.*, 336 (2001) p. 234-241.

[3]. A.M. Brouwer, *Pure Appl. Chem.*, 83 (2011) p. 2213-2228.

[4]. J.W. Verhoeven, *Pure Appl. Chem.*, 68 (1996) p. 2223-2286.

[5]. L.O. Pålsson and A.P. Monkman, *Adv. Mater.*, 14 (2002) p. 757-758.

[6]. L. Porres, A. Holland, L.O. Palsson, A.P. Monkman, C. Kemp, and A. Beeby, *J. Fluoresc.*, 16 (2006) p. 267-72.

Samenvatting

Inleiding

In het eerste hoofdstuk van dit proefschrift wordt een algemene inleiding tot de energiebehoefte van kunstverlichting gegeven, evenals een beschrijving van de werkingsprincipes van lampen en kleurenzicht. Er kan een substantiële hoeveelheid energie bespaard worden wanneer de huidige lampen worden vervangen door meer energie-efficiënte lichtbronnen. Er worden verschillende benaderingen besproken voor zeer efficiënte, op licht-emitterende diodes (LEDs) gebaseerde vastestof lichtbronnen (*Solid State Light sources*, SSLs). Ofschoon SSLs die wit licht uitstralen al bestaan, kunnen eigenschappen zoals de efficiëntie en het emissiespectrum aanzienlijk verbeterd worden. De benadering waarbij gebruik wordt gemaakt van een in het nabij-UV (nUV) emitterende LED gecombineerd met een laag van verbindingen die deze hoog energetische straling naar zichtbaar licht kunnen omzetten, zogenaamde fosforen, is veelbelovend. Echter, de hiervoor vereiste fosforen die efficiënt kunnen worden geëxciteerd middels nUV straling ontbreken vooralsnog. Vanuit dit oogpunt bezien zijn complexen van driewaardige lanthanoide-ionen interessante verbindingen. Bij dergelijke verbindingen kan de lijnemissie van het lanthanoide-ion efficiënt aangeslagen worden *via* ligandgecentreerde absorptiebanden. De liganden op hun beurt kunnen op de excitatiebron, in dit geval de LED, worden afgestemd, bijvoorbeeld door het aanbrengen van substituenten. Naast details van de energieoverdrachtsmechanismen en de fotofysische eigenschappen van de driewaardige lanthanoide-ionen, wordt de coördinatiechemie van de lanthanoiden beschreven. Het laatste onderdeel van dit hoofdstuk behelst een overzicht van de verschillende benaderingen tot het verkrijgen van hoogefficiënte fotoluminescente complexen die in dit proefschrift staan beschreven.

Gesubstitueerde fenantrolines als antennes

Het is reeds bekend dat 1,10-fenantroline in staat is om als antenne voor luminescentie door het Eu(III) ion te dienen. Helaas bevindt het excitatiemaximum van een dergelijke verbinding zich bij 355 nm. Om deze reden kan 1,10-fenantroline niet aangewend worden om Eu(III) emissie aan te slaan met een In:GaN gebaseerde LED emitterend in het nabij-UV. Teneinde te onderzoeken of het mogelijk is om dit excitatiemaximum te verschuiven naar grotere golflengtes is een serie van acht nieuwe Eu(III) coördinatieverbindingen gesynthetiseerd met 1,10-fenantroline beschikkend over een chloro-, methoxy-, ethoxy-, cyano-, carboxylzuur, methylcarboxylaat-, ethylcarboxylaat, en een amino-substituent op de 2-positie. Dit werk is beschreven in hoofdstuk 2. Er is vastgesteld dat alle verbindingen behalve [Eu(2-amino-1,10-fenantroline)$_2$(NO$_3$)$_3$] de voor het Eu(III) ion karakteristieke fotoluminescentie vertonen bij excitatie met nabij-UV straling. Er is geconstateerd dat in de genoemde verbinding de luminescentie wordt gedoofd door een laag energetische ligand-

naar-metaal ladingsoverdracht. Een hoog kwantumrendement van 78% is gevonden voor [Eu(2-chloro-1,10-fenantroline)$_2$(NO_3)$_3$], maar het excitatiemaximum van deze verbinding is incompatibel met de emissie van een nabij-UV LED. Het excitatiemaximum van de verbindingen [Eu(2-(ethylcarboxylaat)-1,10-fenantroline)$_2$(NO_3)$_3$] en [Eu(2-methoxy-1,10-fenantroline)$_2$(NO_3)$_3$] ligt bij 370 nm, maar het lage kwantumrendement (resp. 11% en 24%) beperkt de toepassing hiervan als fosformateriaal. In alle gevallen wordt het totale kwantumrendement van de verbindingen beperkt door het lage intrinsieke kwantumrendement van het Eu(III) ion (17-52%). Tevens wordt in hoofdstuk 2 de allereerste toepassing van 1-methyl-1,10-fenantrolin-2(1*H*)-on, een synthetisch intermediair, als een ligand beschreven, gebruikmakend van Eu(III) als centraal ion. Met behulp van röntgenkristallografie is vastgesteld dat het ligand het metaal bindt *via* de carbonylzuurstof, wat resulteert in een verbinding die gematigd efficiënte fotoluminescentie vertoont met een kwantumrendement van 22% bij aanslaan op 355 nm.

Ln(III)-complexen met kleine aromatische liganden

Zoals beschreven in het eerste hoofdstuk van dit proefschrift kunnen kleine aromatische liganden gebruikt worden als antennes voor het aanslaan van emissie door lanthanoide ionen. Zowel mononucleaire complexen als metaal-organische roosters kunnen worden gevormd met dergelijke liganden en de lanthanoide-ionen. In hoofdstuk 3 wordt de synthese van verbindingen met Eu(III) en Tb(III) en furaan-2,5-dicarboxylzuur (H_2fda) beschreven alsmede een verbinding van Tb(III) met 2-hydroxytrimesinzuur (H_4tma). In de eerste instantie werden met H_2fda en $EuCl_3$ of $TbCl_3$ verbindingen verkregen met de formule $(H_2NMe_2)_6Ln_4(fda)_7Cl_4$. Herkristallisatie van deze verbindingen leidt tot de vorming van een eendimensionaal metaal-organisch polymeer. Alle verbindingen vertonen fotoluminescentie welke karakteristiek is voor het lanthanoide ion. De intensiteit van de luminescentie is laag voor alle verbindingen, in het bijzonder voor de geherkristalliseerde verbindingen. Dit kan eenvoudig worden verklaard, omdat het *Ln*(III)-ion hierin omringd is door vijf watermoleculen die de luminescentie kunnen uitdoven. Reactie van het H_4tma ligand met $TbCl_3$ in water onder hydrothermale condities resulteert in de vorming van een rigide driedimensionaal metaal-organisch rooster met een hoge dichtheid. Deze verbinding vertoont intense fotoluminescentie met een kwantumrendement van 67%. Tezamen met deze hoge efficiëntie maakt het excitatiemaximum bij 378 nm deze verbinding een ideale kandidaat voor een groene fosfor voor toepassing in LEDs.

Fenol-type liganden als antennes

In hoofdstuk 4 is de synthese van tien nieuwe Eu(III) en Tb(III) complexen met 2-(4,5-dihydro-1,3-oxazol-2-yl)fenol (H**L1**) en het thiazolylderivaat 2-(4,5-dihydro-1,3-thiazol-2-yl)fenol (H**L2**) als liganden beschreven. Er is vastgesteld dat deze fenol-type liganden kunnen worden gebruikt voor het aanslaan van emissie door zowel Eu(III)- als Tb(III)-ionen. De intensiteit van de fotoluminescentie van met name de Eu(III)-

complexen blijkt sterk afhankelijk van de metaal-tot-ligand (M:L) verhouding. De verbindingen met een M:L verhouding van 1:4 vertonen tamelijk heldere luminescentie met kwantumrendementen van 20% (Eu**L2**_4) en 43% (Eu**L1**_4). De 1:3 Eu(III)-complexen zijn niet luminescent, hetgeen verklaard kan worden door de aanwezigheid van een laag-energetische ligand-naar-metaal ladingsoverdracht toestand. Een extra band in de absorptiespectra van de Eu(III)-verbindingen in vergelijking met de Tb(III)-analoga bevestigt dit. De intensiteit van de luminescentie van de Tb(III)-complexen lijkt minder sterk af te hangen van de M:L verhouding. De intensiteit van de luminescentie der Tb(III)-complexen met **L2** als ligand is betrekkelijk zwak. Zo vertoont de verbinding Tb**L1**_4 zeer intense fotoluminescentie met een kwantumrendement van maar liefst 79% wanneer deze bij 360 nm wordt aangeslagen, terwijl Tb**L2**_4 zeer zwakke luminescentie vertoont. Dit kan worden verklaard door een slechte spectrale combinatie van **L2** en het Tb(III)-ion. Over het geheel gezien lijkt **L1** een betere antenne te zijn dan **L2** voor zowel Eu(III)- als Tb(III)-ionen. Een poging tot herkristalliseren van Eu**L1**_3 en Tb**L1**_3 leidde tot de vorming van een octanucleair complex waarin de metaalionen nauw bijeen gehouden worden door carbonaationen welke ontstaan zijn uit ingevangen atmosferisch CO_2. De Eu(III)-verbinding vertoont zwakke fotoluminescentie bij excitatie met nabij-UV straling, terwijl het Tb(III)-complex een tamelijk hoog kwantumrendement van 51% heeft.

Afstemmen van Eu(III)-complexen met dibenzoylmethanaten

Dibenzoylmethaan (Hdbm) is een molecuul welke met grote efficiëntie de emissie van het Eu(III) ion kan aanslaan. Op dit moment zijn studies waarin de invloed van substituenten op Hdbm op het vermogen om Eu(III)-luminescentie aan te slaan wordt onderzocht erg schaars. Ook over de invloed van de kationen (A^+) op de luminescente eigenschappen van anionische complexen zoals $A^+[Eu(dbm)_4]^-$ is weinig bekend. In hoofdstuk 5 wordt de synthese van zeven europiumcomplexen met halogeengesubstitueerde Hdbm-liganden beschreven. Afhankelijk van de positie van de substituenten op de fenylgroepen ten opzichte van het chelerende 1,3-diketo-fragment, (ortho, meta of para) kunnen de verbindingen in drie groepen worden geclassificeerd. De emissiespectra van de complexen zijn geanalyseerd met de Judd-Ofelt theorie. Verschillen tussen de ligandsubstitutiepatronen komen tot uiting in de intensiteitparameters $\Omega_{2,4,6}$. De liganden met een 4-Br en een 4-F substituent hebben beiden een hoge antenne-efficiëntie van 90%, maar het intrinsieke kwantumrendement van het Eu(III)-ion is zeer laag in de verbindingen met deze liganden. De Eu(III)-verbindingen met de liganden met een 3-F, 3-Cl, 3-Br of 3-I substituent vertonen lagere antenne-efficiënties (54 tot 62%). Het intrinsieke kwantumrendement van het Eu(III)-ion is hoger in deze verbindingen, hetgeen leidt tot fotoluminescentie kwantumrendementen van 22-35%. De verbinding met de 2-Cl substituent op het ligand vertoont veruit de langste experimentele halfwaardetijd (0.89 ms) en de laagste Ω_2 parameter van de gehele serie. Er wordt in hoofdstuk 5 getoond dat deze eigenschappen ten minste kwalitatief begrepen kunnen worden door beschouwing van de

elektronen-zuigende eigenschappen van de substituenten. De sterke invloed van het tegenion op de luminescente eigenschappen van $[Eu(dbm)_4]^-$ is aangetoond door het vergelijken van de luminescente eigenschappen van de verbindingen met $HNEt_3^+$, Li^+ en NBu_4^+ tegenionen. Bovendien is de kristalstructuur van de twee laatstgenoemde verbindingen bepaald en beschreven.

Triboluminescentie

Een klein aantal verbindingen met driewaardige lanthanoide-ionen vertoont luminescentie wanneer de kristallieten worden gebroken, een fenomeen dat bekend staat als triboluminescentie (TrL). Hoewel nog niet volledig opgehelderd, lijkt het erop dat het TrL-mechanisme energieoverdracht van een ligandgecentreerde geëxciteerde toestand naar een aangeslagen toestand van het lanthanoide-ion behelst, wat in overeenstemming is met het mechanisme voor fotoluminescentie van dergelijke verbindingen. Daarbij bestaat er nog onenigheid over de stelling dat slechts verbindingen welke kristalliseren in een niet-centrosymmetrische ruimtegroep triboluminescentie kunnen vertonen. Een van de verbindingen met de meest intense TrL-emissie is de Eu(III)-coördinatieverbinding $HNEt_3$[Eu(dibenzoylmethanaat)$_4$], welke sterk gerelateerd is aan de verbindingen die besproken worden in hoofdstuk 5. Om deze redenen is er een serie lanthanoide coördinatieverbindingen gesynthetiseerd met de algemene formule $HNEt_3$[*Ln*(dibenzoylmethanaat)$_4$] (*Ln* = La, Nd, Sm, Eu, Tb, Dy, Ho, Er, Tm, Yb). De kristalstructuren van de verbindingen met *Ln* = La, Nd en Sm worden in hoofdstuk 6 beschreven en foto- en triboluminescentie-metingen wijzen uit dat de enige verbindingen die zichtbare fotoluminescentie vertonen (*Ln* = Eu, Sm) tevens de enige zijn die TrL vertonen. Dit is in overeenstemming met het mechanisme waarin het *Ln*(III) ion wordt aangeslagen *via* het ligand. De Sm-verbinding is geïdentificeerd als een nieuwe triboluminescente verbinding; omdat deze kristalliseert in een niet-centrosymmetrische ruimtegroep kan de relatie tussen triboluminescentie en de afwezigheid van centrosymmetrie niet worden weerlegd.

List of publications

'Crystal structures of the double perovskites $Ba_2Sr_{1-x}Ca_xWO_6$'
W.T. Fu, S. Akerboom, D.J.W. IJdo, *J. Sol. St. Chem.* **180** (2007) 1547-1552.

'Crystal structures of the double perovskites $Ba_2M(II)M'(VI)O_6$ (M = Ca, Sr, M' = Te, W, U'
W.T. Fu, Y.S. Au, S. Akerboom, D.J.W. IJdo, *J. Sol. St. Chem.* **181** (2008) 2523-2529.

'The intermediate tilt systems in the double perovskites $Ba_{1-x}Sr_xCaWO_6$ and $Ba_{1-x}Sr_xYSbO_6$'
W.T. Fu, S. Akerboom, D.J.W. IJdo, *J. Alloys Compd.* **476** (2009) L11-L15.

'Crystal structure and luminescence of complexes of Eu(III) and Tb(III) with furan-2,5-dicarboxylate'
S. Akerboom, W.T. Fu, M. Lutz, E. Bouwman, *Inorg. Chim. Acta* **387** (2012) 289-293.

'Synthesis, structure and luminescence of new dinuclear cyanido-bridged AgI–AuI one-dimensional coordination polymer'
M. Ghazzali, M.H. Jaafar, K. Al-Farhan, S. Akerboom, J. Reedijk, *Inorg. Chem. Commun.* **20** (2012) 188-190.

'Substituted phenanthrolines as antennae in luminescent Eu(III) complexes'
S. Akerboom, J.J.M.H van den Elshout, I. Mutikainen, M.A. Siegler, W.T. Fu, E. Bouwman, *Eur. J. Inorg. Chem.* (2013), in press.

'1-Methyl-1,10-phenanthrolin-2(1*H*)-one (L) as a ligand to Eu(III): Crystal structure and luminescent properties of $[Eu(L)_3(NO_3)_3]$'
S. Akerboom, J.J.M.H van den Elshout, I. Mutikainen, W.T. Fu, E. Bouwman, *Polyhedron* (2013), in press.

'Structure, photo- and triboluminescence of the lanthanoid dibenzoylmethanates: $HNEt_3[Ln(dbm)_4]$'
S. Akerboom, M.S. Meijer, M.A. Siegler, W.T. Fu, E. Bouwman, *J. Lumin.* **145** (2014) 278-282.

'A novel metal organic framework from Tb(III) and 2-hydoxytrimesic acid showing very intense photoluminescence'
S. Akerboom, X. Liu, S.H.C. Askes, I. Mutikainen, W.T. Fu, E. Bouwman, submitted for publication.

A series of bimetallic coordination polymers bearing $[Ag(PPh_3)_2]$ chromophores: synthesis, structure and luminescence'
M. Ghazzali, M.H. Jaafar, S. Akerboom, A. Alsalme, K. Al-Farhan, J. Reedijk, *Inorg. Chem. Commun*., **36** (2013) 18-21.

'Phenol oxazolines as antennae in luminescent *Ln*(III) complexes, *Ln*(III)=Eu(III), Tb(III)'
S. Akerboom, E.T. Hazenberg, I. Schrader, S.F. Verbeek, W.T. Fu, E. Bouwman, manuscript in preparation.

'Influence of the substituents on the antenna properties of dibenzoylmethane ligands in luminescent Eu(III) complexes'
S. Akerboom, W.T. Fu, E. Bouwman, manuscript in preparation.

Curriculum Vitae

Sebastiaan Akerboom werd op 6 december 1985 te ’s Gravenhage geboren. In 2004 behaalde hij het atheneumdiploma aan het Fioretticollege te Lisse. In het najaar van datzelfde jaar begon hij met de studie scheikunde aan de Universiteit Leiden. Op 31 augustus 2005 werd het propedeutisch examen van deze opleiding *cum laude* afgelegd. In de herfst van 2006 begon de auteur een stage vastestofchemie onder leiding van dr. W.T. Fu en dr. D.J.W. IJdo, welke in maart 2007 werd afgerond. Op 1 oktober 2007 werd het baccalaureaatsdiploma aan de auteur uitgereikt met het judicium *cum laude*. In 2008 begon hij met een afstudeerstage in de vastestofchemie, met als doel de systematiek in faseovergangen in dubbelperofskieten te onderzoeken. Deze stage werd afgelegd onder leiding van dr. W.T. Fu, en leidde samen met het onderzoek uit 2007 tot de publicatie van een drietal wetenschappelijke artikelen op dit gebied. In oktober 2008 werd begonnen met een onderzoeksstage bij het Energieonderzoekcentrum Nederland (ECN) te Petten, onder leiding van dr. F.P.F. van Berkel en dr. D.J.W. IJdo. In dit project werd gekeken naar de mogelijkheid om op metaaloxide-gebaseerde protonengeleidende elektrolytmembranen toe te passen in vast-oxide brandstofcellen. De studie scheikunde werd op 9 september 2009 afgerond met het *cum laude* behalen van het masterdiploma.

De auteur in was van 1 september 2009 tot 1 september 2013 dienst van de Universiteit Leiden als promovendus. Het in dit proefschrift beschreven werk werd tijdens deze periode verricht onder leiding van prof. dr. E. Bouwman en dr. W.T. Fu. Naast het onderzoek werden de hiermee samenhangende onderwijstaken vervuld op eerstejaars practica voor studenten *Life Science and Technology* (LST) en *Molecular Science and Technology* (MST) alsmede door de begeleiding van een drietal onderzoeksprojecten voor eerste- en tweedejaarsstudenten MST in het kader van ‘Leren onderzoeken’. Daarnaast heeft de auteur zes onderzoeksprojecten voor studenten in de masterfase en drie onderzoeksprojecten voor studenten in de bachelorfase begeleid.

De tijdens de promotieperiode gevolgde en met goed gevolg afgeronde cursussen zijn: ‘Advanced Metal-Organic Chemistry’ (HRSMC, september 2010), ‘Communication in Science’ (Graduate School, 2010), ‘Timemanagement, zelfmanagement' (Graduate School, 2011), ‘Effectieve Comunicatie’ (Graduate School, 2011).

Gedeelten van het in dit proefschrift beschreven werk werden door de auteur gecommuniceerd middels poster of presentatie op verschillende congressen, te weten: ‘the 1st International Conference on the Luminescence of Lanthanides’ (ICLL-1) in Odessa, Oekraïne, 2010, de HRSMC autumn school ‘Advanced Metal-Organic Chemistry’ in Doorn, 2010, het eerste Jan Reedijk Symposium in Leiden, 2010, het HRSMC symposium in Leiden, 2010, de NWO CW bijeenkomst ‘Chemistry related to Physics and Materials Sciences’ in Veldhoven, 2011, de NWO bijeenkomst ‘Chemistry as an Innovative Science’

(CHAINS) in Maarssen, 2011, het HRSMC symposium in Amsterdam, 2011, 'the 8th International Conference on f-Elements (ICfE8)' in Udine, Italië, 2012, de NWO CW bijeenkomst 'Chemistry in Relation to Physics and Materials Science' in Veldhoven, 2013.

Acknowledgements

I kindly acknowledge dr. Ilpo Mutikainen (University of Helsinki, Finland), dr. Maxime Siegler (Johns Hopkins University, USA) and dr. Martin Lutz (Utrecht University) for determining the crystal structures of the compounds described in this work. Ing. John van Dijk performed mass analysis and Mr. Jos van Brussel carried out elemental analyses. The author acknowledges Mrs. Trudie Brouwer and Mr. Arjan Oudshoorn for the use of the fluorimeter. Prof A. Meijerink (Utrecht University) is acknowledged for the use of his spectrometer to determine luminescence lifetime and quantum yields. Mr. Jos van den Elshout contributed to Chapter 2. Mr. Sven Askes and Mr. Xue Liu contributed to Chapter 3. Mr. Tom Hazenberg, Ms. Sarah Verbeek, Ms. Ireen Schrader and Mr. Florian Kettner (University of Leipzig) are acknowledged for their contributions to Chapter 4. Misters Jannick Rooijmans, Kevin Felter, Lucas van der Saag and Loïc LeClerq contributed to Chapter 5. I kindly acknowledge Mr. Michael Meijer for his contribution to Chapter 6.